



Australian Government
Geoscience Australia

POST-CRUISE REPORT

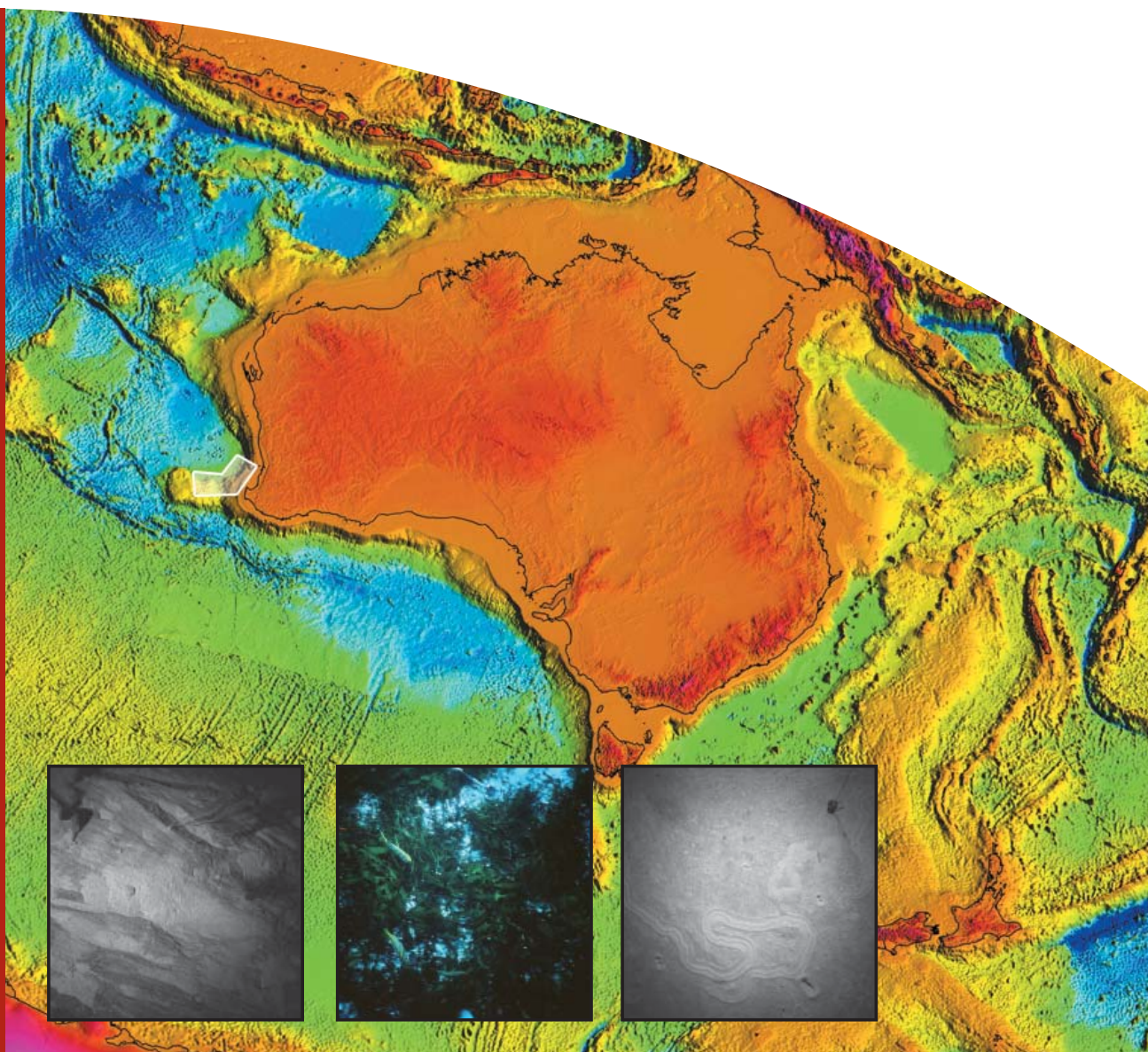
Geomorphology, Sedimentology and Stratigraphy of Submarine Canyons on the SW Australian Slope

RV Southern Surveyor, September – October 2005

*Andrew D. Heap, Jonathan Edwards, Leharne Fountain, Michele Spinnocia,
Michael Hughes, Emma Mathews, Jonathan Griffin, Irina Borissova,
Jane Blevin, Cameron Mitchell and Andrew Krassay*

Record

2008/16



Geoscience Australia Survey SS08/2005

Post-survey Report

**Geomorphology, Sedimentology and
Stratigraphy of Submarine Canyons on the
SW Australian Slope**

RV Southern Surveyor

September – October 2005

Andrew D. Heap, Jonathan Edwards, Leharne Fountain, Michele Spinnocia,
Michael Hughes, Emma Mathews, Jonathan Griffin, Irina Borissova, Jane Blevin,
Cameron Mitchell and Andrew Krassay

Geoscience Australia, GPO Box 378, Canberra, ACT 2601



Australian Government

Geoscience Australia

Department of Resources, Energy and Tourism

Minister for Resources, Energy and Tourism: The Hon. Martin Ferguson, AM MP

Secretary: Dr Peter Boxall, AO

Geoscience Australia

Chief Executive Officer: Dr Neil Williams, PSM

© Commonwealth of Australia 2008

This work is copyright. Apart from any fair dealings for the purposes of study, research, criticism or review, as permitted under the *Copyright Act 1968*, no part may be reproduced by any process without written permission. Copyright is the responsibility of the Chief Executive Officer, Geoscience Australia. Requests and enquiries should be directed to the **Chief Executive Officer, Geoscience Australia, GPO Box 378, Canberra City, ACT 2601, Australia.**

ISSN: 1448-2177

ISBN: 978-1-921498-13-8 Hardcopy

ISBN: 978-1-921498-14-5 CD-ROM

GeoCat No. 66341

Bibliographic reference: Heap, A.D., Edwards, J., Fountain, L., Spinnocia, M., Hughes, M., Mathews, E., Griffin, J., Borissova, I., Blevin J., Mitchell, C., and Krassay, A., (2008). *Geomorphology, Sedimentology and Stratigraphy of Submarine Canyons on the SW Australian Slope – post survey report*. Geoscience Australia, Record 2008/16, 138pp.

Correspondence for feedback:

Sales Centre

Geoscience Australia

GPO Box 378

Canberra

ACT 2601

Sales@ga.gov.au

Geoscience Australia has tried to make the information in this product as accurate as possible. However, it does not guarantee that the information is totally accurate or complete. **Therefore, you should not rely solely on this information when making a commercial decision.**

Contents

	Page
List of Figures	vi
List of Tables	ix
Executive Summary	xi
1. Introduction	1
1.1. Background	1
1.1.1. <i>Submarine Canyons and Biological Hotspots</i>	2
1.2. Study Area	3
1.2.1. <i>Submarine Canyon Geomorphology</i>	3
1.2.2. <i>Shelf Geomorphology and Sedimentology</i>	5
1.2.3. <i>Oceanography</i>	6
1.2.4. <i>Regional Geology</i>	6
1.3. Survey Objectives	11
1.4. Survey Participants	12
1.4.1. <i>Scientific Personnel</i>	12
1.4.2. <i>Ship's Crew</i>	13
2. Geophysics	14
2.1. Data Acquisition	14
2.1.1. <i>Multi-beam (Swath) Sonar</i>	14
2.1.2. <i>Shallow Seismic Reflection</i>	14
2.1.3. <i>Side Scan Sonar</i>	15
2.2. Data Processing and Analysis	15
2.2.1. <i>Multi-beam (Swath) Sonar</i>	15
2.2.2. <i>Shallow Seismic Reflection Data</i>	16
2.2.3. <i>Side Scan Sonar Data</i>	16
2.3. Results	16
2.3.1. <i>Multi-beam (Swath) Sonar</i>	16
2.3.2. <i>Shallow Seismic Reflection</i>	22
2.3.3. <i>Side Scan Sonar</i>	34
3. Oceanography	35
3.1. Data Acquisition	35
3.1.1. <i>Mooring Description</i>	35
3.2. Data Processing and Analysis	35
3.2.1. <i>Wind Waves</i>	35

	Page
3.2.2. <i>Tides</i>	42
3.2.3. <i>Currents</i>	44
4. Sedimentology	50
4.1. Sample Acquisition	50
4.1.1. <i>Water Samples</i>	51
4.1.2. <i>Still Camera</i>	52
4.1.3. <i>Surface Sediment Sampling</i>	53
4.1.4. <i>Subsurface Sediment Sampling</i>	55
4.1.5. <i>Other Survey Samples</i>	56
4.2. Sample Processing and Analysis	56
4.2.1. <i>Water Samples</i>	56
4.2.2. <i>Still Camera</i>	56
4.2.3. <i>Surface Sediment Samples</i>	58
4.2.4. <i>Subsurface Sediment Samples</i>	60
4.3. Results	61
4.3.1. <i>Water Samples</i>	61
4.3.2. <i>Still Camera</i>	63
4.3.3. <i>Surface Sediments</i>	73
4.3.4. <i>Subsurface Sediments</i>	91
5. Basin Geology	97
5.1. Petroleum Potential	97
5.1.1. <i>Vlaming Sub-basin</i>	97
5.1.2. <i>Mentelle Basin</i>	98
5.2. Preliminary Dredge Results	98
5.2.1. <i>Basin Sediments</i>	99
6. Discussion and Summary	100
6.1. Discussion	100
6.1.1. <i>Seabed and Shallow Sub-surface Sedimentology</i>	100
6.1.2. <i>Benthic Biota</i>	101
6.1.3. <i>Petroleum Prospectivity</i>	102
6.2. Summary	103
7. References	104
8. Acknowledgements	111
9. Appendices	112

	Page
9.1. Appendix A – Survey Leaders Log	112
9.2. Appendix B – Shallow Seismic Profiles	119
9.3. Appendix C – CTD Data and Water Samples	120
9.4. Appendix D – Still Photographs	121
9.4.1. <i>Summary Details of Still Photographs</i>	121
9.4.2. <i>Photograph Descriptions</i>	124
9.5. Appendix E – Dredge Descriptions	127
9.6. Appendix F – Textural Characteristics of Seabed Sediments	130
9.7. Appendix G – Core Logs.....	138
9.8. Appendix H – Textural Characteristics of Sub-surface Sediments.	138
9.9. Appendix I – Multi-sensor Core Logger Data.....	138
9.10. Appendix J – Slope Stability Report.	138

List of Figures

	Page
1. Introduction.....	1
Figure 1.1. Map of SW Australian margin geomorphology and study area.....	4
Figure 1.2. Map of major geologic structure of SW Australian margin.....	8
Figure 1.3. Stratigraphy, petroleum systems and basin events for Perth Basin.	9
Figure 1.4. Cross-section of seismo-stratigraphic units for Perth Basin.	10
Figure 1.5. Interpreted cross-section of the Mentelle Basin.....	10
Figure 1.6. Graph of total number of samples by water depth for AEEZ.	11
Figure 1.7. Photograph of RV <i>Southern Surveyor</i>	12
2. Geophysics.....	14
Figure 2.1. Map of multi-beam (swath) sonar and sub-bottom profiler lines.....	17
Figure 2.2. Map of multi-beam (swath) sonar coverage of Perth Canyon.....	19
Figure 2.3. Map of multi-beam (swath) sonar bathymetry for the head of the Perth Canyon.	19
Figure 2.4. Map of multi-beam (swath) sonar bathymetry for the Mentelle Basin region.	21
Figure 2.5. Map of multi-beam (swath) sonar bathymetry and sub-bottom profile for several small tributaries of the Perth Canyon.	23
Figure 2.6. Map of multi-beam (swath) sonar bathymetry and sub-bottom profile for large tributary of the Perth Canyon.....	25
Figure 2.7. Map of multi-beam (swath) sonar bathymetry and sub-bottom profile across a slumped next to the Perth Canyon.	26
Figure 2.8. Map of multi-beam (swath) sonar bathymetry and sub-bottom profile across a thickly sedimented section near the Perth Canyon. ...	27
Figure 2.9. Map of multi-beam (swath) sonar bathymetry and sub-bottom profile across possible fluid escape features south of the Perth Canyon.....	29
Figure 2.10. Distribution of acoustic facies in the Perth Canyon region.....	31
Figure 2.11. Distribution of acoustic facies in the Mentelle Basin region.....	31
Figure 2.12. Multi-beam (swath) sonar and side-scan sonar images of two shipwrecks on the Rottneest Shelf.....	33
Figure 2.13. Multi-beam (swath) sonar bathymetry image of the wreck of HMAS <i>Derwent</i>	33
3. Oceanography	35
Figure 3.1. Photo of ADCP current meter mooring.....	36
Figure 3.2. Graphs of hourly time series of significant wave height.....	37
Figure 3.3. Graphs of directional wave spectra.....	38
Figure 3.4. Graphs of wave autospectra.....	38
Figure 3.5. Cumulative frequency and normal probability plots of significant wave height.....	39

	Page
Figure 3.6. Cumulative frequency and normal probability plots of near-bed wave orbital velocity amplitude.....	40
Figure 3.7. Cumulative frequency and normal probability plots of wave-induced skin friction bed shear stress.....	41
Figure 3.8. Graphs of hourly time series of water depth from the tidal data.	43
Figure 3.9. Graphs of tide and wave current speed and direction at the surface and bed.....	45
Figure 3.10. Graphs of 20 minute time series of current speed and direction at the surface and near the bed.	46
Figure 3.11. Cumulative frequency and normal probability plots of near-surface current speed.....	47
Figure 3.12. Cumulative frequency and normal probability plots of near-bed currents speed.	47
Figure 3.13. Progressive vector plot showing displacement of the near-surface and near-bed currents.	48
Figure 3.14. Cumulative frequency and normal probability plots of skin friction bed shear stress.	48

4. Sedimentology50

Figure 4.1. Multi-beam (swath) sonar bathymetry image showing location of sample stations for survey SS082005.....	50
Figure 4.2. Photograph of CTD rosette.....	52
Figure 4.3. Photograph of benthos deep-sea film camera and strobe.....	53
Figure 4.4. Diagram of typical camera two configuration.....	53
Figure 4.5. Photograph of rock dredge.	54
Figure 4.6. Photograph of Smith-McIntyre grab sampler.....	54
Figure 4.7. Photograph of benthic sled.....	55
Figure 4.8. Photographs of gravity corer and deployment system.	56
Figure 4.9. Multi-beam (swath) sonar bathymetry image showing location of samples from previous surveys in the study area.	57
Figure 4.10. Photograph of water filtering system.	57
Figure 4.11. CTD profile showing four major water bodies in study area.....	62
Figure 4.12. Graphs of temperature, oxygen, salinity and transmission with water depths from CTD casts.....	63
Figure 4.13. Graph of suspended sediment concentrations versus transmission..	64
Figure 4.14. Graph of water depth versus suspended sediment concentration....	64
Figure 4.15. Multi-beam (swath) sonar bathymetry image showing the location of camera stations.	65
Figure 4.16. Multi-beam (swath) sonar bathymetry images showing detailed locations of camera stations.	66
Figure 4.17. Photographs of the seabed from CAM11 and CAM12.....	68
Figure 4.18. Photographs of the seabed from CAM13.	68
Figure 4.19. Photographs of the seabed from CAM13 and CAM09.....	69
Figure 4.20. Photographs of the seabed from CAM09 and CAM10.....	69
Figure 4.21. Photographs of the seabed from CAM07 and CAM04.....	70

	Page
Figure 4.22. Photographs of the seabed from CAM04 and CAM06.	70
Figure 4.23. Photographs of the seabed from CAM06.	71
Figure 4.24. Photographs of the seabed from CAM03.	71
Figure 4.25. Photographs of the seabed from CAM08.	72
Figure 4.26. Photographs of the seabed from CAM08 and CAM14.	72
Figure 4.27. Multi-beam (swath) sonar bathymetry image showing locations of cores.	74
Figure 4.28. Multi-beam (swath) sonar bathymetry image showing locations of dredges, benthic sleds, and grab samples.	74
Figure 4.29. Multi-beam (swath) sonar bathymetry image showing fragmentation index for samples collected in the lower Perth Canyon.	78
Figure 4.30. Multi-beam (swath) sonar bathymetry image showing fragmentation index for samples collected in the Mentelle Basin region.	78
Figure 4.31. Graph of fragmentation index versus water depth.	79
Figure 4.32. Multi-beam (swath) sonar bathymetry image showing mean grainsize for samples in the Perth Canyon region.	79
Figure 4.33. Multi-beam (swath) sonar bathymetry image showing the gravel fraction for samples in the Perth Canyon region.	81
Figure 4.34. Multi-beam (swath) sonar bathymetry image showing the sand fraction for samples in the Perth Canyon region.	81
Figure 4.35. Multi-beam (swath) sonar bathymetry image showing the mud fraction for samples in the Perth Canyon region.	82
Figure 4.36. Multi-beam (swath) sonar bathymetry image showing grainsize bar graphs for samples in the Perth Canyon region.	82
Figure 4.37. Multi-beam (swath) sonar bathymetry image showing bulk carbonate contents for samples in the Perth Canyon region.	83
Figure 4.38. Multi-beam (swath) sonar bathymetry image showing carbonate (sand) contents for samples in the Perth Canyon region.	83
Figure 4.39. Multi-beam (swath) sonar bathymetry image showing carbonate (mud) contents for samples in the Perth Canyon region.	84
Figure 4.40. Multi-beam (swath) sonar bathymetry image showing mean grainsize for samples in the Mentelle Basin region.	86
Figure 4.41. Multi-beam (swath) sonar bathymetry image showing the gravel fraction for samples in the Mentelle Basin region.	86
Figure 4.42. Multi-beam (swath) sonar bathymetry image showing the sand fraction for samples in the Mentelle Basin region.	87
Figure 4.43. Multi-beam (swath) sonar bathymetry image showing the mud fraction for samples in the Mentelle Basin region.	87
Figure 4.44. Multi-beam (swath) sonar bathymetry image showing grainsize bar graphs for samples in the Mentelle Basin region.	88
Figure 4.45. Multi-beam (swath) sonar bathymetry image showing carbonate (bulk) contents for samples in the Mentelle Basin region.	88
Figure 4.46. Multi-beam (swath) sonar bathymetry image showing carbonate (sand) contents for samples in the Mentelle Basin region.	89
Figure 4.47. Multi-beam (swath) sonar bathymetry image showing carbonate (mud) contents for samples in the Mentelle Basin region.	89

List of Tables

	Page
1. Introduction	1
Table 1.1. Scientific survey personnel and their role on the survey.....	12
Table 1.2. Ship's crew and their role on the survey.....	13
2. Geophysics	14
Table 2.1. Echo-types in the study area.	32
3. Oceanography	35
Table 3.1. Amplitudes, phases and errors of the tidal harmonics.	42
4. Sedimentology	50
Table 4.1. Station operations.	51
Table 4.2. Mean grainsize descriptions.....	59
Table 4.3. Summary details of CTD casts collected on the survey.	62
Table 4.4. Summary details of temperature, salinity, dissolved oxygen and transmission for the water bodies present in the study area.....	63
Table 4.5. Camera station locations and photographs collected.....	65
Table 4.6. Summary details of cores collected on the survey.....	75
Table 4.7. Summary details of benthic sleds collected on the survey.	75
Table 4.8. Summary details of grab samples collected on the survey.....	76
Table 4.9. Summary details of dredges collected on the survey.....	76
Table 4.10. Summary details of physical properties of Perth Canyon cores.....	93
Table 4.11. Summary details of physical properties of Busselton Canyon cores.	94
Table 4.12. Summary details of physical properties of Geographe Canyon cores.	95
Table 4.13. Summary details of physical properties of Bunbury Canyon cores.	96
Table 4.14. Summary details of physical properties of sediment contained in cores from the canyon interfluves.	96
9. Appendices	112
Table 9.1. Summary details of suspended sediment samples collected on the survey.....	120
Table 9.2. Summary details of camera SS08/2005/02CAM01.....	121
Table 9.3. Summary details of camera SS08/2005/07CAM02.....	121
Table 9.4. Summary details of camera SS08/2005/09CAM03.....	121
Table 9.5. Summary details of camera SS08/2005/12CAM04.....	121
Table 9.6. Summary details of camera SS08/2005/19CAM05.....	122
Table 9.7. Summary details of camera SS08/2005/19CAM06.....	122
Table 9.8. Summary details of camera SS08/2005/25CAM07.....	122

	Page
Table 9.9. Summary details of camera SS08/2005/27CAM08.....	122
Table 9.10. Summary details of camera SS08/2005/05CAM09.....	123
Table 9.11. Summary details of camera SS08/2005/07CAM10.....	123
Table 9.12. Summary details of camera SS08/2005/30CAM11.....	123
Table 9.13. Summary details of camera SS08/2005/02CAM12.....	123
Table 9.14. Summary details of camera SS08/2005/29CAM13.....	123
Table 9.15. Summary details of camera SS08/2005/01CAM14.....	124
Table 9.16. Descriptions of still photographs collected on the survey.....	124
Table 9.17a. Sedimentology descriptions of dredge sub-samples.	127
Table 9.17b. Sedimentology descriptions of dredge sub-samples continued.	129
Table 9.18. Textural characteristics of seabed sediment samples collected on the survey.....	130
Table 9.19. Textural characteristics of seabed sediment samples collected on previous surveys.	131
Table 9.20. Mean grainsize and Folk classification of seabed sediments samples collected on the survey.....	132
Table 9.21. Mean grainsize and Folk classification of seabed sediment samples collected on previous surveys.	133
Table 9.22. Composition point counting results for seabed sediment samples collected on the survey.....	134
Table 9.23. Composition point counting results for seabed sediment samples collected on the survey, expressed as percentages.....	135
Table 9.24. Percent total foraminifera and total fragments for seabed sediment samples collected on the survey.	136
Table 9.25. Composition point counting results for seabed sediments samples collected on previous surveys.	137
Table 9.26. Composition point counting results for seabed sediment samples collected on previous surveys, expressed as percentages.....	137
Table 9.27. Percent total foraminifera and total fragments for seabed sediment samples collected on previous surveys.....	137

Executive Summary

This report contains the preliminary results of Geoscience Australia survey SS08/2005 to the SW margin of Australia. The survey was completed between 28 September and 20 October 2005 using Australia's national facility research vessel *Southern Surveyor*. The survey included scientists from Geoscience Australia, CSIRO – Marine and Atmospheric Research, and Victoria Museum. The survey was co-funded by Geoscience Australia and the Department of the Environment and Heritage (now the Department of the Environment, Water, Heritage and the Arts). The principal scientific objectives of the survey were to:

1. develop an understanding of deep-water sedimentary processes and benthic biota and habitats in “blind” submarine canyons on the SW Australian margin;
2. document the geological and biological transitions between shelf, slope and offshore platform seabed environments; and
3. investigate the stratigraphy and geology of the Mentelle Basin and assess its implications for petroleum potential.

Generally, the sedimentology of the seabed for the blind canyons and shelf-intruding Perth Canyon is very similar, with the texture and composition of the seabed for both of the study regions consistent with that found across the other Australian margins. The shallow (<5 mbsf) sub-surface sedimentology shows very similar texture and composition to the seabed, being primarily composed of unconsolidated spiculitic, foraminiferal/nannofossil ooze. Very little terrigenous material is present in the seabed sediments, concomitant with the overall aridity of the Australian continent and absence of large modern river systems in the southwest. A higher mud content in the Perth Canyon implies that it may be a conduit for the small amounts of terrigenous material that are sourced from the shelf to the deeper ocean, similar to other large shelf cutting canyons from other continents (e.g., Monterey Canyon, California). Transport of sediment and organic matter from the shelf to the upper slope is implied from oceanographic data with the west and northwest net displacement of water over the study period. The data also reveal that waves are the principal mechanism for resuspending material from the seabed, and were representative of relatively energetic wave conditions, although not extreme conditions, experienced during the survey.

Several peaks in magnetic susceptibility coinciding with intervals of darker (organic-rich?) sediment, and horizontal laminations and inter-beds occur in cores from the blind canyons. These regional trends are implied to reflect consecutive higher-order (4th – 5th) Quaternary sea-level cycles with the lowstands representing a time when organic and terrigenous material from shelf (neritic) sources was being transported to the canyons in greater amounts/rates, which has been recorded in the cores. Detailed bathymetry data also revealed numerous examples of seabed instability on the mid to lower slope in the Mentelle Basin although the causes of the mass movements could not be ascertained from our data and their timing is unknown.

Biota sampled and observed in the study area are typical of the benthic and demersal fauna for the mid- to lower-bathyal zone (200-3,000 m) for Australia and for the world's oceans. Comparison with global distributions of bathyal benthic fauna indicates that the benthic biota observed on the present survey comprise the South Australian faunal element. All environments sampled are depauperate reflecting the generally oligotrophic conditions

of Australian waters. However, a relatively abundant and active infauna is apparent with bioturbation marks, including burrows, tracks and mounds common.

Rocks collected on the survey provide the first samples of basin sediments and contribute to our understanding of geological evolution of this frontier area. Interpreted ages for organic-rich terrigenous mudstones are Albian and Aptian to Cenomanian and Albian-Cenomanian, which assign them to the Coolyena Group that was deposited during a thermal subsidence basin phase. Preliminary assessment of the basement rocks suggests they are from the Pinjarra Orogen. Despite these good samples the petroleum prospectivity of the Vlaming Sub-basin and Mentelle Basin could not be conclusively assessed.

Major highlights of the survey are:

- A total of 6,480 km² (3,230 line-km) of swath sonar data, 3,280 line-km of shallow sub-bottom profiler data, and 250 line-km of dual frequency side-scan sonar data. These data cover a new area of the seabed and have revealed the true extents of the blind submarine canyons in SW Australia (including two previously unknown canyons), many examples of mass movements including a 75 km² slump block at the head of Geographe Canyon, numerous tributary canyons on the mid-slope, details of the shallow hemi-pelagic and pelagic sedimentary stratigraphy of the SW Australian margin, and several unknown sunken wrecks on the Rottnest Shelf. A total of 278 line-km of geophysical data were collected in the Perth Canyon region to fill in remaining gaps and 2,354 line-km in the Mentelle Basin region. A total of 246 line-km were collected on the outer and mid Rottnest Shelf and 352 line-km were collected on transit lines between the study areas and Fremantle;
- Obtained first rocks ever to be collected from the Mentelle Basin (terrigenous mudstones);
- Obtained basement rocks close to the surface indicating the extent of the Mentelle Basin sequence along its northern margin;
- Obtained the first ever images of the seabed below 2,000 m from this margin. The seabed images revealed that the deep sea is mostly covered with spiculitic ooze with sub-cropping rocks restricted to steep flanks and incised canyons. The benthic biota are sparse, but the photographic evidence indicates that there is an abundant and active infauna; and
- Collected the most comprehensive SBP data for the SW margin, which revealed the sediment thickness and sub-surface architecture of the study area.

These data combined have greatly improved our understanding of the nature and processes of the seabed associated with blind submarine canyons on the SW margin of Australia and surrounding areas, as well as the geology of the East Mentelle Basin, and fulfilling the scientific objectives of the survey.

1. Introduction

This record contains the substantive results of Geoscience Australia marine survey SS08/2005 to the SW margin of Australia. The survey was completed between 28 September and 20 October 2005 using Australia's national facility research vessel *Southern Surveyor*. The survey included scientists from Geoscience Australia, CSIRO – Marine and Atmospheric Research, and Victoria Museum. The survey was co-funded by Geoscience Australia and the Department of the Environment and Heritage (now the Department of the Environment, Water, Heritage and the Arts). The principal aims of the survey were to explore deep-sea habitats and processes in submarine canyons on the SW margin, and examine the geology of the underlying Mentelle Basin as an assessment for its petroleum potential.

1.1. BACKGROUND

Of particular significance to our understanding of deep-sea habitats are studies of submarine canyons which are known to support a diverse range of biological communities that are comparatively well documented in the literature (e.g., Shepard & Dill, 1966; Sheppard, 1972; Inman *et al.*, 1976; Vetter, 1994, 1998; Vetter & Dayton, 1999; Puig *et al.*, 2003; Bosley *et al.*, 2004; Lin & Liu, 2004). This diversity is attributed to submarine canyons being geomorphologically complex features that contain a variety of environments such as steep-sides of exposed lithified strata that provide hard-grounds for sessile organisms and flat sedimented floors that support burrowing organisms.

Two main types of submarine canyon exist. The first type extends from the slope to the shelf. Often these canyons are located in close proximity to present-day river systems such as: Sepik River, PNG (Kineke *et al.*, 2000); Eel Canyon, California (Mullenbach & Nittrouer, 2000); and Monterey Canyon, California (Shepard *et al.*, 1979). River sediment, nutrients and organic matter can be directly deposited into this submarine canyon type. Submarine canyons that cut the shelf are subject to more regular and vigorous sedimentary processes and are able to intercept shelf and terrigenous sediment, as well as nutrients and organic matter.

The second and most common type of submarine canyon is separated from the shelf. The canyon head is located on the upper slope in water depths of a few hundred to a few thousand metres. These canyons, known as 'blind canyons', do not necessarily occur adjacent to major rivers, and are less likely to intercept shelf and river-derived sediments, nutrients and organic matter.

Three hydrodynamic processes are important in transporting terrigenous and shallow marine sediments, nutrients and organic matter to submarine canyon heads. Delivery of material can be directly from river plumes (e.g., Kineke *et al.*, 2000). On the shelf, swell waves and regional currents, including tidal currents, up-welling and down-welling currents transport material to the canyon head (Granata *et al.*, 1999). In areas of high terrigenous deposition, wave-resuspension of the seabed sediment and density-driven fluid mud can also aid delivery of sediment and organic matter on the shelf to the head of a submarine canyon (Mullenbach & Nittrouer, 2000; Ogston *et al.*, 2000).

Submarine canyons with their heads close to the shelf break act as conduits for the transfer of material to the deep ocean (Puig, 2003). A build up of shelf sediments along the shelf break in the vicinity of the canyon head, followed by rapid mobilisation downslope via gravity-controlled mechanisms (turbidity currents, debris flows, slumps) or during storms

are the primary mechanisms for delivering organic rich sediment to the deep ocean in canyons (Shepard, 1973; Inman *et al.*, 1976; Shanmugam *et al.*, 1985; Gardner, 1989; Puig *et al.*, 2003; Exon *et al.*, 2005). Less dramatically, sediment can also be delivered to the deep ocean by continuous sediment creep (Shepard, 1972).

Relatively less is known about the processes that transport sediment, nutrients and organic matter to blind canyons. Because these canyons are confined to the slope, they are less likely to intercept shelf sediments, nutrients and organic matter. The seabed environments and abundance and distribution of the associated biota in blind canyons are therefore likely to be similar to the adjacent slope regions. They are also likely to contain less sediment, less direct evidence of active sedimentation, and presumably less diverse and abundant biota.

Effective settling velocity influences sediment particle movement in a submarine canyon. When shelf or terrigenous sediments are delivered to a submarine canyon rim, coarse grained particles quickly settle leaving finer sediments to be transported further down the canyon (Liu & Lin, 2004).

Submarine canyon floor sediments in active canyons typically comprise of sand interbedded with mud, gravel, shell debris and even cobbles. Shallow-water fossils and land plants are also common in canyon floor sediments (Shepard, 1972). Graded, laminated, or cross laminated sediments are common reflecting a dynamic and episodic sedimentary regime (Kennett, 1982). Active submarine canyons may contain coarse-grained sediments tens to hundreds of kilometres from the source, deposited by turbidity currents and other sediment gravity flows (Pickering *et al.*, 1989). At the base of the slope, submarine canyons empty onto fans, where the slope decrease causes sediment settling (Kennett, 1982).

During Pleistocene sea-level lowstands, large volumes of sediment were able to be transported into submarine canyons via rapid, episodic gravity-controlled mechanisms and storms (Shanmugam *et al.*, 1985). However, Holocene sea-level rise has reduced the supply of terrigenous and shelf sediment to most submarine canyons (Puig *et al.*, 2003). Shelves have become wider and have further separated from their sediment supply. Estuaries and lagoons that formed in the Holocene trap terrigenous sediment before they can reach the canyon head (Emery & Uchupi, 1972). Slow, continuous transport mechanisms are thought to dominate transport of sediments into submarine canyons during the Holocene (Carson *et al.*, 1986).

1.1.1. Submarine Canyons as Biological Hotspots

Submarine canyons are recognised worldwide as being biological “hotspots” compared to the adjacent slope regions. This is because they contain a range of sedimentary environments and act as conduits for sediment, nutrients and organic matter. Submarine canyons are often associated with enhanced productivity, which can affect the structure of canyon communities compared with adjacent environments (Vetter & Dayton, 1999; Bosley *et al.* 2004).

Submarine canyons act as traps for sediment and organic matter which provides nourishment for a diverse and abundant microfauna (Vetter, 1994; Vetter & Dayton, 1999). Evidence indicates that the presence of organic detritus in shelf-cutting submarine canyons leads to higher growth rates and/or higher abundances of benthic fauna compared with the neighbouring slope regions (Snelgrove, 1994; Vetter & Dayton, 1999). Suspension feeders

benefit from increased plankton and micronekton and also through enhanced currents related to tidal cycles (Shepard, 1979).

Most studies of canyon fauna have reported increased density in canyons compared to adjacent slope environments (Rowe, 1971; Haedrich *et al.*, 1975, 1980; Cartes *et al.*, 1994). Fish abundances are enhanced in submarine canyons due to increased availability of benthic and planktonic food sources (Stefanescu *et al.*, 1994; Vetter, 1994). Submarine canyons may serve as important nursery grounds for fishes (Vetter & Dayton, 1994). At depths greater than about 500 m the enrichment effect of submarine canyons is generally reduced (Vetter & Dayton, 1998). However, in geologically active canyons enrichment may only occur in deep water and no enrichment at shallow water depths where active sedimentary processes (slumps, flows) are present (Rowe *et al.*, 1982; Vetter & Dayton, 1999).

Deeply-incised submarine canyons are also biological hotspots because they act as conduits for up-welling of cooler nutrient-rich water from the deep ocean (Freeland & Denman, 1982; Hooker *et al.*, 1999). Submarine canyons are recognised world-wide as being important feeding grounds for whales with higher diversity and abundance observed compared to neighbouring shelf and slope waters (Hooker *et al.*, 1999).

1.2. STUDY AREA

1.2.1. Submarine Canyon Geomorphology

Previous studies of submarine canyons on the Australian margin have revealed that they are sites of considerable geological (and biological) diversity (e.g., Von der Borch, 1967; McCauley *et al.*, 2000; Exon *et al.*, 2005; Hill *et al.*, 2005). Along the southwest margin of Australia, adjacent to the Rottnest Shelf, lie a series of well-developed submarine canyons (Fig. 1.1).

Submarine canyon development along the southwest margin is related to various tectonic phases including subsidence and rapid seafloor spreading which commenced in the Mid Eocene (43 Ma; Exon *et al.*, 2005). They are structurally controlled, with the orientation of many submarine canyons influenced by original rift structures (Stagg & Willcox, 1991; Hill & De Deckker, 2004; Exon *et al.*, 2005).

Perth Canyon is the largest of the named canyons on the southwest margin (Fig. 1.1). It is a shelf-intruding canyon that dissects the slope about 30 km west of the city of Perth. The morphology and extent of the canyon is well known with almost 100% of the canyon now mapped with high-resolution bathymetry data. The canyon head occurs at the shelf break in approximately 170 m water depth (Collins, 1988).

Perth Canyon is about 120 km long, up to 20 km wide, and dissects the slope to a depth of about 2,000 m. From the head, Perth Canyon extends in a SW direction for ~40 km, then in a NW direction for ~40 km, and then west for ~40 km. The floor of the canyon descends from 170 m at its head to over 4,000 m at its termination. The main canyon axis occurs from 170 m water depth and is intercepted by two smaller tributaries at ~500 m and ~600 m water depth. Slopes on the canyon walls have gradients up to 40° and the underlying bedrock of the Perth Sub-basin is exposed. At the base of the canyon is a large submarine fan (Marshall *et al.*, 1989). During BMR Surveys 80/81 twenty dredge samples were recovered from the Perth Canyon walls. Rocks recovered consisted mainly of limestones, with some sandstones, shales

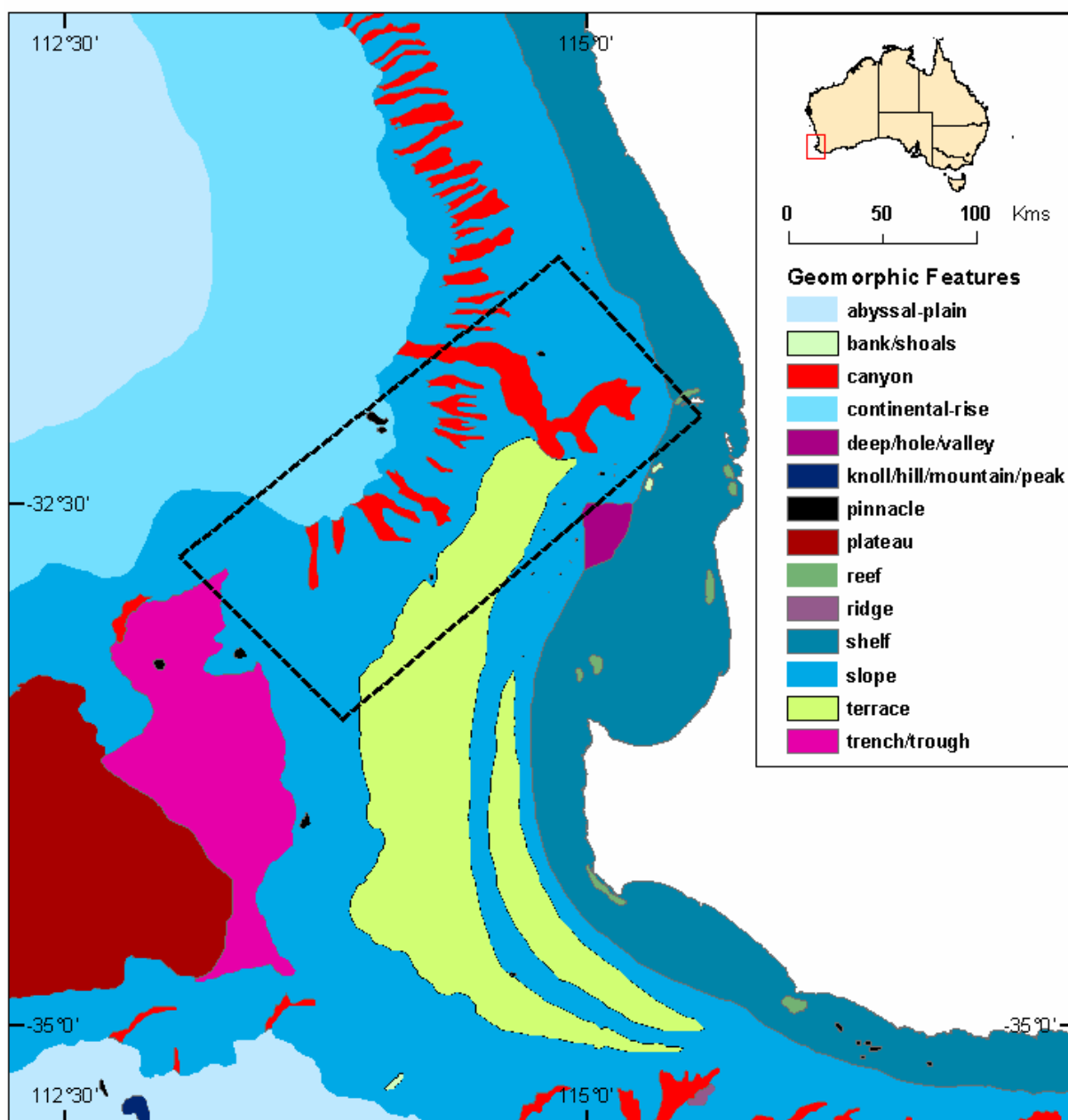


Figure 1.1. Map of SW margin of Australia showing the main geomorphic features and the study area of the present survey.

and mudstones (Marshall *et al.*, 1989). Most of the dredge samples were recovered from the Perth Canyon walls with a few samples from the canyon floor and slope, which also contained deep-sea oozes. Ages of dredged samples range from Late Cretaceous to Early Miocene based on nannofossil assemblages and Early Cretaceous to Early Miocene based on foraminiferal assemblages (Marshall *et al.*, 1989).

Limestones recovered from BMR Surveys 80/81 are relatively similar. Colour varies from white to medium grey. Glauconite is present in some samples. Limestones are bioclastic calcilutites or calcarenites, and common skeletal components include foraminifera, nannofossils, sponges, radiolarian, diatoms, echinoids and bryozoans. Minor clay minerals and trace fine to medium size quartz grains are present. For all limestones an outer shelf to upper slope environment is suggested based on the presence of mature glauconite pellets, minor terrigenous material and relatively fine-grained skeletal material. Sandstones

recovered are medium to coarse grained, quartzose sandstones, finely laminated silty sandstones, some showing cross-bedding. Shales recovered are dark brown or grey and finely laminated. Some consisted of alternating light and dark layers. Mudstones recovered are soft, fissile, dark grey to pale brown to black in colour. Some are finely laminated and others more massive.

Even though it cuts the outer shelf, there is no observable channel connecting the Perth Canyon to the present coast, even though it probably was connected to the Swan River during sea-level lowstands (Fig. 1.1; Marshall *et al.*, 1989). This is in contrast to many submarine canyons around the continental margin of Australia, that are normally located at or directly below the shelf break, and have not incised the shelf (Von der Borch, 1968; Davies, 1973; Gingele *et al.*, 2004; Hill *et al.*, 2005).

Existing bathymetry data indicates that to the north and south of the Perth Canyon, the southwest Australian margin is extensively cut by a series of “blind” submarine canyons on the slope. These canyons are much smaller and do not cut the shelf. These ‘blind’ canyons initiate in water depths of between 1,500 and 2,500 m and serve as nice comparisons to the well-developed shelf-intruding Perth Canyon. These canyons have been poorly-mapped and poorly-studied.

‘Blind’ submarine canyons do not intercept terrigenous or shelf sediments and are thus likely to be similar to the neighbouring slope and contain relatively less terrigenous sediment, less direct evidence of active sedimentary processes, and presumably less diverse and abundant benthic biota compared to the Perth Canyon.

1.2.2. Shelf Geomorphology and Sedimentology

East of the submarine canyons, the Rottnest Shelf is a 45-100 km wide, relatively low-gradient shelf (Carrigy & Fairbridge, 1954; Playford *et al.*, 1976; Collins, 1998). Rottnest Shelf sediments have a distinct shelf-parallel zonation (Collins, 1988). An offshore ridge system, located between 50-60 m water depth separates a broad inner shelf plain (0-60 m) and a narrow, steeper outer shelf ramp (100-170 m), which terminates at the shelf break. Between 0-20 m ridges, reefs, depressions and topographic highs occur.

Rivers that empty onto the Rottnest Shelf deliver little sediment to the coast by world standards. As such, shelf sediments are mainly biogenic sands and sandy-gravels, with very little organic matter accumulation. River-derived sediment is principally trapped in estuaries and the coastal plain and terrigenous sediment is a minor component of the shelf seabed. Shelf sediments are mostly composed of calcareous algae and the skeletal remains of foraminifers, bryozoans, molluscs, with minor amounts of chemical precipitation (i.e., ooids; Harris *et al.*, 1991).

Two sediment facies comprise the southern Rottnest Shelf in the vicinity of the Perth Canyon and other blind canyons (Collins, 1988), as follows:

1. *Fremantle Blanket* which forms a discontinuous, thin (0-0.5 m) and mobile sediment blanket composed of coarse to medium calcareous sand in water depths of 20-90 m. The sand comprises quartz grains and the skeletal remains of bryozoans, foraminifers and molluscs with relatively small amounts of lithic material; and
2. *Rottnest Blanket* which forms a thin (0.5-1.0 m) sediment layer below 90 m water depth across the outer shelf and upper slope. Sediments are moderate- to poorly-sorted fine to medium calcareous sand, fining seawards. The sediment is composed of mainly skeletal remains of bryozoans, foraminifers, echinoderms and molluscs, with a small amount of

lithic material. Below 170 m, the concentrations of calcareous mud increases and the occurrence of bryozoans decrease considerably (Collins, 1988).

Comet marks and linear, low-amplitude ridges found on the seabed below 150m water depth, indicate that shelf currents are principally uni-directional to this water depth, inferring a reduction in the influence of tidal currents on the shelf. The dominant shelf current on the southwest margin is the south-flowing Leeuwin Current. This predominant current is probably responsible for the uni-directional features present on the shelf (Collins, 1988).

1.2.3. Oceanography

The Rottnest Shelf and adjacent slope environment is effected by the Leeuwin Current and by S-SE swell waves generated in the Southern Ocean (Harris *et al.*, 1991). The south-flowing Leeuwin Current brings relatively warm, low-salinity, nutrient-poor water from the tropics to the southwest margin (Creswell & Golding, 1980). The current is shallow (<300 m water depth) and narrow (<100 km wide) and is located over the upper slope. The current flows southward along the coast of Western Australia, against the prevailing wind and wave directions, and is strongest in autumn and winter (Creswell & Golding, 1980; Creswell, 1991; Pattiaratchi & Buchan, 1991). Due to the shallow depth of the Leeuwin Current, it only interacts with the Perth Canyon near its head. The current impedes up-welling in the region, resulting in nutrient-poor waters and low-productivity on the adjacent shelf regions (Thompson, 1984; Godfrey & Ridgeway, 1985; James *et al.*, 1999).

Below 300 m water depth, adjacent to the slope, the Leeuwin Undercurrent flows north towards the equator (Smith *et al.*, 1991). This undercurrent interacts strongly with the Perth Canyon (and presumably other canyons), generating eddies and up-welling (Rennie, 2006). Up-welling in the canyon and along the canyon rims driven by this current and also by storm activity induces significant mixing of deep- and shallow-ocean water. Despite this, up-welling of this deeper water does not reach the surface due to the presence of the Leeuwin Current (Rennie, 2006).

Inshore of the Leeuwin Current, the cooler, higher-salinity, wind-driven Capes Current flows along the coast in a northerly direction between Cape Leeuwin and Shark Bay during summer (Cresswell & Peterson, 1993; Pearce & Pattiaratchi, 1999). Up-welling caused by eddies associated with this current allows nutrients into the surface waters and can result in large-scale phytoplankton blooms (Webb and Morris, 1984). However, terrigenous and coastal sediments and associated organic matter are advected along the coast with very little being transported across the shelf to the canyons.

Sediment mobility due to storm and normal swell waves is related to water depth such that in depths of less than 50 m medium to coarse sand is mobile 50% of the time (Harris *et al.*, 1991). On the outer shelf, fine sand to silt and clay of the outer shelf and upper slope are occasionally to infrequently reworked (Collins, 1988). Sediment mobility, to a lesser degree, is also influenced by the Leeuwin current and tidally induced currents (Harris *et al.*, 1991).

1.2.4. Regional Geology

The SW margin of Australia is a geologically complex region comprising the Vlaming Sub-basin (of the southern Perth Basin) and the Mentelle Basin (Fig. 1.2). The Mentelle Basin is

separated from the Vlaming Sub-basin by a large basement high comprising the Yallingup and Vasse Shelves.

1.2.4.1. Vlaming Sub-basin

The Vlaming Sub-basin is a deep (<15 km), elongate, N-S trending depocentre that extends across the shelf and slope in water depths ranging from 0 to 3,000 m (Fig. 1.2). The main part of the Vlaming Sub-basin contains a very thick (<8 km) Middle Jurassic–Lower Cretaceous syn-rift succession, which is overlain by up to 2 km of Lower Cretaceous–Cainozoic post-breakup succession (Backhouse, 1978; Seggie, 1990). No wells in the Vlaming Sub-basin have penetrated below Middle Jurassic strata. However, it has been estimated that up to 5 km of older Permian–Lower Jurassic strata may be present (Seggie, 1990).

Comprehensive descriptions of the stratigraphy for the Vlaming Sub-basin are provided in Marshall *et al.* (1993) and Crostella & Backhouse (2000). A summary of the stratigraphy for the southern Perth Basin is illustrated in Figure 1.3. The oldest unit penetrated in the Vlaming Sub-basin is the Upper Jurassic Yarragadee Formation comprising a feldspathic sandstone succession deposited by a northward flowing fluvial system (Marshall *et al.*, 1993; Crostella & Backhouse, 2000; Norvick, 2003). Syn-rift sedimentation continued into the Berriasian–Valanginian with fluvio-deltaic and lacustrine facies of the Parmelia Group (Crostella & Backhouse, 2000). Faulting prior to and during the breakup produced a half-graben style of basin architecture (Fig. 1.4) with predominantly north, north-northeast and north-northwest oriented bounding faults. Throughout the rifting history the basin developed in a transtensional setting with northwest-southeast trending strike-slip faults accommodating north-south component of the movement. This tectonic setting resulted in complex structuring with multiple stages of fault reactivation, reverse faulting, formation of anticlinal rollovers (Fig. 1.4) and crestal collapse systems.

Continental breakup in the Valanginian was associated with extensive uplift and erosion throughout the Perth Basin, and was followed by a post-breakup period of high subsidence in the Valanginian–Aptian. This post-breakup period in the Vlaming Sub-basin was associated with the deposition of a 1.5 km thick complex assemblage of fluvio-deltaic, shelfal and submarine fan deposits from the Warnbro Group that unconformably overlie deformed and eroded strata from the Parmelia Group (Spring & Newell, 1993; Crostella & Backhouse, 2000; Norvick, 2003). Early post-breakup deposits from the Warnbro Group are overlain by a relatively thin succession (generally <1.0 km thick) of passive margin siliciclastics and carbonates from the Lower–Upper Cretaceous Coolyena Group and younger Cainozoic units.

1.2.4.2. Mentelle Basin

The Mentelle Basin is a large sedimentary basin lying beneath the Naturaliste Trough and the Yallingup Shelf in water depths of 500 to 3,500 m (Fig. 1.2). The basin has never been drilled or sampled and its stratigraphy has been deduced from the nearby Vlaming Sub-basin and DSDP wells on the adjacent Naturaliste Plateau. The Mentelle Basin comprises two parts (Fig. 1.5): the western depocentre (17,400 km²) beneath the Naturaliste Trough containing at least 5 km of sediments, and the shallow eastern part (19,000 km²) with a series of small rift basins which may represent a faulted hinge zone of the original depocentre (Bradshaw *et al.*, 2003).

The Mentelle Basin stratigraphy has been deduced from petroleum exploration wells in the southern Vlaming Sub-basin and DSDP sites 258 and 264 on the Naturaliste Plateau (Borissova, 2002). Both DSDP wells penetrated only the Latest Early Cretaceous to recent section. The oldest sediments recovered were mid-Albian to Cenomanian ferruginous detrital clays at Site 258 and Cenomanian or older volcanoclastic conglomerates at site 264 (Hayes *et al.*, 1975). The presence of at least 4 km of section in the Mentelle Basin beneath the inferred Albian sediments suggests that it is likely to be pre-Valanginian syn-rift succession similar to that of the Vlaming Sub-basin (Fig. 1.5).

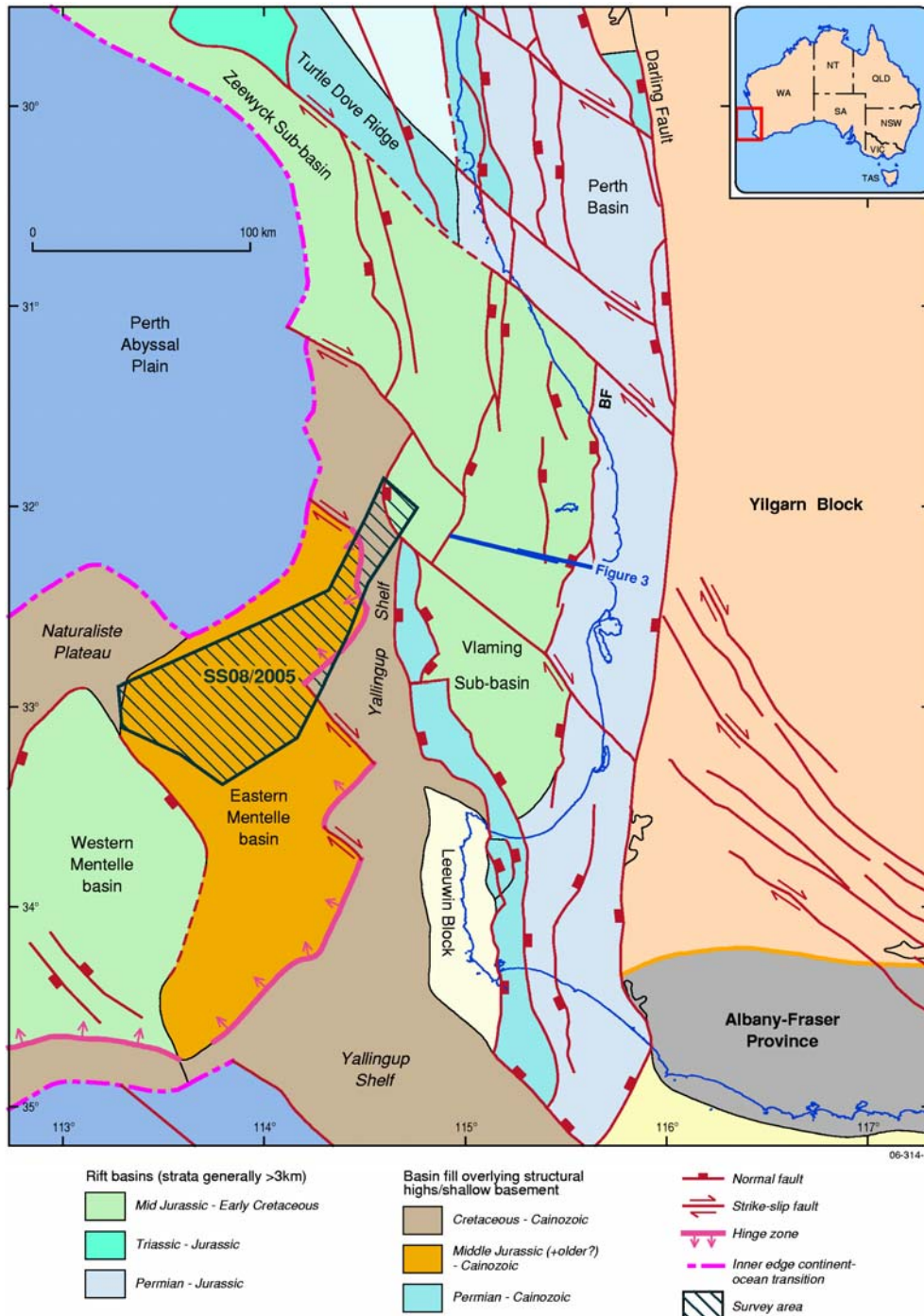


Figure 1.2. Survey area (black hatched polygon) in respect to major structural sub-divisions of the southern Perth and Mentelle Basins (from Bradshaw *et al.*, 2003). Location of the cross-section presented in Fig. 1.3 is shown by the blue line.

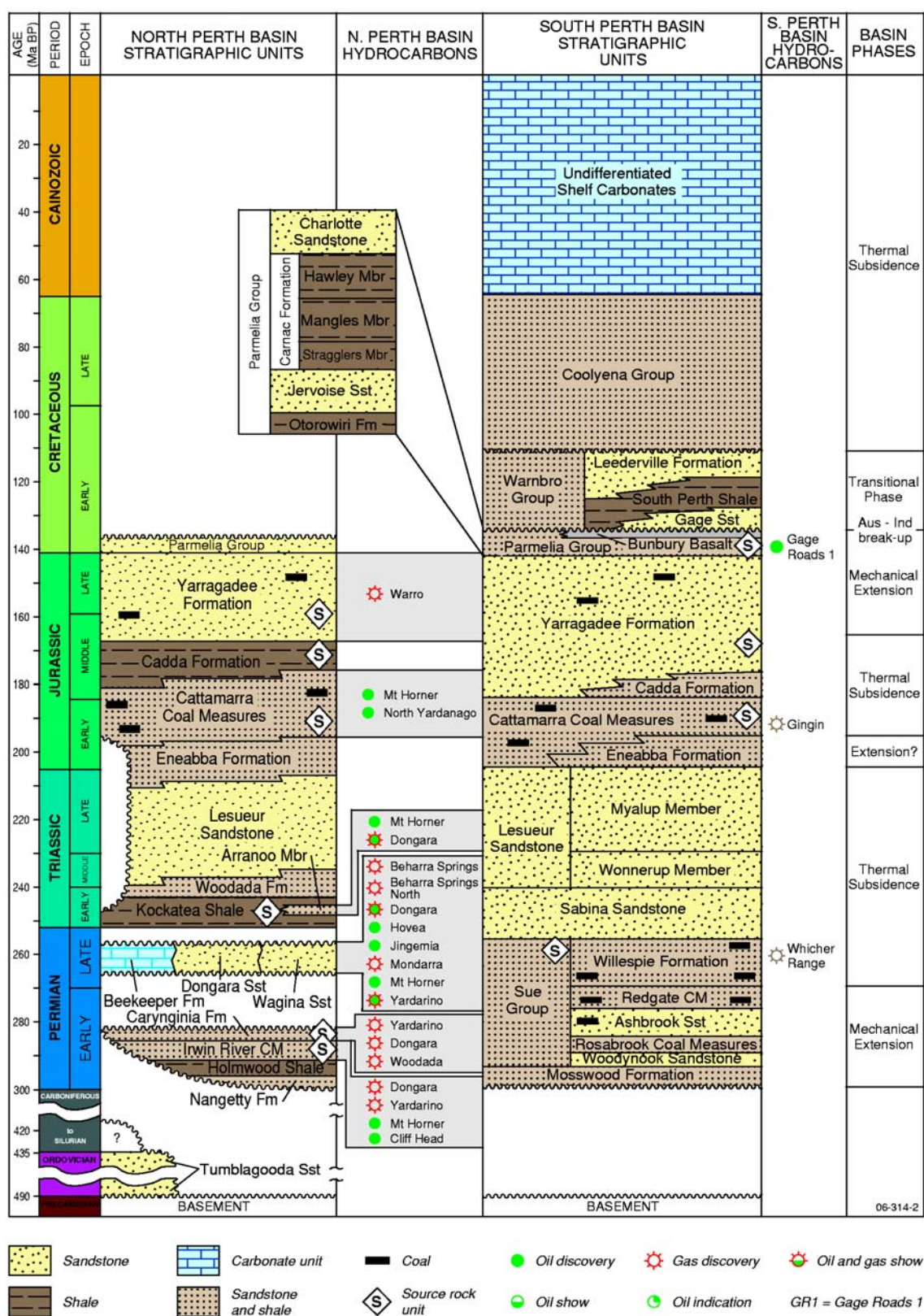


Figure 1.3. Stratigraphy, petroleum systems and basins events for the Vlaming Sub-basin (southern Perth Basin).

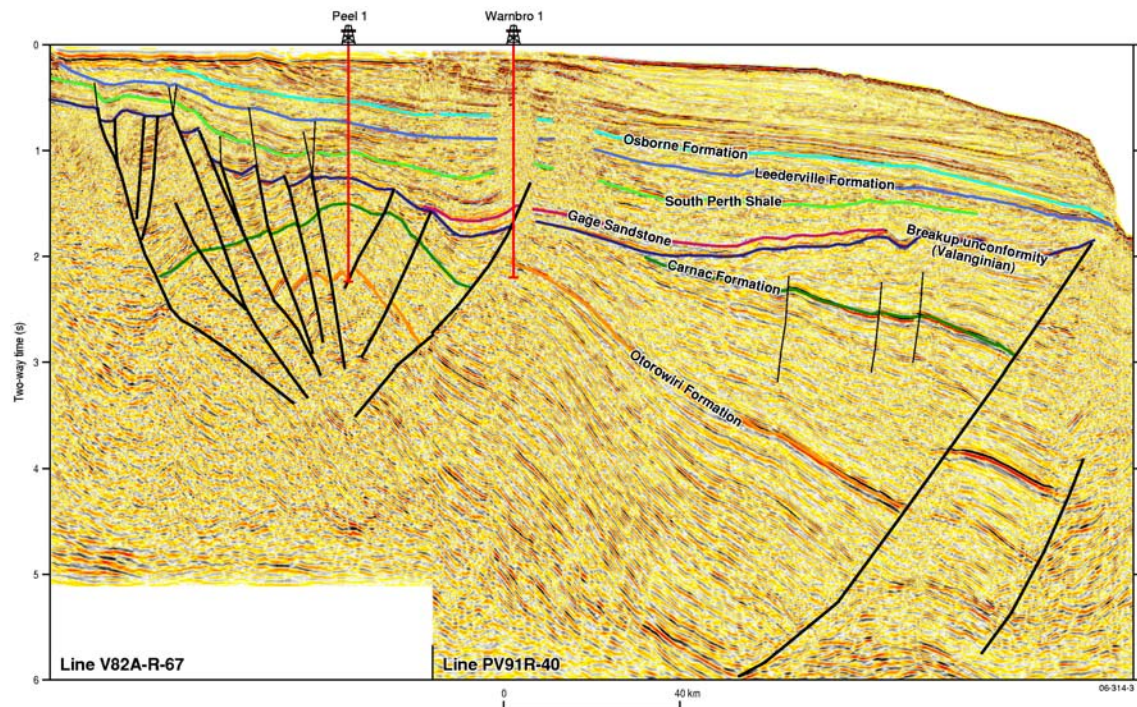


Figure 1.4. Representative cross-section from the northern Vlaming Sub-basin, showing major seismostratigraphic units (from DITR, 2005).

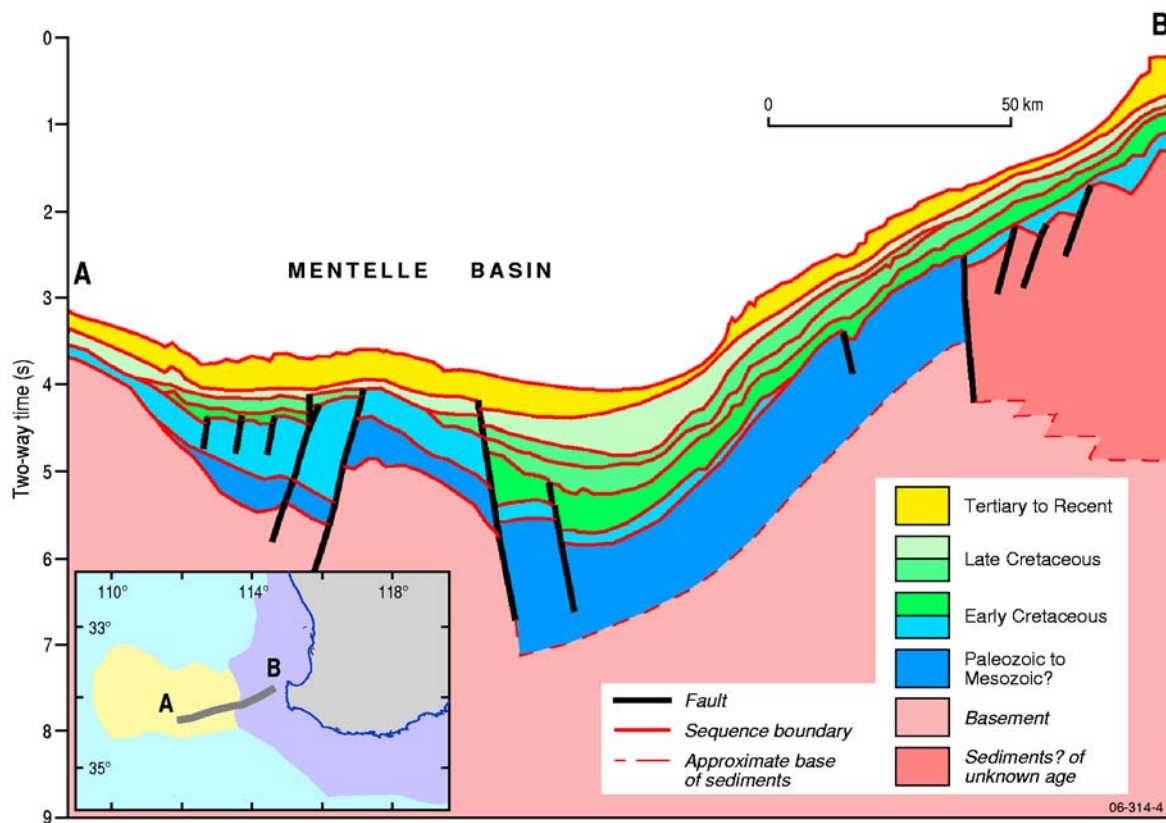


Figure 1.5. Interpreted geological cross-section of the Mentelle Basin (modified from Borissova, 2002).

1.3. SURVEY OBJECTIVES

This survey represented a valuable opportunity to sample key seabed environments and benthic biota together in two fundamentally different types of submarine canyons. For the first time, deep-sea seabed environments and associated processes and benthic biota were compared and contrasted in a large well-developed shelf-intruding canyon (i.e., Perth Canyon) versus several blind canyons. In addition, key data was also collected on the outer shelf and upper and lower slope of the SW Australian margin. Concentrating on deep-sea sampling at depths greater than 1,000 m water depth this survey increased the relatively low sample density of deep-sea samples compared to upper slope and shelf samples (Fig. 1.6). A further objective of the survey was to assess the petroleum potential of the Mentelle Basin.

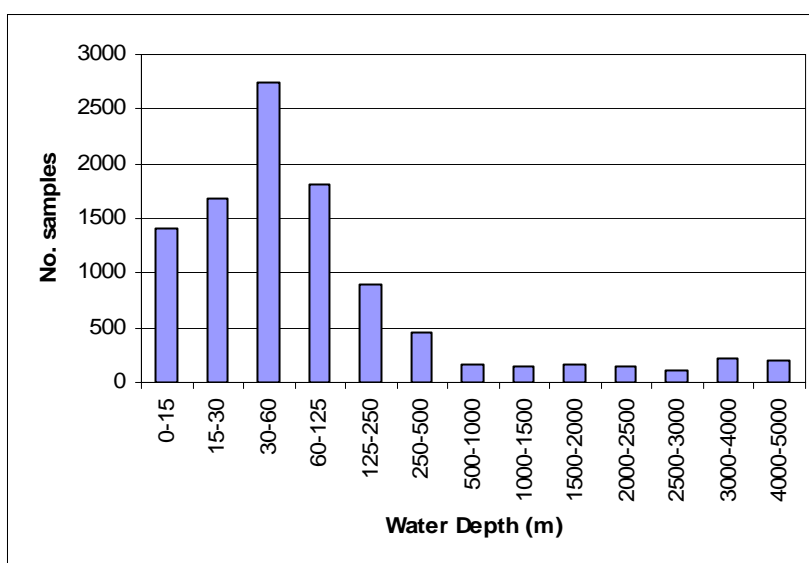


Figure 1.6. Graph of total samples versus water depth within the Australian Exclusive Economic Zone (EEZ). Note the higher abundance of samples from water depths less than 1000 m. (Source: Marine Samples Database (MARS), Geoscience Australia).

The principal scientific objectives of this marine survey (GA Survey SS08/2005) were to:

4. develop an understanding of deep-water sedimentary processes and benthic biota and habitats in “blind” submarine canyons on the SW Australian margin;
5. document the geological and biological transitions between shelf, slope and offshore platform seabed environments; and
6. investigate the stratigraphy and geology of the Mentelle Basin and assess its implications for petroleum potential.

The seabed of the slope environments separating the submarine canyons is relatively deep and flat. Sediments and associated benthic marine biota on the relatively flat regions of the slope will also be a target for the survey in comparison to those of the rugged submarine canyons. Targeting these regions will provide key data on the seabed and benthic biota for deep-water slope environments. Establishing the rock succession in the Mentelle Basin by targeting the blind canyons will permit an assessment of its petroleum potential. The survey leader’s log is detailed in [Appendix A](#).

1.4. SURVEY PARTICIPANTS

The vessel used for the survey was Australia's national facility research vessel *Southern Surveyor* (Fig. 1.7). The RV *Southern Surveyor* is 66 m long, with accommodation for 13 scientists.



Figure 1.7. Australia's national facility research vessel *Southern Surveyor* which was used in this survey.

1.4.1. Scientific Personnel

The multi-disciplinary nature of the research required the efforts of a group of scientists with a wide variety of complementary skills to make it successful. The survey personnel, representing organisation, and their substantive roles are listed in Table 1.1.

Table 1.1. Scientific survey personnel, representing organisation, and their substantive roles.

Name	Organisation	Role
Andrew Heap	Geoscience Australia	Chief Scientist
Jane Blevin	Geoscience Australia	Scientist/watch leader
Irina Borissova	Geoscience Australia	Scientist/GIS/Database
Emma Mathews	Geoscience Australia	Scientist/Database
Michele Spinoccia	Geoscience Australia	Swath processor
Cameron Mitchell	Geoscience Australia	Swath processor/GIS
Ian Atkinson	Geoscience Australia	Electronics Technician
Franz Villagran	Geoscience Australia	Electronics Technician
Colin Tindall	Geoscience Australia	Geological Technician
Petar Vujovic	Geoscience Australia	Geological Technician
Craig Wintle	Geoscience Australia	Mechanical Technician
Karen Gowlett-Holmes	CSIRO	Biologist
Julian Finn	Victoria Museum	Biologist
Drew Mills	CSIRO	Electronics (Voyage Manager)
Hiski Kippo	CSIRO	Computer support

1.4.2. Ship's Crew

In addition to the scientific crew, the ship's crew provided tireless support throughout the survey. The ship crew and their substantive roles are listed in Table 1.2.

Table 1.2. Ship's crew and their substantive roles.

Name	Role
Les Morrow	Master
Arthur Staron	First Mate
Brent Middleton	Second Mate
Roger Thomas	Chief Engineer
John Elfstrom	1st Engineer
Chris Heap	2nd Engineer
Tony Van Rooy	Boatswain
Russell Williams	Integrated Rating
Les Webster	Integrated Rating
Marcus Gaffney	Integrated Rating
Phil French	Integrated Rating
Andy Goss	Chief Cook
Kevin Shenahan	2nd Cook
Charmayne Aylett	Chief Steward

2. Geophysics

A comprehensive geophysical survey was conducted to determine the seabed morphology and composition of the seabed features. The survey consisted of high-resolution multi-beam sonar and shallow seismic data. In addition, side scan sonar data were collected on the outer and mid Rottneest Shelf. The geophysical survey was used to design the sampling program.

2.1. DATA ACQUISITION

2.1.1. Multi-beam (Swath) Sonar

The Simrad EM300 on the R/V *Southern Surveyor* is a 30 kHz multi-beam sonar system comprising 135 beams each covering a 1° arc. The performance of the multi-beam system during the survey was excellent based on the coverage achieved and quality of the data acquired. The survey was generally laid out in a NE-SW direction with line spacing designed to give maximum overall coverage. Gaps were left between some lines to obtain a regional assessment of seabed habitats.

During the survey, the sea state ranged from rippled to rough, with regular swells of between 1 m and 6.5 m. Wind speeds were between 7.7 m s⁻¹ and 20.6 m s⁻¹ from S and SW. Data was collected at a vessel speed of between 6 and 10 knots; higher speeds of up to 8 knots were achieved when the vessel was travelling with the swell (i.e., towards the NE). During the survey, tidal currents were faster toward the south. Generally, noise in the data was most noticeable at water depths between 100 m and 150 m. However, this was also greatly affected by the sea state.

Sound velocity profiles (SVP) were obtained to account for changes in the speed of sound in the water column due to changes in temperature and salinity. SVP's on the transits to and from the survey area were generated using the SVP Builder utility on board the ship. This method uses global climatology data to derive an SVP for a given set of coordinates. This method proved effective at generating accurate SVP's during deep water transits.

In addition, a total of 8 CTD (conductivity/temperature/depth) casts were undertaken throughout the study area. The CTD data were used to generate accurate SVP's for the study region that complimented those generated from the global climatology data. The spatial coverage of the CTD casts provided excellent results. The data were used to calculate the absorption co-efficient, which was used to improve the backscatter returns by correcting the transducer gains for changes to the speed of sound through the water column as a result of changes in salinity and temperature.

2.1.2. Shallow Seismic Reflection

The R/V *Southern Surveyor*'s hull-mounted Topas PS 18 parametric sub-bottom profiler was used to record the acoustic response of surface and shallow sub-bottom sediments during the survey. The Topas PS 18 system is a narrow beam, high resolution and full ocean depth sub-bottom profiler. The system is capable of substrate penetration of greater than 150 m in water depths of 1,000 m and a range resolution of 0.30 m. In practice, sub-bottom penetration was dependent on sediment character, water depth and the transmitted signature. Penetration of up to 100 ms (~75 m) was attained during this survey, for the thick sediments on the outer shelf and mid slope.

The Topas sub-bottom profiler has two main waveforms that can be used to achieve maximum sub-bottom penetration and bottom tracking for different water depths and for different sediment types and/or variable terrain. In shallow water (<600 m), the Ricker pulse was used, and sub-bottom penetration was well maintained. In deeper water, the linear Chirp pulse, which is a linearly swept frequency over time, was used to achieve sub-bottom penetration. Full details of each waveform can be found in the Topas user documentation.

Data from the Topas PS 18 sub-bottom profiler was filtered to remove boat-induced noise, and a time-varying gain, controlled by the automatic bottom tracker, was applied to the data before output in IEEE 32 bit Seg-Y format. The raw data was also output in proprietary Topas format. The sub-bottom profiler was operated in-conjunction with the multi-beam sonar system. The two systems were synchronised to minimise interference.

2.1.3. Side Scan Sonar

Geoscience Australia's EdgeTech 4200-FS towed side scan sonar system was used to record the acoustic response of the seabed during the survey. The side scan system was operated in high speed mode (HSM), using the low frequency band (120 kHz). The range setting was 200 to 250 m, providing a 2.5 m resolution along track, and around 10 cm resolution across track. A depressor was used during most deployments to minimise the length of cable required to tow the "fish" close to the seabed. Minimising cable length is important as the longer the cable, the more time it takes time to deploy and retrieve the fish. Long cables also inhibit ship manoeuvrability, requiring larger turn radii. Use of the side scan depressor during this survey however, only led to a 3–5 % reduction in cable length used.

2.2. DATA PROCESSING AND ANALYSIS

2.2.1. Multi-beam (Swath) Sonar

Minimal post processing of the raw data was undertaken due to the exceptionally good quality data acquired. The multi-beam data were processed using Caris HIPS/SIPS V5.4. Initially, a vessel configuration file was created that the co-ordinates of the motion sensor and DGPS antenna and patch test offsets were obtained. A new project for survey SS082005 was then created and the vessel configuration file was attached to the project file. The raw data was then acquired in the form of "raw.all" format for each line. The motion sensor, DGPS and heading data were then cleaned using a filter that averaged adjacent data to remove artefacts. The SVP's for each of the study regions were attached to the corresponding raw multi-beam sonar data files to correct the water depths. Then a new blank field area was defined that encompassed the geographic area of study and the co-ordinate system (WGS84) was specified.

Once loaded, the data were then cleaned by applying several filters that removed any remaining spikes using user defined threshold values. A visual inspection of the data for each line was then undertaken where artefacts and noisy data not removed by the filtering process were removed manually using the swath editor module of the Caris HIPS/SIPS software.

Parameters for the motion sensor, DGPS, ship's heading, tidal height, and sound velocity profile data were then merged with the raw depth data to produce the final processed data file. A weighted grid of the processed data was then created for each of the study regions. The processed data was finally exported as grid soundings or false coloured

images for presentation and reporting and as final processed data in GSF (Generic Sensor Format) format.

The acquired multi-beam bathymetry data is presented as a 35 m spatial-resolution grid. This resolution was chosen as it is close to the beam footprint (at nadir) for the average water depth of the survey area. A second, coarser grid of 175 m spatial-resolution was also created to cover “holes” in the data. These two grids were then super-imposed on top of Geoscience Australia’s 250 m spatial resolution bathymetry grid for regional context.

2.2.2. Shallow Seismic Reflection Data

The Seg-Y data from the Topas PS 18 were loaded into IESX, the seismic interpretation and evaluation module within the UNIX-based geoscience application GeoFrame™. The acoustic character of the data was interpreted using the classification scheme devised by Damuth (1974; 1980) in which the clarity, continuity and morphology of reflections are used to classify them into a number of distinctive echo-types.

Damuth (1980) identifies three main seabed echo-types: Type I—distinct; Type II—prolonged indistinct; and Type III—hyperbolic indistinct; each of which is further subdivided based on the presence or absence of sub-bottom reflectors, extent of prolongation, and the relationship of hyperbolae to the seafloor.

Horizons were defined for each type within IESX and the water-bottom digitised according to the interpreted acoustic facies. Poor data quality in regions of dramatic deep-sea morphology prevented interpretation of all lines across the entire study area.

Seabed horizons were exported as ASCII files that were then imported into ArcGIS together with the multi-beam bathymetry so that the distribution of acoustic facies and the relationship of these with seafloor geomorphology could be analysed.

2.2.3. Side Scan Sonar Data

At the time of writing the side scan data has not been processed. The side scan data was replayed in the acquisition software and a number of screen captures were taken.

2.3. RESULTS

In total, the geophysical survey resulted in 6,480 km² of multi-beam sonar data, 3,280 line-km of shallow sub-bottom profiler data (Fig. 2.1), and 250 line-km of dual frequency side-scan sonar data. Figure 2.1 is a composite image of swath data from several surveys carried out between 1988 and 2005, including this survey. This survey’s swath (multi-beam) sonar and sub-bottom profiler lines highlight the extent of coverage from this survey (Fig. 2.1). The geophysical survey completed swath coverage of the Perth Canyon and covered a completely new area of the slope of the SW Australian margin. Features that were revealed by the geophysical survey include: the true extents of the “blind” submarine canyons in SW Australia, including one previously unknown canyon; a previously unknown 75 km² slump block at the head of Geographe Canyon; and numerous tributary canyons on the mid-slope.

2.3.1 Multi-beam (Swath) Sonar

A total of 3,230 line-km of multi-beam data were acquired during the survey, comprising two study areas; the Perth Canyon region and Mentelle Basin region (Fig. 2.1).

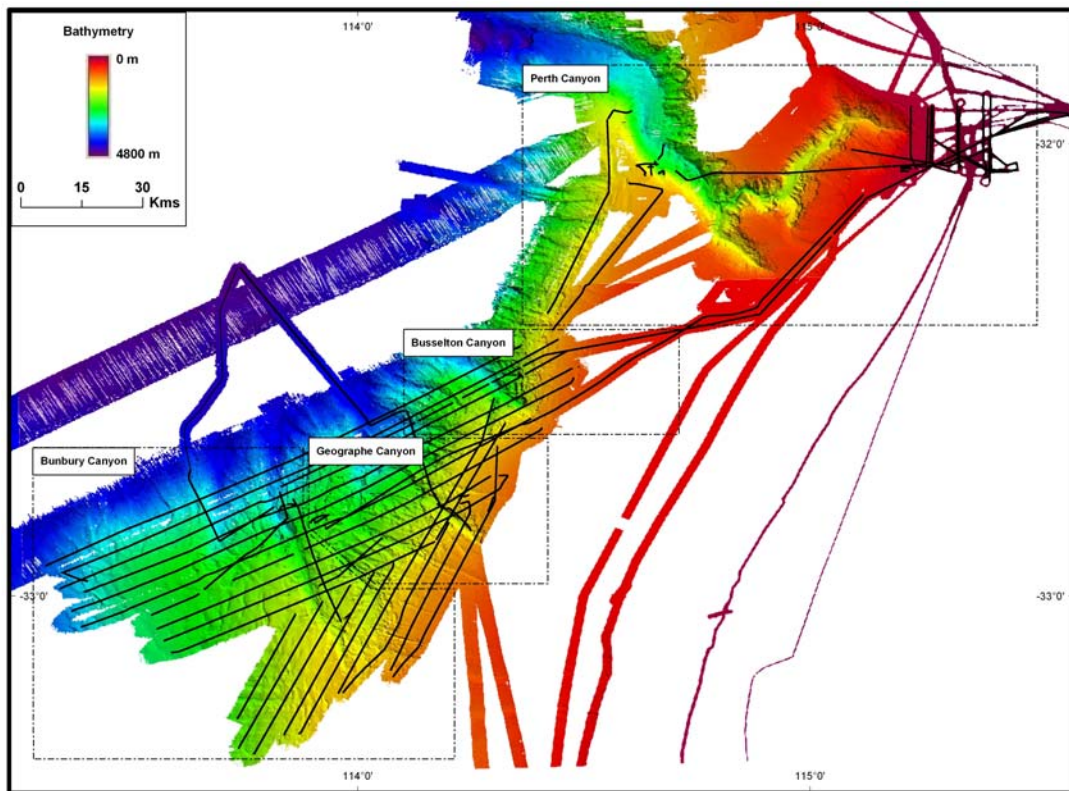


Figure 2.1. Map showing the location of multi-beam (swath) sonar and Topas sub-bottom profiler lines acquired during the survey. Boxes indicate areas described in the text.

A total of 278 line-km were collected in the Perth Canyon region and 2,354 line-km in the Mentelle Basin region. A total of 246 line-km were collected on the outer and mid Rottneest Shelf and 352 line-km were collected on transit lines between the study areas and Fremantle. The total area of the seabed covered in the survey was >6,480 km².

Water depths for the survey ranged from 11 m to >4,500 m. Shallowest depths were recorded in Fremantle Harbour, and water depths on the Rottneest Shelf were generally <150 m. In the Perth Canyon region, water depths ranged from 44 m on the shelf east of the canyon head to 1,160 m on the canyon flank. In the Mentelle Basin region, water depths ranged from 840 m on the upper slope to >4,500 m on the Perth Abyssal Plain.

Data coverage was variable throughout the survey due to rapid changes in water depth, particularly in the Mentelle Basin region. In the Perth Canyon region, data coverage ranged from between ~3.9x the water depth in water depths of 600 m and provided a maximum swath width of 2,345 m. In deeper water, the swath width is much narrower as the beams are steered closer to the vertical to ensure a strong enough signal is received. A maximum swath width of 1.3x the water depth or 3,000 m was attained in 2,300 m water depth from this area. In the Mentelle Basin region, maximum data coverage of 3x the water depth was obtained in 1,200 m water depth giving a swath width of 3,600 m. In water depths over >3,900 m, data coverage was only 0.6x the water depth, giving a swath width of 2,300 m in 3,900 m water depth.

2.3.1.1. Perth Canyon

The geophysical component of this survey completed swath coverage of the Perth Canyon (Fig. 2.2). The insert map in Fig. 2.2 shows the swath coverage of the Perth Canyon from this survey. The Perth Canyon has previously been described (Marshall *et al.*, 1988). However,

the complete swath coverage of the Perth Canyon presented below reveals many features previously not described. The Perth Canyon is broadly characterised by a steep walled and active upper canyon and a broad, deep and flat lower canyon. The slope of the canyon walls range from 10° to 30°. Localised areas of the canyon wall are steeper.

The main channel of the Perth Canyon forms close to the shelf break at around 170 m and the canyon axis trends to the west for ~11 km, then changes direction to the SW for ~45 km. Two secondary tributaries intersect the main channel at ~500 m and ~600 m. The main canyon axis then heads in a NW direction where the canyon becomes broad with a flat canyon floor. The main channel is very narrow (<100 m) near the canyon head and widens to 6-8 km in the lower canyon.

The main channel is surrounded by a broad, gently sloping fan (2° to 5°; Fig. 2.3). The fan is bound by a rim of steep walls. A series of stepped walls form down the slope of the fan into the main channel and indicate slumping of sediment. Several narrow feeder channels incise the fan directly adjacent to where the main channel forms. Sand waves are visible on the upper slope and shelf break adjacent to the canyon head and extend around the rim of the canyon to the south. These sand waves form in a north-west to north direction with a variable wavelength of 300-500 m near the canyon head increasing to 900-1,500 m to the south. Taken together these features indicate active sedimentary processes occurring at the canyon head with the down canyon transport of upper slope and shelf sediments.

Along the southern wall the gently sloping fan and short steep wall continues to rim the southern canyon wall, extending around a secondary tributary, which forms at ~500 m water depth. The fan around the tributary is 4.5-12 km wide with a slope of 2° to 5°. Slumping and narrow incising channels at the secondary tributary head indicate active sedimentary processes. A narrow and shallow feeder channel ~8.5 km long and ~1,400 m wide joins the upper slope to the tributary and may act as a pathway for the transport of shelf and upper slope sediments into the canyon. Along the eastern side of the tributary the lower slope of the fan ends abruptly with a series of stepped walls followed by a steep canyon wall.

The deeper secondary tributary, ~19 km long, trends to the NW. The NE wall of the tributary is steep and the NW wall relatively gentle sloping. A broad feeder channel 1-3 km wide joins the upper slope to the tributary and may also act as sediment transfer pathway. Slumping features rim the tributary. This tributary joins the main Perth Canyon channel at a point where the main channel becomes broad with a relatively flat floor.

Between the two secondary tributaries lies an interfluvial comprising of a large area of smooth gently sloping sea floor. To the N-NW of this interfluvial the main channel of the Perth Canyon narrows to 200-500 m wide and changes direction from SW to NW to SW over a distance of ~14 km. Both the north and south canyon walls are extremely steep. At the end of this narrow section the canyon axis trends to the NW then N for ~37 km. The canyon floor begins to broaden forming a relatively flat and smooth surface. The NE-E wall remains steep whilst gradient of the SW-W wall decreases. Steep walls rimming the NE-E wall and channels incising this wall are visible, possibly indicating transfer of slope sediments directly to the deep canyon floor. From ~3,000 m the canyon axis changes direction to the west for ~35 km at which point swath coverage ends at ~4,400 m depth. The canyon floor widens to 7.5-9 km. Canyon walls decrease in size as does their gradient.

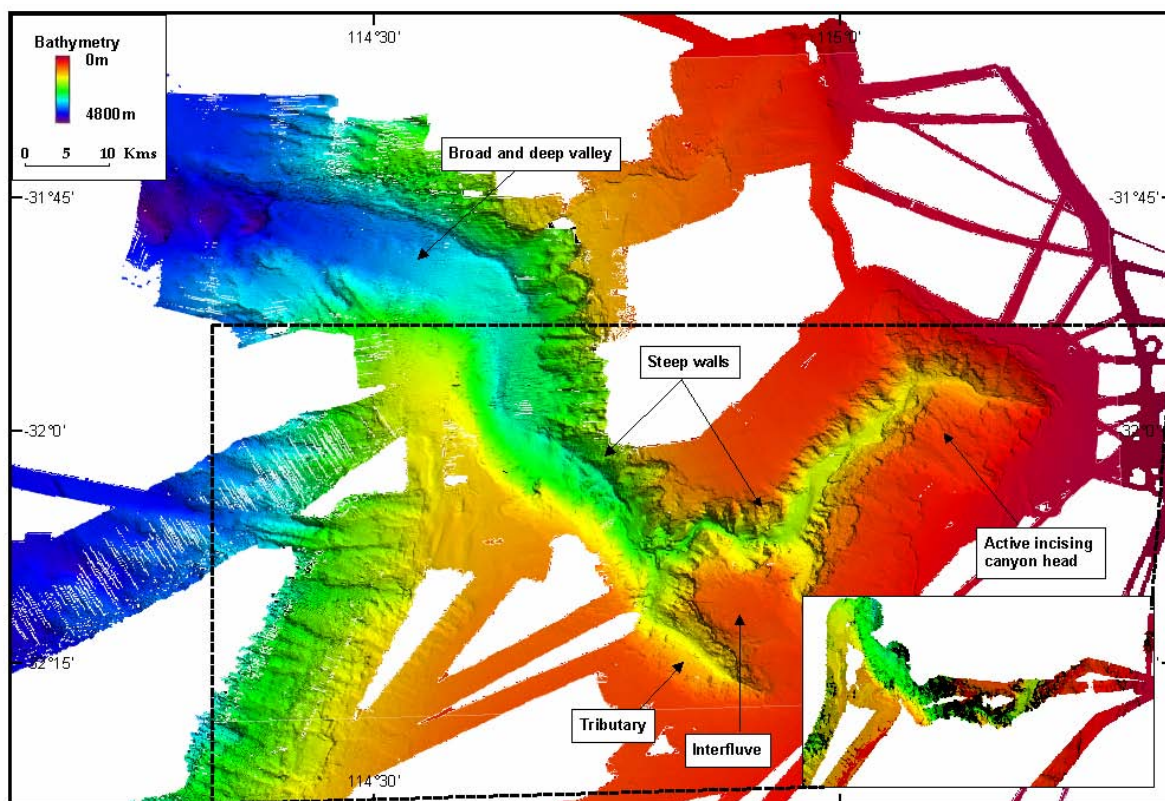


Figure 2.2. Multi-beam (swath) coverage of Perth Canyon. Inset map shows new swath coverage obtained from this survey.

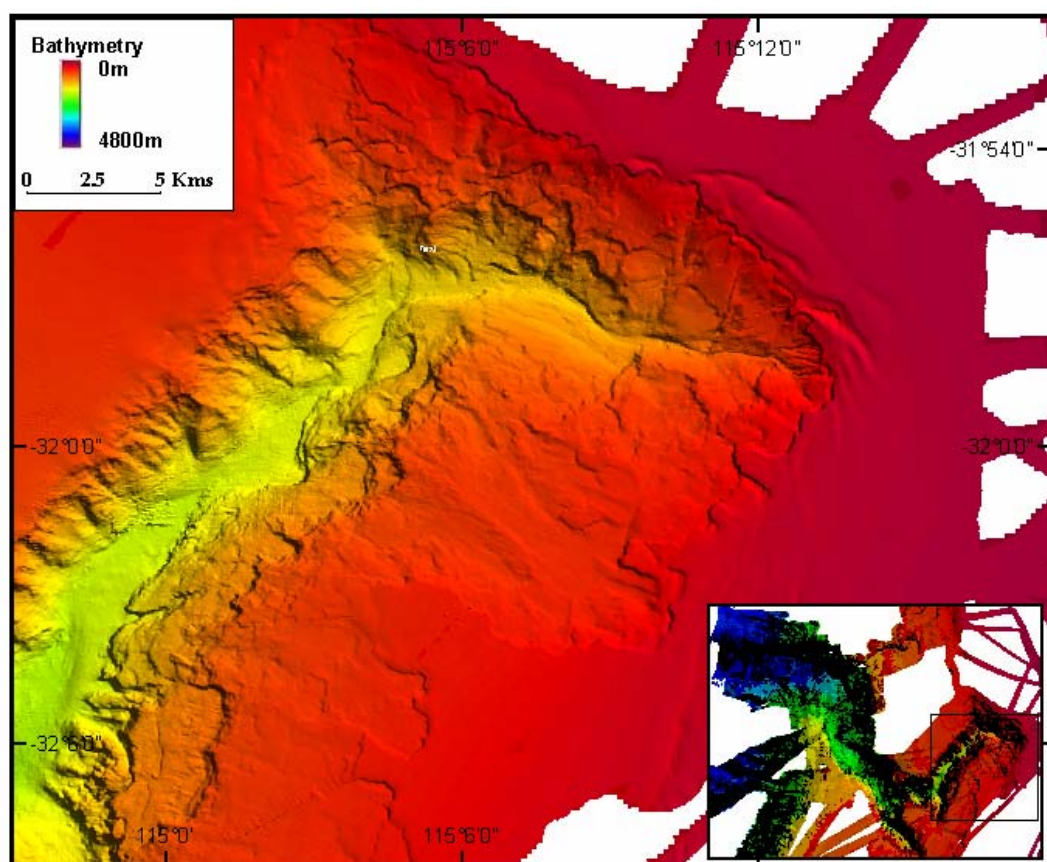


Figure 2.3. Head of Perth Canyon. Sand waves visible adjacent to the canyon head, narrow tributaries cutting the canyon head and series of steep walls indicate that the upper Perth Canyon is active with shelf sediments being transferred into the canyon.

2.3.1.2. Busselton Canyon

Busselton Canyon is the first submarine canyon found to the south of Perth Canyon (Fig. 2.4). It is a relatively straight, NW-trending, blind submarine canyon, about 25 km long, which dissects the slope at ~1,200 m. A gentle sloping (~8°) slump 3-4 km wide rims the canyon head. A series of stepped walls are visible down the fan and signs of active mass-movement including discrete slump deposits are displayed. The fan ends at 1,700 m where a 20° to 30° steep wall extends down to a water depth of 2,400 m. Steep walls with a gradient of 8° to 10° also extend to the north of the fan in a broad arc. Several steep, narrow channels incise these steep walls. Above the steep northern walls, a broad gentle sloping fan exhibiting active sedimentary flows extends for several kilometres to water depths around 1,200-1,400 m. In contrast to the northern wall the southern wall is gentle sloping and is not incised with channels.

Beyond the steep-sided head the canyon broadens considerably and the floor becomes relatively flat and slopes gently downwards at a ~3° gradient for 13 km to >3,000 m water depth. A shallow-incised tributary canyon to the south forms at 1,350 m and extends for ~17 km where it intersects the main canyon at ~2,500 m.

2.3.1.3. Geographe Canyon

Geographe Canyon is about 35 km long and dissects the slope at ~1,200 m (Fig. 2.4). Distinct from Busselton Canyon, which has a steep canyon head, Geographe Canyon initiates with a gentle sloping (1° to 2°) and narrow channel 15 km long. The northern wall is relatively steep (10° to 15°) compared to a gentle sloping southern wall. The gentle sloping channel terminates at ~1,950 m with a steep wall (15° to 20°) extending to 2,300 m. From this point a large gentle sloping (5°) slump block (75 km²) occurs. This slump block is up to 15 km long and 10 km wide. A steep wall almost entirely encircles the lower slump block boundary. In the SW corner of the slump block, at 2,700 m, a narrow and steep channel extends for several kilometres to a water depth of 3,500 m where it leads to a broad and flat canyon floor. This canyon floor joins with several steep narrow channels incising the slope to the NE of the slump block.

2.3.1.4. Bunbury Canyon

Bunbury Canyon is a newly discovered canyon about 55 km long that dissects the slope at 1,350 m (Fig. 2.4). Similar to Geographe Canyon, Bunbury Canyon initiates with a gentle sloping (~2°) narrow and long (35 km) channel extending from a water depth of 1,450 m to 2,475 m. The NE wall is relatively steep (8° to 10°) compared to the SW wall. At 2,475 m the narrow channel terminates leading to a steep sloping headwall (8° to 10°) which extends to 2,800 m. Again the NE wall is steeper than the SW wall. From the bottom of the headwall a broad, flat and gentle sloping (1° to 3°) canyon floor with a steep-sided NE wall extends to a water depth of ~3,600 m where the canyon ends in a broad flat plain.

2.3.1.5. Slope and Shelf

Swath coverage of the shelf is restricted to around the Perth Canyon head and reveals a smooth sea floor surface. Towards the Perth Canyon head sand waves are visible as described in 2.3.1.1 (Fig. 2.3).

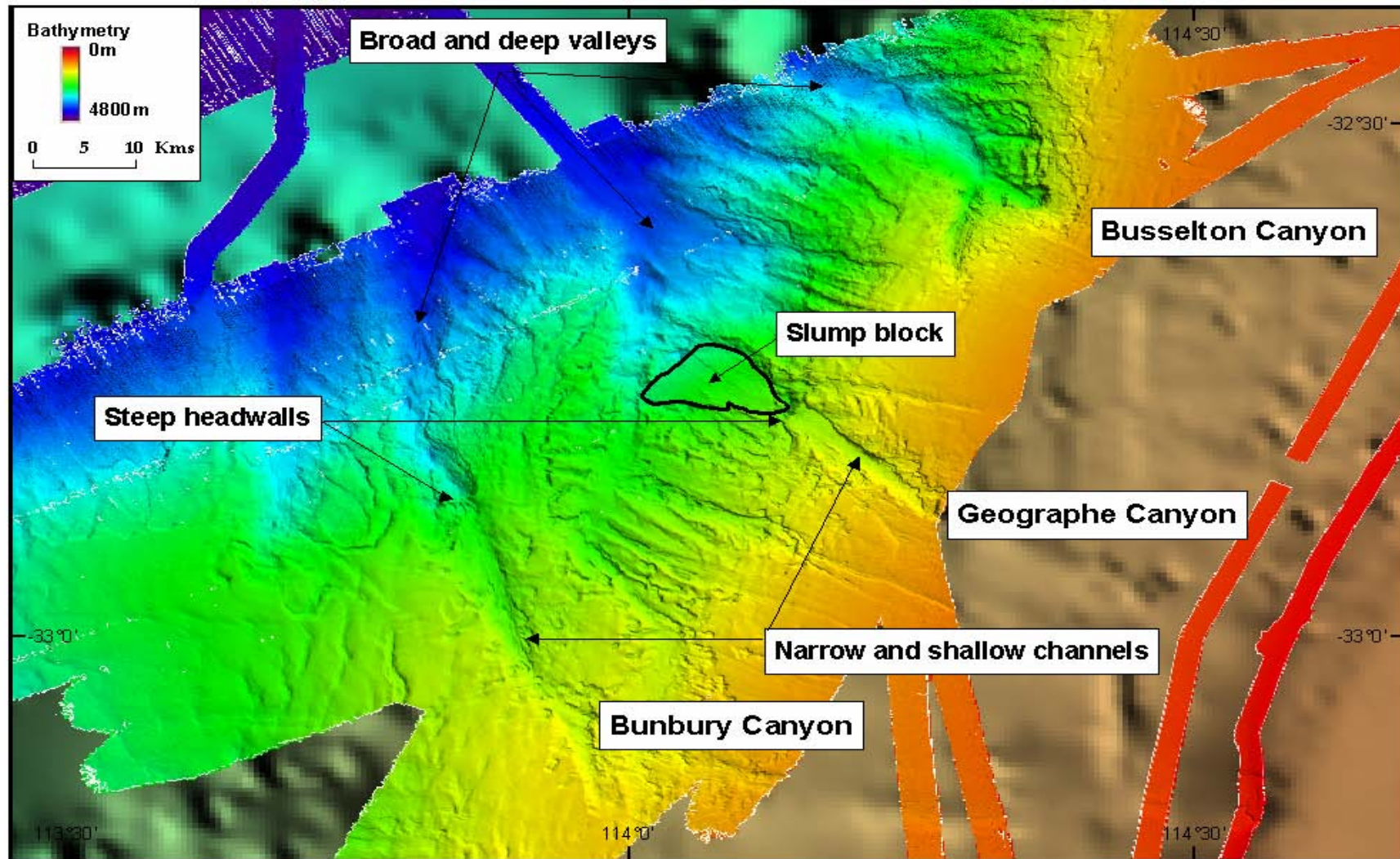


Figure 2.4. Multi-beam (swath) bathymetry image from this survey showing Busselton and Geographe Canyons and the newly discovered Bunbury Canyon.

The slope can be divided into an upper and lower slope based on changes in morphology and slope of the sea floor (Figs. 2.2 & 2.4). The gentle sloping smooth surfaced upper slope lies between 170 m and 1,100-1,500 m and the steeper, rugged and incised lower slope lies between 1,100-1,500 m to ~4,000 m.

The gentle sloping (1-2°) smooth upper slope has localised regions of small depressions and knolls. Progressing towards the lower slope the smooth sea floor becomes increasingly disturbed. Between Perth and Busselton Canyon at 1,000-1,300 m depth the smooth upper slope increases in gradient to ~3° and is disturbed by slumping and small channels indicating down slope movement of sediments. Below this depth small cliff lines are visible and a series of channels trending east dissect the lower slope, which steepens to >5°. The channel closest to Perth Canyon is ~20 km long. Swath coverage of the channels to the south is not complete.

Between Geographe and Bunbury Canyons the smooth upper slope is dissected by several straight, narrow, and shallow WNW-trending channels, 8-14 km long. These tributaries feed into a number of channels, 10-20 km long, which dissect the lower slope at the same bearing. The series of channels feed into one large broad north trending channel, ~12 km long, which connects to the lower Geographe Canyon at ~2,700 m depth.

2.3.2. Shallow Seismic Reflection

A total of 3,280 line-km of digital shallow seismic reflection data (8 GB) was acquired during the survey (Fig. 2.1); the most comprehensive shallow seismic dataset ever collected for the SW margin. Screen captures of select shallow seismic reflection profiles are contained in Appendix B. Rough seas as described earlier, combined with rapid and dramatic changes in seabed morphology, and water depths of up to 4,500 m, resulted in variable data quality. Across the steep-sided canyons and deeper abyssal areas, data quality is typically poor. However, high resolution and significant sub-bottom penetration was attained in shallower areas on the shelf and slope, and in deeper regions with less variable seabed morphology. Penetration of sub-bottom sediments was generally good, ranging from 10 (~7.5 m) to 100 ms (~75 m). Sediment thickness and sub-surface architecture of the study area is revealed, including rocky substrates in the narrow, steep-sided tributary canyons and extensive sedimented areas containing sediment drapes on the slope. Slumping around the head of the Perth canyon, and the large slump block at the foot of the Geographe Canyon are also observed in the data.

2.3.2.1. Perth Canyon

In the vicinity of the Perth Canyon, one transect crossed the canyon at two locations. Several lines to the east of the main canyon head reveal the nature of the nearby shelf, and lines to the south and west identify the character of the upper and mid slope in this region (Fig. 2.1).

Data on the shelf show a high amplitude reflector (up to 2 ms) that traces a flat to subtly inclined smooth surface, with intermittent irregular, rugged prominences with reduced amplitude. This upper reflector is interpreted to be the present seabed as it is the first distinct reflector beneath the sea surface. Very few sub-bottom reflectors are evident on the shelf in this region. The morphology of the rugged prominences and minimal sub-bottom penetration beneath the features indicates these are probably rocky reef outcrops, which are observed in the data to a water depth of around 80 m (~110 ms).

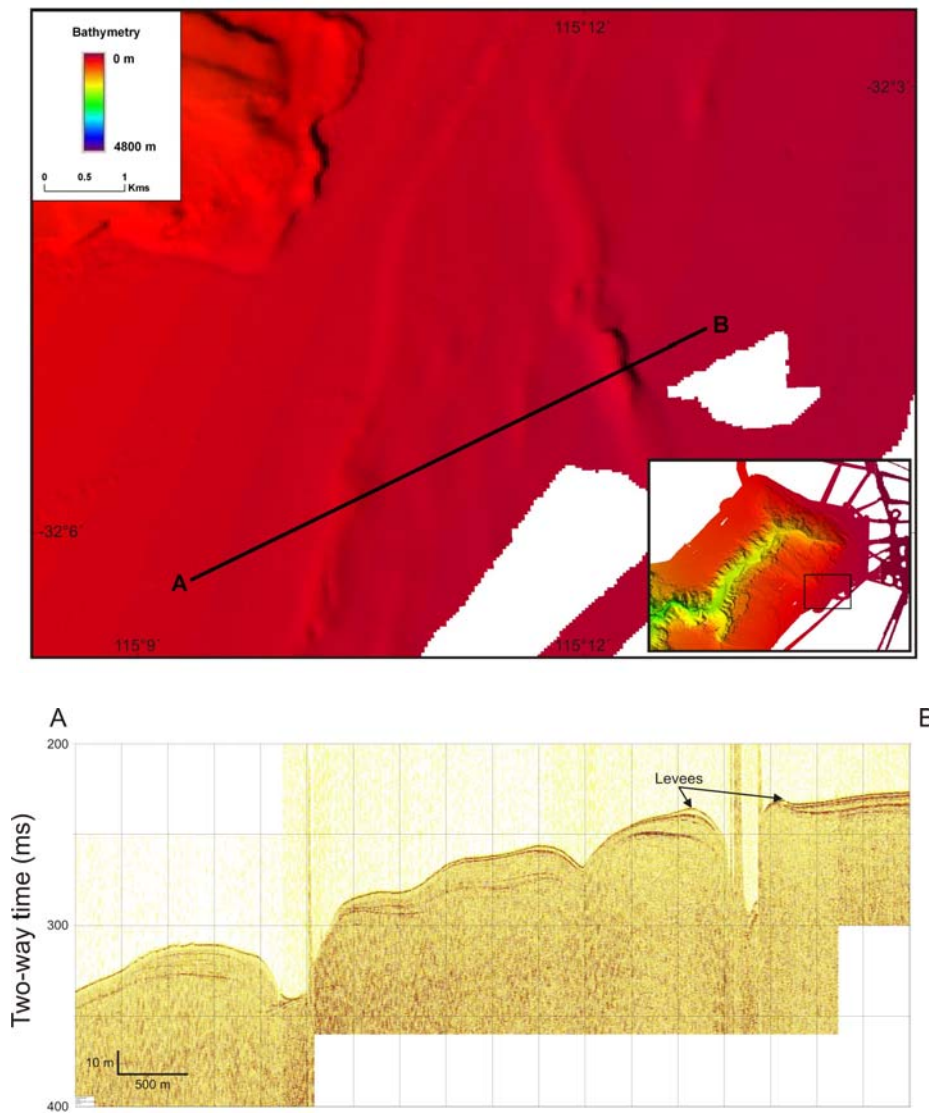


Figure 2.5. Multi-beam (swath) sonar bathymetry (top) and sub-bottom profile (bottom) of several small tributaries of the Perth Canyon.

On the slope, the seabed reflector forms a distinct (typically less than 1 ms) smooth surface gently dipping to the north-west, towards the head of the Perth Canyon. Several semi-parallel subsurface reflections can be traced regionally, although their strength, continuity and depth are variable across the area. These sub-bottom reflections onlap at the shelf edge and generally diverge down the slope reaching a maximum thickness of around 12 m (15 ms) before converging again at several small tributaries of the Perth Canyon, where they form sediment drapes. The tributary channels are also visible in the multi-beam (swath) bathymetry (Fig. 2.5).

Data on the upper slope to the south of the canyon reveal an abrupt increase in the number of sub-bottom reflectors and depth of penetration. This change in data quality was likely influenced by a change in the acquisition parameters. The event log records that the transmit waveform was changed from a Ricker pulse to a linear chirp, which generally provides greater depth penetration. Multiple, distinct (less than 1 ms), coherent, semi-parallel sub-bottom reflectors are evident from the seabed to a depth of around 30 to 38 m (40 to 50 ms). Beneath this series of reflectors, a single, distinct (around 2 ms) locally coherent, non conformable reflector is evident, ranging in depth from 30 m down to a

maximum of 75 m (40 to 100 ms) below the seabed. The reflector diminishes towards the Busselton Canyon as it deepens beyond the penetration of the system.

These data also reveal a broad (1.5 km wide) channel which feeds a secondary tributary into the Perth Canyon as evident in the swath data. Sub-bottom reflections appear draped on the northern wall, while the southern wall displays terminating strata. A 1.5 km wide tilted slump block, apparently detached from the southern wall, is also evident at the base of the channel (Fig. 2.6).

This series of sub-bottom reflectors continue west to the broad rim of slumping, which surrounds the canyon head and extends along its southern side. Here the seabed reflector appears to rapidly step down 150 to 200 m. The quality of the data at the rim is poor however, limiting interpretation of the nature of the headwall.

The profile across the canyon reveals great diversity in the nature of the seabed and sub-bottom. The seabed across the broad, low angled region of slumped sediments feeding into the canyon forms a distinct (less than 2 ms) undulating surface (Fig. 2.7). A series of largely conformable, parallel sub-bottom reflectors is also evident to a depth of around 45 m (60 ms). Bedforms within the slumped sediments are largely preserved, although somewhat altered; while the sequence of sub-bottom reflectors evident in the adjacent upper slope reach a depth of around 75 m (100 ms) and are fairly uniform, those in the slump are limited to just 50 m (65 ms). They are also non-uniform, with several very high amplitude bands of apparently “amalgamated” reflectors interbedded with sequences of comparatively low amplitude.

Moving across the steep canyon walls, data quality is poor, particularly over the steep northern wall, where little coherent data were collected. However, across the lesser sloping southern wall of the south-east trending arm of the tributary, and the eastern wall of the north-western trending arm, data quality is marginally better. Where visible, the seabed forms an indistinct, prolonged or hyperbolic reflector with no coherent sub-bottom reflectors present.

Lines to the west of the Perth canyon reveal the nature of the mid slope in the region. The seabed reflector is distinct although more variable in amplitude and continuity than the upper slope, and defines a more undulating morphology, with large irregular hyperbolae. Sub-bottom reflectors occur locally and are faint to indistinct, prolonged and of variable amplitude. A 7.5 km long lobe of draped sediment, up to 25 m thick is evident as the slope begins to decline northwards towards the lower reaches of the Perth Canyon (Fig. 2.8).

As the slope deepens in the west, the seabed morphology becomes quite rugged and the seabed reflector becomes irregular and indistinct, defined by large irregular hyperbolae and small overlapping hyperbolae at varying elevations, with local pockets of prolonged reflections. Sub-bottom penetration is minimal with faint, indistinct generally low amplitude reflections locally. The swath reveals a series of northwest trending channels between 1 and 2 km wide which extend north-west from this area.

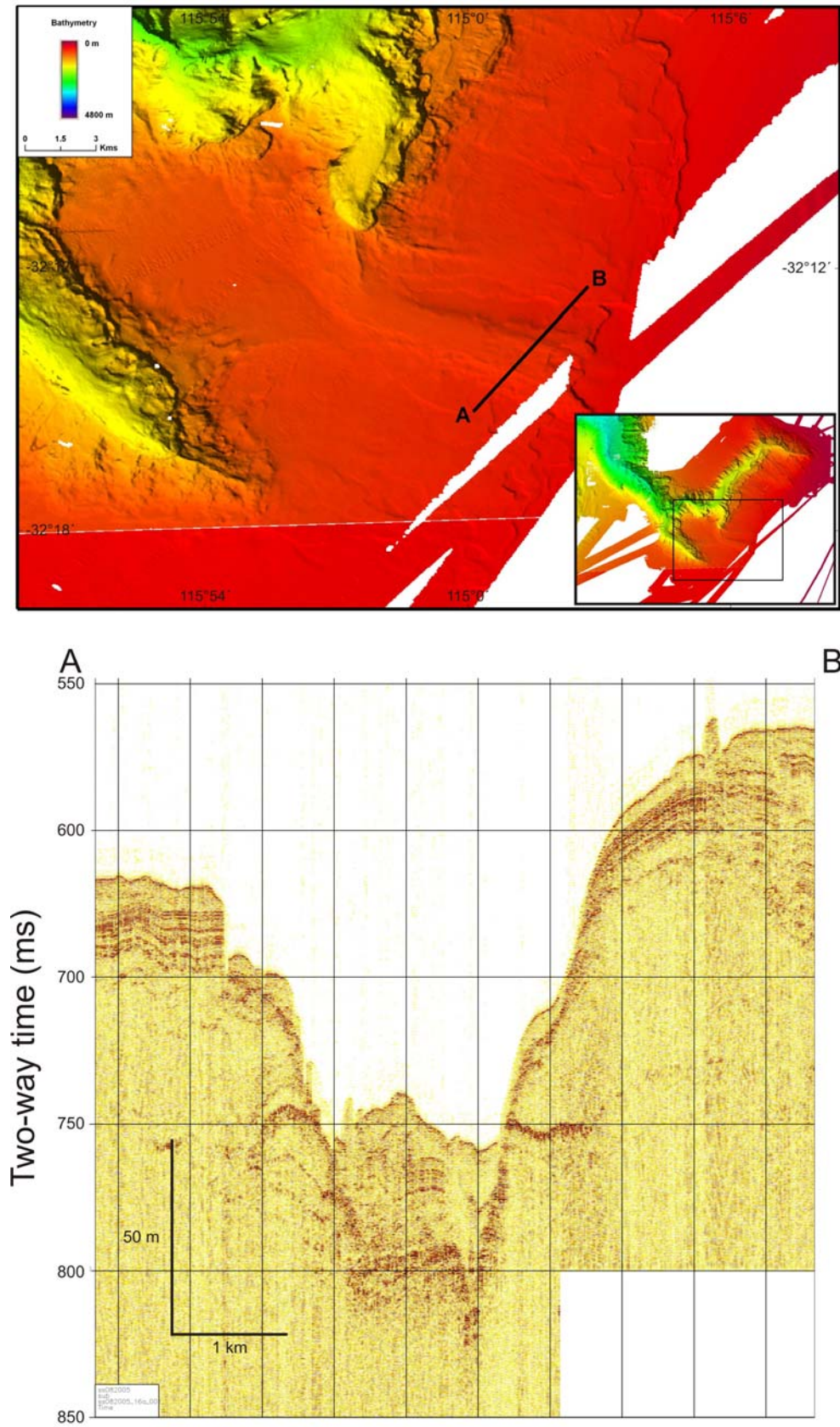


Figure 2.6. Multi-beam (swath) sonar bathymetry (top) and sub-bottom profile (bottom) across a broad tributary channel of the Perth Canyon.

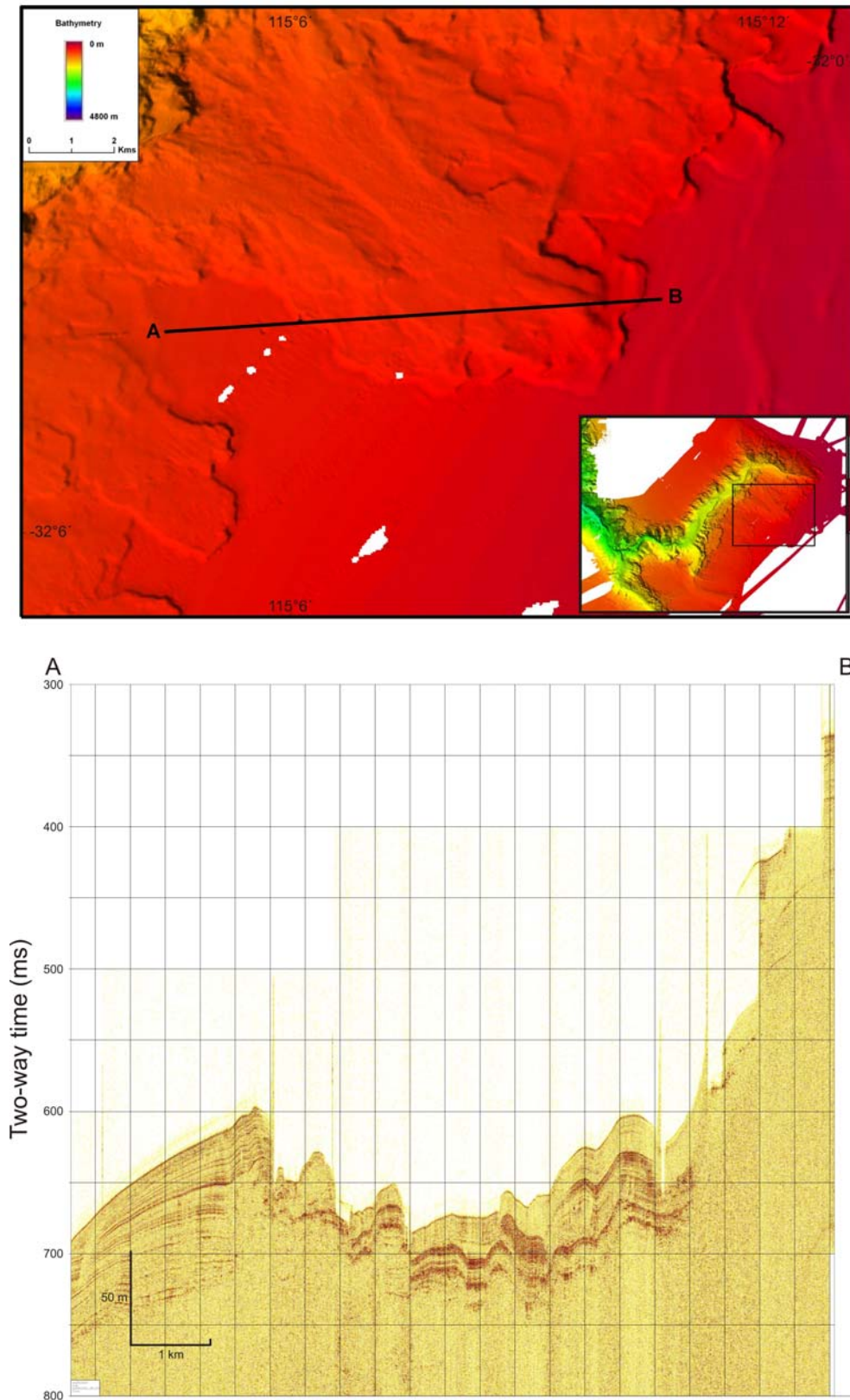


Figure 2.7. Multi-beam (swath) sonar bathymetry (top) and sub-bottom profile (bottom) across a slumped section of the upper slope feeding into the Perth Canyon.

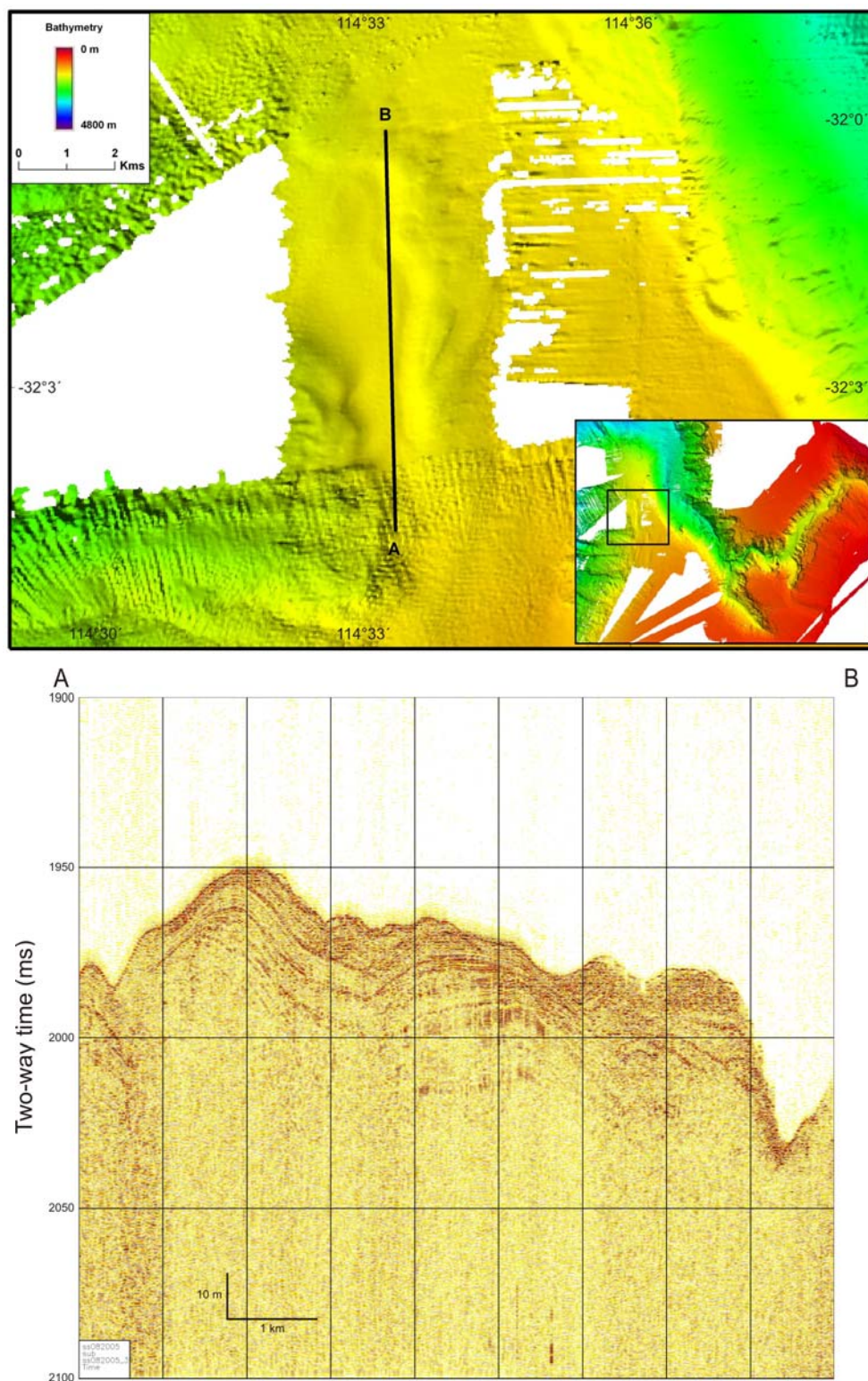


Figure 2.8. Multi-beam (swath) sonar bathymetry (top) and sub-bottom profile (bottom) across a thickly sedimented portion of the mid slope near the lower reaches of the Perth Canyon.

2.3.2.2. Busselton Canyon

Two shallow seismic lines were acquired over the Busselton Canyon; one across the main channel, and a second along the axis of the secondary tributary. There are also several lines across the adjacent slope, one of which intersects the top of the canyon head. Across the

canyon data quality is generally poor, although some patches of reasonable quality provide some information on the nature of the canyon walls.

Data in the upper to mid slope area show a strong distinct (2 ms) reflector which defines a smooth, gently undulating seabed. Small depressions and prominences occur intermittently on the seabed between the Perth and Busselton Canyons. These surface irregularities are visible on the swath bathymetry and appear as clusters of small circular features, around 80 to 100 m in diameter. The sequence of multiple distinct, coherent, semi-parallel sub-bottom reflectors evident on the slope south of the Perth Canyon extends to the mid slope in this region. In the vicinity of these irregular seabed features however, the sub-bottom reflectors change dramatically (Fig. 2.9). In more distal areas, a number of round to elliptical transparent zones on the order of 100 m wide appear to intrude into the sequence of multiple parallel reflectors, truncating the reflections. Some doming of overlying reflectors occurs above these zones. These acoustically transparent ellipses appear to join at depth to form a broad transparent zone that extends south around 35 km towards the Busselton Canyon. Proximal to the surface features, shallow sub-bottom reflectors (to a depth of around 7.5 to 12 m) appear amalgamated and of elevated amplitude. Below this depth is the broad acoustically transparent zone, which is bounded at its lower surface by the deep distinct (around 2 ms) locally coherent, non conformable reflector which extends south from the Perth Canyon region. Directly beneath the surface features, doming of the overlying shallow amalgamated sub-bottom reflectors occurs. These features may be fluid escape features (pockmarks) or may be associated with some diagenetic process.

Within the broad, gently sloping fan which extends north from around the canyon head, the seabed reflection becomes less distinct, and the sub-bottom reflectors less coherent. As the wall steepens into the canyon, the seabed reflection becomes indistinct and is defined by multiple small overlapping hyperbolae at varying elevations, and few sub-bottom reflections are evident. The data along the secondary tributary is patchy, but where visible the seabed reflector is prolonged (around 10 ms) with no sub-bottom reflectors evident.

2.3.2.3. Geographe Canyon

Several shallow seismic lines cross the Geographe Canyon, yielding information about the seabed and sediments within and around the canyon. The data quality is generally better than over the Perth and Busselton Canyons, most likely due to the comparatively gently dipping, broad and flat bottomed morphology of the Geographe Canyon.

The canyon floor is defined by an indistinct, prolonged (up to 10 ms) reflection with no sub-bottom reflectors. The canyon walls are characterised by multiple small overlapping hyperbolae at varying elevations with no coherent sub-bottom reflections evident. The large slump block at the foot of the Geographe Canyon can be observed in the data as an area with very diffuse and prolonged seabed reflection, defining an irregular surface. No sub-bottom reflectors occur within the slumped sediment.

Data on the mid slope reveal a somewhat changed character of the seabed and sub-bottom reflectors compared with areas further north. While the seabed reflection is still distinct (less than 2 ms), it traces a more uneven and undulating morphology. Sub-bottom reflections are variable across the slope in this area and are generally less coherent than in areas further north. Where visible, sub-bottom reflectors form an indistinct, high amplitude interval around 7.5 m (~10 ms) deep, underlain by a series of faint, incoherent reflections 20 to 25 m thick (~30 to 35 ms). A semi- prolonged (between 5 and 10 ms), generally non-

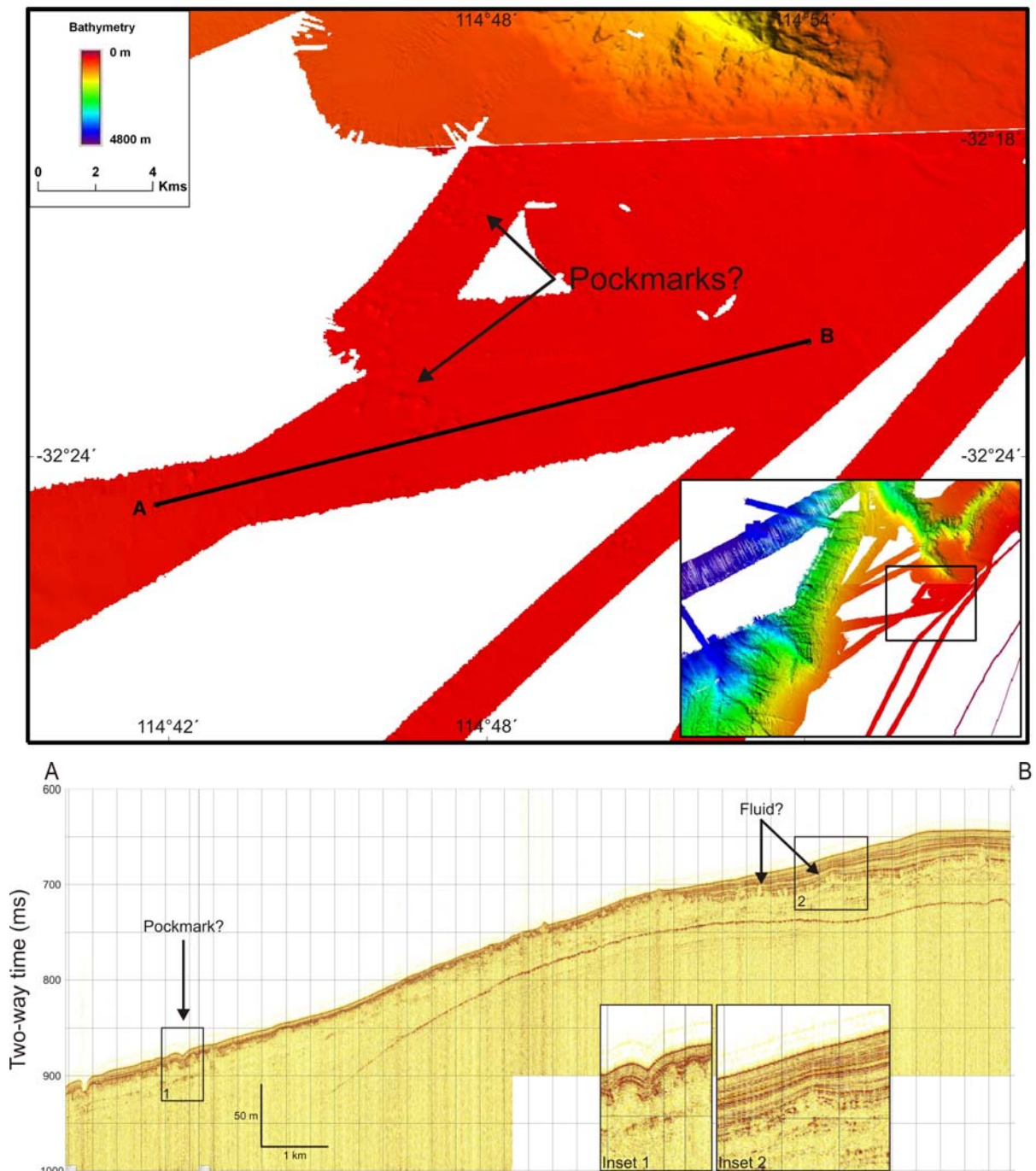


Figure 2.9. Multi-beam (swath) sonar bathymetry (top) and sub-bottom profile (bottom) across a series of surface irregularities that may be caused by fluid escape (pockmarks) or may be diagenetic features.

conformable and locally coherent reflector occurs below this largely transparent zone. A shallow, possibly fault-controlled channel oblique to the Geographe Canyon is also evident in the data with reflections abruptly terminating at the edge of the lineament.

The seabed on the mid slope to the south of the Geographe Canyon forms a distinct, smooth, gently undulating reflector intersected by several straight, narrow, and shallow west-north-west trending tributaries. These tributaries feed into a number of channels cutting the lower slope at the same bearing. Sub-bottom penetration on the mid slope in this region is good, with between 35 and 75 m (around 50 to 100 ms) achieved across the area. Two distinct sequences of sub-bottom reflectors are evident; a series of shallow, high

amplitude (less than 1 ms), semi-parallel, conformable reflectors up to 20 m thick (~25 ms); and an underlying series of, less coherent, semi-parallel, reflectors up to 50 m thick (~65 ms) with a more level morphology. The upper set of reflections sit unconformably above the lower set in some areas, while in other locations an acoustically transparent zone up to 20 m thick separates the upper and lower reflection sequences.

Data quality on the rugged lower slope, to the southwest of the Geographe Canyon, is variable. The seabed reflection here is predominantly defined by multiple overlapping hyperbolae with vertices at varying elevation, and with no coherent sub-bottom reflectors visible.

2.3.2.4. Bunbury Canyon

Sixteen lines of shallow seismic data were collected in the Bunbury Canyon region. Data quality across the canyon itself is generally poor, with few lines yielding information about the canyon walls or floor. On the mid and lower slope, data is of better quality with coherent seabed and sub-bottom reflections visible.

The seabed reflection of the steep canyon walls is defined by small discrete hyperbolae with varying vertex elevations. The canyon floor forms an indistinct and prolonged reflector. No sub-bottom reflections are observed within the canyon. Data on the mid-slope south and west of the Bunbury Canyon reveal a distinct, smooth seabed reflection, interrupted by a number of localised crack-like depressions between 10 and 22 km west of the gently sloping section of the canyon. These fissures, evident on the swath data, are around 8 km in length with a sigmoidal form. The seabed within the fissures tends to be indistinct with a prolonged reflection.

To the west of the canyon, multiple, faint but distinct, uniform, parallel sub-bottom reflectors are observed to a depth of around 38 m (~50 ms). Further south, the sub-bottom reflections become less regular and non-conformable, forming sediment drapes in some areas.

A broad area of the mid slope near the head of the gently sloping Bunbury Canyon displays a prolonged seabed reflection with small areas of hyperbolic reflections, and with no sub-bottom reflectors evident. This area is bounded linearly on its western side where it appears to join the Bunbury Canyon, and arcs around to the north joining the southern-most of the north-east trending channels that cut the shelf between the Bunbury and Busselton Canyons.

2.3.2.5. Acoustic Facies

A total of seven major acoustic echo-types were observed in the study area (Table 2.1). Generally the shelf and slope are defined by distinct echo-types, while indistinct reflections characterise the canyons, channels and rugged areas of the mid and lower slope (Figs. 2.10 & 2.11).

Distinct, continuous seabed reflections with no apparent sub-bottoms (Type IA) are mostly limited to the shelf and upper slope. Distinct, continuous seabed reflections with either numerous distinct, continuous, parallel sub-bottoms (Type IB) or distinct, continuous, converging sub-bottoms (Type IC) have the widest distribution, representing most of the slope across the study area.

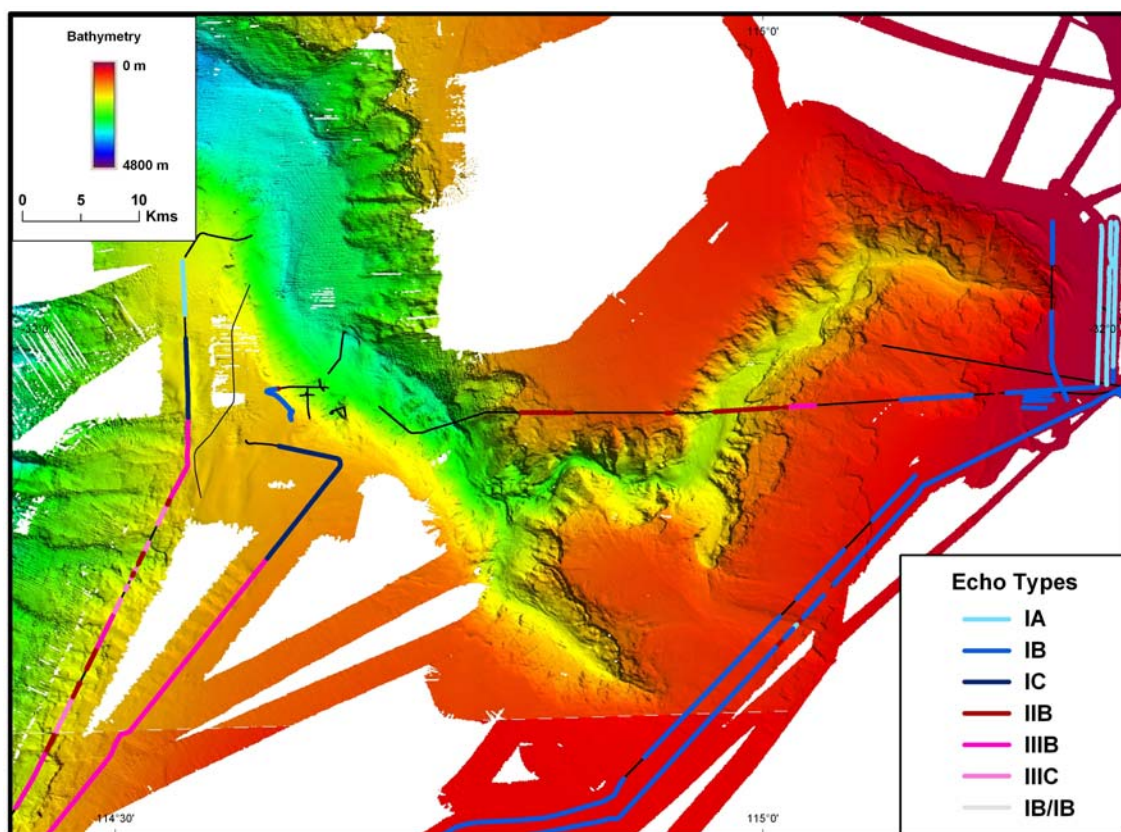


Figure 2.10. Distribution of acoustic facies in the Perth Canyon region.

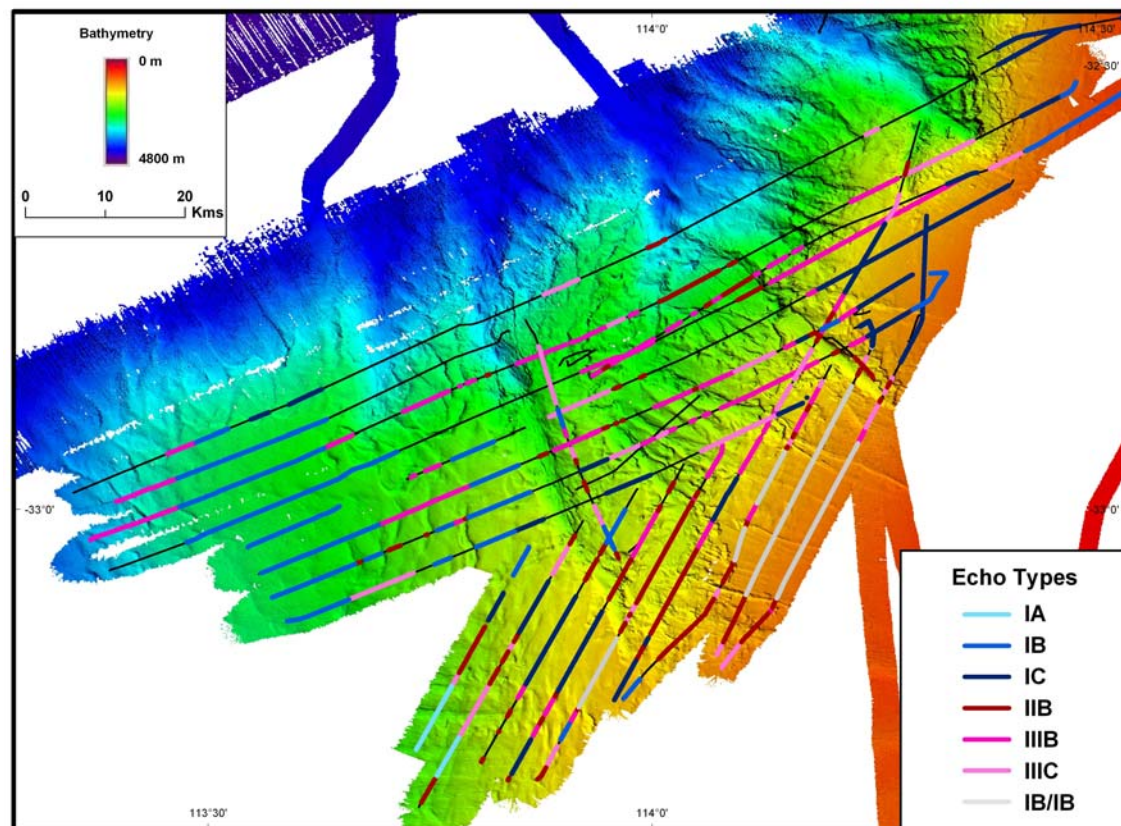
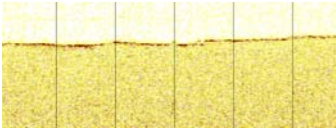
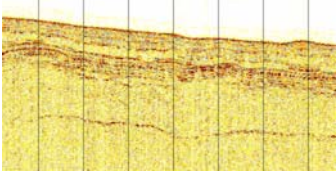
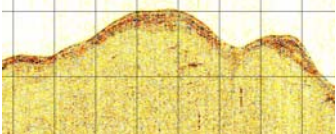
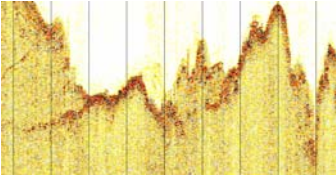
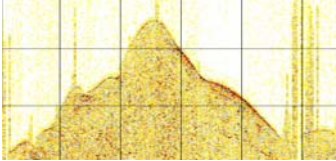
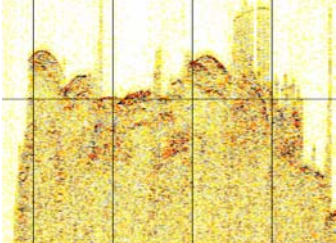
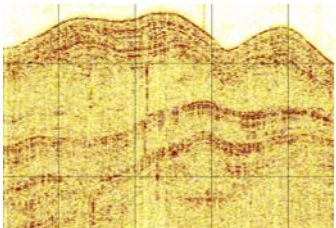


Figure 2.11. Distribution of acoustic facies in the Mentelle Basin region encompassing the Busselton, Geographe and Bunbury Canyons.

Table 2.1. Descriptions of echo-types observed in the study area. Echo types defined after Damuth (1974; 1980).

Class	Type	Example	Description	Distribution
Distinct echoes (Class I)	IA		Distinct (~2 ms), continuous water bottom reflection with no apparent sub-bottom reflectors	Shelf
	IB		Distinct, continuous water bottom reflection with numerous distinct, continuous parallel sub-bottom reflectors	Thickly sedimented areas of the upper and mid slope
	IC		Distinct, continuous water bottom reflection with distinct, continuous, converging (non-conformable) sub-bottom reflectors	Areas on the mid slope with thin sediment layer, often draped
Indistinct echoes: Prolonged	IIB		Prolonged (~10 ms) water bottom reflection with no clear sub-bottom reflectors	Canyon floors, areas of outcrop on the mid slope
Indistinct echoes: Hyperbolae (Class III)	IIIB		Large, irregular, overlapping hyperbolae to broad irregular single hyperbolae with varying vertex elevations above the seafloor.	Localised areas on the lower slope with variable morphology
	IIIC		Regular, overlapping hyperbolae with varying vertex elevations above the seafloor	Areas of steep morphology such as canyon walls and rugged areas on the lower slope with little sedimentation
Composite	IB/IB		Distinct, continuous water bottom reflection with two discrete sub-bottom reflection sequences. Both sequences are defined by multiple, distinct, continuous, parallel reflections (Type IB), although the upper sequence lies unconformably above the lower sequence	Mid slope between the Geographe and Bunbury Canyons, intersected by narrow, linear channels

Indistinct, prolonged seabed reflections with no clear sub-bottoms define the canyon floors and some areas of interpreted rocky substrate on the mid slope; in particular the broad arc-shaped depression at the head of the Bunbury Canyon. The large slump at the foot of the Geographe Canyon also produces a predominantly indistinct, prolonged seabed reflection. Indistinct, hyperbolic reflections occur in rugged areas of the mid and lower slope. Large, irregular, overlapping hyperbolae to broad irregular single hyperbolae with varying vertex elevations above the seafloor (Type IIIB) occur in localised areas on the lower slope with variable morphology, such as across the northwest trending channels which intersect the

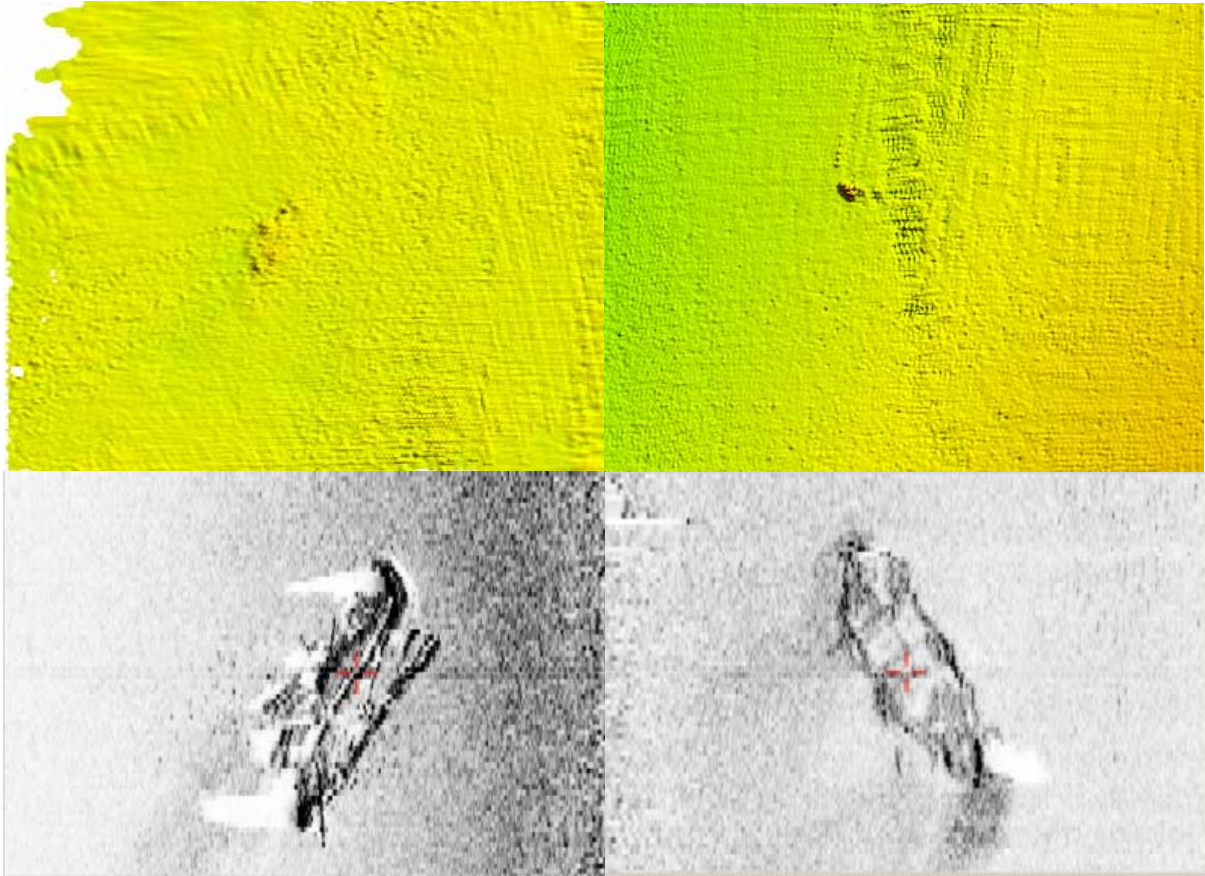


Figure 2.12. Images of the shipwrecks located during the survey. The first wreck (left) is located at $-32^{\circ}01.887652'$ and $115^{\circ}19.541413'$ at a depth of 110 m. The second wreck (right) is located at $-32^{\circ}01.668323'$ and $115^{\circ}13.588796'$ at a depth of 187 m. The wrecks are visible on the reprocessed 2 m grid swath bathymetry (top) although much greater detail is obtained from the side scan sonar (bottom).

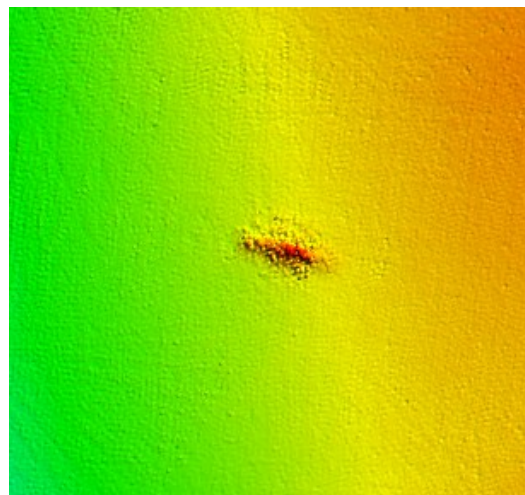


Figure 2.13. Swath bathymetry image of the 112 m long HMAS *Derwent* located at $-32^{\circ}03.455892'$ and $115^{\circ}12.288817'$ at a depth of around 200 m. No side scan data were collected over the HMAS *Derwent*.

slope between the Geographe and Bunbury Canyons. Smaller more regular, overlapping hyperbolae with varying vertex elevations above the seafloor (Type IIIC) define areas of steep morphology along the canyon walls and some rugged areas of the lower slope.

Across the mid-slope between the Geographe and Bunbury Canyons, a composite reflection type is observed (Type IB/IB). This reflection type consists of an upper and lower

reflection sequence; both are defined by multiple, distinct, continuous, parallel reflections (Type IB), although the upper sequence lies unconformably above the lower sequence.

2.3.3. Side Scan Sonar

A total of 7.6 GB of side scan sonar data were acquired during the survey, limited to a small area of the shelf nearby Rottnest Island. The surveyed area encompassed a well-known deepwater graveyard, used as a dumping ground for vessels abandoned after the Second World War.

The side scan data revealed two previously unknown ship wrecks. These wrecks, as well as the river class destroyer HMAS *Derwent* scuttled in 1994, are also visible in the swath bathymetry data when reprocessed with a 2 m grid ([Figs. 2.12 & 2.13](#)).

3. Oceanography

3.1. DATA ACQUISITION

3.1.1. Mooring Description

An RD Instruments Workhorse Sentinel 600 kHz acoustic Doppler current profiler (ADCP Serial No. 5581) was deployed southwest of Rottnest Island (Fig. 3.1). The mooring consisted of a benthic frame supporting both the ADCP and an acoustic release (Serial No. 117), as well as a 60 m long ground line to a second acoustic release (Serial No. 154) suspended between a bottom weight and sub-surface floats. A 50 m line connected this second acoustic release to a string of surface floats. The mooring was located in approximately 32 m water depth at 32° 2.713'S 115° 26.795'E. The mooring was deployed at 09:27 hrs on 28/09/2005 (GMT) and retrieved at 23:32 hrs on 18/10/05 (GMT). On retrieval the benthic frame was found to be entangled in seaweed, and the metal shroud surrounding the ADCP was partially bent over and shadowing one of the transducers. The mooring line may have caused this damage during recovery. Four heavy gauge fishing hooks and 250 g sinkers on nylon fishing line were also entangled with the mooring line running from the second acoustic release to the surface floats.

The ADCP measures directional currents from the Doppler shift of sound reflected from the water column using two pairs of orthogonal acoustic beams. ADCP Serial No. 5581 contains the following feature upgrades: Mode 5, 8, and 11 high resolution modes; high ping rate mode 12; and the waves array upgrade. The instrument was programmed to obtain profiles of currents from 1.6 m above the seabed to near the water surface with measurements (bin elevations) spaced 0.5 m apart. A total of 50 pings were averaged every 1,200 s to provide current speed and direction time series with a sampling interval of 20 minutes for each bin elevation. The instrument was also programmed to measure waves by burst sampling at 2 Hz for 20 minutes beginning on the hour. Hourly measurements of mean water depth (waves removed) and near-bed water temperature were also recorded.

3.2. DATA PROCESSING AND ANALYSIS

3.2.1. Wind Waves

The significant wave height (average of the highest 1/3 of waves in the record) varied from 0.95 m to 3.95 m (Fig. 3.2). There were three occasions when significant wave height ramped up to values larger than 3 m: 30th September, 3rd October and 9th October. Peak wave period varied between 5 and 10 s, although the upper limit is artificially clipped (the reason for this was not apparent at the time of writing).

Wave power P was calculated assuming deep water waves, as follows (e.g. Masselink and Hughes, 2003):

$$P = ECn \quad (1)$$

where $n=0.5$, E is the energy density, and C is the wave speed calculated as:



Figure 3.1 Mooring showing acoustic release system (front) and ADCP (rear).

$$E = \frac{1}{8} \rho g H_s^2 \quad (2)$$

and

$$C = \frac{g T_p}{2\pi} \quad (3)$$

respectively, where ρ is the water density, g is the gravitational acceleration, H_s is the significant wave height and T_p is the peak wave period. A more accurate estimate of the wave power can be obtained using the general form of the wave dispersion equation, rather than the deep water approximation. This was not pursued here for two reasons; (1) only an approximate estimate of wave power was required, and (2) solving the general form of the dispersion equation is not straightforward because it is implicit. Estimated wave power varied between 0.53 kW m^{-1} and 15.32 kW m^{-1} , and follows closely the pattern of variation observed for significant wave height. Wave direction throughout the study period was persistently from the SW and to lesser extent NW quadrants (Fig. 3.2).

The first example (30th September) is representative of the first high energy event in the record, and shows a narrow directional window ($<25^\circ$ span) for the peak wave energy, centred on 252° magnetic (Fig. 3.3). The peak period of 8.53 s is suggestive of swell waves rather than locally generated sea, and ship-board wind speed and direction measurements (39.5 knots from 25° magnetic) at the time are consistent with this interpretation (Fig. 3.4). The second example (3rd October) is representative of relatively low wave energy during the deployment period (Fig. 3.3). It shows a larger directional window for the peak wave energy that spans up to 90° and is centred on 244° magnetic. The third example is also representative of relatively low energy conditions, and clearly shows waves originating from two directionally distinct sources; the southeast and the north. The two distinct peaks in the autospectra demonstrate that the two directional sources also occupied discrete frequency bands.

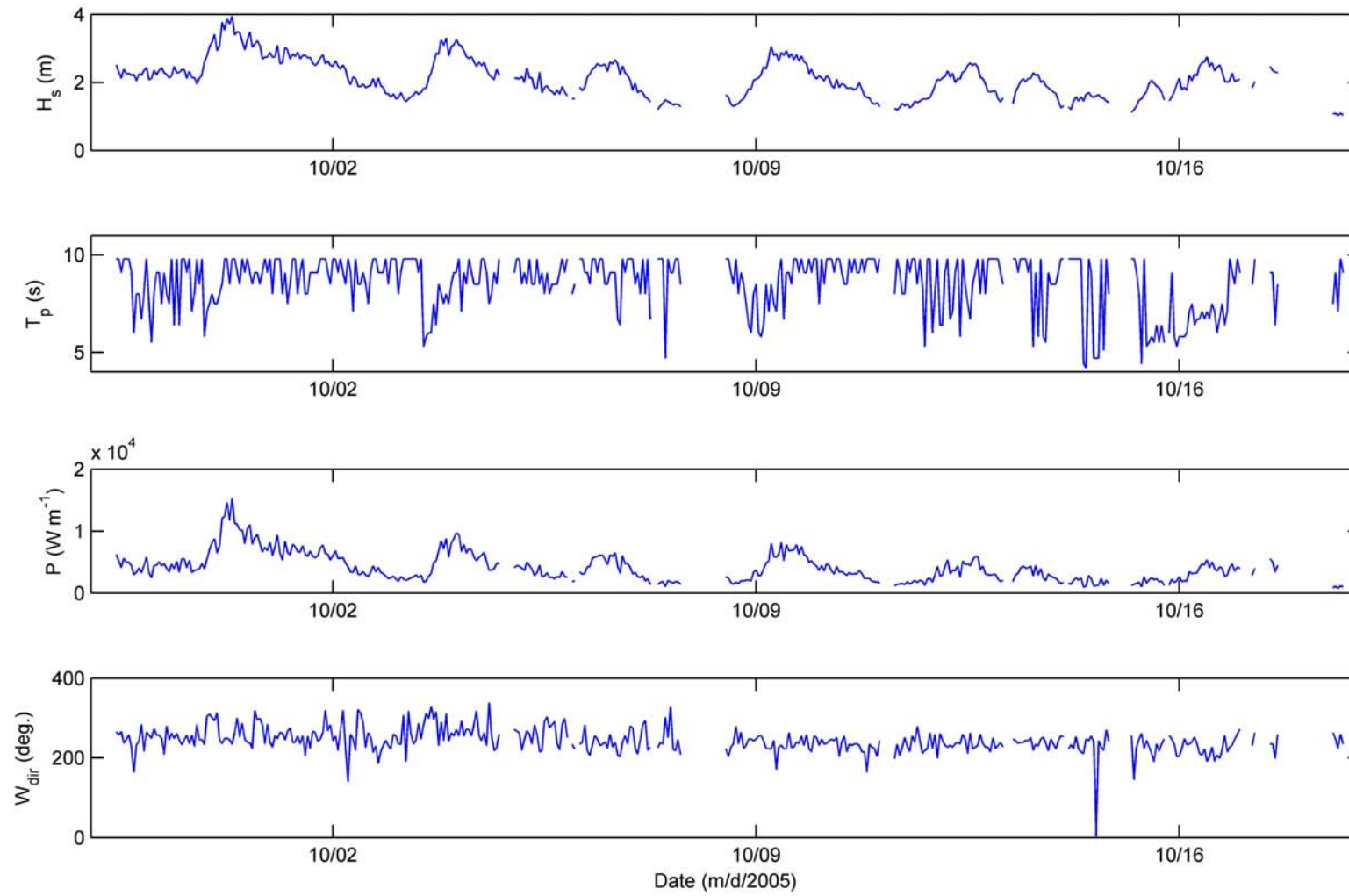


Figure 3.2. Hourly time series of significant wave height H_s , spectral peak wave period T_p , wave power P and wave direction W_{dir} . Wave power was computed using Equation 1.

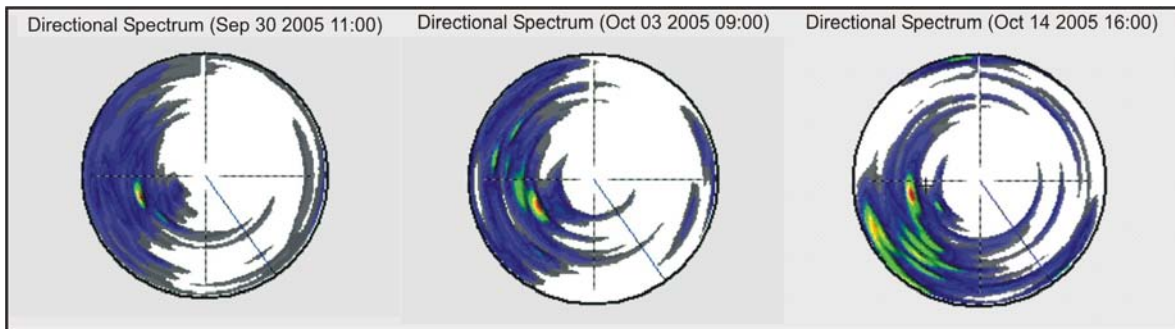


Figure 3.3. Examples of directional wave spectra for a single sampling burst (20 minutes) at the time and dates indicated.

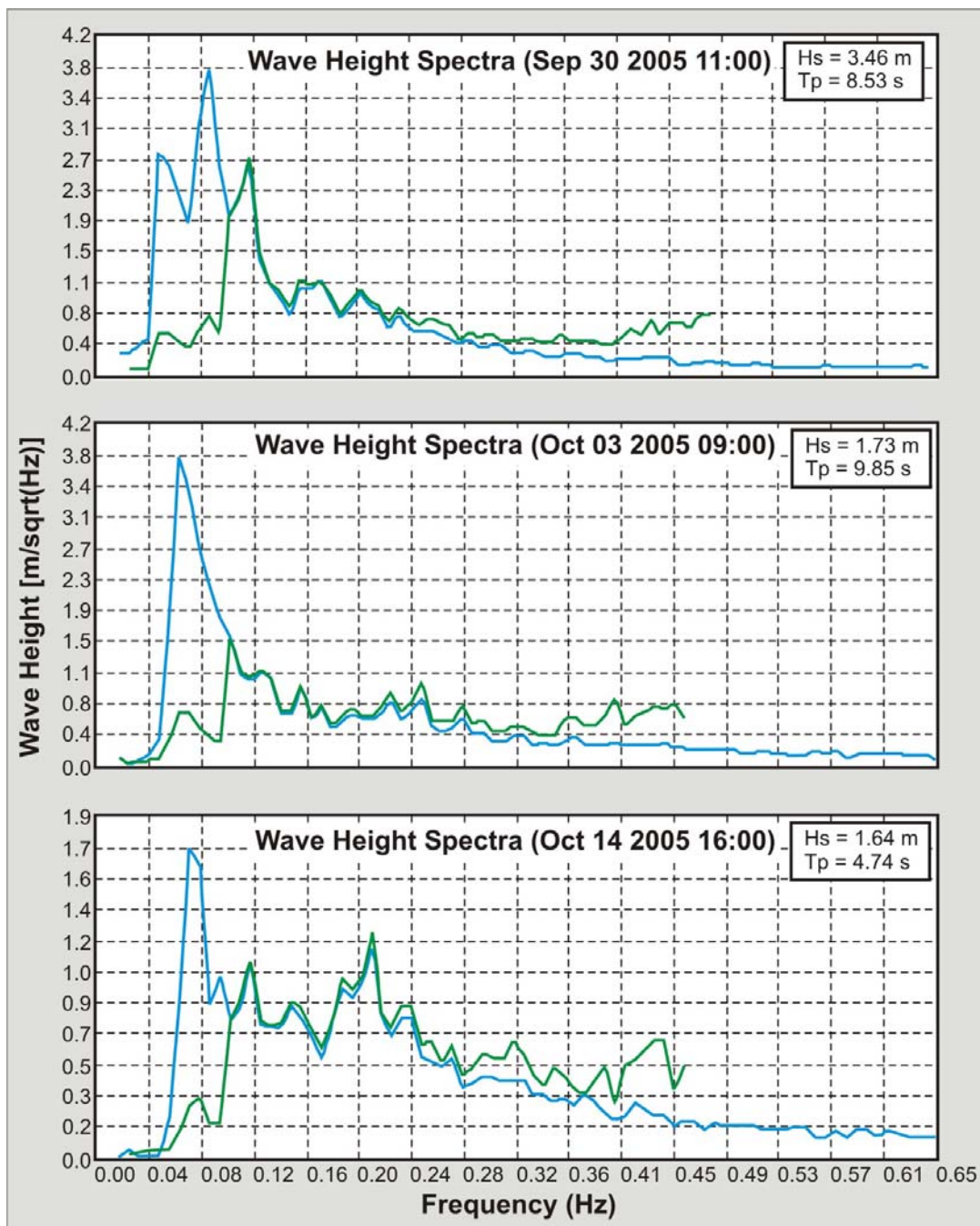


Figure 3.4. Examples of wave autospectra for a single sampling burst (20 minutes) at the time and dates indicated.

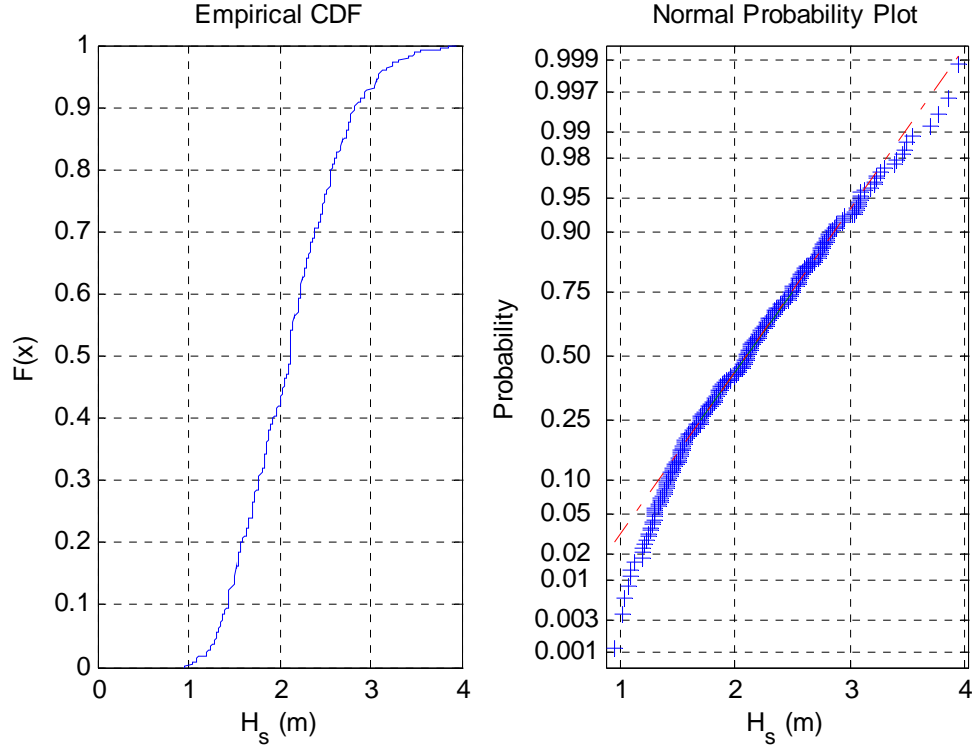


Figure 3.5. Cumulative frequency plot (left) and normal probability plot (right) of significant wave heights H_s measured over the deployment period.

Over the deployment period the significant wave height exceeded 2.1 m 50% of the time and exceeded 3.5 m 1 % of the time (Fig. 3.5). The data have been plotted on normal probability axes to provide a quick test for normality. The data deviates from a normal distribution, particularly in the lower tail. The Kolmogorov-Smirnov test was also applied to determine if the data conformed to the Rayleigh distribution, and the null hypothesis was rejected at the 95% confidence level. The fact that the distribution of hourly significant wave heights does not conform to either the normal or Rayleigh distributions is probably a reflection of the fact that the record is relatively short and biased away from the smaller wave heights. Lemm *et al.* (1999) analysed 2.5 years (1994-1996) of wave data collected by a waverider buoy located approximately 15 km southwest of Rottneet Island in 50 m water depth. Their longer term record indicates that significant wave height exceeds 1.8 m 50% of the time and 4.9 m 1% of the time. The data obtained during the deployment period are therefore representative of more energetic than typical conditions, but not representative of extreme conditions.

Near-bed wave orbital velocity amplitude U_w (Fig. 3.6) was calculated using the method of Soulsby (1997), as follows:

$$U_w = \frac{\pi H_s}{T_p \sinh(kh)} \quad (4)$$

where the wave number $k = 2\pi/L$, h is the water depth and the wavelength L was calculated using the deepwater approximation of

$$L = gT_p^2 / 2\pi \quad (5)$$

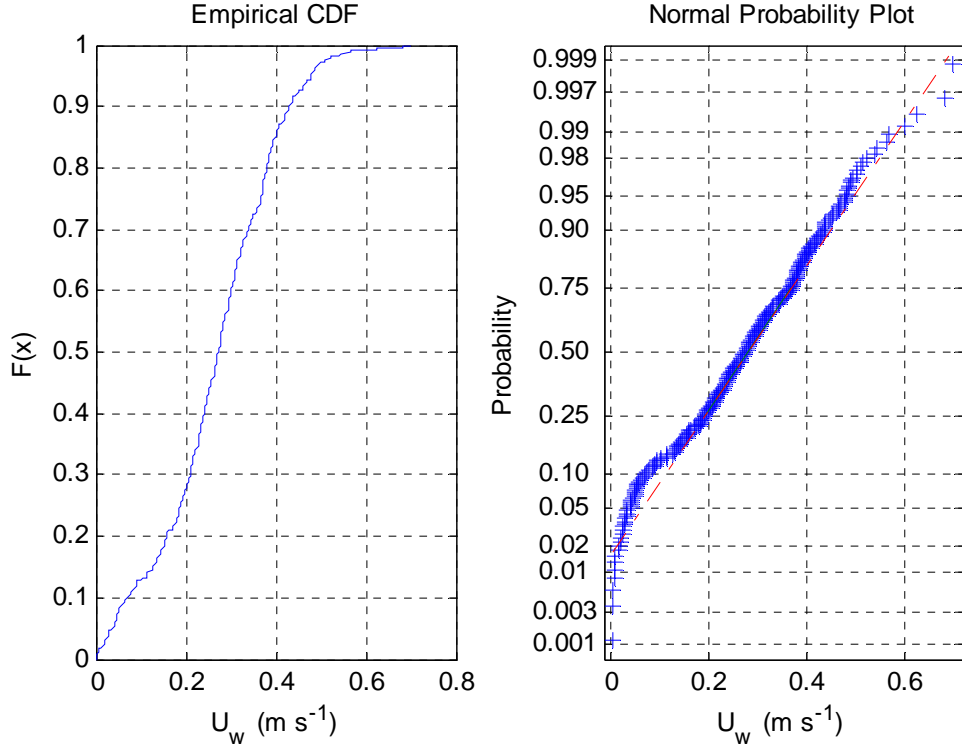


Figure 3.6. Cumulative frequency plot (left) and normal probability plot (right) of near-bed wave orbital velocity amplitude U_w over the deployment period. U_w was estimated using Equation 4.

The near-bed wave orbital velocity amplitude exceeded 0.28 m s^{-1} 50% of the time and exceeded 0.6 m s^{-1} 1% of the time. These velocity estimates were used to determine the wave induced bed shear stress τ_w (e.g., Soulsby, 1997), as follows:

$$\tau = 0.5 \rho f_w U_w^2 \quad (6)$$

where the wave friction factor f_w was calculated as (Nielsen, 1992):

$$f_w = \exp \left(5.5 \left(\frac{r}{A} \right)^{0.2} - 6.3 \right) \quad (7)$$

The bed roughness $r = 2.5 \bar{D}$ was calculated using a mean grain diameter $\bar{D} = 0.25 \text{ mm}$ of a grab sample taken at the mooring location (01GR03). The wave orbital diameter A was calculated, as follows:

$$A = \frac{U_w T_p}{2\pi} \quad (8)$$

This approach yields the skin friction value, τ_w , for which a cumulative frequency distribution can be derived (Fig. 3.7). The skin friction bed shear stress exceeded 0.36 N m^{-2} 50% of the time and 1.14 N m^{-2} 1% of the time. The distribution of bed stresses is clearly not normal, but in the absence of any theoretical distribution no other probability distributions were tested. The critical bed shear stress, τ_{cr} , required to initiate grain motion, given a mean grain diameter of $\bar{D} = 0.25 \text{ mm}$ (Fig. 3.7), can then be calculated using Soulsby and Whitehouse (1997), as follows:

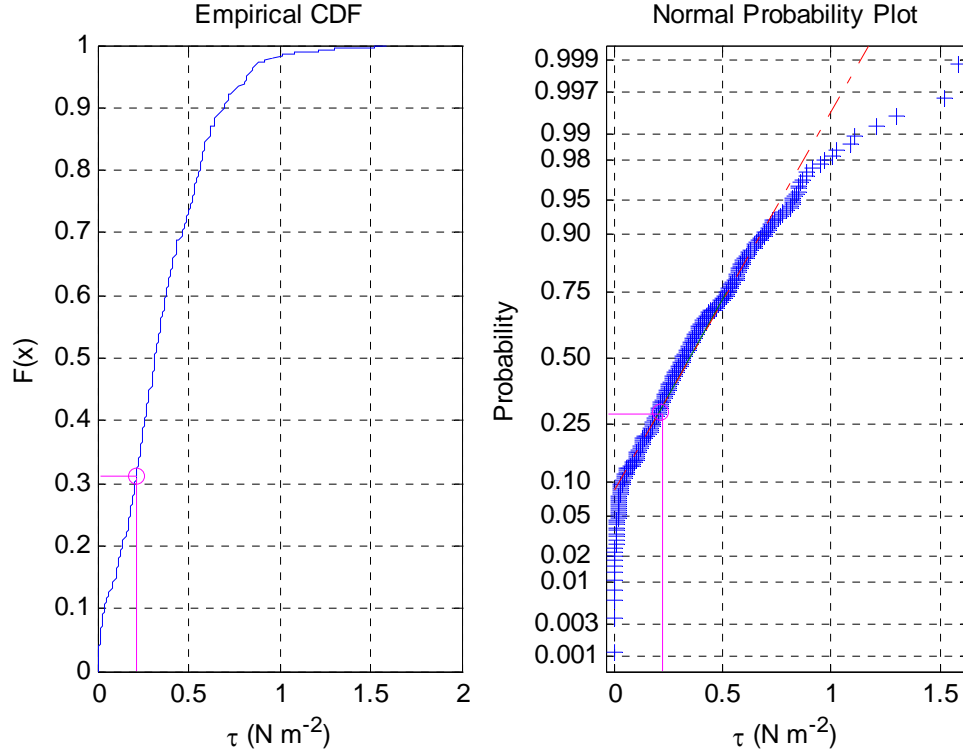


Figure 3.7. Cumulative frequency plot (left) and normal probability plot (right) of wave-induced skin friction bed shear stress τ_w over the deployment period. τ_w was estimated using Equation 6. Also shown by the magenta line is the critical bed shear stress required to initiate sediment motion, estimated using Equation 9.

$$\theta_{cr} = \frac{0.24}{D_*} + 0.055[1 - \exp(-0.020D_*)] \quad (9)$$

where θ_{cr} is the critical Shields parameter (or non-dimensional bed shear stress) and D_* is the non-dimensional grain diameter. The non-dimensional grain diameter was calculated, as follows:

$$D_* = \bar{D} \left(\frac{g(s-1)}{\nu^2} \right)^{1/3} \quad (10)$$

where s is the ratio of sediment to seawater density and ν is the kinematic viscosity of seawater. The value of θ_{cr} was converted to τ_{cr} by multiplying the former by $g\bar{D}(s-1)$.

For the grain diameter $\bar{D} = 0.25$ mm the critical bed shear stress is 0.21 N m^{-2} , which was exceeded over 70% of the time. It should be noted that the skin friction bed shear stress represents the minimum wave-induced bed shear stress, and will significantly under-represent the total bed shear stress in the presence of a rippled bed. Given the available data it is possible to determine the likely presence and dimensions of bedforms over the deployment period, and therefore obtain a more accurate estimate of the excess bed shear stress due to waves. The effects of wave-current interaction could also be explored using the available data. Such a sophisticated analysis, however, is beyond the scope of this report. The necessary information to undertake such an analysis can be found in Nielsen (1992) or Soulsby (1997).

Table 3.1. Listing of the amplitudes, phases and errors of the harmonic constituents resolved from the available 20.5 day deployment record. The Greenwich phase was computed with nodal corrections.

Tide	Frequency (cycles hr ⁻¹)	Amplitude (m)	Amplitude error*	Phase (degrees)	Phase error*	Signal-to-noise ratio
MSF	0.002822	0.0597	0.011	23.72	9.51	29
O1	0.038731	0.1258	0.017	170.26	6.39	57
K1	0.041781	0.1327	0.014	166.71	5.96	85
M2	0.080511	0.0570	0.006	55.36	5.46	1.00E+02
S2	0.083333	0.0738	0.006	38.22	5.04	1.70E+02
M3	0.120767	0.0036	0.003	227.55	41.47	1.6
SK3	0.125114	0.0027	0.002	55.88	49.55	1.7
M4	0.161023	0.0044	0.002	167.85	23.52	6.7
MS4	0.163845	0.0039	0.001	221.82	23.86	6.8
S4	0.166667	0.0022	0.001	275.92	39.86	3.4
2MK5	0.202804	0.0005	0.001	186.56	156.19	0.2
2SK5	0.208447	0.0013	0.001	114.23	55.73	1.5
M6	0.241534	0.0001	0.001	259.16	229.19	0.016
2MS6	0.244356	0.0016	0.001	45.11	55.59	1.6
2SM6	0.247178	0.0019	0.001	175.42	39.11	2.1
3MK7	0.283315	0	0.001	291.94	255.17	0.0025
M8	0.322046	0.0018	0.002	203.06	56.49	1.4

* = errors are for a 95% confidence interval.

3.2.2. Tides

A classical harmonic analysis was undertaken of the actual water depth time series to determine the predicted tidal signal and amplitudes and phases of the tidal constituents (Fig. 3.8). The method used followed Pawlowicz *et al.* (2002), which is based on a method initially proposed by Foreman (1977) and includes nodal corrections. Using this method a total of 45 astronomical and 101 shallow-water constituents can be resolved, depending on the record length. The 20.5 days of data available from the deployment yielded the amplitudes and phases of 17 tidal constituents along with their 95% confidence limits (Table 3.1).

The harmonic amplitudes and phases were used to compute a predicted tidal water depth record, which was subtracted from the observed record to obtain a residual time series (Fig. 3.8). The ratio of the variances of the measured and predicted time series is 91.8%. This represents a reasonable fit with the residuals limited to ± 0.1 m. There is an overall trend in the residual record from positive at the start of the deployment to negative at the end, which is consistent with the overall trend of increasing atmospheric pressure over the deployment period (viz. the ‘inverse barometer effect’, e.g. Masselink & Hughes, 2003). There is also a cyclical, but non-tidal variation in the residual record with a period of roughly 2.5 days. This may be due to the passage of shelf waves, but there is currently insufficient information available to assess this. It does not appear to be related to cycles in atmospheric pressure (Fig. 3.8).

The tide can be classified according to the ratio of key diurnal to semi-diurnal tidal constituents. This is represented by the form factor F (e.g., Pugh, 2004), as follows:

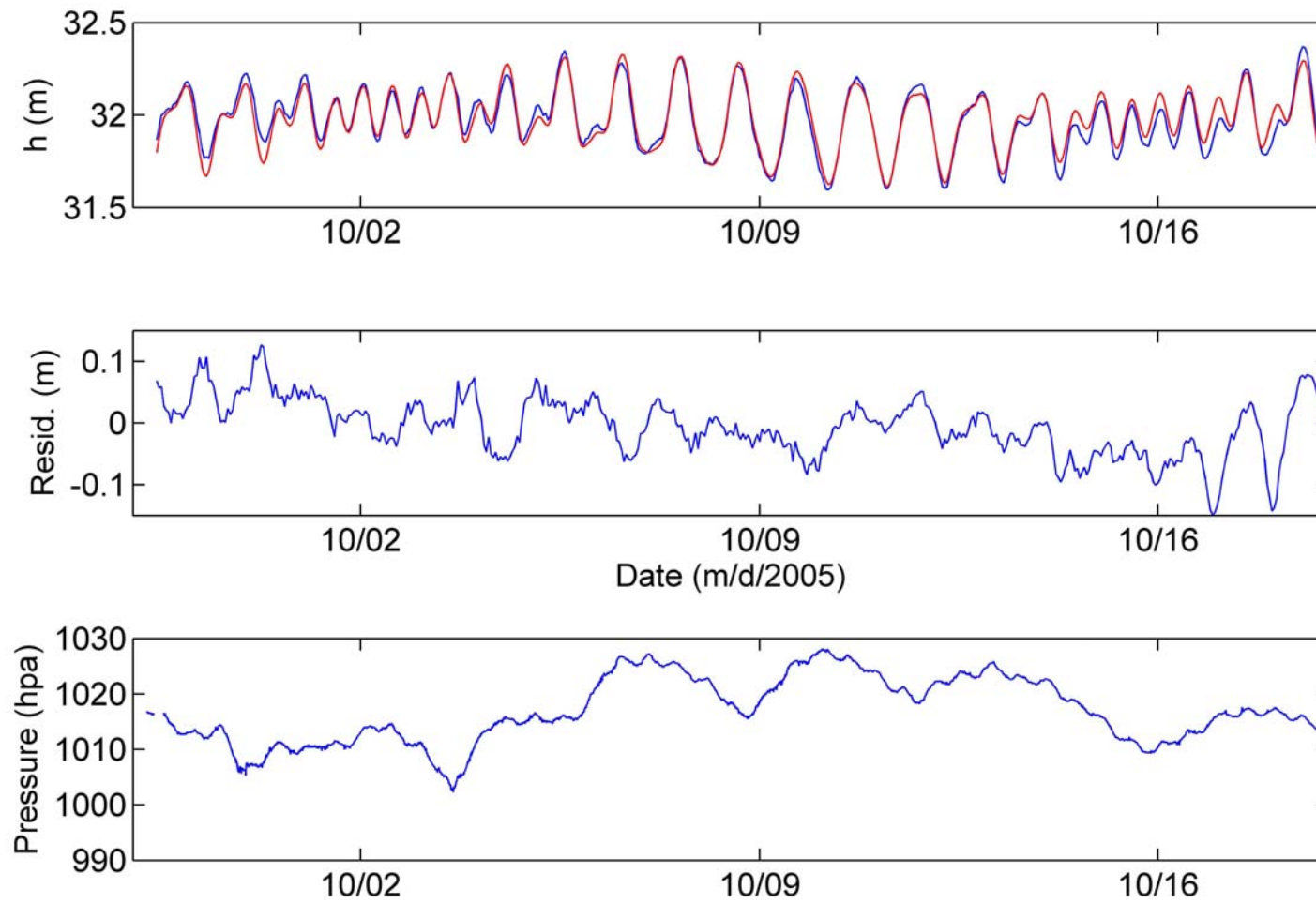


Figure 3.8. Hourly time series of measured water depth h (blue line), predicted tidal water depth h (red line), residual water level (observed minus predicted), and atmospheric pressure. The predicted tide was based on the harmonic constituents listed in [Table 3.1](#).

$$F = \frac{a_{K1} + a_{O1}}{a_{M2} + a_{S2}} \quad (11)$$

where a is amplitude and the subscript denotes the relevant constituent. The amplitudes indicate a value for F of 1.9763 (Table 3.1), which is indicative of a mixed, mainly diurnal tide.

3.2.3. Currents

The currents recorded during the deployment show the surface 5 m of the water column contain noisy results with respect to both current speed and direction, which are difficult to interpret (Fig. 3.9). This may be due to the wave activity present and/or acoustic reflections off the sea surface. The lowest and highest bins containing consistent data are Bins 1 and 56, respectively. These bins are located 1.6 m above the bed and 5 m below the mean sea surface, respectively. Across this bin range the current speeds consistently increased with elevation above the bed, and flowed in a direction that was persistent throughout the entire water column (Fig. 3.9). These observations are characteristic of a shelf current boundary layer. The first half of the record displays a highly variable current direction, whereas the second half of the record is characterised by a persistent roughly northward flow (Fig. 3.9). The reason for the switch from one regime to another is not clear, but may be related a change in the regional geostrophic current and its interaction with the nearby Rottneet Island. This issue could be investigated further using satellite imagery of sea-surface elevations during the deployment period.

Bins 1 and 56 were analysed in more detail to elucidate some key aspects. Figure 3.10 shows the near-bed and near-surface current speeds and directions as 20-minute time series. As expected, the near-surface current speeds are roughly a factor of five larger than the near-bed speeds. Near surface current speeds exceeded 0.22 m s^{-1} 50% of the time and 0.51 m s^{-1} 1% of the time (Fig. 3.11), whereas near-bed speeds exceeded 0.04 m s^{-1} and 0.12 m s^{-1} , respectively (Fig. 3.12). Figures 3.11 and 3.12 indicate that the current speeds are not normally distributed, with a larger than expected kurtosis. While there is some evidence of weak variation in the magnitude of the current speed at diurnal tidal frequencies, there is no evidence of current reversals related to the tide (Fig. 3.10).

A progressive vector plot of the near-surface and near-bed currents indicates that during the time period when the current direction was highly variable (Fig. 3.9), there was a residual displacement directed towards the east-southeast at the surface and to the southeast at the bed (Fig. 3.13). In the second half of the deployment period the displacement was considerably larger and directed towards the north-northwest at the surface and northwest at the bed. The final net displacements of the near-surface and near-bed waters were 130 km to the north and 20 km to the west, respectively.

The near-bed current speed can be used to estimate the current-induced bed shear stress, τ_c , using the quadratic stress law (e.g. Soulsby, 1997), as follows:

$$\tau_c = \rho C_D \bar{U}^2 \quad (12)$$

where C_D is the drag coefficient and \bar{U} is the time-averaged horizontal velocity measured at 1 m above the bed. In this case we only have the velocity at 1.6 m above the bed available, which will result in a slight over-estimate of τ_c . A C_D value representative of the grain size at the deployment site, assuming an unrippled bed, is 0.0026 (see Soulsby, 1997). This approach

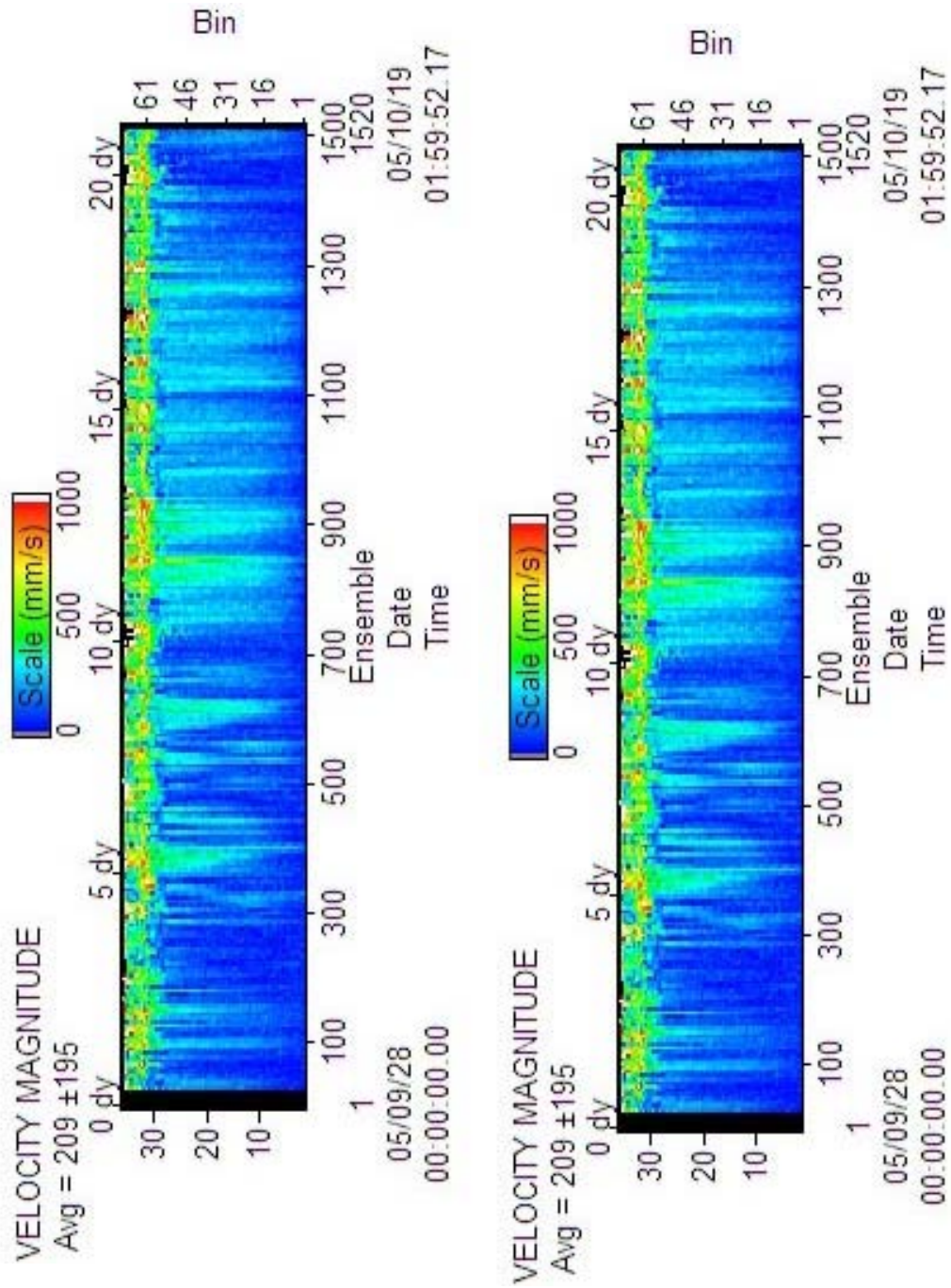


Figure 3.9. Twenty minute time series of current velocity magnitude and direction measured across sixty-nine 0.5 m bins extending from 1.6 m above the bed to the sea surface.

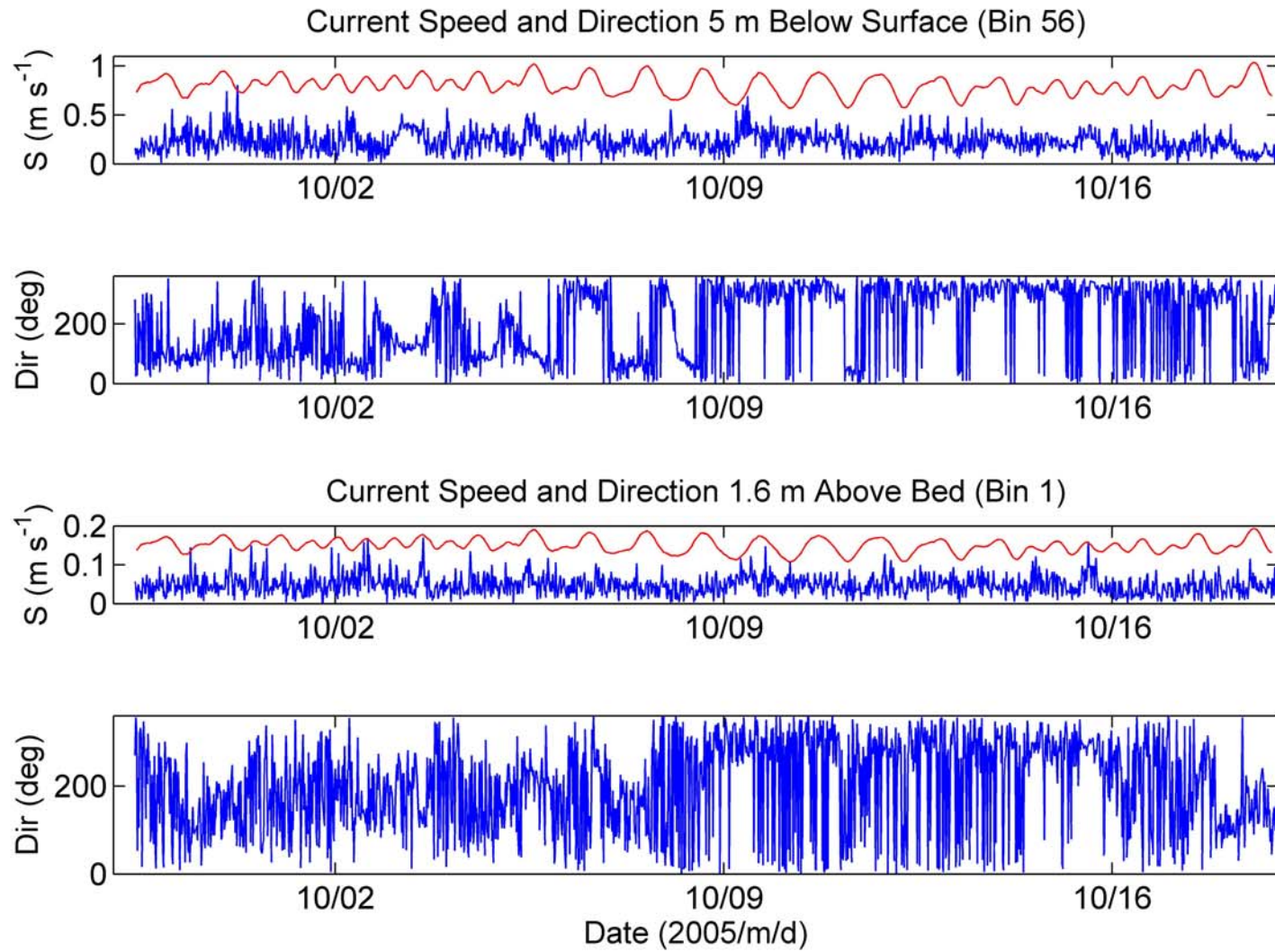


Figure 3.10. Twenty-minute averages of current speed (S) and direction (Dir.) measured 5 m below the sea surface (top two panels) and 1.6 m above the bed (bottom two panels). The red line shows the tidal elevation (arbitrary scale) for comparison

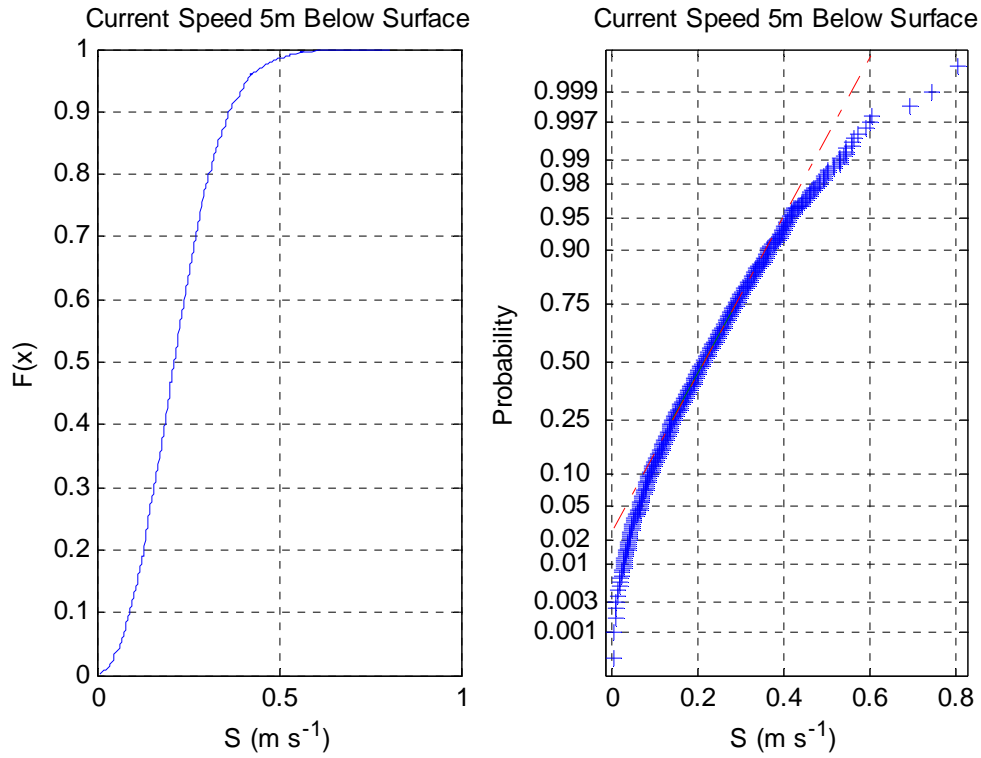


Figure 3.11. Cumulative frequency plot (left) and normal probability plot (right) of near-surface (Bin 56) current speed S .

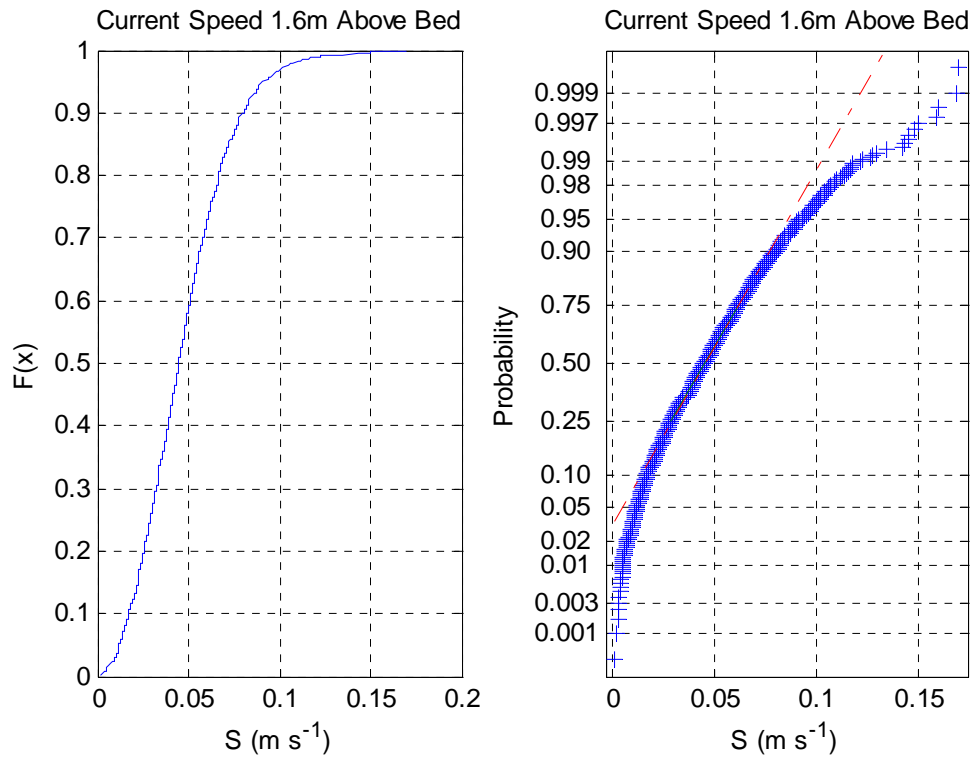


Figure 3.12. Cumulative frequency plot (left) and normal probability plot (right) of near-bed (Bin 1) current speed S .

yields the skin friction value of the current-induced bed shear stress and a cumulative frequency distribution (Fig. 3.14). The bed stresses are clearly not normally distributed, but in the absence of any theoretical distribution no other probability distributions were tested.

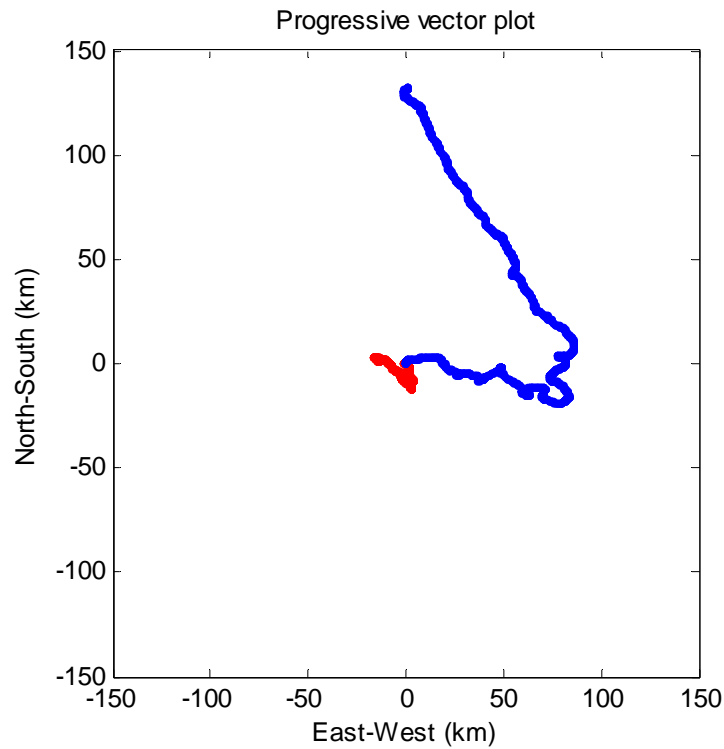


Figure 3.13. Progressive vector plot showing the displacement of the near-surface (blue) and near-bed (red) currents. The origin represents the beginning of the deployment.

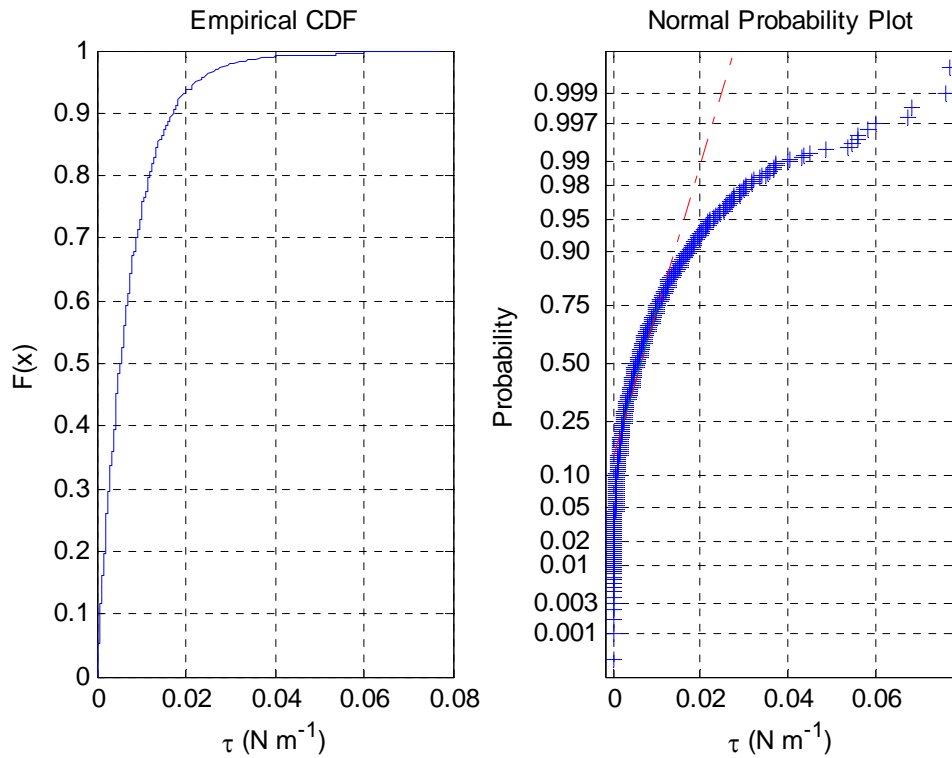


Figure 3.14. Cumulative frequency plot (left) and normal probability plot (right) of skin friction bed shear stress τ over the deployment period. τ was estimated using Equation 12.

The bed shear stress due to currents exceeded 0.005 N m^{-2} 50 % of the time and 0.04 N m^{-2} 1% of the time. The critical bed shear stress required to initiate sediment motion $\tau_{cr} = 0.21 \text{ N m}^{-2}$

(calculated in [section 3.2.1](#)) was not exceeded. Even assuming wave ripples were present, thus increasing the drag coefficient threefold and the bed shear stress correspondingly, the critical stress was still not exceeded by currents alone. It appears then that, at least during the deployment period, waves would have been the only effective mechanism for stirring the bed sediment (see [section 3.2.1](#)). It should be noted that the sediment mobilising effects of waves and currents combined are non-linear and should not be considered a simple sum of the wave- and current-induced bed shear stresses estimated here. The effects of wave-current interaction could be explored using the available data. Such a sophisticated analysis, however, is beyond the scope of this report. The necessary information to undertake such an analysis can be found in Nielsen (1992) or Soulsby (1997).

4. Sedimentology

4.1. SAMPLE ACQUISITION

A total of 30 stations were occupied during the survey (Fig. 4.1; [Table 4.1](#)). The location of the stations were designed to capture the full spectrum of sedimentary environments and habitats including shelf environment (station 1), the near shelf cutting Perth Canyon (stations 2, 26 and 28-30), deep water “blind” canyons (stations 5-8, 10-19, 23-25) and adjacent slope (stations 3, 4, 9, 20-22 and 27). Several operations were undertaken at each station in order to characterise the seabed sediments, sedimentary processes, and biota and habitats.

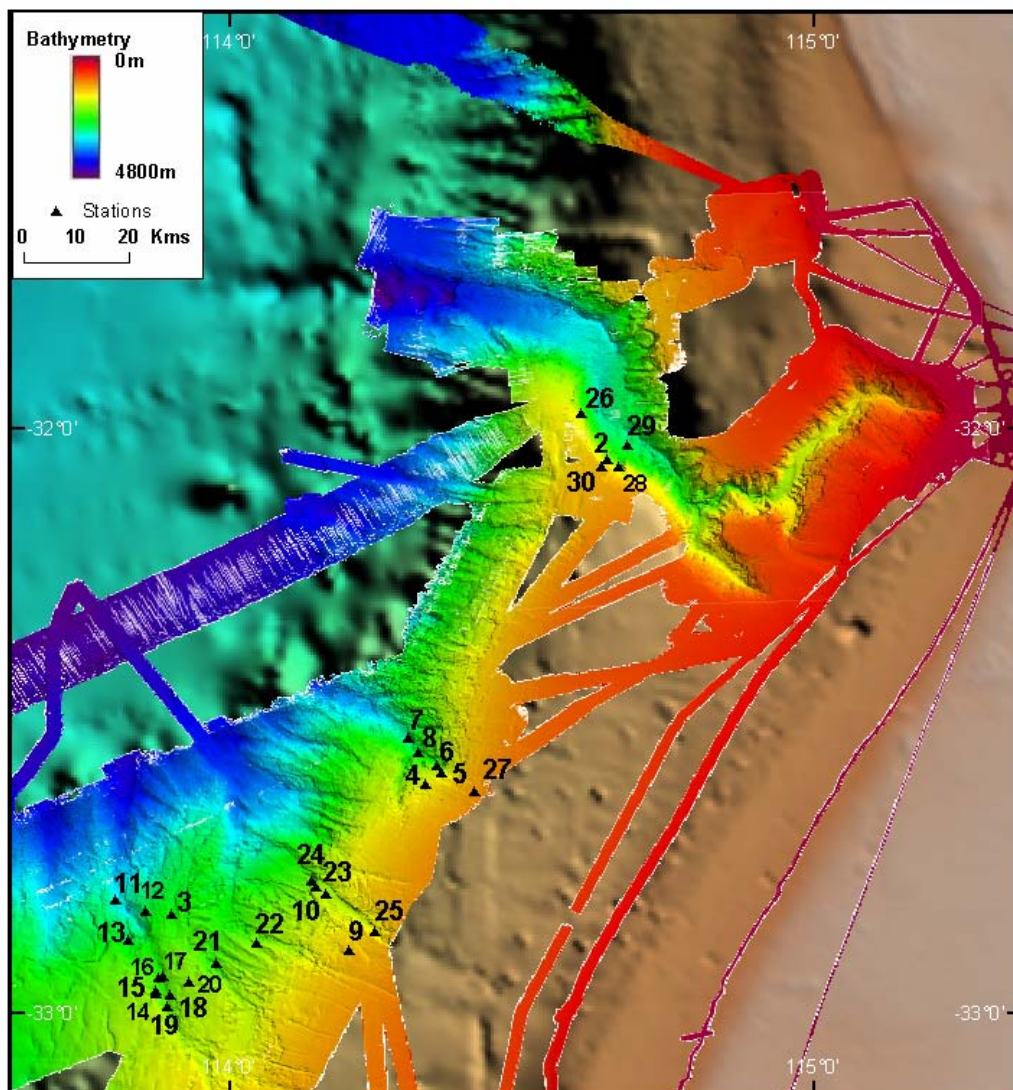


Figure 4.1. Multi-beam (swath) bathymetry image showing sample stations for SS08/2005 Survey. Stations were occupied in the Perth Canyon (stations 2, 26, and 28-30), Busselton Canyon (stations 5-8), Geographe Canyon (stations 10, 23-25), Bunbury Canyon (stations 11-19), canyon interfluvies and slope (stations 3, 4, 9, 20-22 and 27).

Table 4.1. Station operations.

Station	Camera	Grab	Core	Dredge	Benthic sled	CTD	Current meter
01	CAM14	GR01, 02, 03	-	-	-	CTD06	TG01
02	CAM12	-	GC23, 24	DR01, 10, 11	-	CTD01	-
03	-	-	GC12	-	-	CTD02	-
04	-	-	GC01	-	-	-	-
05	CAM09	-	GC02	-	-	-	-
06	-	-	GC03	-	-	-	-
07	CAM02, 10	-	GC04	-	-	-	-
08	-	-	GC05	-	-	-	-
09	CAM03	-	GC06, 07	-	-	-	-
10	-	-	GC08, 09	-	-	-	-
11	-	-	GC10	-	-	-	-
12	CAM04	-	GC13	-	BS01	CTD03	-
13	-	-	-	DR02	-	-	-
14	-	-	-	DR03	-	-	-
15	-	-	-	DR04	-	-	-
16	-	-	GC11	-	-	-	-
17	-	-	GC14	-	-	-	-
18	-	-	GC15	-	-	-	-
19	CAM06	-	GC16, BC01	-	-	CTD04	-
20	-	-	-	DR05	-	-	-
21	-	-	GC17	-	-	-	-
22	-	-	-	DR06	-	-	-
23	-	-	GC18A	DR07	-	CTD05	-
24	-	-	GC18	-	-	-	-
25	CAM07	-	GC19	-	BS02	-	-
26	-	-	GC21	DR09	-	-	-
27	CAM08	-	GC20	DR08	-	-	-
28	-	-	GC22	DR12	-	-	-
29	CAM13	-	-	-	-	-	-
30	CAM11	-	-	-	-	-	-

4.1.1. Water Samples

A Seabird™ SBE911 CTD was deployed with a Seatech transmissometer, calibrated to measure suspended sediment concentration using surface and near-bed water samples (Fig. 4.2). The CTD was deployed from the starboard A-frame and automatically recorded salinity (‰), temperature (°C), and transmission (%). Water samples were collected using Niskin bottles fixed to the CTD rosette, which were fired remotely from the ship. Samples were collected at 10 m from the bed, from each of the different water masses, and 2 m from the water surface.



Figure 4.2. Photograph of CTD rosette deployed from starboard A-frame. Niskin bottles were attached to the rosette to collect water samples from the water column.

4.1.2. Still Camera

A Benthos deep-sea 35 mm colour film camera (serial #135) and strobe (serial #087) was hired from the Department of the Environment and Heritage, Australian Antarctic Division (<http://www.aad.gov.au>) and used to take high-resolution still images of the seabed. The camera was mounted onto a 3 m x 1 m steel frame and connected to the strobe that fired once the trigger weight touched the seabed (Fig. 4.3). The camera and trigger weight were set up to take pictures approximately 3 m above the seabed, which corresponded to an area of the seabed of approximately 1.8 m by 1.8 m. To accurately locate the camera on the seabed, a pinger was also attached to the frame. The height of the camera above the seabed was accurately located using the ship's echo-sounder display which recorded the soundings from the pinger (Fig. 4.3). Because of its relatively light weight compared with the weight of the wire, the camera was deployed at 20 m min⁻¹ to prevent the wire overtaking the frame; recovery was at 40-45 m min⁻¹.

At each camera station, photographs were taken at up to 6 positions spaced approximately 200 m along a 600-1,200 m transect, with repeat photographs taken at each position (Fig. 4.4). Between each position, the camera was raised up to 50 m above the seabed and the ship moved to the next position. Each roll of film contained 800 frames. In practice, only 60-100 frames were exposed at each camera station. However, most frames were taken in the water column during deployment and recovery due to the heaving and pitching of the ship and were not useful for analysis.

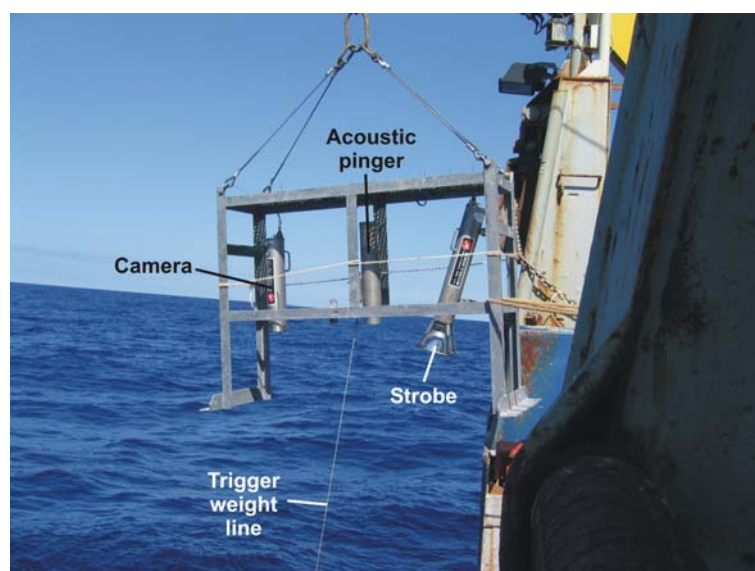


Figure 4.3. Benthos deep-sea 35 mm colour film camera and strobe. The camera frame was fitted with an acoustic pinger for accurate location above the seabed. The camera was triggered by a weight 3 m beneath the frame, which resulted in a still image of the seabed of 1.8 m x 1.8 m.

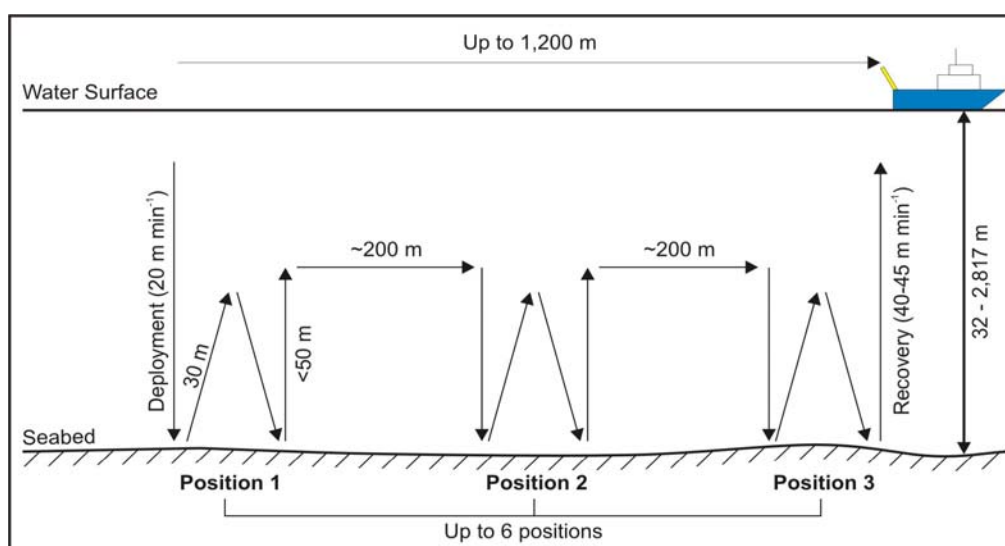


Figure 4.4. Diagram showing the typical configuration of camera tows collected at each station. Photographs were taken at up to six positions spaced approximately 200 m apart along a transect up to 1,200 m long. Two photographs were taken as replicates at each position. The camera was raised up to 30 m between photographs and up to 50 m between positions.

4.1.3. Surface Sediment Sampling

Surface sediments were collected using a rock dredge, Smith McIntyre grab, and epibenthic sled (Figs. 4.5-4.7). Station locations included the Perth Canyon, “blind” canyons to the south and several slope and shelf locations (Table 4.1; Fig. 4.1). Details of samples and sub-samples were entered into Geoscience Australia’s Marine Samples database (MARS; <http://www.ga.gov.au/oracle/mars>).

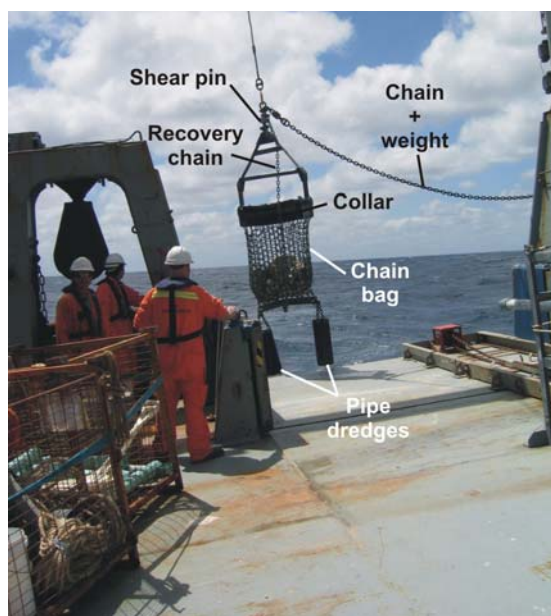


Figure 4.5. Rock dredge used to sample lithified, partially-consolidated and unconsolidated deep-sea sediments. The dredge consists of metal collar, chain bag and pipe dredges to sample all fractions. The dredge was towed behind the vessel for 500 m to several km depending on seabed slope, extent of sediment outcrop and water depth.



Figure 4.6. Photograph of Smith-McIntyre grab sampler used on the survey. The grab collects about 0.1 m³ of sediment in the jaws. The jaws are released when the pads hit the seabed releasing the trigger mechanism. The Smith-McIntyre grab was deployed from the starboard A-frame. A total of three grabs were obtained from Station 01 in 32 m of water SW of Rottneest Island.

4.1.3.1. Rock Dredge

Lithified, partially-lithified and unconsolidated seabed samples were recovered with a rock dredge towed behind the vessel. The rock dredge comprises a 0.5 x 1 m rectangular-shaped metal collar to which is attached a 1 x 1 m chain bag. Attached to the base of the chain bag are two pipe dredges to collect finer material (Fig. 4.5). Dredging was undertaken using the port trawl winch. To ensure successful recovery of rocks a 500 kg weight was attached 10 m in front of the dredge to a chain connected to the trawl wire. In each case a shear pin and recovery chain were attached to the dredge as a 'weak-link' in case of hook-ups and to prevent too much strain being imparted to the wire. In all cases, the total wire paid out for dredging was twice the water depth. Dredges were typically 500 m to several km in length depending on the extent of suitable rock outcrop, seabed slope, and water depth.

4.1.3.2. Smith McIntyre Grab

Samples of the seabed at Station 01 were collected using a Smith-McIntyre grab deployed from the starboard A-frame (Fig. 4.6). Sediment sub-samples were double bagged, labelled (including an aluminium tag), and stored in a refrigerated container. The sub-samples were analysed for grainsize distribution and carbonate content analysis at Geoscience Australia.

4.1.3.3. Epibenthic Sled

An epibenthic sled hired from Woods Hole Oceanographic Institute (WHOI) was used at two stations to collect samples of epibenthic biota (Table 4.1). The benthic sled comprised a plastic net attached to a 1 m wide metal frame that was lowered to the seabed and then towed along the seabed behind the ship (Fig. 4.7). Surface sediments and the epibenthic biota collected in the net were then brought on board with the sled. Sub-samples were taken for

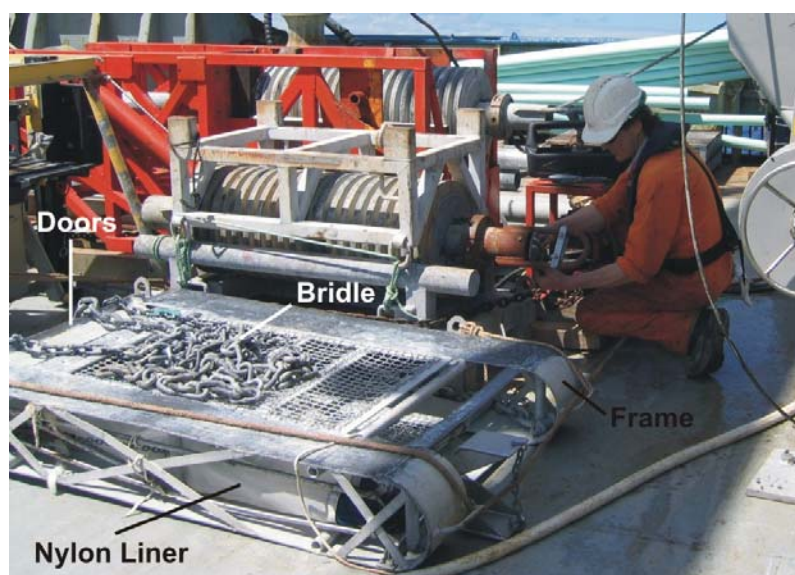


Figure 4.7. Photograph of benthic sled used on the survey, which is towed along the seabed behind the ship. Benthic biota collects in the nylon liner, and the doors close over the liner when the sled is raised off the seabed to prevent the sample from being lost on recovery.

sediment grainsize distribution and carbonate analysis (e.g., 25BS02A) and biology (e.g., 25BS02B). The biological sub-sample was sieved on board and the remaining biota picked, sorted, identified and photographed. Biological samples were frozen for transport to the Victoria Museum for formal identification. Sub-samples of the sediment were also frozen and transported to the Victoria Museum for formal identification of the meiofauna (<1 mm) fraction. At the time of writing, the formal analysis of the biological samples had not commenced.

4.1.4. Subsurface Sediment Sampling

Sub-surface sediments were sampled using a gravity corer that consisted of a 90 mm diameter, 6 m-long steel barrel connected at the top to a 1.5 ton lead “bomb” fitted with a flapper valve to let water out of the barrel (Fig. 4.8a). A 84 mm diameter, 6 m-long PVC liner was used to contain the sediment inside the barrel and a core catcher was fitted to the base of the barrel to enhance core recovery. The core was deployed and retrieved using a hydraulically-powered cradle and the ship’s main coring wire and winch (Fig. 4.8b). Once the core was clear of the transom, it was lowered to approximately 50 m above the seabed at 30 m min⁻¹ and then left to stabilise for up to 5 minutes. The brake on the winch was then released to allow the corer to “free-fall” under its own weight to the seabed (speeds reached >110 m min⁻¹ on impact), and extra wire payed-out to ensure maximum penetration. Recognition that the core had penetrated the seabed was determined by a sharp decrease in the tension on the wire. Usually, good core recovery could be estimated by a sharp and large increase in tension associated with pulling the corer out of seabed. The core was then brought to the surface at 40-45 m min⁻¹. Previous experience has shown that this procedure produces excellent recovery (up to 6 m) in deep-sea sediments.

Once recovered on board the ship, the PVC core liners containing the sediment were cut into 1.0 m sections, sealed with end caps (and packed with high-density foam biscuits where necessary), labelled, engraved, and stored in a refrigerated container before being

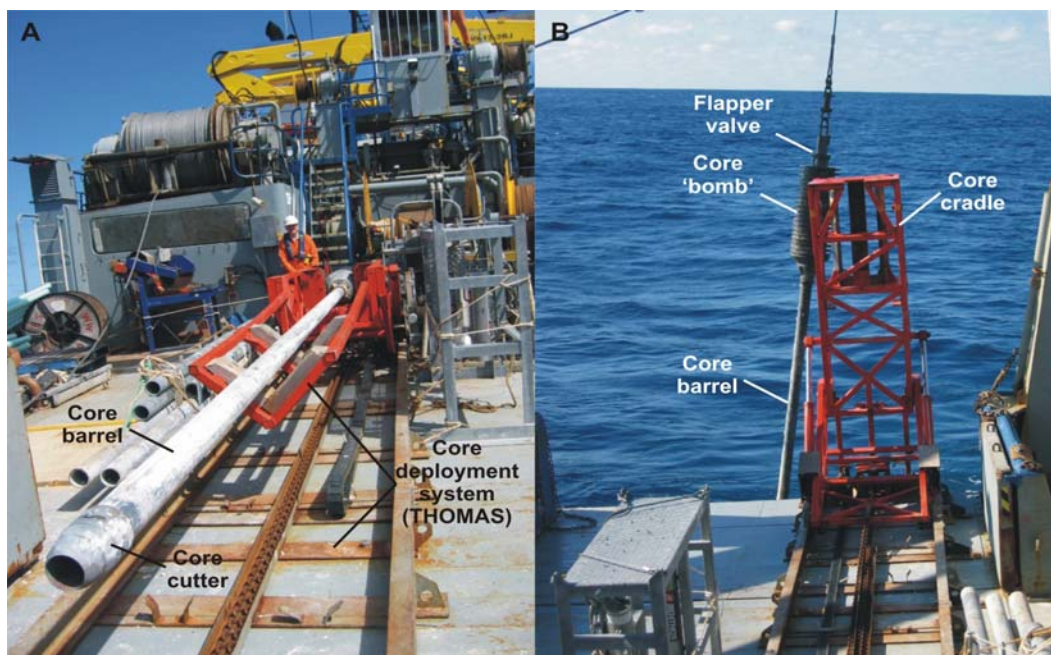


Figure 4.8. Photographs showing: a) gravity core configuration, and b) deployment using the hydraulically-powered cradle.

transported to Canberra for geophysical logging and sub-sampling for grainsize distribution and carbonate content analysis (see below). All sample and sub-sample details were entered into the MARS database.

4.1.5. Other Survey Samples

Thirty-one samples from previous surveys conducted in the region were incorporated into the results for the SS08/2005 survey for regional context (Fig. 4.9). These samples were collected by rock dredge and gravity cores. Analyses of sediment texture and composition have been included from: 19 samples from Bureau of Mineral Resources surveys 80 and 81 conducted in 1988, 8 samples from Geoscience Australia survey SS07/2005 (GA296) conducted in 2005, and 4 samples from national facility survey SS09/2005 conducted in 2005, have been used as supporting data in drawing our regional comparisons on the seabed environments and associated benthic habitats.

4.2. SAMPLE PROCESSING AND ANALYSIS

4.2.1. Water Samples

One litre of water was filtered through pre-weighed 0.45 μm mesh glass filter papers using a vacuum system on board the vessel (Fig. 4.10). The filter papers were then stored in a dry freezer and oven dried at 60° C and re-weighed to ± 0.0001 g to obtain the weight of suspended sediment.

4.2.2. Still Camera

Each 100 ft roll of 35 mm colour positive slide film was developed on the vessel. The slides were then digitally scanned at 1200 dpi. The digital images were cropped to remove as much of the dark portion of the image that was not within the range of the flash. Images were then

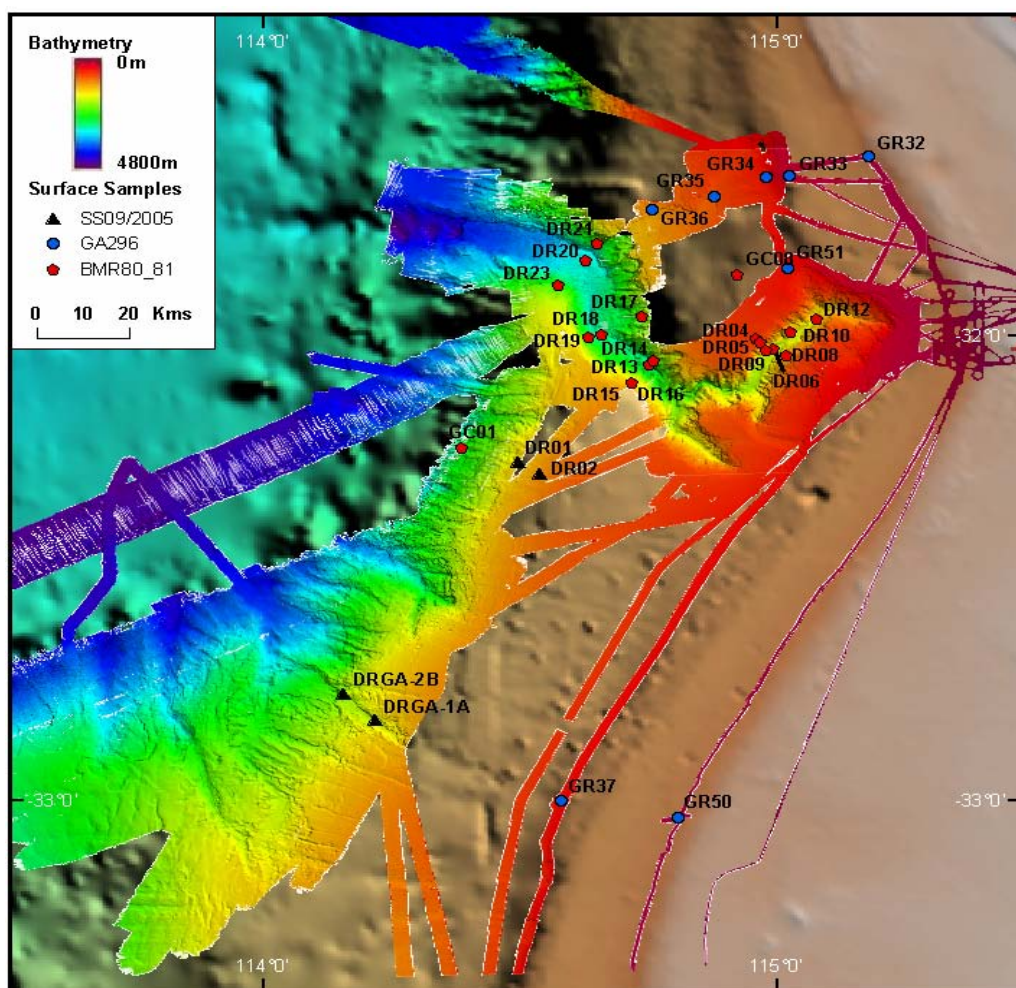


Figure 4.9. Multi-beam (swath) bathymetry image showing location of other survey surface samples incorporated into the results of SS08/2005 survey for regional context.

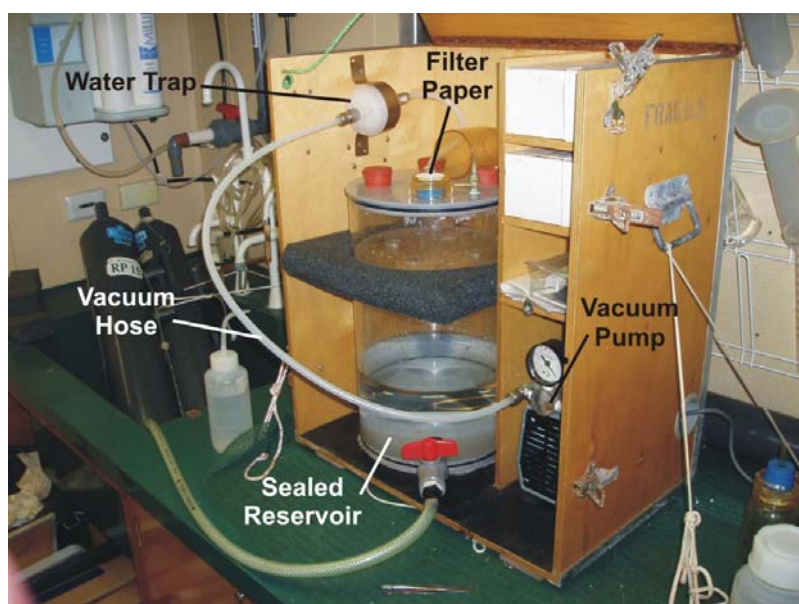


Figure 4.10. Photograph showing Geoscience Australia's purpose-built water filtering system. A total of 1 litre of seawater is filtered through 45 μm mesh filters. The filter papers are then weighed in the laboratory to determine total suspended solids (sediments).

converted to black and white to aid contrast and identification of biota and physical structures. Finally, photo station location, water depth, time and scale bar were added.

4.2.3. Surface Sediment Samples

4.2.3.1. Calculation of Dredge Layback

The location of the dredge path is often several kilometres behind the vessel. The distance the dredge is behind the vessel is the layback, which must be accounted for when determining the location of samples collected in the dredge. Variables required to estimate the dredge path include: the length of wire out, the seabed profile, vessel location, and direction of travel. The following procedure was used to estimate the layback and dredge path for this survey:

- i. The vertical geometry (i.e., the seabed profile and the sea surface) of the dredge path was plotted at a constant scale on graph paper, noting any rapid changes in water depth.
- ii. The locations of the vessel at the start and end of dredging, using the first bite as the start point and the last bite as the end point, were then used to determine the distance over the seabed the dredging occurred by applying the Vincenty Inverse Method calculator (Vincenty, 1975). This calculator is available on Geoscience Australia's website (http://www.ga.gov.au/geodesy/datums/vincenty_inverse.jsp). In cases where no bites were recorded the location of the vessel when the dredge first hit the seabed was used as the start point. If wire was still being paid out at this location, then the position of vessel when all wire was paid out was used. The Vincenty Inverse Method calculator provides the direction of travel, which is needed for step v. The calculated distance was then plotted on the same scale as the water depth on the graph paper.
- iii. The total wire out (m) was then reduced by between 5% and 10% to account for the bow in the wire. This distance was then plotted on the graph paper so that the end of the wire intersected the seabed; this location on the seabed is the position of the dredge. Where bites were used to determine the start and end points of the dredge path was assumed that the bow was 5% to account for the additional stretch on the wire, otherwise 10% was used.
- iv. The position of the dredge was then extrapolated to the sea surface and the distance between this point and the vessel position is the estimated layback.
- v. The layback, position of vessel, direction of travel (step ii), at the start and end points of the dredge were then used to determine the dredge path using the Vincenty Direct Method calculator (http://www.ga.gov.au/geodesy/datums/vincenty_direct.jsp).

Start and finish locations and dredge path are only estimates and errors of >100 m are likely using this method. Errors arise from inaccuracies associated with plotting the profile on the graph paper, changes of vessel direction during dredging, and from inaccurate estimates of the amount of bow in the wire.

4.2.3.2. Sediment Texture

Initially, the bulk sample was split into two sub-samples for grain size analysis. Bulk grain size distributions and mean grain size were determined for the first sub-sample using a Malvern™ Mastersizer-2000 laser particle size analyser (e.g., Heap *et al.*, 1999). After rinsing

Table 4.2. Mean grainsize descriptions after Krumbein and Sloss (1963).

Mean grainsize interval (μm)	Description	
0 – 2	Fine-medium clay	
2 – 4	Coarse clay	
4 – 8	Very fine silt	Mud
8 – 16	Fine silt	
16 – 31	Medium silt	
31 – 63	Coarse silt	
63 – 125	Very fine sand	
125 – 250	Fine sand	
250 – 500	Medium sand	Sand
500 – 1,000	Coarse sand	
1,000 – 2,000	Very coarse sand	
2,000 – 4,000	Granules	Gravel
>4,000	Pebbles and larger	

thoroughly with distilled water, the sample was placed in an ultrasonic bath for up to 2 mins to break up any remaining aggregates before being analysed by the laser particle size analyser. Mean laser grainsize results are divided into 13 descriptive categories based on the commonly used sedimentological descriptions of Krumbein and Sloss (1963) (Table 4.2).

4.2.3.3. Sediment Composition

Carbonate concentrations were determined on all of the bulk samples, as well as the sand and mud fractions using the “carbonate bomb” method of Muller and Gastner (1971). Initially the 3-5 g of bulk sample was dried in an oven at 40° C for 24 hours. This sample was then ground to a fine powder and exactly 0.8 g was reacted with 10 ml of orthophosphoric acid (H_3PO_4). The flask was agitated until the entire sample had reacted with the acid (usually about 60 s). The pressure of the gas liberated was then compared to a standard curve that converted the pressure into carbonate concentrations (the curve is constructed by reacting known amounts of pure calcium carbonate between 0.1 – 0.8 g and recording the corresponding pressure). The carbonate content of the gravel fraction was estimated from a visual inspection for all samples.

Samples were also visually inspected in the laboratory for composition within the sand fraction (63-2000 μm). Point counting of individual grains was carried out on the 125-2000 μm fraction. The sand fractions were dry sieved through a 125 μm mesh resulting in a 63-125 μm and a 125-2000 μm fraction. Due to the difficulty examining small grains within the 63-125 μm fraction samples were briefly examined to determine the main components and no point counting of the grains in this fraction was carried out. A small portion of the 125-2000 μm fraction was spread over a gridded picking tray and examined using a standard binocular microscope. Approximately 300 individual grains were counted and separated into planktic and benthic foraminifera, sponge spicules, ostracods, radiolarians, pteropods, mineral grains, fragments, other/unknown, and the results converted to percentage.

The abundance of foraminifera was compared to the number of fragments in a sample and expressed as a fragmentation index as follows:

$$\text{Fragmentation Index (\%)} = F/(W+F)*100 \quad (13)$$

where F = foraminifera fragments and W = whole foraminifera (Berger, 1970).

The foraminifera fragmentation index in deep-sea sediments can provide information about carbonate dissolution, the energy levels at the sea floor, and the transfer of shelf sediments down slope (Berger, 1970). Shelf sediments are exposed to higher energies from the actions of waves and tides, resulting in greater fragmentation of foraminifera and other bioclasts on the shelf compared with the deeper-water environments (i.e., slope, rise, abyssal plain/deep ocean floor). Samples from this survey were not separated into individual fragment categories (e.g., foraminifera, ostracod, or pteropod fragments). However, in most samples foraminiferal fragments comprised >95% of all fragments. Samples with relatively high proportions of other fragments are noted in the results.

4.2.4. Subsurface Sediment Samples

4.2.4.1. Physical Properties

After equilibration with ambient laboratory conditions (between 18° and 20°C), wet bulk density (WBD), P-wave Velocity (Vp), Fractional Porosity (FP), Magnetic Susceptibility (MS), and the sediment colour spectrum (RGB) were determined at 0.01 m intervals down GC01-24 using a GEOTEK™ MS2 multi-sensor core logger (e.g., Heap *et al.*, 2001).

Wet bulk density (WBD) was determined by measuring the gamma attenuation of the sediment from a Cs-137 source. WBD of the sediment is positively correlated with gamma attenuation. The relationship between density and gamma attenuation was initially calibrated using a graduated density standard consisting of 13 water/aluminium density components (e.g., Best and Gunn, 1999). This procedure corrects for gamma attenuation (caused by the Al liner), count rate effects (e.g., Weber *et al.*, 1997), and the different scattering properties of seawater and sediment (e.g., Gerland & Villinger, 1995). The calibration was undertaken using a water density of 1.001 g cm⁻³, and aluminium density of 2.71 g cm⁻³, which is approximately equal to the mineral densities of siliciclastic (2.65 g cm⁻³) and carbonate (2.67 g cm⁻³) grains.

P-wave velocity (Vp) was determined by measuring the travel time of a 500 kHz ultrasonic compressional pulse across the core. The pulse propagates through the core from the transmitter and is detected by the receiver. Vp is directly related to changes in the composition and texture of the sediments (e.g., mineral composition, grain shape and size, packing, etc.). To prevent variations in the ambient conditions masking differences between sedimentary units, the Vp was also corrected for temperature of the water and sediment and salinity of the interstitial fluid for each core.

Fractional Porosity (FP) was calculated directly from the WBD using Equation 14:

$$FP = (MGD - WBD) / (MGD - WD) \quad (14)$$

where FP = fractional porosity, MGD = mineral grain density, WBD = wet bulk density, and WD = fluid density (i.e., sea water). This calculation assumes that the sediment was fully saturated with seawater, a mineral density of siliciclastic and carbonate sediment of ~2.65 g cm⁻³, and a fluid (i.e., seawater) density of 1.024 g cm⁻³.

Magnetic susceptibility (MS) was determined by measuring variations in the frequency of the AC waveform with a tuned oscillator circuit using a Bartington Instruments MS2 meter and magnetic loop attached to the multi-sensor core logger. Variations in the

frequency of the AC waveform associated with magnetically susceptible sediment are directly proportional to the MS of the samples (Robinson, 1990). Because magnetically susceptible grains (e.g., magnetite grains) have terrigenous origins, MS can be used as a measure of terrigenous versus marine input. The system was operated with an AC field strength of 80 A/m rms and at a frequency of 0.58 kHz (10 s integration time).

The colour spectrum (RGB) of the subsurface sediment was measured using the GEOTEK Geoscan digital imaging system attached to the multi-sensor core logger. The Geoscan system consists of a 3 megapixel CCD digital camera mounted vertically to the track of the multi-sensor core logger. The whole cores were split and the archived half selected for colour imaging of the exposed surface. After calibrating the camera with black and white standards, and focussing it on the core surface, colour samples were collected at 0.01 m intervals down the core in a 0.05 m wide band located between 4.0–4.5 cm across the surface. Individual objects that skewed the measurements (e.g., voids) were avoided.

4.2.4.2. Sediment Texture

Grainsize distributions were determined from sub-samples of the core-tops (0–2 cm). Initially, the bulk sample was split into two sub-samples for grain size analysis. Bulk grain size distributions were determined using a Malvern™ Mastersizer-2000 laser particle size analyser and through sieving using the same procedures for the surface sampling (see [section 4.2.3.2](#)). At time of writing no down-core samples have been analysed.

4.2.4.3. Sediment Composition

Carbonate content concentrations were determined on bulk core-top (0–2 cm) sub-samples, as well as the sand and mud fractions using the “carbonate bomb” method of Muller and Gastner (1971). The procedure used is the same as that for the surface sediments (see [section 4.2.3.3](#)).

4.2.4.4. Headspace Gas Geochemistry

Two cores (GC07 and GC09) were sub-sampled for headspace gas geochemistry. At the time of writing these samples have not been analysed.

4.3. RESULTS

4.3.1. Water Samples

A total of six CTD casts were taken during the survey ([Fig. 4.1](#); [Table 4.3](#)). CTD and water sample data are located in [Appendix C](#). The CTD data reveal the presence of four major water masses throughout the region ([Fig. 4.11](#)). These water masses are: 1) well-mixed surface layer (0–100 m); 2) stratified oxygen-rich water (100–600 m); 3) stratified oxygen-poor water (600–1200 m); and 4) stratified cold bottom water (>1200 m). All CTD stations have a similar ~100 m deep well mixed surface layer. The oxygen-rich and oxygen-poor water mass boundary varies between 500–600 m. The oxygen-poor and cold bottom water mass boundary is consistent at ~1,200 m.

Minimum, maximum and average values of temperature, salinity, dissolved oxygen and transmission at the water mass boundaries are shown in [Table 4.4](#). Minimal variation in the four parameters occurs at each water mass boundary, except for dissolved oxygen in surface waters (0–10 m), which range from 241.7 mmol l⁻¹ (19CTD04) to 324.4 mmol l⁻¹ (23CTD05).

Table 4.3. Summary details of CTD casts collected on the survey.

SampleID	Location	Latitude	Longitude	Water depth	No. of water samples
02CTD01	Perth Canyon	-32° 03.61'	114° 38.39'	1,356 m	5
03CTD02	Slope	-32° 49.97'	113° 54.22'	2,425 m	9
12CTD03	Bunbury Canyon	-32° 49.49'	113° 51.27'	2,623 m	4
19CTD04	Mentelle Canyon	-32° 59.20'	114° 53.64'	2,199 m	11
23CTD05	Geographe Canyon	-32° 46.90'	114° 08.84'	1,950 m	11
01CTD06	Rottneest Shelf	-32° 02.65'	114° 26.83'	32 m	4

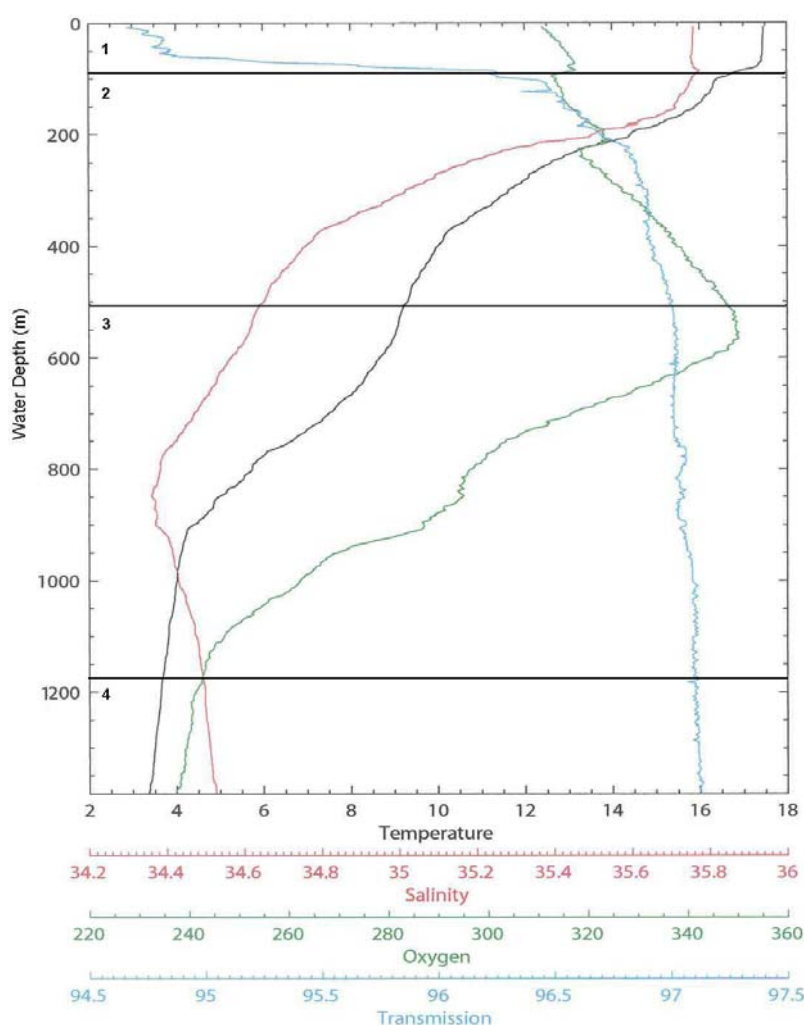


Figure 4.11. CTD profile of 02CTD01. The four main water bodies are labelled 1-4 as in text above.

Surface water (0-10 m) temperature ranges from 17-18°C and salinity from 35.69 to 35.78 ‰. Between 0 and 100 m water depth, the water temperature decreases gradually by ~1-1.5°C. There is a rapid drop in water temperature between 100-1200 m, from ~16°C to ~3.5°C. Below 1,200 m the water temperature decreases much more gradually, with a minimum recorded temperature of 1.8°C at 2,570 m (12CTD03).

Profiles of depth versus temperature, oxygen, salinity and light transmission for the six

Table 4.4. Minimum, maximum and average values for temperature, salinity, dissolved oxygen and transmission at the water mass boundaries shown in Fig. 4.11.

Water depth (m)	Temperature (°C)			Salinity (‰)			Dissolved oxygen (mmol l ⁻¹)			Transmission (%)		
	Min.	Max.	Av.	Min.	Max.	Av.	Min.	Max.	Av.	Min.	Max.	Av.
10	16.93	18.11	17.48	35.69	35.78	35.75	241.7	324.4	302.1	94.69	95.16	95.06
100	15.91	16.45	16.14	35.71	35.75	35.73	311.0	338.3	319.6	95.00	96.43	96.00
600	8.16	8.63	8.31	34.52	34.56	34.53	317.8	343.4	331.7	96.86	97.02	96.96
1,200	3.43	3.64	3.52	34.50	34.51	34.51	230.4	242.8	239.4	97.02	97.08	97.08
2,570*			1.80			34.70			267.6			97.11

*= Maximum water depth of all CTD stations (12CTD03).

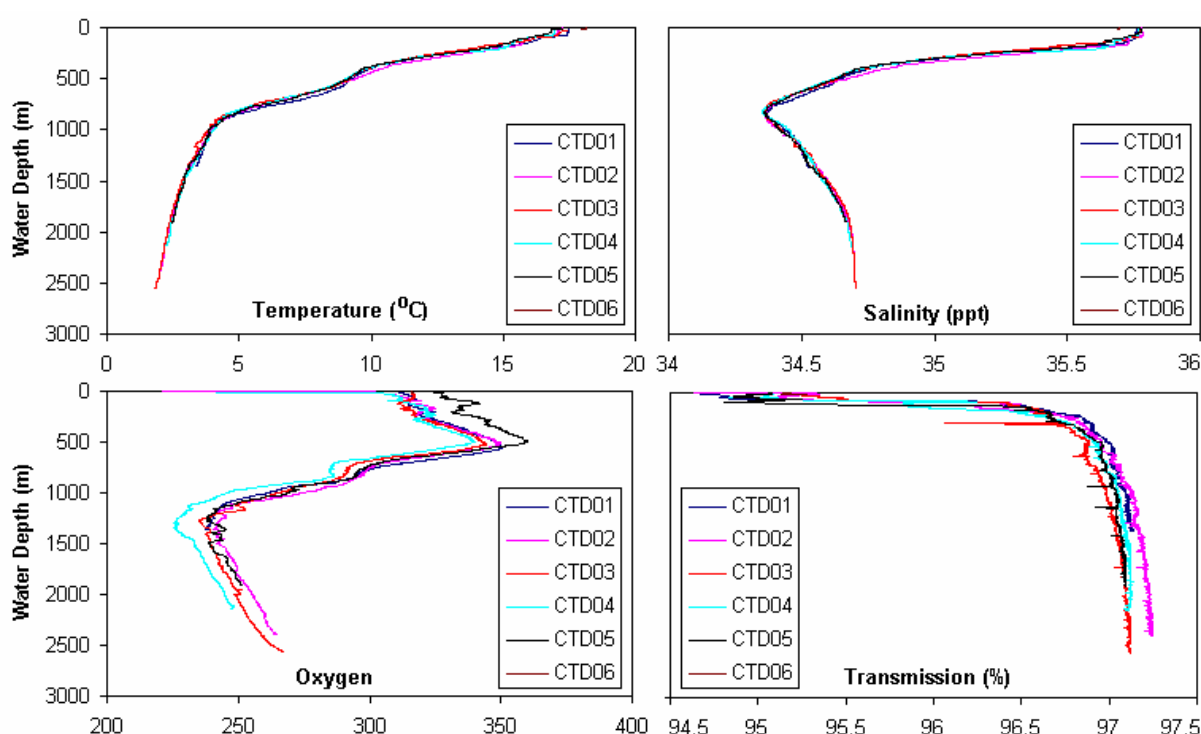


Figure 4.12. Graphs of temperature, oxygen, salinity and transmission profiles for the 6 CTD stations versus water depth.

CTD stations are very consistent (Fig. 4.12). Greatest variation occurs in dissolved oxygen and transmission profiles. Temperature and salinity vary only slightly with depth. There is no correlation between transmission and suspended sediment concentration (SSC) obtained from the filter papers (Fig. 4.13). SSC is highest in the well mixed surface layer (0-100 m) relative to deeper waters (Fig. 4.14).

4.3.2. Still Camera

A total of 12 camera stations were occupied during the survey with a total of 121 photographs taken (Fig. 4.15; Table 4.5; Appendix D). Camera stations were occupied in Perth Canyon, the three “blind” canyons further south (Busselton, Geographe, Bunbury Canyons), and at several locations on the slope and shelf (Figs. 4.15-4.16). This survey recovered the first images of deep sea environments in water depths of >2,000 m for the SW region of Australia. Photographs from most stations reveal varying degrees of mottled and bioturbated soft sediment. Seabed features include a diverse and abundant range of deep-sea

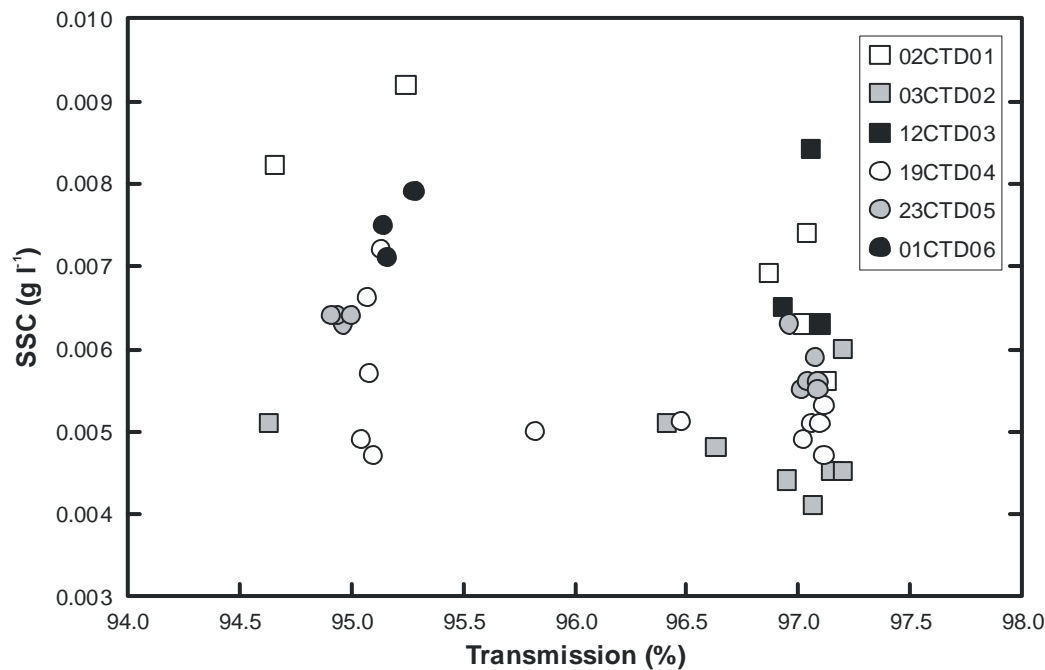


Figure 4.13. Graph of suspended sediment concentration (SSC) versus transmission.

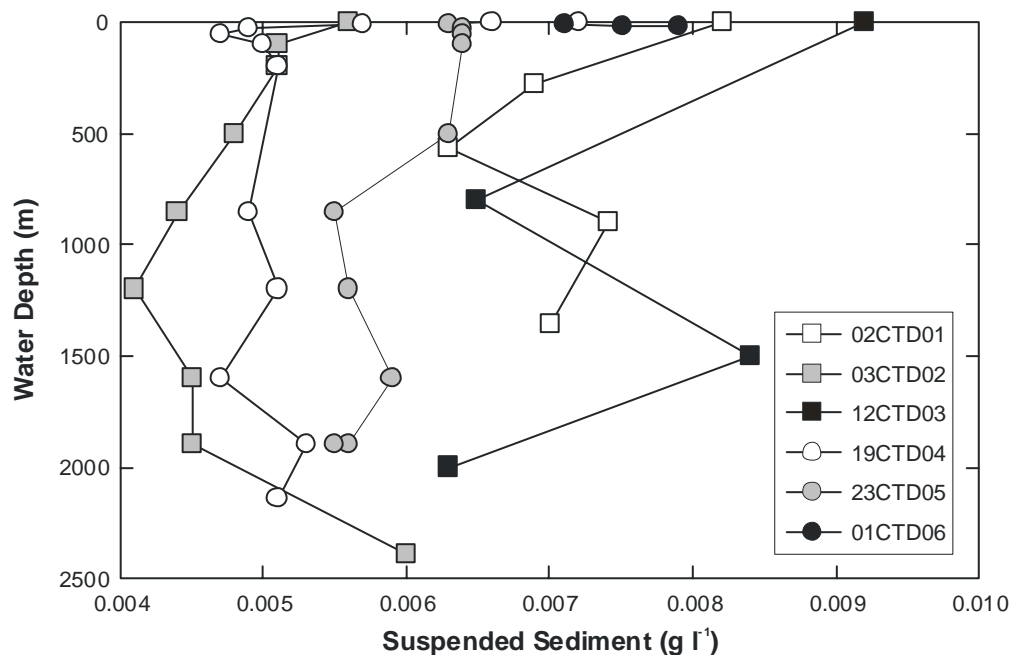


Figure 4.14. Graph of water depth versus suspended sediment concentration.

fauna in both the canyons and on the adjacent slope areas. Crustaceans, burrows, trails, faecal pellets and small infaunal mounds are common at most camera stations.

Small ball-shaped sponges are abundant at several stations on the canyon floors (19CAM06, 25CAM07, 07CAM10, 29CAM13) and less abundant on the upper canyon slopes (07CAM02, 12CAM04). At 25CAM07 between 20 and 40 of these sponges are visible in several photographs (see below). Photographs at the two camera stations on the slope (09CAM03 and 27CAM08) show no ball-shaped sponges, possibly indicating this sponge species prefers canyon floor environments.

Table 4.5. Camera station locations and number of photographs taken.

SampleID	Start latitude	Start longitude	Finish latitude	Finish longitude	Start water depth (m)	Finish water depth (m)	No. of photos
02CAM01	-32° 04.76'	114° 37.12'	-32° 04.76'	114° 37.12'	1,291	1,291	0
07CAM02	-32° 31.11'	114° 19.56'	-32° 31.11'	114° 19.56'	2,369	2,369	1
09CAM03	-32° 53.30'	114° 12.59'	-32° 53.48'	114° 12.59'	1,290	1,290	36
12CAM04	-32° 49.39'	113° 51.48'	-32° 49.75'	113° 51.22'	2,594	2,610	16
19CAM05	-32° 59.23'	113° 53.64'	-33° 00.28'	113° 53.42'	2,160	2,060	0
19CAM06	-32° 59.26'	113° 53.62'	-32° 59.37'	113° 53.62'	2,150	2,150	5
25CAM07	-32° 51.43'	114° 14.95'	-32° 51.60'	114° 15.06'	1,515	1,520	13
27CAM08	-32° 37.31'	114° 25.27'	-32° 37.34'	114° 25.25'	1,090	1,092	11
05CAM09	-32° 35.30'	114° 21.73'	-32° 35.52'	114° 21.77'	1,665	1,657	9
07CAM10	-32° 31.72'	114° 18.36'	-32° 31.95'	114° 18.36'	2,764	2,817	9
30CAM11	-32° 03.69'	114° 38.20'	-32° 04.05'	114° 38.13'	1,280	1,250	7
02CAM12	-32° 03.01'	114° 38.92'	-32° 03.08'	114° 38.92'	2,035	2,030	1
29CAM13	-32° 01.68'	114° 40.87'	-32° 02.05'	114° 40.80'	2,680	2,605	11
01CAM14	-32° 02.64'	114° 26.62'	-32° 02.65'	114° 26.65'	32	34	2

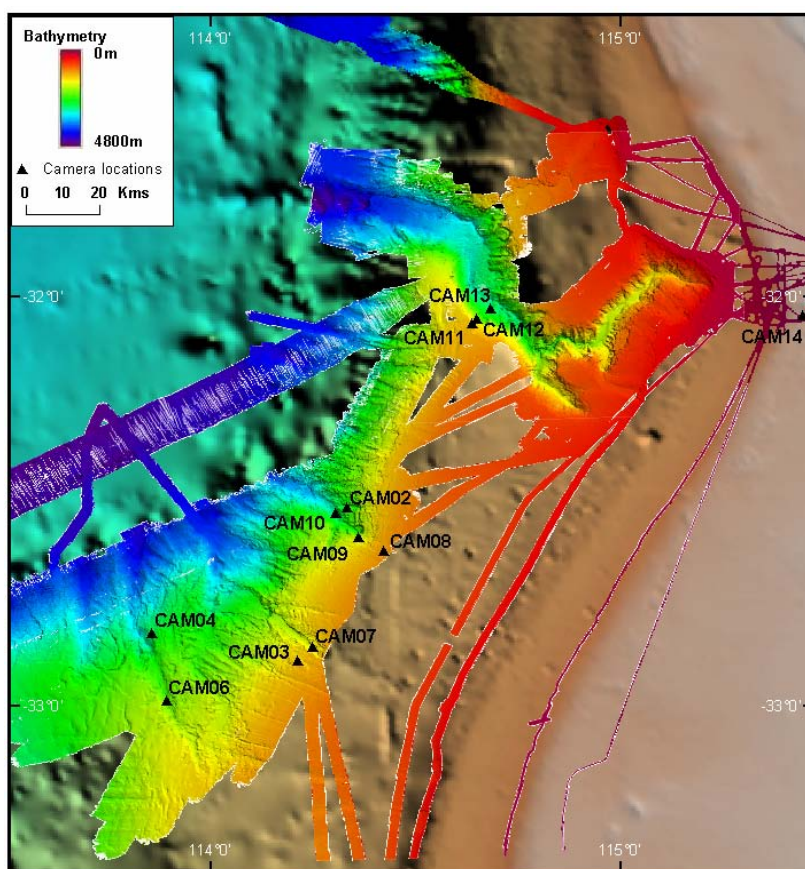


Figure 4.15. Multi-beam (swath) sonar bathymetry image showing the location of camera stations.

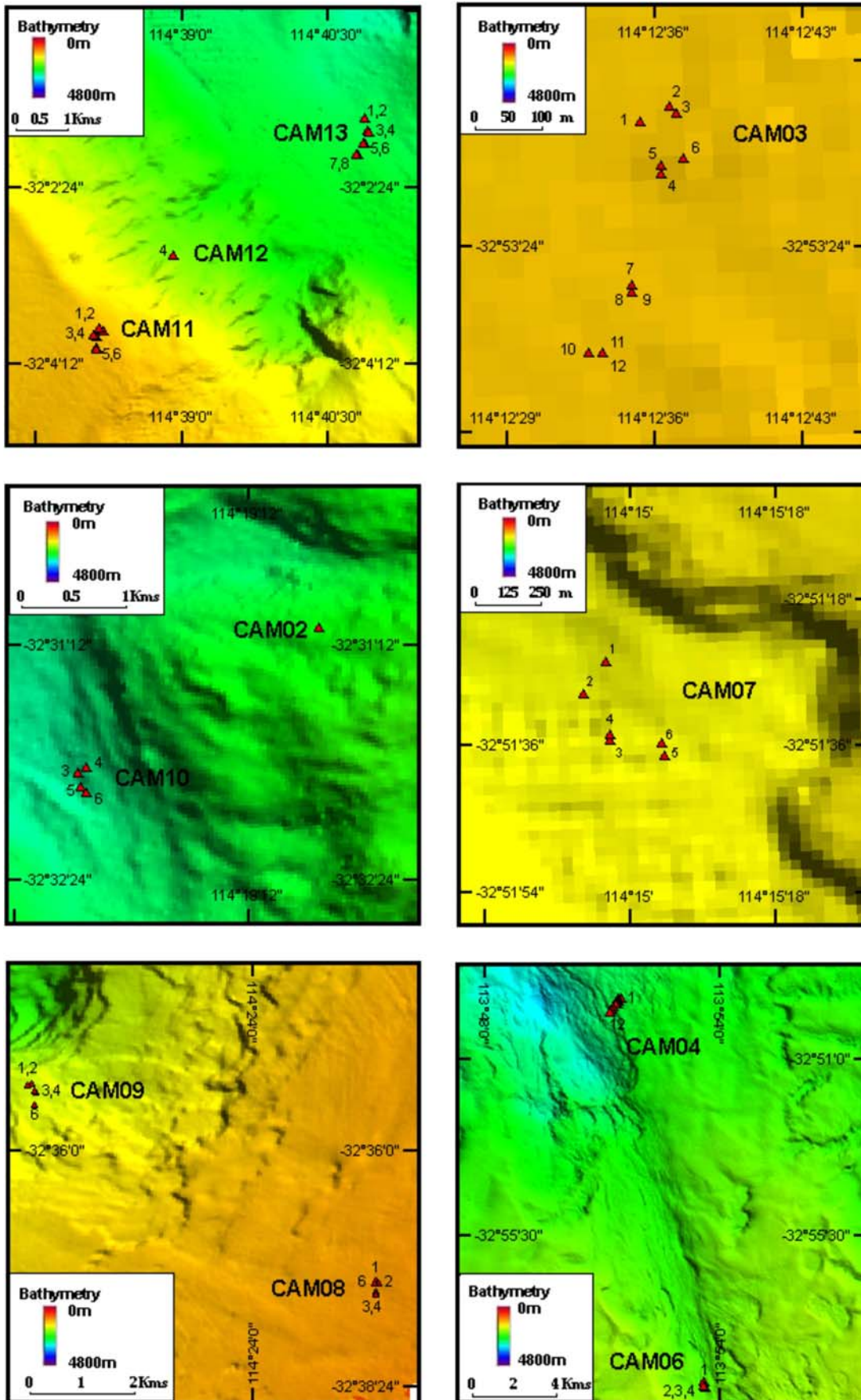


Figure 4.16. Multi-beam (swath) sonar bathymetry images showing detailed locations for camera stations.

Other diagnostic fauna captured in the photographs include: octocorals (27CAM08, 29CAM13), anemones (29CAM13), whiptail fish (30CAM11), shrimp (09CAM03, 27CAM08), *Hexactinellid* glass sponge (09CAM03), *Galatheid* squat lobster (12CAM04), holothurian (12CAM04), commensal brittlestar (29CAM13), and fish (27CAM08).

A brief description of each camera station is provided below with the photographs. All individual photographs and descriptions are presented in [Appendix D](#).

4.3.2.1. Perth Canyon

30CAM11 (upper SE wall; 7 photographs): Mottled sediment with small mounds and holes visible in all photographs (e.g., photograph 04; [Fig. 4.17a, b](#)). Other features include faint trails and a whiptail (photograph 04; [Fig. 4.17a](#)).

02CAM12 (mid-SE wall; 1 photograph): Parallel marks possibly man made trawl marks, but look very irregular spacing so possibly a natural feature ([Fig. 4.17c](#)). Trails and bioturbation cut over parallel marks.

29CAM13 (lower canyon floor; 11 photographs): Mottled sediment, cylindrical shaped holothurian faeces, ball shaped sponges (photograph 05; [Fig. 4.19a](#)), small mounds, trails and burrow holes are visible in most photos. Several long trails are visible in photograph 02 ([Fig. 4.18a](#)). Five large holes most likely crustacean burrows are visible in photograph 03 ([Fig. 4.18b](#)). Photograph 04 ([Fig. 4.18c](#)) reveals long straggling colonies covering most of the surface. Other features in photograph 04 include two branching octacorals, one with a commensal brittlestar attached, and an anemone. In photograph 06 ([Fig. 4.19b](#)) large spiral trail of *Enteropneust* (Acorn worm) faeces is visible.

4.3.2.2. Busselton Canyon

07CAM02 (NE canyon wall; 1 photograph): Mottled, bioturbated sediment with trails, faecal pellets and a ball shaped sponge visible.

05CAM09 (canyon head; 8 photographs): Mottled sediment is visible in all photos. Trails likely from molluscs, small holes and mounds are visible in most photos (e.g., photographs 02 and 08; [Fig. 4.19c](#) and [Fig. 4.20a](#), respectively).

07CAM10 (canyon floor; 7 photographs): Mottled sediment, trails and small mounds are visible in all photographs (e.g., Photographs 01 and 07; [Fig. 4.20b, c](#)). Other features include small ball-shaped sponges (photographs 01 and 07), fan trail (photograph 01), crustacean in burrow (photograph 01) and cylindrical faeces (photograph 01).

4.3.2.3. Geographe Canyon

25CAM07 (upper canyon floor; 13 photographs): Mottled sediment with holes and trails are visible in most photographs. Two large burrows are visible in photograph 04 ([Fig. 4.21a](#)). Small ball-shaped sponges are visible in all photographs with extensive coverage (20 to 40 individuals) (e.g., photograph 10; [Fig. 4.21b](#)).

4.3.2.4 Bunbury Canyon

12CAM04 (upper canyon wall; 11 photographs): All photographs show mottled sediment. A holothurian about 0.25 m long is visible in photograph 11 ([Fig. 4.21c](#)), and a *Galatheid* squat lobster is visible in photograph 16 ([Fig. 4.22b](#)). Camera station 12CAM04 is located on the steep NE flank of Bunbury Canyon and photograph 04 reveals a piece of rubble possibly indicating hard ground below a thin veneer of sediment. The presence of

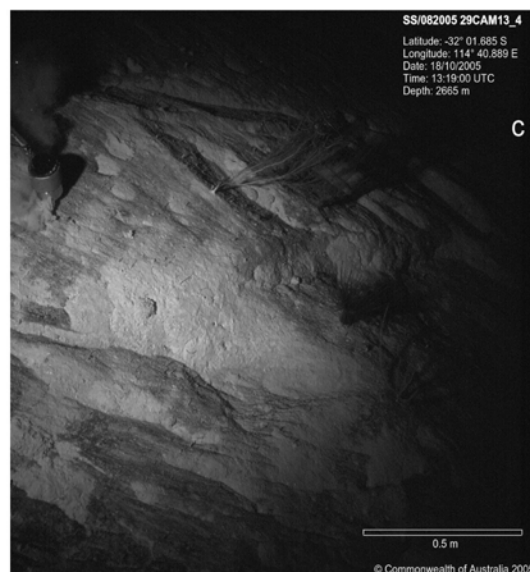
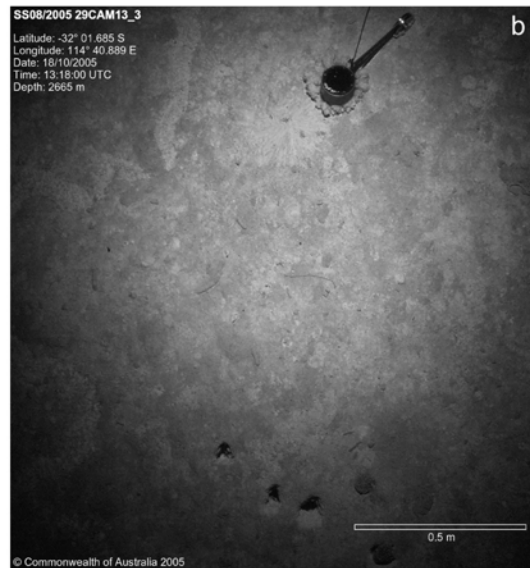
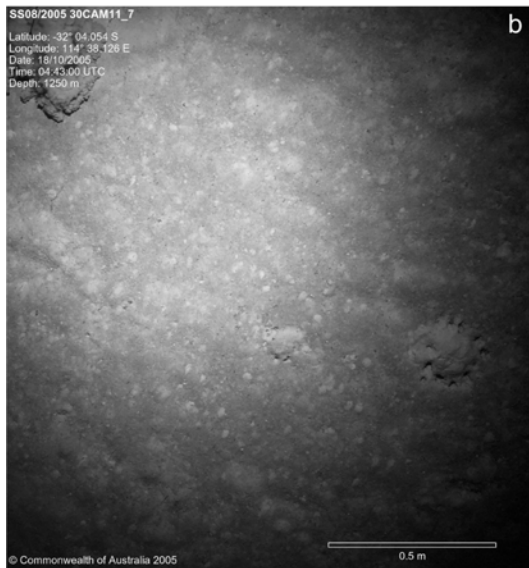
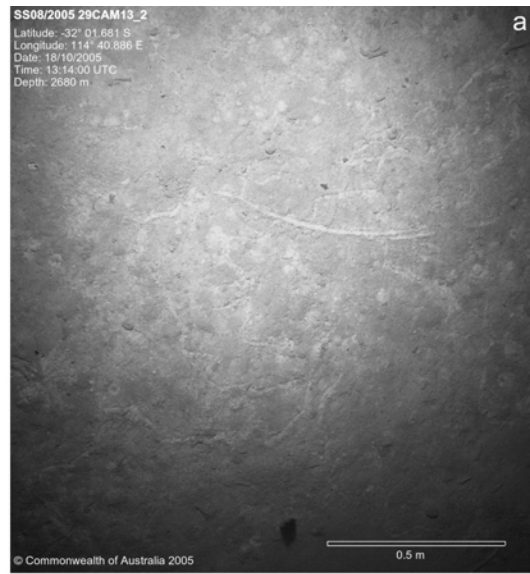


Figure 4.17. a) 30CAM11_4, b) 30CAM11_7, c) 02CAM12_1 (Perth Canyon).

Figure 4.18. a) 29CAM13_2, b) 29CAM13_3, c) 29CAM13_4 (Perth Canyon).

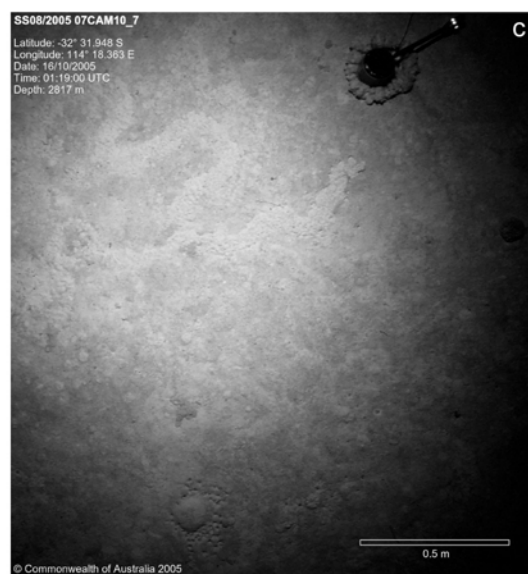
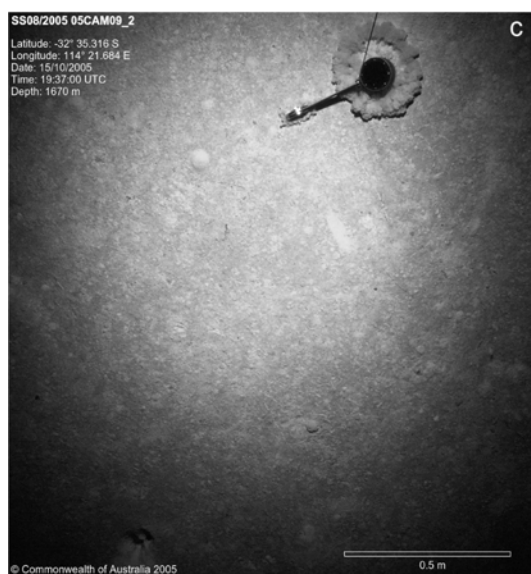
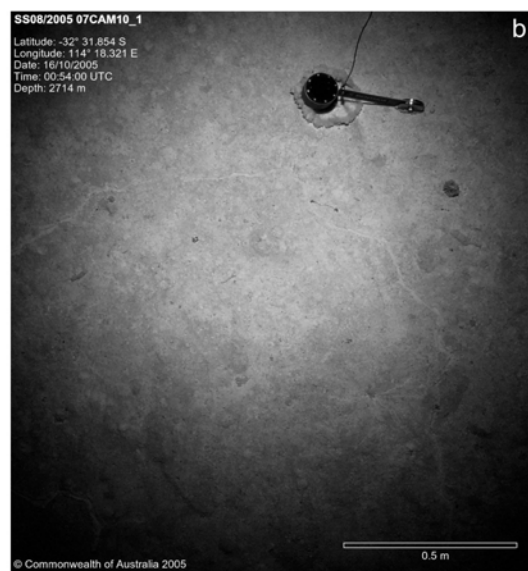
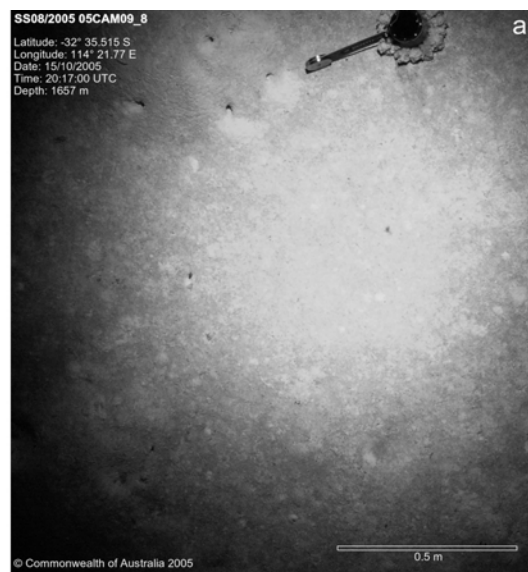
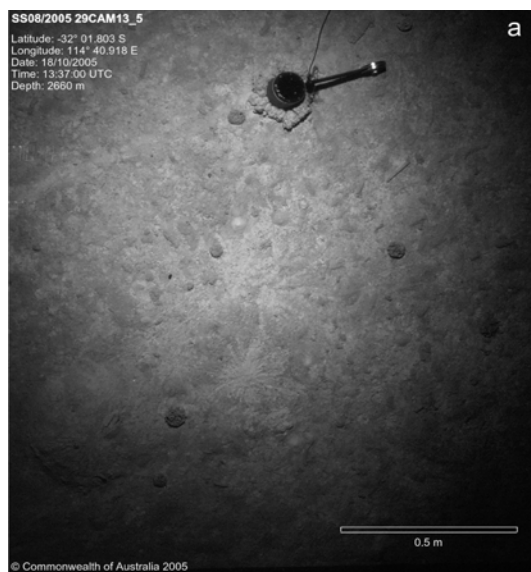


Figure 4.19. a) 29CAM13_5, b) 29CAM13_6 (Perth Canyon), c) 05CAM09_2 (Busselton Canyon).

Figure 4.20. a) 05CAM09_8, b) 07CAM10_1, c) 07CAM10_7 (Busselton Canyon)

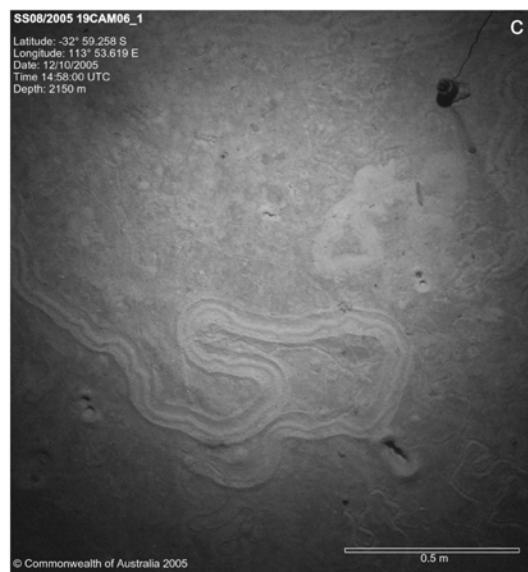
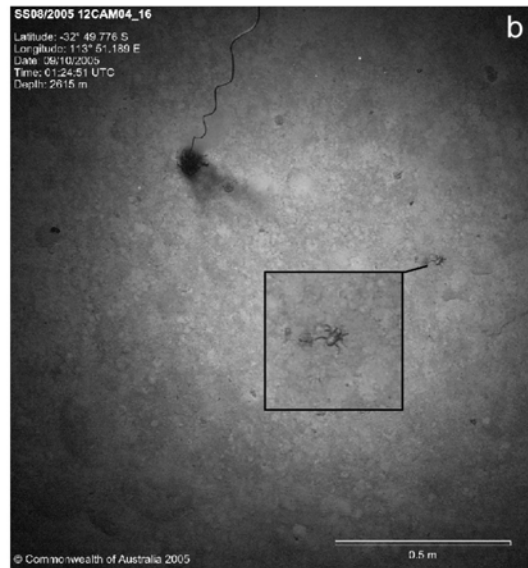
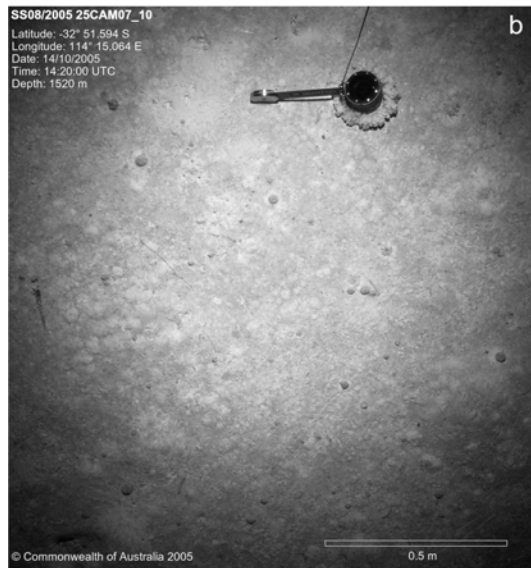


Figure 4.21. a) 25CAM07_4, b) 25CAM07_10 (Geographe C.), c) 12CAM04_11 (Bunbury C.).

Figure 4.22. a) 12CAM04_12, b) 12CAM04_16, c) 19CAM06_01 (Bunbury Canyon).

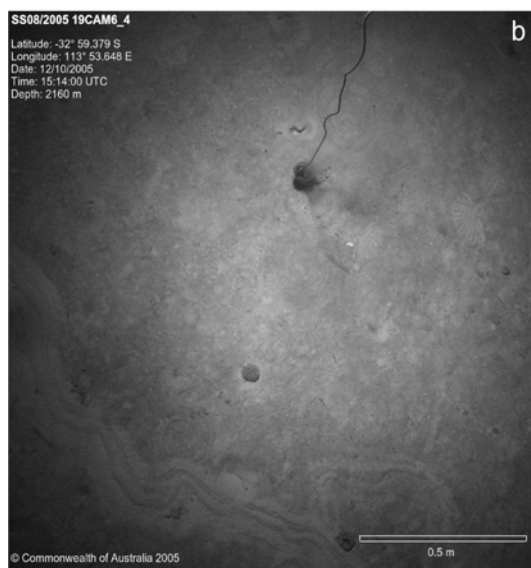
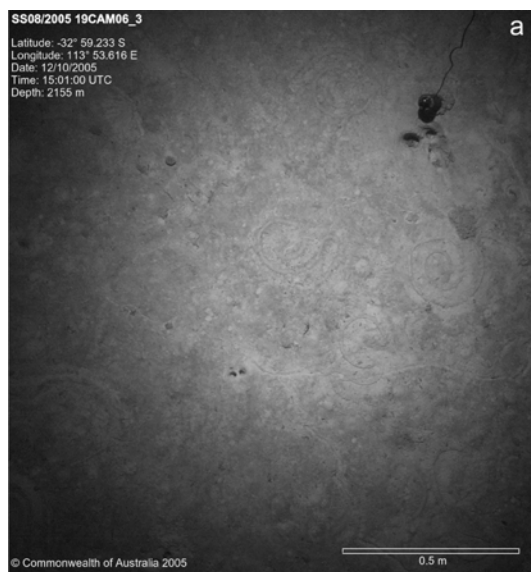


Figure 4.23. a) 19CAM06_3, b) 19CAM06_4, c) 19CAM06_5 (Bunbury Canyon).

Figure 4.24. a) 09CAM03_14, b) 09CAM03_17, c) 09CAM03_29 (Slope).

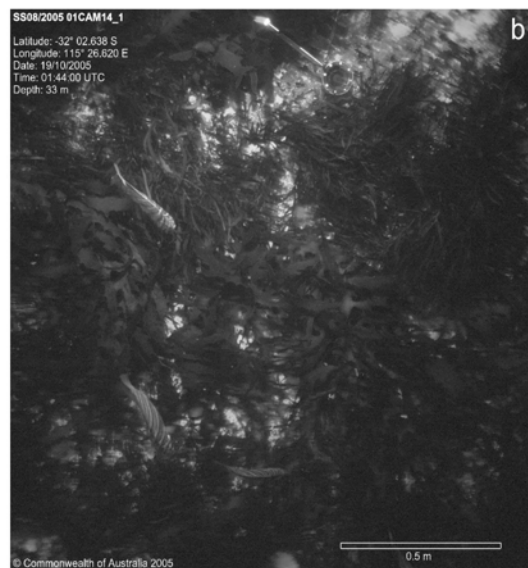
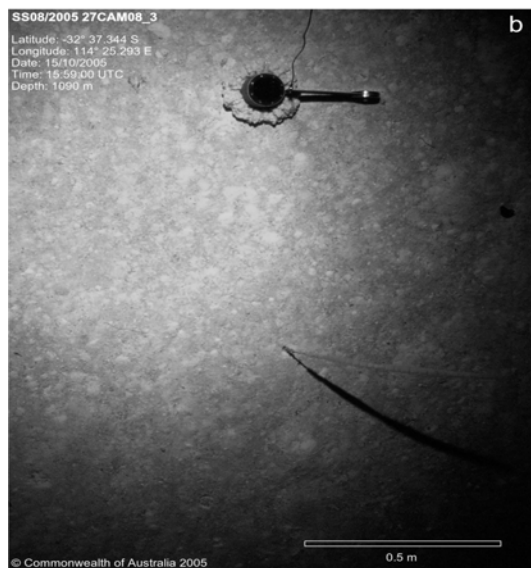
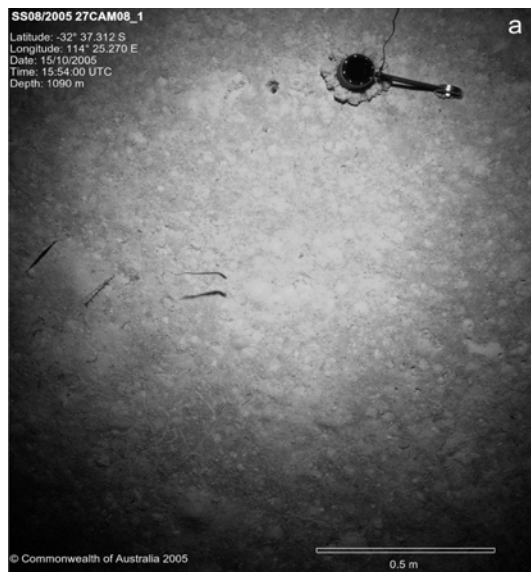


Figure 4.25. a) 27CAM08_1, b) 27CAM08_3 (Slope).

Figure 4.26. a) 27CAM08_7 (Slope), b) 01CAM14_1 (Shelf).

rubble may indicate the presence of hard ground that sessile organisms could attach too. The recovery of a variety of hard rocks from the dredging program within the canyons also indicates that these hard-grounds are common and located just below the surface sediments.

19CAM06 (upper canyon floor; 5 photographs): Mottled and bioturbated sediment with small and large trails and holes are visible. A wide trail is visible in photograph 01 and is probably formed by a mollusc (Fig. 4.22c). Other features include a raised spiral trail of *Enteropneust* (Acorn worm) faeces (photograph 03; Fig. 4.23a), several holes and fan-shaped feeding trails probably from crustaceans or worms, and small ball-shaped sponges (photograph 04 and 05; Fig. 4.23b, c).

4.3.2.5. Canyon Interfluvies and shelf camera stations

09CAM03 (slope near Geographe Canyon; 29 photographs): All sea floor photographs reveal mottled sediment commonly with trails, small mounds and crustacean and worm holes (e.g., photograph 17; Fig. 4.24b). A stalked glass sponge (hexactinellid) is visible in

photograph 14 (Fig. 4.24a). Other features included a small shrimp (photograph 29; Fig. 4.24c). A shrimp on the seafloor is also visible in photograph 31.

27CAM08 (slope near Busselton Canyon; 11 photographs): Mottled sediment with holes, trails and mounds are visible in most photographs. Other features include two species of stalked octocoral (photograph 01; Fig. 4.25a), single stalked octocoral (photograph 03; Fig. 4.25b), fish or eel (photograph 01; Fig. 4.25a), swimming shrimp (photograph 07; Fig. 4.26a). Swimming shrimps are also visible in photographs 09 and 11.

01CAM14 (shelf east of Perth Canyon; 1 photograph): One photograph (Fig. 4.26b) with *Eckolonia* kelp, other brown algae and two footballer sweep fish (*Neafypus obliquus*).

4.3.3. Surface Sediments

A total of 66 surface samples were analysed for grain size, carbonate content and 42 samples were inspected for composition. Thirty-five samples were from this survey (Figs. 4.27 & 4.28; Tables 4.5-4.8) and 31 from previous surveys (Fig. 4.9 & 4.10). Brief compositional descriptions and colour of samples are provided in Tables 4.5-4.8. Full sedimentological descriptions of dredge samples are contained in Appendix E.

4.3.3.1. Regional surface sediment composition

Forty-two surface samples were inspected for composition. Thirty-five samples were from this survey, two from SS07/2005 (GA296), three from SS09/2005 and two from BMR80. Most surface samples are very poorly sorted, nannofossil oozes. Visual examination of the fine sand fraction (63-150 μm) revealed that radiolarians, sponge spicules, planktic foraminifera and biogenic fragments are abundant in all samples. Sediments of the coarse fraction (125-2,000 μm) are principally composed of nannofossils, including: planktic and benthic foraminifera, radiolarians, ostracods, and pteropods. Sponge spicules are also common in many samples. Planktic foraminifera are the dominant constituent of sediments of the lower slope and submarine canyons. By contrast, the upper slope sediments are primarily composed of benthic foraminifera. Two samples located in the upper Perth Canyon (80/DR04 and 80/DR05) are mostly composed of skeletal fragments of shelf origin. Results of the quantitative analysis of the individual grains in the 125-2,000 μm sediment fraction are described in this section. The full results are located in Appendix F.

Foraminifera: The primary constituent in most samples are planktic foraminifera which make up between 12.2% and 97.1% of the sample, with an average of 73.5%. Only seven samples comprise <50% planktic foraminifera (09GC06, 27GC20, 26GC21, BMR80/DR04 and DR05, and SS07/2005/GR36 and SS07/2005/GR51). Apart from 27GC20, these samples are located on the upper slope and upper Perth Canyon, between 950-1,400 m water depth. Sample 27GC20, located in the lower Perth Canyon, comprises skeletal fragments (38.1%), sponge spicules (34.2%) and planktic foraminifera (22.4%).

Globigerinoides ruber is the most common planktonic foraminifera present in all samples. Common planktonic foraminifera include *Globigerinoides sacculifer*, *Globorotalia inflata*, *Globorotalia menardii*, *Globigerinita glutinata*, *Globoquadrina dutertrei*, *Globigerina bulloides*, and *Orbulina universa*. Benthic foraminifera are rare in all samples and comprise between 0% and 6.1%, with an average of 1.7%.

Sponge spicules: Generally rare in all samples, ranging in content from 0% to 34.2%, with an average of 3.1%. Five samples (10GC08, 27GC20, 26GC21, 02GC24 and

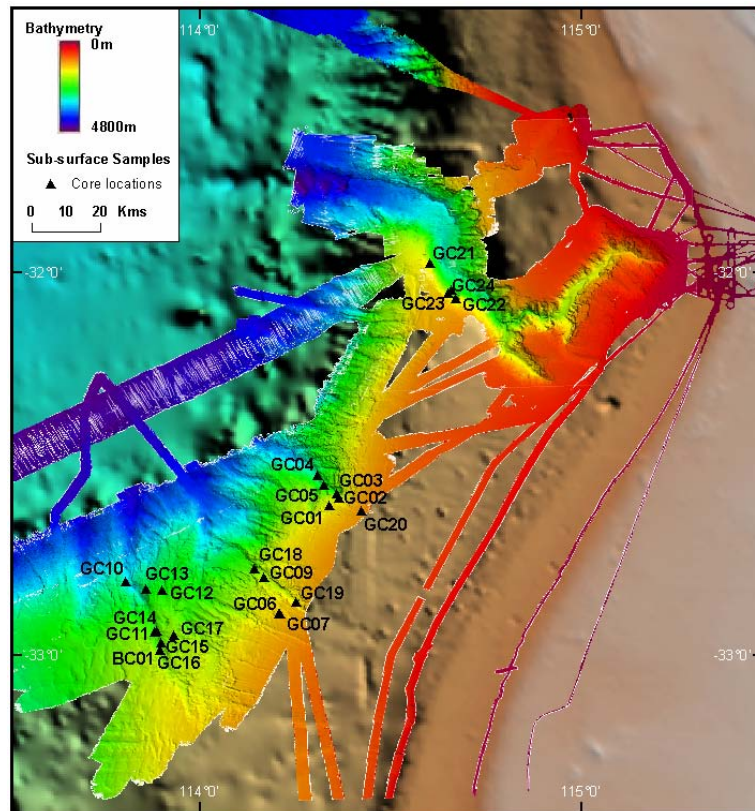


Figure 4.27. Multi-beam (swath) sonar bathymetry image showing sample locations of core samples for SS08/2005.

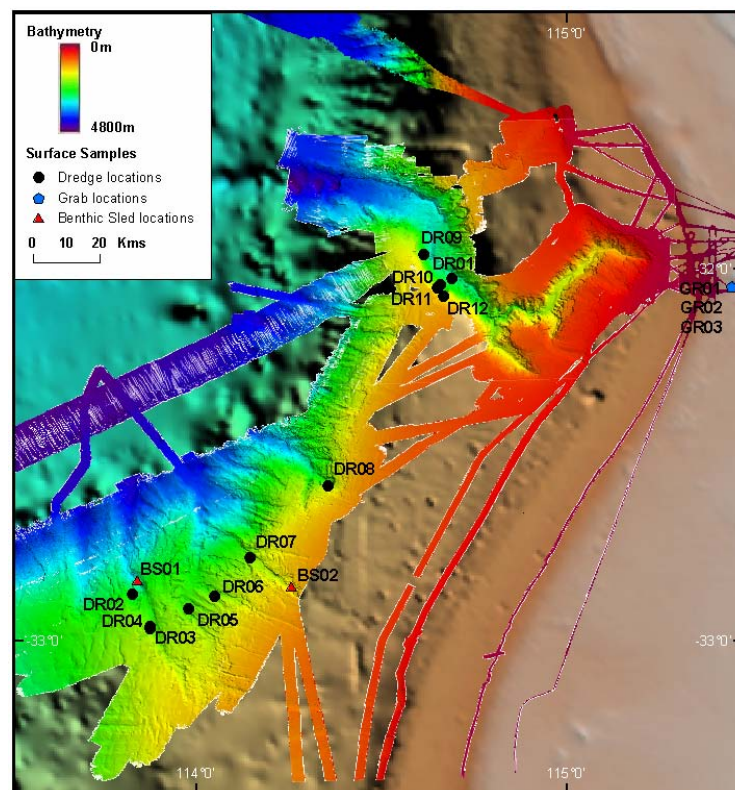


Figure 4.28. Multi-beam (swath) sonar bathymetry image showing locations of dredges, benthic sleds and grab samples.

Table 4.6. Core locations, water depths, core lengths and descriptions.

SampleID	Latitude	Longitude	Water depth (m)	Length (m)	Sample description
04GC01	-32° 36.43'	114° 20.24'	1,630	2.32	White-to-light grey nannofossil ooze.
05GC02	-32° 35.24'	114° 21.76'	1,708	3.99	Unconsolidated spiculitic nannofossil ooze.
06GC03	-32° 34.57'	114° 21.38'	2,386	0.34	Spiculitic nannofossil ooze.
07GC04	-32° 31.70'	114° 18.44'	2,719	0.3	Compacted nannofossil ooze. (core catcher sample only)
08GC05	-32° 33.27'	114° 19.39'	2,530	3.28	White-to-light grey nannofossil ooze.
09GC06	-32° 53.52'	114° 12.53'	1,308	2.06	Light grey nannofossil ooze.
09GC07	-32° 53.55'	114° 12.51'	1,308	3.3	Light grey nannofossil ooze. (not retained)
10GC08	-32° 47.80'	114° 09.93'	1,872	3.60	Stiff grey-white spiculitic nannofossil ooze.
10GC09	-32° 47.81'	114° 09.97'	1,535	4.83	White spiculitic nannofossil ooze. (not retained)
11GC10	-32° 48.35'	113° 48.29'	3,138	0.38	Light grey nannofossil ooze.
16GC11	-32° 56.36'	113° 52.80'	2,338	0.10	Unconsolidated white to grey-white calcareous spiculitic nannofossil ooze. (core catcher sample only)
03GC12	-32° 49.84'	113° 54.05'	2,475	1.96	White-to-tan, spiculitic and nannofossil ooze.
12GC13	-32° 49.57'	113° 51.38'	1,824	2.95	Spiculitic nannofossil ooze.
17GC14	-32° 56.14'	113° 53.22'	2,192	0.78	Very stiff, dewatered spiculitic ooze.
18GC15	-32° 58.05'	113° 53.88'	2,085	1.78	Calcareous nannofossil ooze with spicules at core top and base.
19GC16	-32° 59.25'	113° 53.64'	2,171	0.30	Semi-consolidated to stiff nannofossil ooze.
21GC17	-32° 56.80'	113° 55.82'	1,939	0.53	White spiculitic nannofossil ooze
24GC18	-32° 46.44'	114° 08.48'	2,340	2.75	White unconsolidated nannofossil ooze.
23GC18A	-32° 46.94'	114° 08.85'	1,946	0.14	Pteropod hash and silty sand with nannofossils and spicules.
25GC19	-32° 51.60'	114° 15.02'	1,562	3.10	Spiculitic nannofossil ooze.
27GC20	-32° 37.32'	114° 25.27'	1,117	5.37	Spiculitic nannofossil ooze.
26GC21	-31° 58.33'	114° 36.16'	2,037	1.18	Spiculitic nannofossil ooze.
28GC22	-32° 03.90'	114° 40.08'	2,218	1.76	Nannofossil ooze at top, calcilutite at base.
02GC23	-32° 03.09'	114° 38.91'	2,080	1.08	Nannofossil ooze at top, weathered consolidated green-grey calcilutite.
02GC24	-32° 02.58'	114° 39.50'	2,360	0.47	Nannofossil ooze at top, weathered consolidated green-grey calcilutite.
19BC01	-32° 59.24'	113° 53.64'	2,200	N/A	Unconsolidated nannofossil ooze.

Table. 4.7. Benthic sled locations, water depths and descriptions.

Sample	Start latitude	Start longitude	Water depth (m)	Finish latitude	Finish longitude	Water depth (m)	Sample description
12BS01	-32° 50.29'	113° 50.51'	2,819	-32° 50.49'	113° 50.25'	2,942	Grey-white spiculitic mud.
25BS02/A	-32° 51.28'	114° 15.41'	1,440	-32° 51.49'	114° 15.02'	1,535	Calcareous nannofossil ooze.
25BS02/A	-32° 51.28'	114° 15.41'	1,430	-32° 51.49'	114° 15.02'	1,535	Calcareous nannofossil ooze.

02DR11) contain relatively high concentrations, ranging from 9.1% to 34.2%.

Ostracods: Generally are in all samples, ranging in content from 0% to 1.4%, with an average of 0.2%.

Pteropods: Generally rare in all samples, ranging in content from 0% to 0.9%, with an average of 0.1%.

Table. 4.8. Grab locations, water depths and descriptions.

Sample	Latitude	Longitude	Water depth (m)	Sample description
01GR01	-32° 02.69'	115° 26.87'	29	Rock fragments, coral, seaweed, some sand. Rocky bottom.
01GR02	-32° 02.73'	115° 26.72'	42	Medium to coarse grained sand
01GR03	-32° 32.27'	115° 26.72'	44.1	Medium to coarse grained sand

Table 4.9. Estimated dredge start and finish locations, dredge layback and descriptions.

Dredge	Start latitude	Start longitude	Layback (m)	Finish latitude	Finish longitude	Layback (m)	Sample description
02DR01	-32° 04.85'	114° 06.17'	1,743	-32° 02.85'	114° 39.29'	2,257	Pelagic nannofossil ooze
13DR02	-32° 52.29'	113° 16.13'	2,700	-32° 52.29'	113° 50.78'	2,774	Unconsolidated to stiff nannofossil ooze
14DR03	-32° 57.82'	113° 18.98'	2,577	-32° 57.82'	113° 53.56'	2,541	Unconsolidated nannofossil ooze
15DR04	-32° 57.73'	113° 18.46'	1,100	-32° 57.73'	113° 52.09'	1,100	Unconsolidated to stiff nannofossil ooze
20DR05	-32° 55.94'	113° 25.54'	1,870	-32° 55.94'	113° 58.88'	1,847	Brown terrigenous mud, nannofossil ooze unconsolidated to stiff
22DR06	-32° 52.89'	113° 25.60'	1,905	-32° 52.89'	114° 02.89'	1,937	Brown terrigenous mud, nannofossil ooze
23DR07	-32° 45.54'	113° 36.77'	2,376	-32° 45.54'	114° 08.50'	2,392	Gneiss, metasediment, nannofossil ooze unconsolidated to stiff
06DR08	-32° 34.31'	113° 48.41'	2,505	-32° 34.31'	114° 21.44'	2,475	Limestone, calcarenite, nannofossil ooze, manganese crusts
26DR09	-32° 57.37'	114° 02.96'	2,529	-32° 57.37'	114° 36.43'	2,238	Calclutite, chalk, nannofossil ooze
02DR10	-32° 01.96'	114° 07.55'	2,268	-32° 01.96'	114° 39.65'	2,641	Calclutite, nannofossil ooze
02DR11	-32° 02.87'	114° 06.55'	1,940	-32° 02.87'	114° 38.92'	1,800	Calclutite, nannofossil ooze, coral
28DR12	-32° 04.01'	114° 08.08'	1,770	-32° 04.14'	114° 40.03'	819	Indurated calclutite and unconsolidated ooze

Radiolarians: Generally rare in all samples, ranging in content from 0% to 3.7%, with an average of 1.1%. Five samples (08GC05, 25GC19, 27GC20, 26GC21 and 28GC22) contain relatively high concentrations, ranging between 3% to 3.7%.

Mineral Grains: Generally, rare in all samples except SS09/2005/DRG1A which contains a concentration of 12.1%. Excluding this high value the average concentration of mineral grains is 0.1%.

Skeletal Fragments: In most samples skeletal fragments were comprised of planktonic foraminifera in concentrations of between 90 and 95%. Visual estimates indicate that skeletal fragments of other organisms (pteropods, radiolarians) comprise between 20% and 90% in 10 samples (04GC01, 23GC18A, 27GC20, 26GC21, 25BS02A, 02DR11, SS07/2005/GR31 and SS07/2005/GR51 and 80/DR04 and 80/DR05). Apart from GC21, these samples are located on the upper slope or upper Perth Canyon in water depths of between 410 and 1,630 m.

Fragmentation Index: Fragmentation (Equation 13) ranges from 2% to 85% (Fig. 4.29-4.30). There is a negative correlation between the fragmentation index and water depth for all samples (Fig. 4.31).

In the Perth Canyon, fragmentation ranges between 5% and 83%, with an average of 26%. In Busselton, Geographe and Bunbury Canyons, fragmentation ranges from 19% to 30%, 14% to 32% and 2% to 24%, respectively. Fragmentation for lower Perth Canyon samples ranges from 5% to 62%, with an average of 17.9%. Lowest fragmentation is observed in samples collected from the lower Bunbury Canyon with an average of 9% compared to 16.3% for Geographe Canyon and 19 % for Busselton Canyon.

Fragmentation indices for the upper canyons range between 10% and 83%, with an average of 27.2%. This average is more than double the value for samples recovered from the lower canyon (27.2% versus 11.7%). Moreover, samples from the upper Perth Canyon contain the highest fragmentation indices of 47% and 83%, with an average of 64.9%, followed by Geographe Canyon (24.9%), Busselton Canyon (23.4 %), and Bunbury Canyon (16.7%). Perth Canyon samples are located closer to the shelf and in shallower waters than samples from the three “blind” canyons. The trends observed in the fragmentation indices reflect greater transport of highly abraded and fragmented shelf sediments into Perth Canyon. If dissolution was a significant factor in the fragmentation of foraminifera, the fragmentation indices would be higher in lower canyon samples.

In Busselton Canyon, the samples are located in the canyon head or at the base of steep canyon walls. The relatively high fragmentation values found at these locations probably reflect increased abrasion of foraminifera test from the down-canyon transfer of upper slope sediments. Similarly, relatively high fragmentation values are found in samples located close to the canyon head of Geographe and Bunbury Canyons and adjacent slope.

On the slope, fragmentation indices range from 14% to 85%. Highest values (48-85%) are located on the upper slope close to the heads of Perth, Busselton and Geographe Canyons. Relatively high fragmentation values on the slope adjacent to canyons probably reflect funnelling of highly fragmented shelf sediments into the canyon head by waves and tides, followed by transfer to greater depth within the canyon by mass movements.

4.3.3.2. Perth Canyon region – grainsize and carbonate content

Within the Perth Canyon a total of 36 samples were analysed for grainsize distribution and carbonate content. Nine samples are from this survey (SS08/2005), 17 samples are from BMR80 Survey and six from SS07/2005 (GA296) Survey (Fig. 4.9, 4.27-28). Twenty-six samples are from within the Perth Canyon, with seven upper canyon and 19 lower canyon samples. Eight samples are from the slope and two samples are from the shelf. Full results are listed in Appendix F.

Mean grainsize: All samples within the Perth Canyon have a mean grain size of coarse silt (31-63 μm) using the sedimentological description system of Krumbien and Sloss (1963) (Fig. 4.32). Slope sediments are very fine (63-125 μm) to fine (125-250 μm) sand and the shelf sediments are coarse sand (500-1,000 μm). Sediments along a NE-SW transect to the north of Perth Canyon (Fig. 4.32) display a general fining trend from coarse sand on the shelf to fine and very fine sand on the slope, to coarse silts on the NE canyon wall and floor.

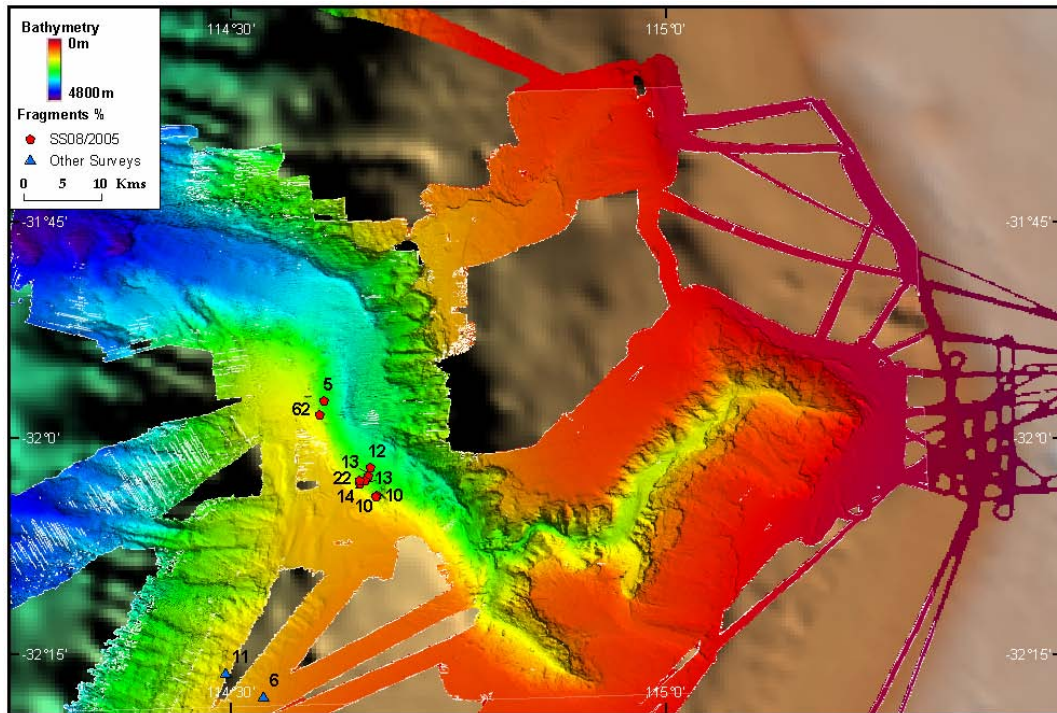


Figure 4.29. Multi-beam (swath) sonar bathymetry image showing fragmentation index (%) for samples collected in the lower Perth Canyon.

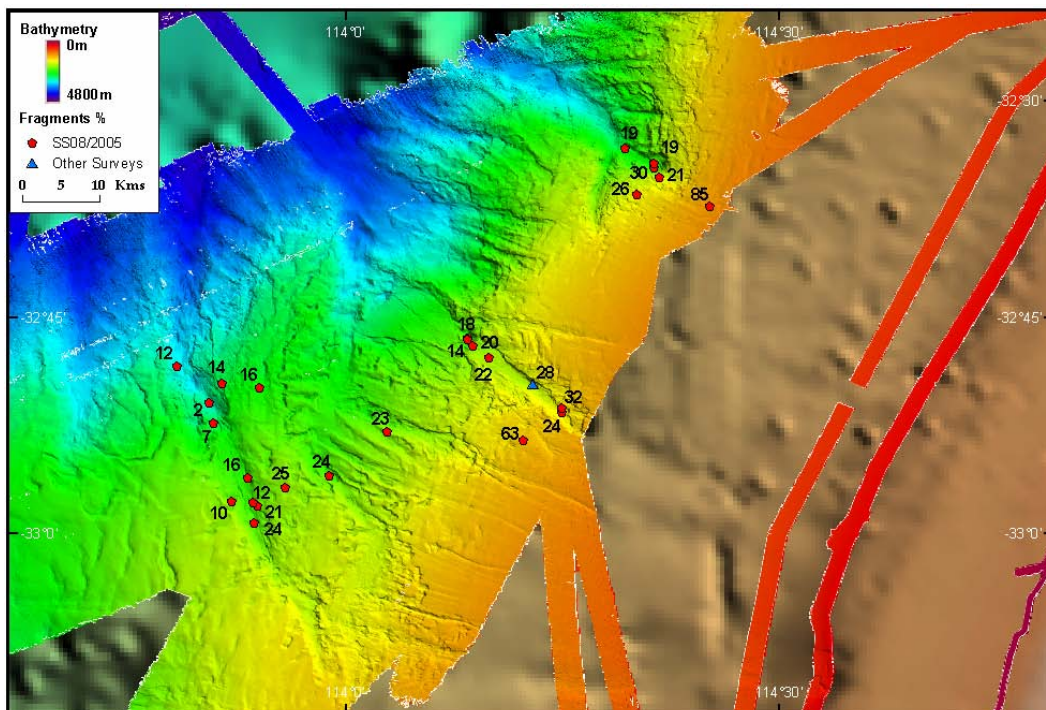


Figure 4.30. Multi-beam (swath) sonar bathymetry image showing fragmentation index (%) for samples collected in the Mentelle Basin region.

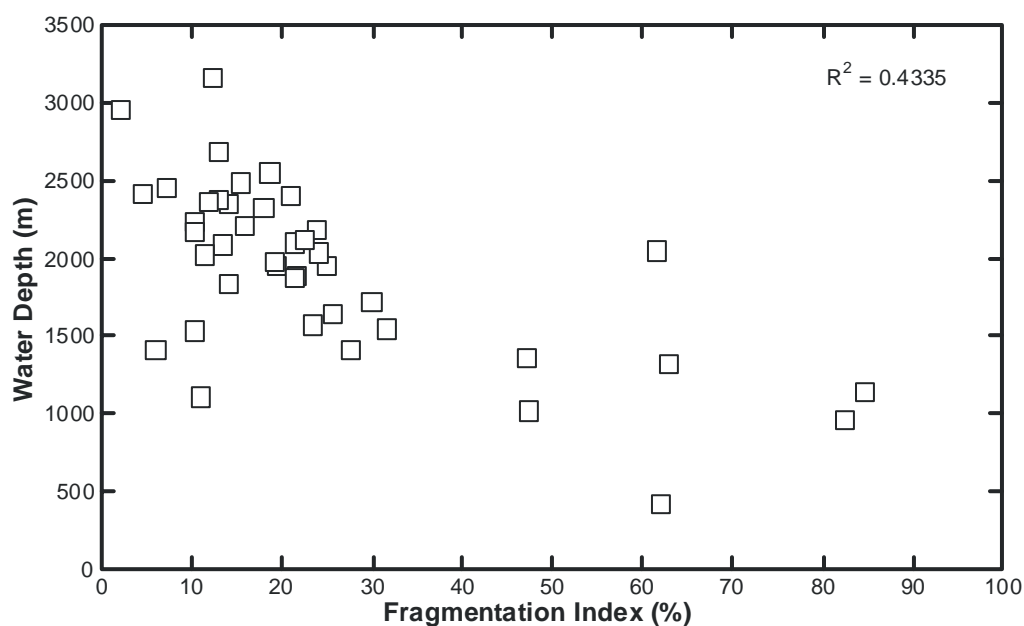


Figure 4.31. Graph of fragmentation index (%) versus water depth (m).

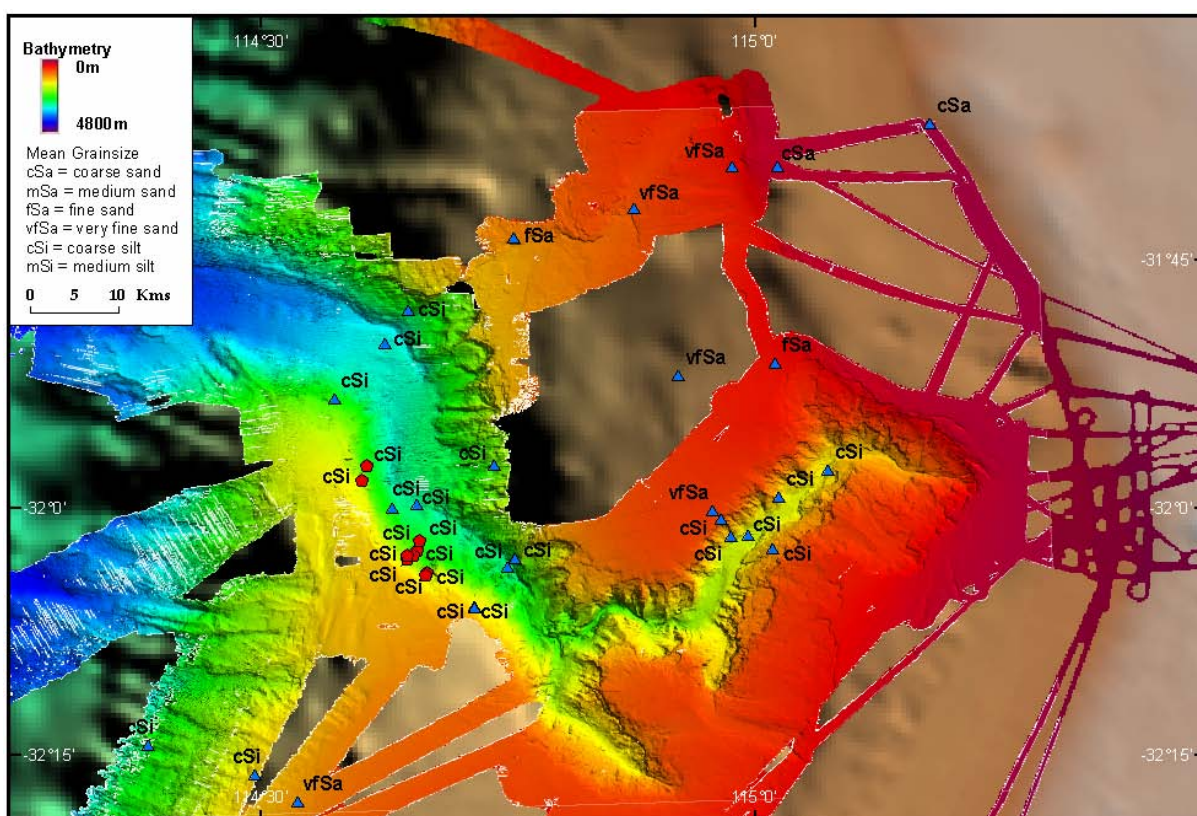


Figure 4.32. Multi-beam (swath) sonar bathymetry image showing mean grainsize for samples in the Perth Canyon region.

Gravel: Gravel is a minor component in all sediments sampled from the Perth Canyon region (Fig. 4.33), with contents between 0% and 4.2%. Gravel is found only in three samples on the NE flank of the Perth Canyon. Six samples from the slope and shelf samples contain no gravel. Only one slope sample, SW of the Perth Canyon, contains 2.9% gravel, and the two shelf samples contain 7.8% and 8.7% gravel.

Sand: Sand contents from the Perth Canyon region range from 6% to 92% (Fig. 4.34). Sediments in Perth Canyon have sand contents of between 6% and 39%. Highest sand contents of 22% to 39% occur on the northern wall in water depths of 730 to 2,500 m. Elsewhere, sand comprises 6% to 16%. Average sand contents for sediments in the Perth Canyon is 14%, with average contents slightly lower on lower canyon slopes (13%) than on the upper canyon slopes (16.85%). Sand contents for sediments on the slope are generally higher than those for sediments in the Perth Canyon, ranging from 14% to 70%, with an average of 36%. Sediments along a SW transect from Perth Canyon show a general decrease in sand content down the slope. Sediments on the shelf have the highest sand contents of 91% and 92%. The sand contents show a clear partitioning between relatively low contents in sediments in Perth Canyon to relatively high contents in sediments on the slope and shelf.

Mud: Mud contents from the Perth Canyon region range from 0% to 94% (Fig. 4.35). Sediments in Perth Canyon are dominated by mud-sized grains with contents between 61% and 92% (average = 85%). Sediments on the lower canyon slope have an average mud content of 86.7% which is very similar to the average mud content of 81.7% for sediments on the upper canyon slope. Highest mud contents in the Perth Canyon are located on the SW slope and canyon floor with values ranging from 86% to 94%. Lowest mud contents are found on the upper slope of the NW flank (61% and 78%) and on the lower slope of the NE flank (72% and 75%). Generally, sediments on the NE and NW canyon flanks have lower mud contents than other locations, which may reflect the relatively steep gradients of the northern canyon margin compared to the southern margin. The steeper northern canyon margin is also incised by channels, and are likely to be more active in transporting sediment downslope than the more gently sloping southern flanks. The southern flanks are likely to be more stable and result in thicker accumulations of fine-grained material over time.

Mud contents for slope samples range from 29% to 86% with an average of 64%. Sediments contained in the two shelf samples contain between 0% and 1% mud. The three slope samples to the SW of the Perth Canyon show increasing mud contents down slope (66%, 74% and 86%). Overall, mud contents of sediments in Perth Canyon are greater than sediments on the slope and shelf, and sediments on the lower canyon slopes contain more mud than sediments on the upper canyon slopes. This confirms previous work that indicates that the Perth Canyon acts as a conduit for fine grained material from the shelf and upper slope, transporting it to the deep ocean floor.

Carbonate (bulk): Bulk carbonate contents range from 52% to 92% (Fig. 4.37). Within the Perth Canyon values range from 52% to 83%, with an average of 78%. Apart from one sample (52%) all samples have bulk carbonate contents greater than 74%. On the lower canyon slope, bulk carbonate contents range from 74 to 81% with an average of 78%. On the upper canyon slope, bulk carbonate contents range from 82 to 88% (except for one sample with 52% carbonate) with an average of 78%. The low value of 52% is located on the upper NE wall of the upper Perth Canyon. This low value may represent sampling of underlying basement sandstones. Excluding this low sample the average value is 83%, which is slightly higher than for the lower Perth Canyon environments. Slope sample bulk carbonate contents range from 77% to 86% with an average of 82%. The two shelf samples have bulk carbonate contents of 92% and 94% possibly indicating enhanced preservation in shallow shelf waters. Overall, there is a slight decrease in bulk carbonate contents with increasing water depth.

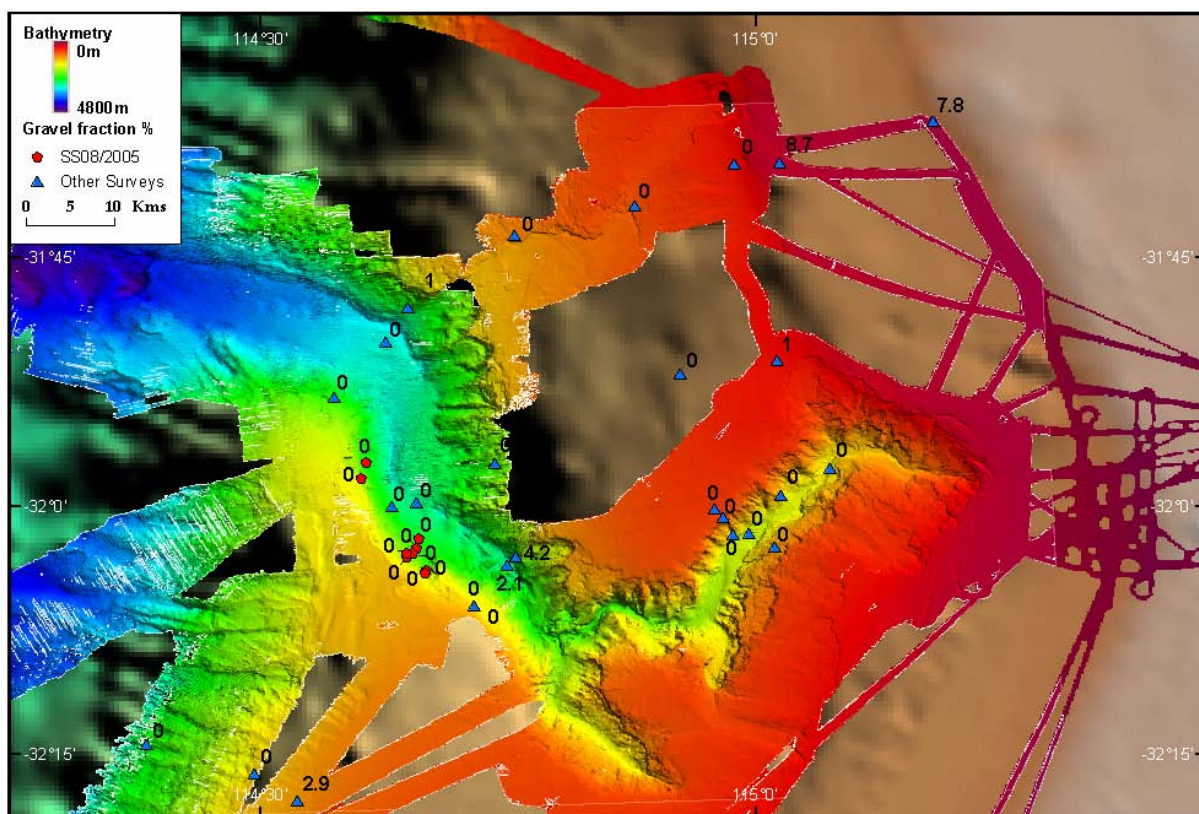


Figure 4.33. Multi-beam (swath) sonar bathymetry image showing gravel fraction (%) for samples in the Perth Canyon region.

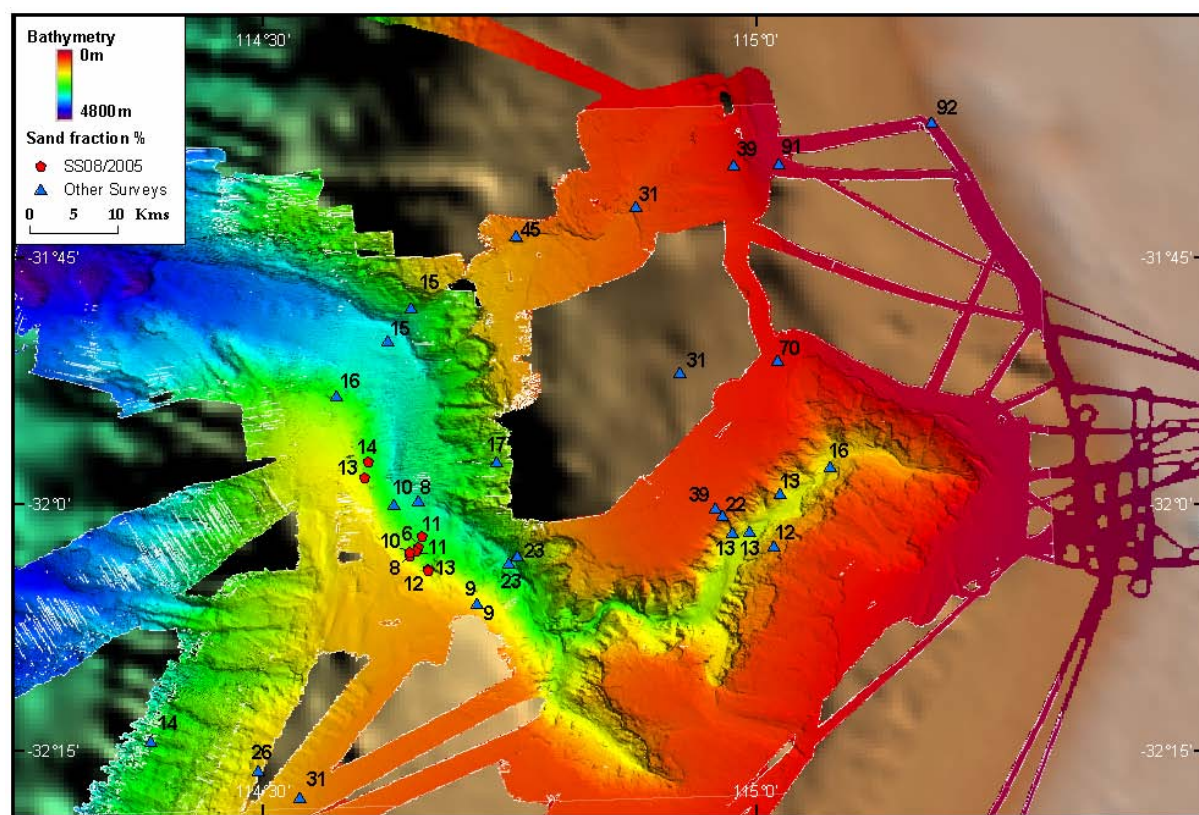


Figure 4.34. Multi-beam (swath) sonar bathymetry image showing the sand fraction (%) for samples in the Perth Canyon region.

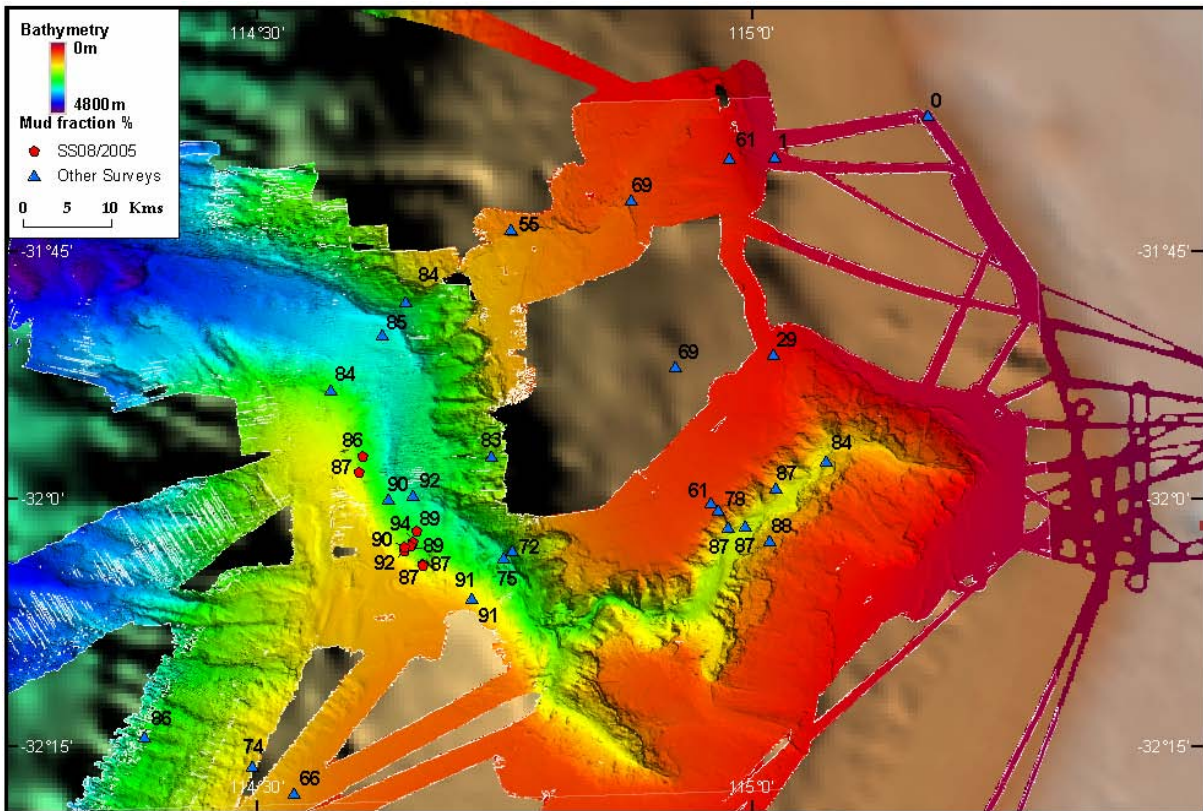


Figure 4.35. Multi-beam (swath) sonar bathymetry image showing the mud fraction (%) for samples in the Perth Canyon region.

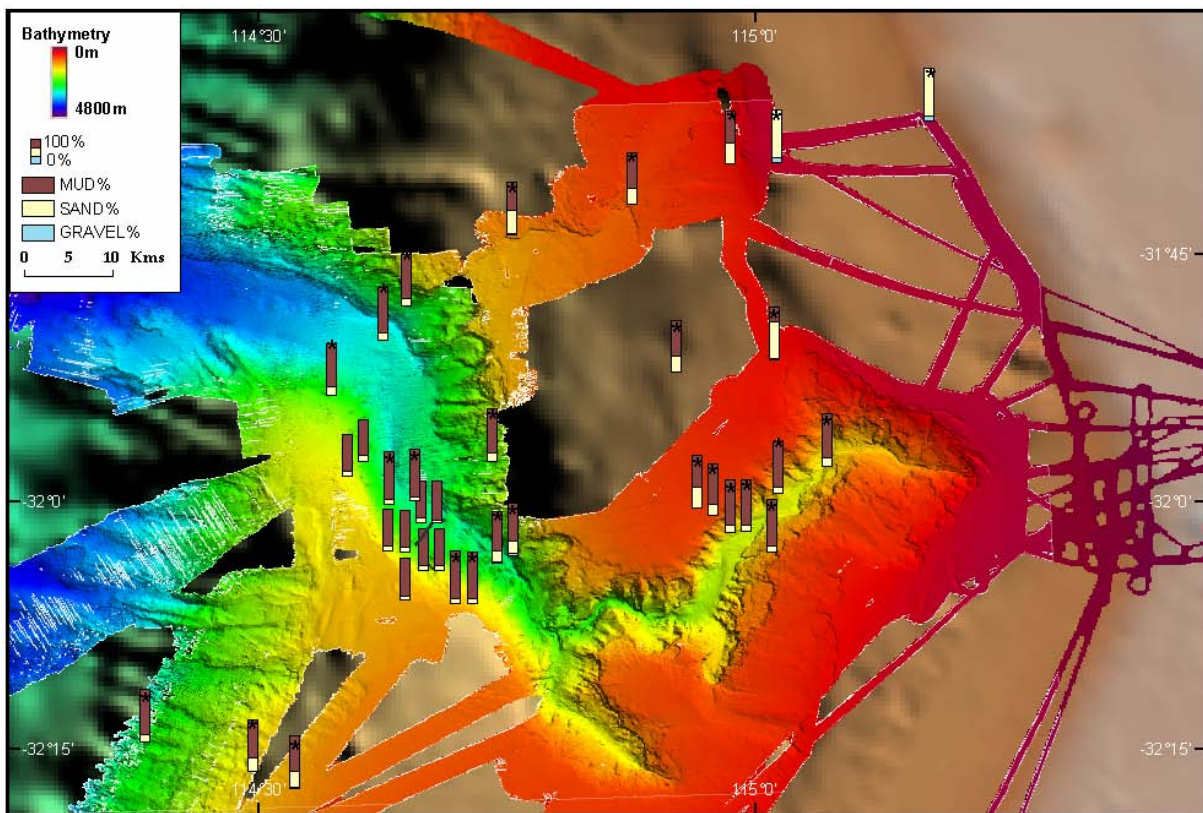


Figure 4.36. Multi-beam (swath) sonar bathymetry image showing grainsize bar graphs for samples in the Perth Canyon region.
* = Other survey samples.

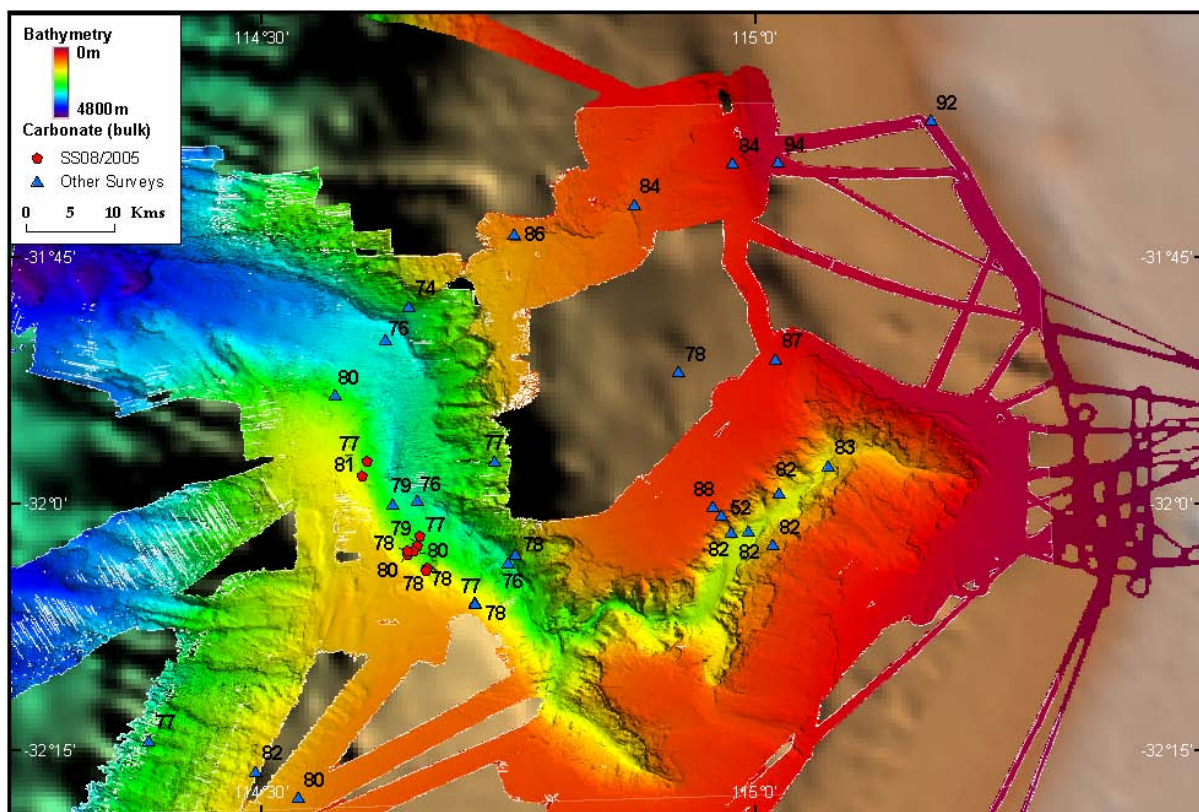


Figure 4.37. Multi-beam (swath) sonar bathymetry image showing bulk carbonate contents (%) for samples in the Perth Canyon region.

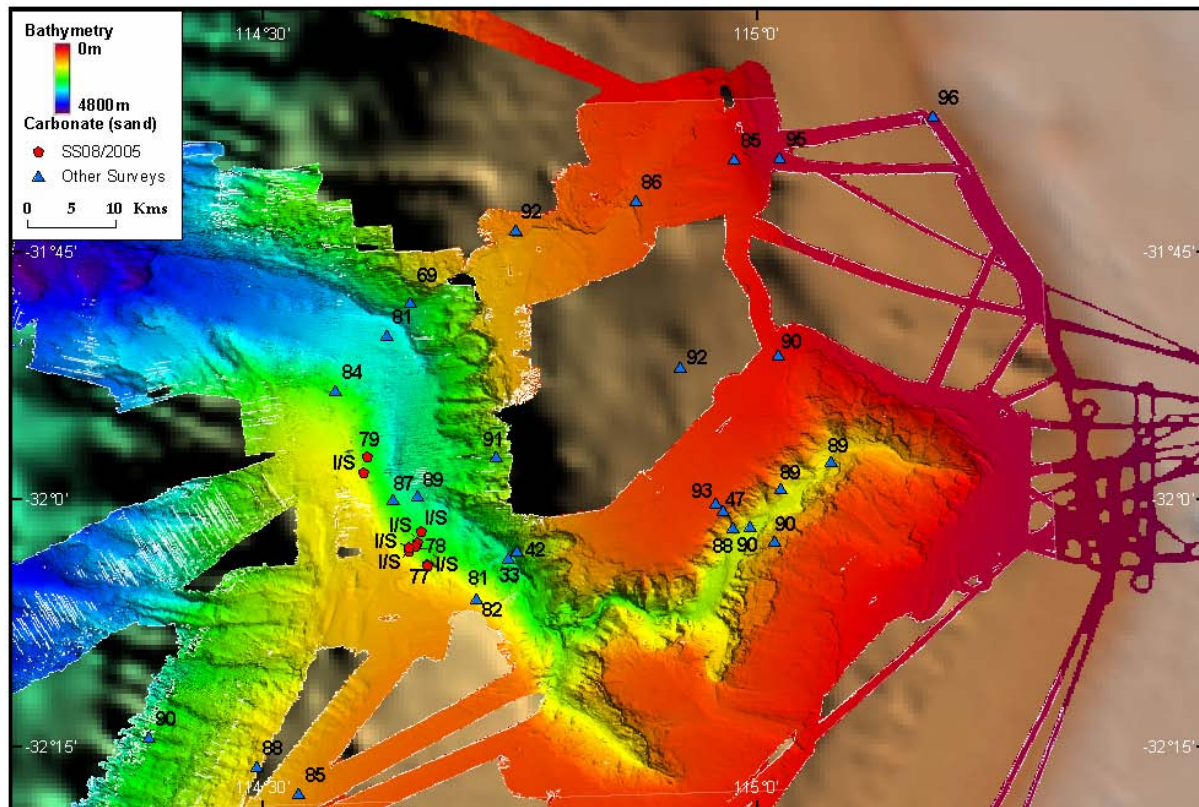


Figure 4.38. Multi-beam (swath) sonar bathymetry image showing carbonate (sand) contents (%) for samples in the Perth Canyon region.

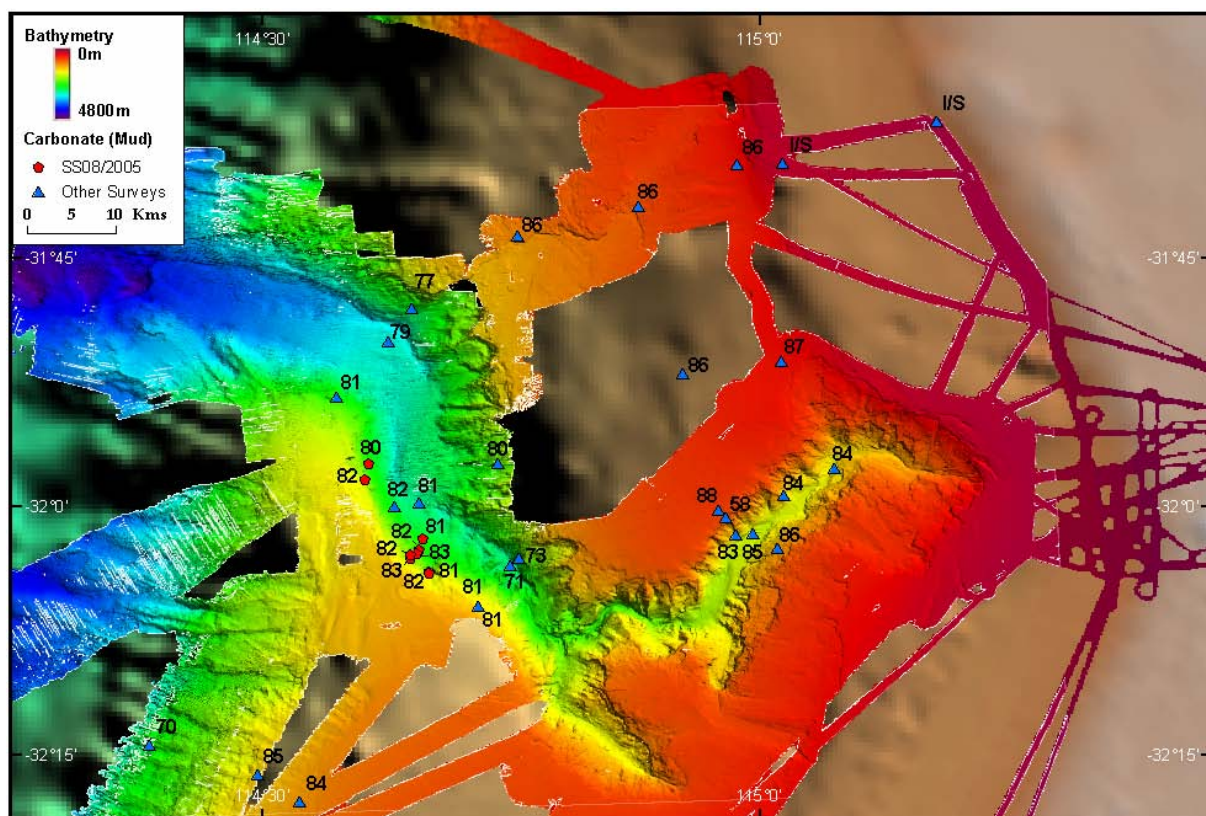


Figure 4.39. Multi-beam (swath) sonar bathymetry image showing carbonate (mud) contents (%) for samples in the Perth Canyon region.

Carbonate (sand): Six samples were of insufficient sample size to be analysed for the carbonate sand fraction. The remaining 30 samples from the Perth Canyon region have carbonate sand contents of between 33% and 96% (Fig. 4.38). Apart from three samples with lower carbonate sand values (33%, 42%, and 47%) carbonate sand content ranges from 69% to 90%. The three samples with lower carbonate values are located on the steep NE and NW canyon walls and probably represent sampling of the underlying basement rocks. Carbonate sand values within the Perth Canyon range from 32% to 93% with an average of 78%. On the lower canyon slope, carbonate sand values range from 33% to 91% with an average of 75%. On the upper canyon slope, carbonate sand values range from 47% to 93%, with an average of 84%. Slope and shelf samples have high carbonate sand values ranging from 85% to 96%. Generally, slope and shelf samples have higher carbonate sand contents than the Perth Canyon samples.

Carbonate (mud): Carbonate mud contents for the Perth Canyon region range from 58% to 88% (Fig. 4.39). The same range of values occurs within the Perth Canyon with an average of 81%. On the lower slope of the Perth Canyon average carbonate mud contents range from 71% to 83% with an average of 80%. On the upper slope average carbonate mud contents range from 58% to 88% with an average of 81%. Carbonate mud contents on the upper slope of the Perth Canyon (except for one at 58%) are higher than those on the lower slope. Low carbonate mud contents are restricted to the NE and NW walls of the Perth Canyon. On the slope adjacent to the Perth Canyon, carbonate mud contents range from 86% to 87% and are higher than those found in the Perth Canyon. Samples collected from the shelf had insufficient sample size to analyse carbonate mud content. The remaining non-carbonate mud fraction comprises terrigenous material and silica, which primarily comprises sponge spicules. Compared with the adjacent slope, the terrigenous mud component is

relatively high within the Perth Canyon. There is also a slight increase in terrigenous mud down the canyon. This suggests that the Perth Canyon may act as a conduit for terrigenous mud derived from the shelf.

4.3.3.3. *Mentelle Basin region - grainsize and carbonate content*

A total of 30 samples from the Mentelle Region were analysed for grain size distribution and carbonate concentration. Eighteen samples are from this survey (SS08/2005), two from SS09/2005 survey and two from GA296 survey. A total of 20 samples are from the three “blind” canyons, with five in Busselton Canyon, seven in Geographe Canyon, and eight in Bunbury Canyon. Seven samples are located on the lower slope adjacent to the canyons. One sample is located on the upper slope and one on the shelf.

Mean grainsize: Within the Mentelle Basin region the dominant surface sediment type is coarse silt (Fig. 4.40). Within Busselton Canyon the surface sediments are all coarse silts. Sediments on the slope close to Busselton Canyon’s entrance are composed of very fine sands, indicating a general fining of sediments from the slope to the canyon. Sediments in Geographe and Bunbury Canyons are predominantly coarse silts, although there is more variability within the canyons with samples comprising very fine sand, and coarse to medium silt. Sediments on the slope between Bunbury and Geographe Canyons are coarse silts except for one sample close to Bunbury Canyon, which is very fine sand. Sediments in the one sample recovered from the upper slope are very fine sand, and in the one sample recovered from the shelf are medium sand. Similar to the Perth Canyon region there is a fining in sediments from predominantly sand to silt with increasing water depth.

Gravel: There is no gravel present in any of the slope and canyon sediments. Gravel was only present on the shelf in a concentration of 5.7% (Fig. 4.41).

Sand: Sand contents for Busselton Canyon range from 9% to 16%, 11% to 38% for Geographe Canyon, and 2% to 32% for Bunbury Canyon (Fig. 4.42). Sediments in Geographe Canyon have the highest average sand contents of 21%. Sediments in Bunbury and Busselton Canyons have average sand contents of 17% and 13%, respectively. Sediments on the lower slope contain sand values of 9% near Bunbury Canyon to 36% near Busselton Canyon, with an average of 21%. Sediments in the only sample recovered from the upper slope have a sand content of 55%, and sediments in the only samples recovered from the shelf comprise 94% sand. Compared to a lower slope average (21%), sand contents in Geographe Canyon are similar to those on the adjacent lower slope, while sediments in Bunbury and Busselton Canyons have slightly lower sand contents. Compared to Perth Canyon, sediments in Geographe and Bunbury Canyons have a slightly higher average sand content (21% and 17%, respectively), with sediments in Busselton Canyon having a lower average sand content (13%).

Mud: Mud concentrations for sediments in Busselton Canyon range from 84% to 89%, 62% to 89% for Geographe Canyon, and 68% to 98% for Bunbury Canyon (Fig. 4.43). Sediments in Busselton Canyon have the highest average mud contents of 87%, which is slightly higher than the average mud content for Perth Canyon (85%). Bunbury and Geographe Canyons have average mud contents of 83% and 79%, respectively. Sediments on the lower slope contain mud contents of between 64% and 91%, with an average of 79%, which is slightly lower than those contained in sediments from Busselton and Bunbury

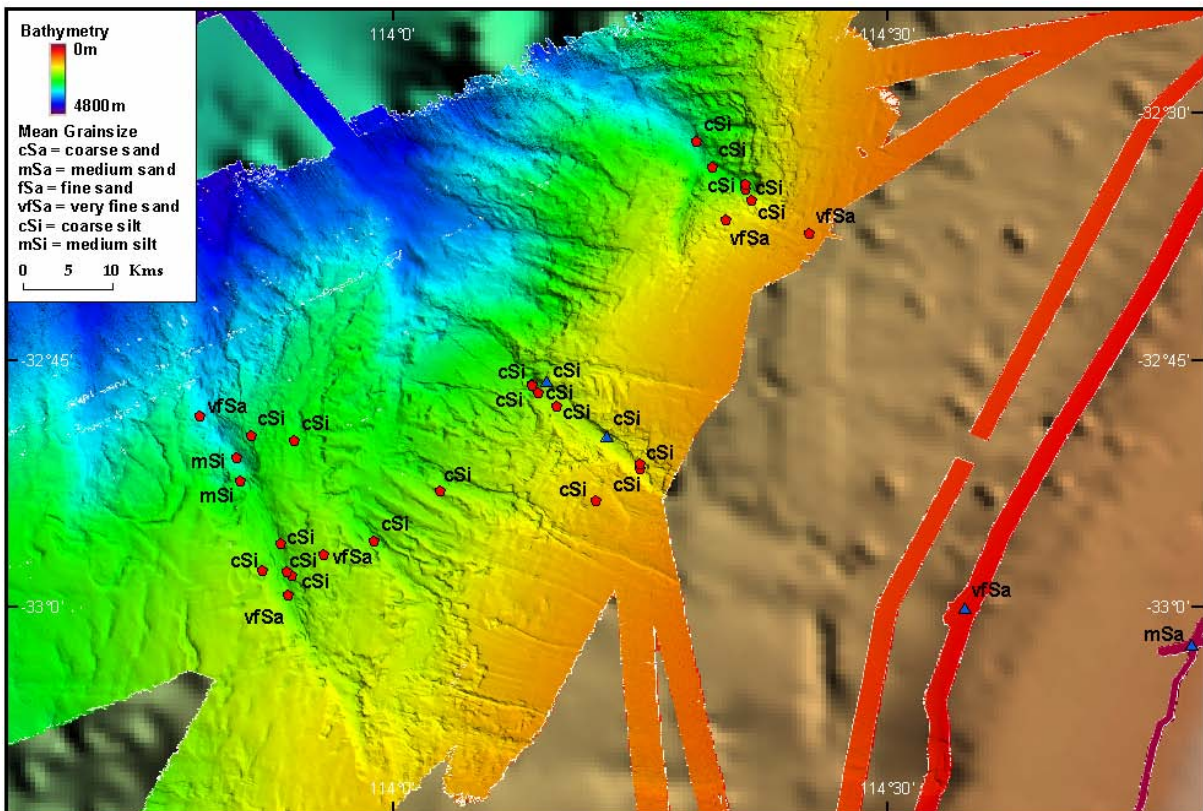


Figure 4.40. Multi-beam (swath) sonar bathymetry image showing mean grainsize for samples in the Mentelle Basin region.

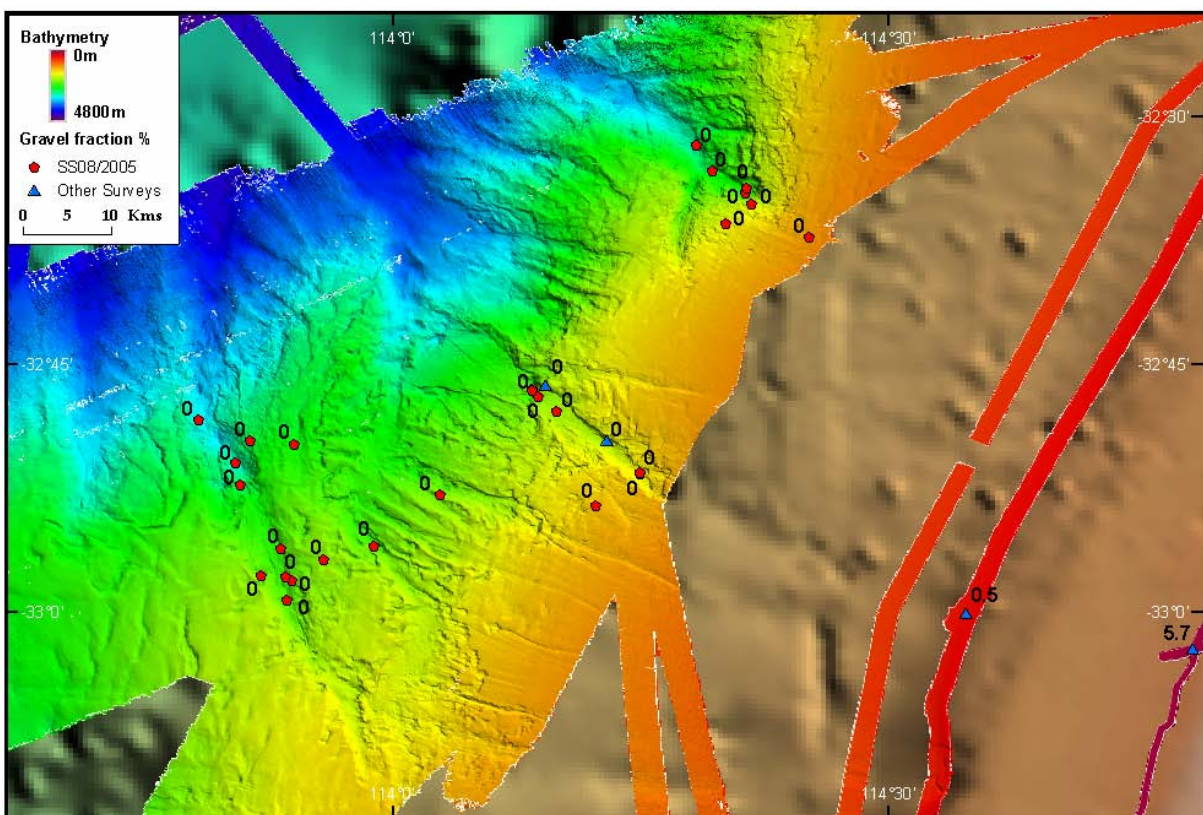


Figure 4.41. Multi-beam (swath) sonar bathymetry image showing the gravel fraction (%) for samples in the Mentelle Basin region.

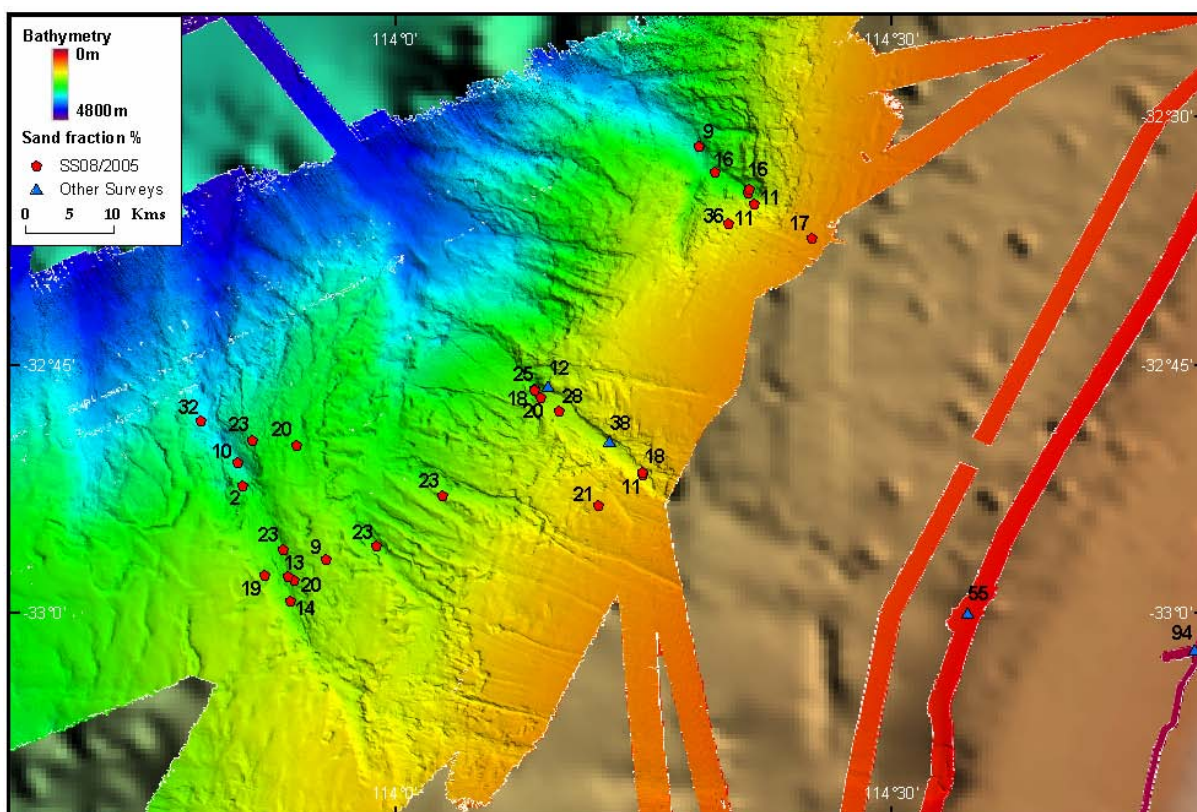


Figure 4.42. Multi-beam (swath) sonar bathymetry image showing the sand fraction (%) for samples in the Mentelle Basin region.

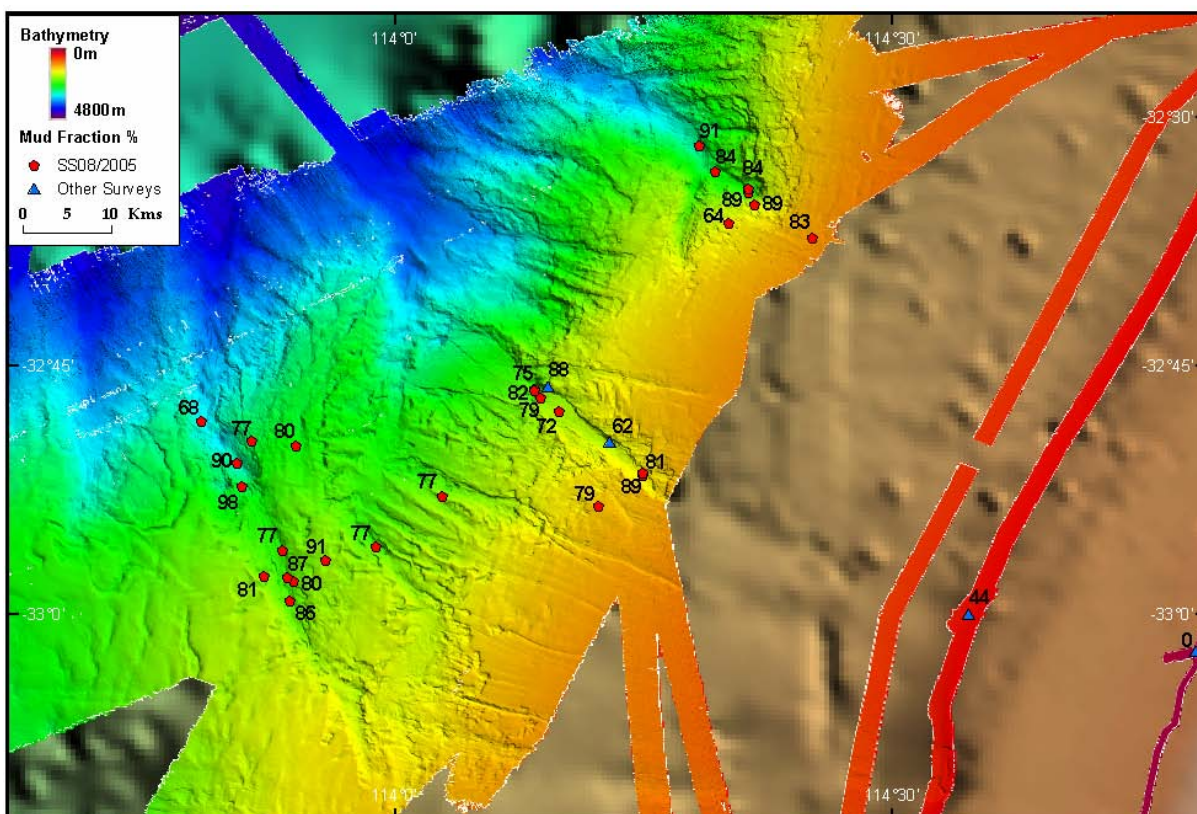


Figure 4.43. Multi-beam (swath) sonar bathymetry image showing the mud fraction (%) for samples in the Mentelle Basin region.

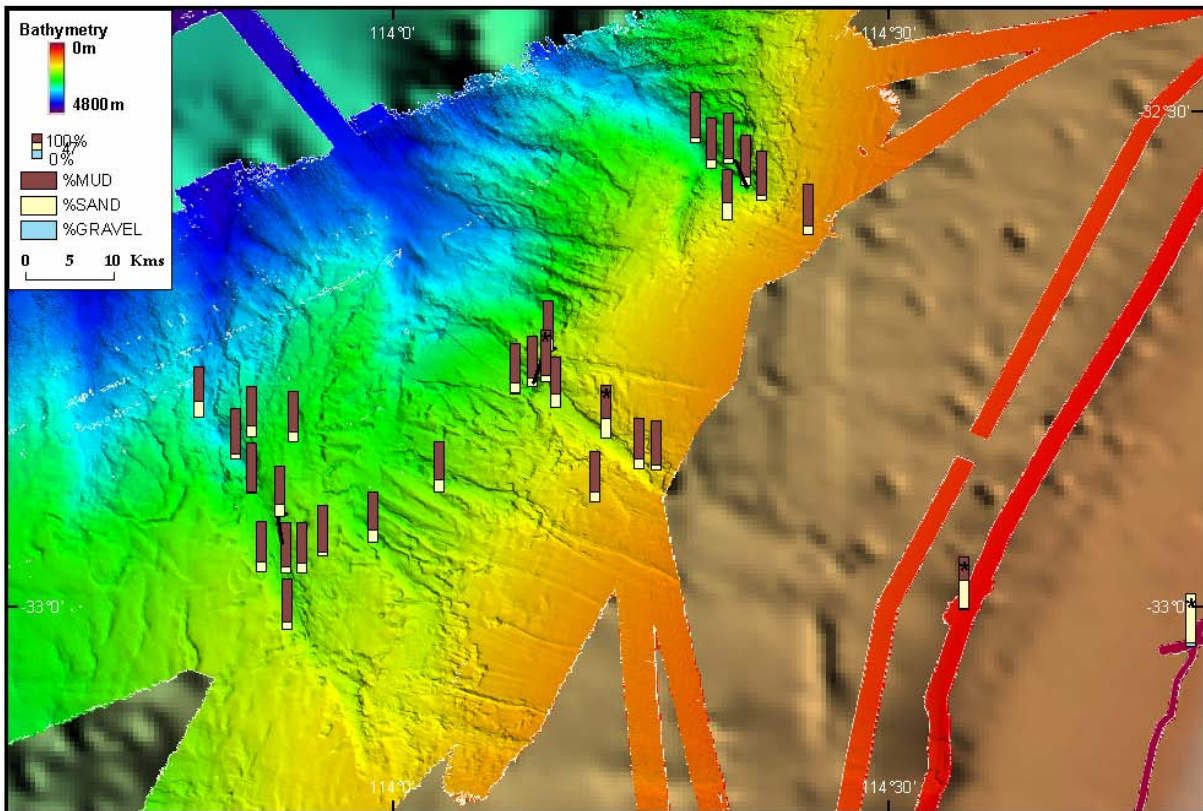


Figure 4.44. Multi-beam (swath) sonar bathymetry image showing grainsize bar graphs for samples in the Mentelle Basin region.

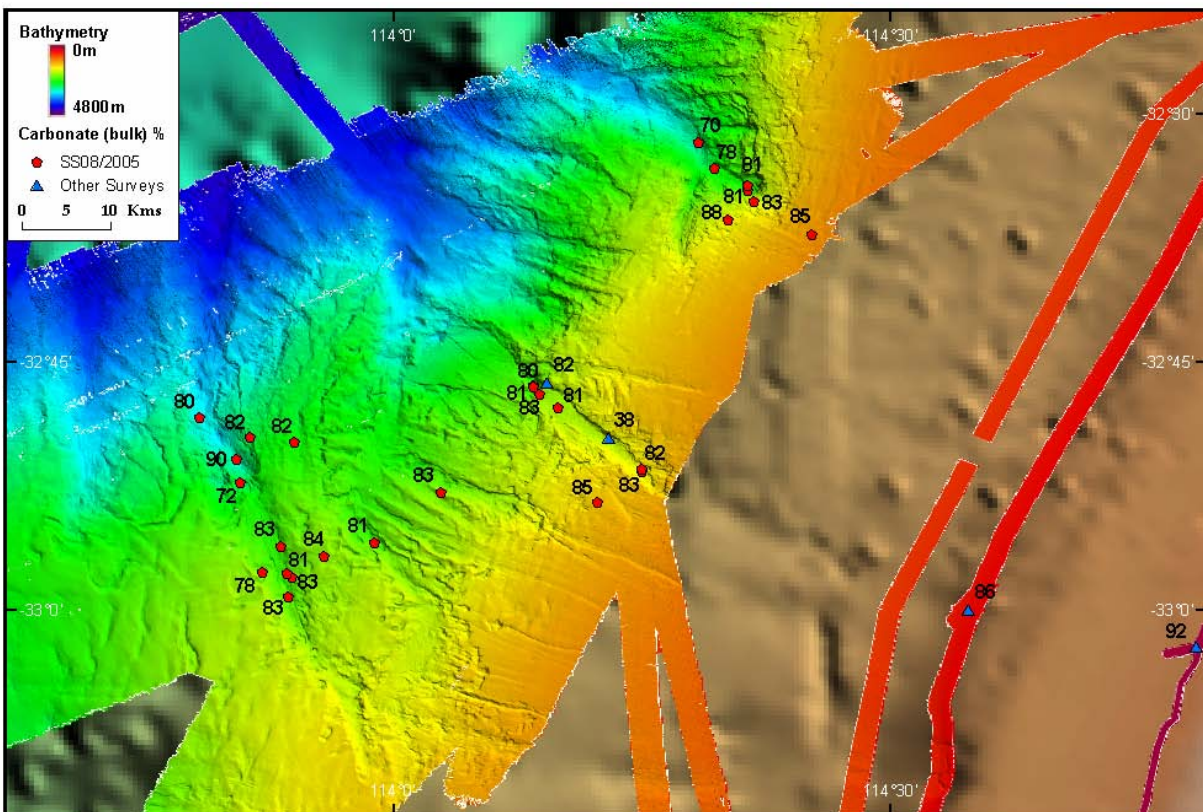


Figure 4.45. Multi-beam (swath) sonar bathymetry image showing carbonate (bulk%) contents for samples in the Mentelle Basin region.

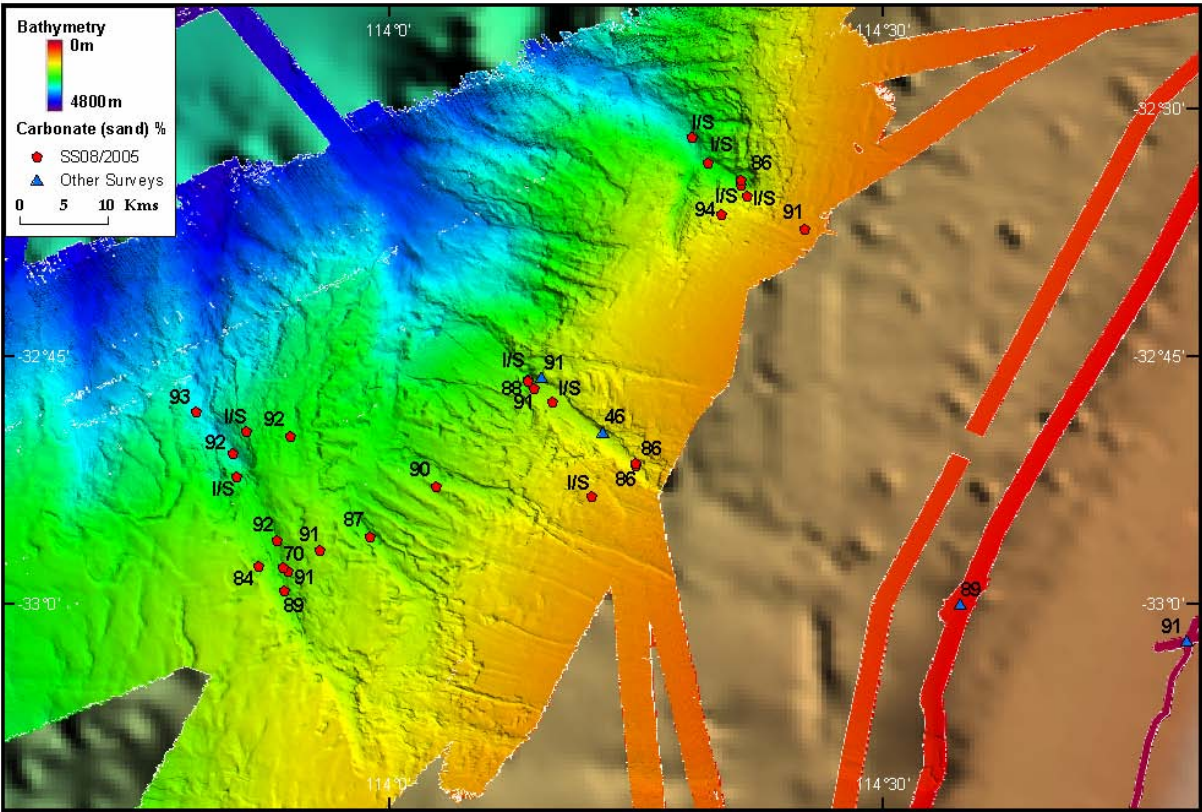


Figure 4.46. Multi-beam (swath) sonar bathymetry image showing carbonate (sand%) contents for samples in the Mentelle Basin region.

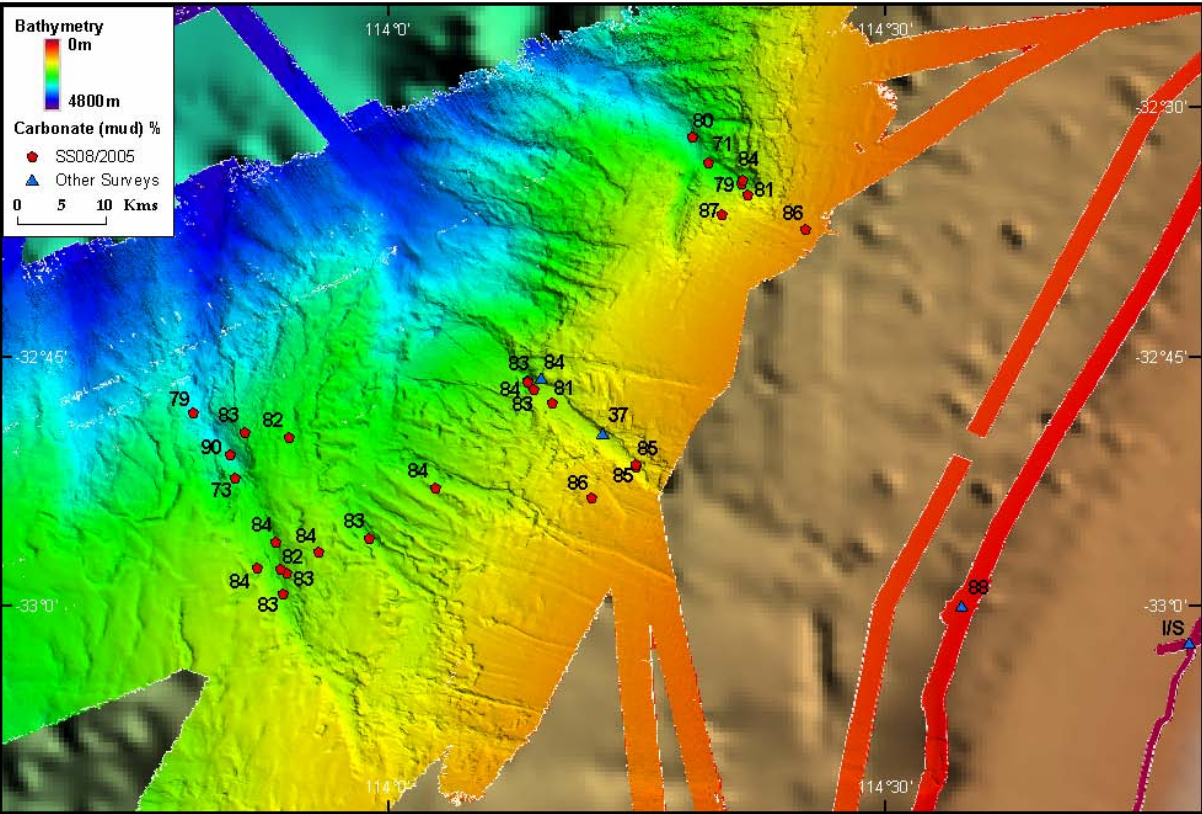


Figure 4.47. Multi-beam (swath) sonar bathymetry image showing carbonate (mud%) contents for samples in the Mentelle Basin region.

Canyons (87% and 83%, respectively), but similar to sediments from Geographe Canyon (79%). Lowest mud contents occur in sediments from the upper slope (44%) and shelf (0%).

Carbonate (bulk): Bulk carbonate contents for Busselton Canyon range from 70% to 83%, 38% to 83% for Geographe Canyon, and 72% to 90% for Bunbury Canyon (Fig. 4.45). Average bulk carbonate contents are 76% for Geographe Canyon, 79% for Busselton Canyon, and 81% for Bunbury Canyon. These values are similar to the bulk carbonate contents for sediments in Perth Canyon (78%). Bulk carbonate contents range from 70% to 83% for all samples, except for one sample in Geographe Canyon which contained a bulk carbonate content of 38%. This low value probably reflects sampling of the underlying basement sandstones present at this location. Apart from this, all Geographe Canyon samples have consistently high bulk carbonate contents of 80-83%. Bulk carbonate contents in Bunbury Canyon exhibit a random distribution throughout the canyon, with no obvious trends either down the canyon or across to the adjacent slope. Bulk carbonate concentrations decrease from 83% to 70% with increasing water depth in Busselton Canyon, which may reflect enhanced carbonate preservation in shallower waters. Slope sediments have bulk carbonate concentrations ranging from 81% to 88% with an average of 84%, which is higher than the average for Busselton, Geographe and Bunbury Canyons. Sediments contained in the shelf sample contain a bulk carbonate concentration of 92%.

Carbonate (sand):- Carbonate sand contents were obtained on 22 samples, with 8 samples of insufficient size to be analysed (Fig. 4.46). Sediments in the single sample from Busselton Canyon have a carbonate sand content of 86%. For Geographe Canyon, carbonate sand contents range from 46% to 91% with an average of 81%. Apart from one low value of 46% Geographe Canyon carbonate sand contents range from 86 to 91%. Bunbury Canyon carbonate sand contents range from 70% to 93%, with an average of 87.3%. Apart from one low value of 70%, Bunbury Canyon carbonate sand contents are consistently between 84% and 93%. Sediments in Geographe and Bunbury Canyons display no obvious trends in carbonate sand content either down the canyon or across to the adjacent slope. All three “blind” canyons have higher average carbonate sand contents than Perth Canyon (78%). Lower slope carbonate sand contents range from 87% to 94% with an average of 91% and are higher than those observed in the sediments from the canyons. Sediments in the sample from the upper slope have carbonate sand contents of 89% and the shelf sediments have a sand content of 91%.

Carbonate (mud): Carbonate mud contents for Busselton Canyon range from 71% to 81%, with an average of 79% (Fig. 4.47). Geographe Canyon carbonate mud values range from 37% to 85%, with an average of 78%. Sediments from this canyon contain carbonate mud contents of between 81% and 85%, apart from one value of 37% which probably reflects sampling of the underlying basement sandstones present at this location. Removing this single anomalous value results in an average carbonate mud content for the sediments in Geographe Canyon of 84%. Sediments in Bunbury Canyon contain carbonate mud contents of between 73% and 90%, with an average value of 81.3%. Sediments in both Geographe and Bunbury Canyons show no trends in carbonate mud contents either down the canyon or across to the adjacent slope. Sediments in Busselton Canyon show a slight decrease in carbonate mud content down the canyon. Average carbonate mud contents are similar to those found in Perth Canyon. Carbonate mud contents for sediments on the slope range from

82% to 87%, with an average of 84.6%, which is slightly higher than the average carbonate mud contents of sediments contained in each of the “blind” canyons.

4.3.4. Subsurface Sediments

In this section the main trends in the sedimentology and physical properties of the shallow sub-surface sediment contained in the cores are described. Each of the cores was collected to sample particular seabed habitats. A total of 24 cores were recovered from the Perth Canyon and Mentelle Basin regions, ranging in length from 0.14 m (23GC18A) to 5.37 m (27GC20) and representing a total length of 37.12 m ([Table 4.5](#)). Cores were collected from a variety of sedimentary environments in water depths of 1,117 m to 3,138 m from Busselton (05GC02-06GC03, 08GC05), Bunbury (11GC10, 12GC13-19GC16), Geographe (10GC08, 24GC18-25GC19) and Perth (26GC21-02GC24) Canyons. In addition, five cores (04GC01, 09GC06, 03GC12, 21GC17, 27GC20) were recovered from the canyon interfluvies to characterise the surrounding slope environments. Cores 07GC04 and 16GC11 comprised only a core catcher sample and are not described. Cores 09GC07 and 10GC09 were sampled for head space gas and the core material was not retained. Sediment cores (09GC06, 10GC08) were also collected at these two sites. Core logs and photographs are presented in [Appendix G](#). Textural data for the sub-surface sediments in the cores are in [Appendix H](#).

Although the overall sediment type is similar throughout all the cores, a total of three distinct facies (A, B, and C) can be defined based on colour, abundance of organic matter, and sedimentary structures. Reliable data were obtained for wet bulk density, magnetic susceptibility, fractional porosity and colour for each of the cores. P-wave velocities were also obtained however the absolute values are low for marine sediments; they are shown because the relative values are probably representative. Similarly, magnetic susceptibility values are generally low (<25 cgs). These values are similar to those observed for marine sediments collected around the Australian margin in distal locations from the mainland and terrigenous sources. While the absolute values are small, reflecting a relatively small terrigenous input, the relative changes between the cores and down each core are considered representative and useful for facies correlation between cores. The textural and compositional analyses of the sediments indicate that there are distinct facies changes between the canyons and with depth. However, the colour spectrum of the sediment shows very little change between the cores and facies, with the red, green and blue phases having very similar pixel intensities in all cores collected from across the study area. Major deviations are only present where significant sediment mottling occurs. These results point to similar sediment composition between the facies in the cores. Further analysis of these data is required to explore the subtle differences observed. Greatest variability in the physical properties of the cores occurs in the bulk density and fractional porosity. Trends in fractional porosity are generally inversely related to those displayed by the bulk density. Physical property data for the cores are in [Appendix I](#).

4.3.4.1. Perth Canyon region – sediment facies

A total of four cores were recovered from the Perth Canyon (26GC21-02GC24) ranging in length from 0.47 m (02GC24) to 1.76 m (28GC22). The cores were collected from the upper (26GC21) and lower slope of the southern canyon wall (28GC22) and from the canyon floor (02GC23-24). In each case the cores recovered poorly-sorted, fossil-rich calcareous ooze ([Appendix G](#)). A total of three distinct facies were contained in the cores.

Facies A occurs at the top of every core to a maximum thickness of 0.45 m (core 26GC21) and comprises a relatively homogenous calcareous, spiculitic ooze. The sediments are principally composed of foraminifers and nannofossils with numerous sponge spicules. The upper-most sections appear oxidised, as revealed by a slightly darker colour. Facies A grades into Facies B which is a homogeneous calcareous ooze ranging in thickness from 0.15 m (02GC23) to 0.78 m (26GC21). This facies is distinguished from Facies A by abundant (presumably) organic matter, giving it a dark appearance. Facies B is present in all cores except for 02GC24. The sediments are principally composed of foraminifers and nannofossils. Facies B also contains organic-rich horizontal laminations, burrows, and interbeds (e.g., 28GC22). In 26GC21, Facies B contains pebbles up to 0.01 m long. Facies C is composed of a relatively homogenous calcareous ooze. The base of Facies C was not sampled in our cores, and it ranges in thickness from 0.12 m (02GC24) to 1.11 m (28GC22). The sediments are principally composed of foraminifers and nannofossils and distinguished from Facies A and B primarily by colour, with the sediments being very light in colour. The upper contact of Facies C with Facies A and B is sharp, suggesting either a diagenetic or non-depositional boundary. Facies C is also characterised by organic-rich horizontal laminations, burrows, and inter-beds (e.g., 28GC22).

4.3.4.2. Mentelle Basin region – sediment facies

A total of three cores were collected from Busselton Canyon (05GC02-06GC03, 08GC05) ranging in length from 0.34 m (06GC03) to 3.99 m (05GC02). The cores were collected from the upper (05GC02) and lower (08GC05) slope of the canyon wall and from the canyon floor (06GC03). In each case the cores recovered poorly-sorted fossil-rich calcareous ooze, which appears oxidised in the upper sections of the cores, as depicted by a slight change in colour. Three distinct facies (A, B, and C) were contained in the cores. These facies are similar to those observed in cores from the Perth Canyon. The significant difference is that the stratigraphic succession of facies is repeated down core in cores recovered from the floors of Busselton (05GC02, 08GC05) and Bunbury Canyons (12GC13, 18GC15).

Facies A occurs at the top of every core and ranges in thickness from 0.10 m (17GC14, 18GC15) to 1.00 m (04GC01), although the base of this facies was not attained in 18GC15 where it occurs at the base of the core. Facies A is composed of a relatively homogenous calcareous, spiculitic ooze. The sediments are principally composed of foraminifers and nannofossils with numerous sponge spicules. The upper most sections appear highly oxidised, as revealed by a slightly darker colour. Facies A has both a sharp and gradational contact with Facies B. Facies B separates the overlying Facies A and underlying Facies C in all cores, except 17GC14, 18GC15, 23GC18A, and 27GC20 where it is absent. Facies B ranges in thickness from 0.03 m (21GC17) to 1.00 m (03GC12), although the base of this facies was not attained in 12GC13 where it occurs at the base of the core. Facies B is composed of homogenous calcareous ooze in all cores, except for 04GC01 and 11GC10 where it is muddy fine sand, and 08GC05 and 03GC12 where it is silty clay. Facies B is distinguished from Facies A by abundant organic matter, giving it a slightly darker appearance in most cases. Facies B also contains organic-rich horizontal laminations, burrows and inter-beds (e.g., 25GC19). Facies C ranges in thickness from 0.66 m (12GC13) to 4.90 m (27GC20) and is composed of relatively homogenous calcareous ooze. The base of Facies C was not sampled, except in those cores where the stratigraphic sequence is repeated and the core terminated in Facies A or B. Facies C is characterised by numerous organic-rich horizontal to inclined laminations, extensive burrowing, and interbeds (e.g., 10GC08, 25GC19). The upper contact

of Facies C with Facies A and B is sharp, suggesting a diagenetic or non-depositional boundary. The lower boundary is also sharp with Facies A, where it occurs in a repeated sequence (e.g., 08GC05).

4.3.4.3. Perth Canyon region - physical properties

Wet bulk densities range from a minimum of 1.0346 g cm⁻³ (26GC21) to a maximum of 1.7262 g cm⁻³ (28GC22), with an average of 1.4691 g cm⁻³ (Table 4.10). The range in wet bulk density down the cores is consistently within ± 0.50 g cm⁻³. These values are comparable to wet bulk densities recorded from slope sediments on other Australian margins (e.g., Dunbar *et al.*, 2000). Wet bulk densities show a slight increase down core in 26GC21 and 02GC24, which may be due to compaction otherwise no trends are observed between the facies. Magnetic susceptibilities range from 0 cgs (28GC22) to 11.4 cgs (28GC22), with an average of 5.11 cgs (Table 4.10). The range in magnetic susceptibility down the cores is relatively consistent at between 2.7-3.0 cgs, except for 26GC21 where the range is slightly lower at 2.0 cgs. In all the cores, the magnetic susceptibility rises to a peak in Facies B where darker (organic-rich?) sediments occur at the base of Facies A. By contrast magnetic susceptibilities for Facies C are generally very low, indicating a lack of organic material, in line with its increased carbonate content. This pattern is also repeated in the cores collected from the Mentelle Basin study area (see below). Fractional porosities range from 0.5938 (28GC22) to 0.9950 (26GC21), with an average of 0.7429 (Table 4.10). The range in fractional porosity down the cores is relatively consistent at 0.29, except for 02GC24 which is slightly lower at 0.20. Because the fractional porosity is inversely related to the wet bulk density the down core trends are also inversely related, with slight decreases in 26GC21 and 02GC24, probably associated with sediment compaction. Significant changes in the red, green and blue colour spectrum occur only in association with the presence of darker (organic-rich) sediment, which occurs as burrows, mottles, and fine laminations or bedding. No consistent relationship occurs between the changes in R:G:B and magnetic susceptibility.

Table 4.10. Details of physical properties of Perth Canyon region cores.

Core	Mean	Max.	Min.	Std dev.	Range	Environment
Wet bulk density (g cm ⁻³) (average = 1.4691 g cm ⁻³)						
26GC21	1.2766	1.5365	1.0346	0.1128	0.50	Upper canyon slope
28GC22	1.6058	1.7262	1.2207	0.0708	0.50	Lower canyon slope
02GC23	1.4505	1.5636	1.0573	0.1171	0.50	Canyon floor
02GC24	1.4838	1.6035	1.2595	0.0666	0.34	Canyon floor
Magnetic susceptibility (cgs) (average = 5.11 cgs)						
26GC21	4.3	9.2	0.2	2.0	9.0	Upper canyon slope
28GC22	4.0	11.4	0.0	3.1	11.4	Lower canyon slope
02GC23	4.4	9.9	1.1	2.7	8.8	Canyon floor
02GC24	7.0	11.0	1.3	3.0	9.7	Canyon floor
Fractional Porosity (average = 0.7429)						
26GC21	0.8546	0.9950	0.7039	0.0654	0.29	Upper canyon slope
28GC22	0.6637	0.8871	0.5938	0.0411	0.29	Lower canyon slope
02GC23	0.7538	0.9819	0.6882	0.0679	0.29	Canyon floor
02GC24	0.7345	0.8645	0.6650	0.0386	0.20	Canyon floor

4.3.4.4. Mentelle Basin region – physical properties

Busselton Canyon: Wet bulk densities range from 1.0697 g cm⁻³ (05GC02) to 1.7389 g cm⁻³ (08GC05), with an average of 1.5331 g cm⁻³ (Table 4.11). The range in wet bulk densities down the cores is similar for 05GC02 and 08GC05 at 0.55 g cm⁻³ and 0.59 g cm⁻³, respectively.

The range of wet bulk densities is slightly lower for 06GC03 at 0.30 g cm^{-3} . These values are comparable to wet bulk densities recorded from slope sediments on other Australian margins (e.g., Dunbar *et al.*, 2000). Wet bulk densities are relatively uniform down each core and there are no consistent trends between the facies. Down core reductions occur in the top 1.3 m of 06GC03, although the abrupt changes in the values are associated with joins in the core and the trends are probably related to sediment settling in the liner. Magnetic susceptibilities range from 0 cgs (08GC05) to 17.6 cgs (05GC02), with an average of 5.28 cgs (Table 4.11). The range of magnetic susceptibilities down the cores is relatively uniform at 3.1–3.4 cgs. In all the cores, the magnetic susceptibility rises to a peak where darker (organic-rich?) sediments occur in Facies B. By contrast magnetic susceptibilities for Facies C are generally very low, indicating a lack of organic material, in line with its higher carbonate composition. In cores 05GC02 and 08GC05 the magnetic susceptibility peaks are repeated several times down the core and are also associated with darker (organic-rich?) laminations and inter-beds. Fractional porosities range from 0.5865 (08GC05) to 0.9747 (05GC02), with an average of 0.7058 (Table 4.11). The range in fractional porosity down the cores is similar for 05GC02 and 08GC05 at 0.32 and 0.35, respectively. The range of fractional porosities is slightly lower for 06GC03 at 0.18. Down-core trends in fractional porosity are inversely related to those observed in the wet bulk densities.

Table 4.11. Details of physical properties of Busselton Canyon cores.

Core	Mean	Max.	Min.	Std dev.	Range	Environment
Wet bulk density (g cm^{-3}) (average = 1.5331 g cm^{-3})						
05GC02	1.5367	1.6293	1.0697	0.0639	0.55	Upper canyon slope
06GC03	1.4331	1.5768	1.2729	0.0631	0.30	Mid canyon slope
08GC05	1.5389	1.7389	1.1426	0.0950	0.59	Lower canyon slope
Magnetic susceptibility (cgs) (average = 5.28 cgs)						
05GC02	5.8	17.6	0.8	3.4	16.8	Upper canyon slope
06GC03	7.0	11.6	1.4	3.1	10.2	Mid canyon slope
08GC05	5.8	13.3	0.0	3.2	13.3	Lower canyon slope
Fractional Porosity (average = 0.7058)						
05GC02	0.7038	0.9747	0.6501	0.0370	0.32	Upper canyon slope
06GC03	0.7639	0.8568	0.6805	0.0366	0.18	Mid canyon slope
08GC05	0.7025	0.9323	0.5865	0.0551	0.35	Lower canyon slope

Geographe Canyon: Wet bulk densities range from 1.1202 g cm^{-3} (25GC19) to 1.6954 g cm^{-3} (24GC18), with an average of 1.5584 g cm^{-3} (Table 4.12). The range in wet bulk densities down the cores is similar for 10GC08 and 25GC19 at 0.52 and 0.57 g cm^{-3} , respectively, and slightly lower at 0.37 g cm^{-3} for 24GC18. There is a down core increase in wet bulk density for all three cores, which may be due to sediment compaction as the peaks do not appear to consistently correlate with any other physical property changes. Most significant changes in wet bulk densities are associated with breaks in the core and are probably artefacts. Magnetic susceptibilities range from 0 cgs (all cores) to 17.8 (10GC08), with an average of 3.16 cgs (Table 4.12). The range in magnetic susceptibilities is high attaining 17.8, 13.1 and 11.2 in 10GC08, 24GC18 and 25GC19, respectively. Peaks in the magnetic susceptibility coincide with darker (organic-rich?) sediment and horizontal laminations and inter-beds. Generally, magnetic susceptibilities for Facies C are very low. In 10GC08 and 25GC19, the peaks are repeated several times down the core, although in 24GC18 and 25GC19, much of the data are missing. Fractional porosities range from 0.6117 to 0.9454, with an average of 0.6911 (Table 4.12). The range in fractional porosities down the cores is similar for 10GC08 and 25GC19 at

0.31 and 0.33, respectively. The range in fractional porosities is slightly lower for 24GC18 at 0.21. Down-core trends in fractional porosity are inversely related to those observed in the wet bulk densities.

Table 4.12. Details of physical properties of Geographe Canyon cores.

Core	Mean	Max.	Min.	Std dev.	Range	Environment
Wet bulk density (g cm^{-3}) (average = 1.5584 g cm^{-3})						
10GC08	1.5607	1.6759	1.1481	0.1128	0.52	Upper canyon floor
24GC18	1.5349	1.6929	1.3256	0.0708	0.37	Mid canyon floor
25GC19	1.5869	1.6954	1.1202	0.1171	0.57	Upper canyon floor
Magnetic susceptibility (cgs) (average = 3.16 cgs)						
10GC08	4.1	17.8	0.0	3.6	17.8	Upper canyon floor
24GC18	2.2	13.1	0.0	2.6	13.1	Mid canyon floor
25GC19	2.6	11.2	0.0	2.6	11.2	Upper canyon floor
Fractional Porosity (average = 0.6911)						
10GC08	0.6895	0.9292	0.6230	0.0421	0.31	Upper canyon floor
24GC18	0.7048	0.8262	0.6132	0.0496	0.21	Mid canyon floor
25GC19	0.6746	0.9454	0.6117	0.0460	0.33	Upper canyon floor

Bunbury Canyon: Wet bulk densities range from 1.0018 g cm^{-3} (19GC16) to 1.6994 g cm^{-3} (12GC13), with an average of 1.5558 g cm^{-3} (Table 4.13). The range in wet bulk densities down the cores is relatively consistent for all cores at $0.28\text{--}0.32 \text{ g cm}^{-3}$, except 19GC16 which has a slightly higher range of 0.55 g cm^{-3} . Except for 19GC16, wet bulk densities are relatively constant down each core with no obvious trends. Wet bulk densities increase down core in 19GC16, although this is likely due to sediment compaction in this short core. Changes in wet bulk density observed in the cores do not consistently correspond to changes in any of the other physical properties. The most significant changes in wet bulk density are associated with breaks in the core and are probably artefacts. Magnetic susceptibilities range from 0 cgs (18GC15) to 22.0 (12GC13), with an average of 6.30 cgs (Table 4.13). The range in magnetic susceptibilities down core is relatively high, attaining 18.4, 12.3, 9.5, 8.9, and 8.0 in 12GC13, 18GC15, 11GC10, 17GC14 and 19GC16, respectively. Peaks in the magnetic susceptibility coincide with darker (organic-rich?) sediment. Peaks occur at the base of Facies A in all of the cores, and in 12GC13 and 18GC15, they are repeated down the core and coincide with Facies A. Fractional porosities range from 0.6094 (12GC13) to 0.9985 (19GC16), with an average of 0.6895 (Table 4.13). The range in fractional porosities down each core is similar at $0.16\text{--}0.18$ for all cores except 19GC16, which is slightly higher at 0.30. Down-core trends in fractional porosity are inversely related to those observed in the wet bulk densities.

Canyon Interfluves: Wet bulk densities range from 1.2098 g cm^{-3} (04GC01) to 1.8204 g cm^{-3} (27GC20), with an average of 1.6372 g cm^{-3} (Table 4.14). The range in wet bulk densities down the cores is relatively consistent for 04GC01, 03GC12 and 27GC20 at 0.43 , 0.41 and 0.43 g cm^{-3} , respectively. The range of down-core wet bulk densities is slightly higher for 09GC06 at 0.54 g cm^{-3} and lower for 21GC17 at 0.15 g cm^{-3} . Wet bulk densities increase slightly down all of the cores. However, variations in wet bulk density do not appear to be associated with any consistent changes in any of the other physical properties, so that trend observed is likely due to sediment compaction. Magnetic susceptibilities range from 0 cgs (04GC01, 09GC06, 03GC12, 27GC20) to 17.4 (03GC12), with an average of 4.19 cgs (Table 4.14). The range in magnetic susceptibilities down core is relatively high, attaining 17.4, 15.9, 10.9, 10.0 and 8.8 in 03GC12, 04GC01, 21GC17, 09GC06 and 27GC20, respectively. Peaks in the magnetic susceptibility coincide with darker (organic-rich?) sediment, as well as

Table 4.13. Details of physical properties of Bunbury Canyon cores.

Core	Mean	Max.	Min.	Std dev.	Range	Environment
Wet bulk density (g cm ⁻³) (average = 1.5558 g cm ⁻³)						
11GC10	1.4919	1.5618	1.2373	0.0749	0.32	Lower canyon floor
12GC13	1.6194	1.6994	1.4097	0.0513	0.28	Lower canyon slope
17GC14	1.5423	1.6275	1.3192	0.0496	0.30	Mid canyon floor
18GC15	1.5285	1.6538	1.3459	0.0523	0.31	Mid canyon floor
19GC16	1.1942	1.5504	1.0018	0.1676	0.55	Mid canyon floor
Magnetic susceptibility (cgs) (average = 6.30 cgs)						
11GC10	6.6	10.8	1.3	2.5	9.5	Lower canyon floor
12GC13	9.9	22.0	3.6	4.1	18.4	Lower canyon slope
17GC14	1.7	9.0	0.1	2.2	8.9	Mid canyon floor
18GC15	2.3	12.3	0.0	3.5	12.3	Mid canyon floor
19GC16	5.9	9.9	1.9	2.5	8.0	Mid canyon floor
Fractional Porosity (average = 0.6895)						
11GC10	0.7297	0.8774	0.6892	0.0434	0.18	Lower canyon floor
12GC13	0.6558	0.7775	0.6094	0.0298	0.16	Lower canyon slope
17GC14	0.7005	0.8300	0.6511	0.0288	0.17	Mid canyon floor
18GC15	0.7085	0.8145	0.6359	0.0303	0.17	Mid canyon floor
19GC16	0.8746	0.9985	0.6958	0.0901	0.30	Mid canyon floor

Table 4.14. Details of physical properties of cores recovered from the canyon interfluvies.

Core	Mean	Max.	Min.	Std dev.	Range	Environment
Wet bulk density (g cm ⁻³) (average = 1.6372 g cm ⁻³)						
04GC01	1.5399	1.6491	1.2098	0.0799	0.43	Upper slope
09GC06	1.5575	1.7559	1.2115	0.0245	0.55	Upper slope
03GC12	1.6068	1.7484	1.3321	0.0787	0.41	Upper slope
21GC17	1.5774	1.6375	1.4874	0.0340	0.15	Upper slope
27GC20	1.7275	1.8204	1.3868	0.0465	0.43	Upper slope
Magnetic susceptibility (cgs) (average = 4.19 cgs)						
04GC01	4.0	15.9	0.0	4.3	15.9	Upper slope
09GC06	1.8	10.0	0.0	2.3	10.0	Upper slope
03GC12	6.2	17.4	0.0	5.1	17.4	Upper slope
21GC17	7.8	12.7	1.8	2.6	10.9	Upper slope
27GC20	3.3	8.8	0.0	2.8	8.8	Upper slope
Fractional Porosity (average = 0.6455)						
04GC01	0.7019	0.8934	0.6386	0.0463	0.25	Upper slope
09GC06	0.6917	0.8924	0.5766	0.0907	0.32	Upper slope
03GC12	0.6631	0.8225	0.5810	0.0457	0.24	Upper slope
21GC17	0.6801	0.7323	0.6453	0.0197	0.09	Upper slope
27GC20	0.5931	0.7907	0.5392	0.0270	0.25	Upper slope

horizontal laminations and inter-beds. In all cases there is a peak at the base of Facies A and B and magnetic susceptibilities of Facies C are very low. Unlike the cores collected from the canyons, none of the interfluvie cores show repetition in the magnetic susceptibility peaks down core. Fractional porosities range from 0.5392 (27GC20) to 0.8934 (04GC01), with an average of 0.6455 (Table 4.14). The range of fractional porosities shows the same trends as the wet bulk densities, with similar values for 04GC01, 03GC12 and 27GC20 at 0.25, 0.24 and 0.25, respectively. The range of down-core fractional porosities is slightly higher for 09GC06 at 0.32 and lower for 21GC17 at 0.09. Down-core trends in fractional porosity are inversely related to those observed in the wet bulk densities.

5. Basin Geology

The second aim of the survey was to establish the basin geology and petroleum potential of the Vlaming Sub-basin and Mentelle Basin, both of which are frontier petroleum areas on the SW margin. Limited regional seismic data are available for both basins and sediments of the Mentelle Basin have never been sampled. Consequently, the stratigraphy of the Mentelle Basin can currently only be deduced from petroleum wells in the nearby Vlaming Sub-basin and through correlations with regional seismic lines. It was a principal objective of this survey to sample the sediments that comprise the Mentelle Basin, to determine its stratigraphy and assess the likelihood of a petroleum resource in the basin. Uncommercial oil has previously been found in one exploration well from the Vlaming Sub-basin which suggests an oil-prone petroleum system may be present.

A total of 12 dredges were deployed during the survey (Table 4.8). The Vlaming Sub-basin sediments were targeted by dredges recovered from the southern margin of the Perth Canyon (02DR01, 26DR09-28DR12), which intersects the central part of the basin. Dredges collected on the survey will supplement those already collected by Marshall *et al.* (1993). Mentelle Basin sediments were targeted by dredges recovered from Busselton, Geographe and Bunbury Canyons (13DR02-06DR08), which intersect the northeastern basin sediments. This sampling aimed to establish the age and composition of the basin-fill deposits to enable characterisation of petroleum system elements of the Mentelle Basin and to assist with comparison to the Vlaming Sub-basin.

High-resolution multi-beam data acquired during the survey in combination with seismic data collected in the area in 2004 allowed accurate delineation of locations where basin fill rocks were expected to be exposed in the canyons. However, positioning of dredge sites was difficult because of rough weather, thick pelagic deposits on the margins of the canyons, and lack of good outcrop.

5.1. PETROLEUM POTENTIAL

5.1.1. Vlaming Sub-basin

In the Vlaming Sub-basin petroleum exploration is active with 16 wells drilled to date. This southern part of the Perth Basin has proven petroleum potential with both oil and gas recovered from wells. Oil has been recovered from the Parmelia Group (Fig. 1.3) in Gage Roads-1, oil and gas bleeding from cores is reported from the Warnbro Group in Gage Roads-2, oil bleeding and staining in cores is reported from Araucaria-1 and gas shows were encountered in Marri-1 (Miyazaki *et al.*, 1996). Subsequent wireline and formation testing analysis suggests the presence of a small oil column in Araucaria-1, a small gas column in Marri-1 and an oil accumulation at the Gage Roads prospect. Seggie (1990) has estimated that there is the potential for 500 million barrels of oil in the Gage Roads structure.

Analysis of seismic data and drilling results by several workers (Miyazaki *et al.*, 1996; Crostella & Backhouse, 2000) suggests that an active petroleum system is present in the Vlaming Sub-basin and hydrocarbon accumulations are likely to be found where valid traps can be identified. Failure to find commercial petroleum accumulations in the past was largely due to misinterpretation of the complex structural geology based on inferior seismic data.

5.1.2. Mentelle Basin

The Mentelle Basin is a rank frontier basin with no wells or any other geological sampling conducted prior to the present survey. As such, the petroleum potential of the Mentelle Basin has been largely ignored in the past, due to the prevailing assumption that the Naturaliste Plateau and the Naturaliste Trough are composed mostly of Early Cretaceous oceanic basalts (Coleman *et al.*, 1982; Storey *et al.*, 1992). New sampling results on the Naturaliste Plateau (Beslier *et al.*, 2004) and recent review of seismic data (Borissova, 2002) showed that most of the plateau and the trough are made of rocks and form part of the west Australian margin. Preliminary analysis of newly acquired and reprocessed seismic data across parts of the Mentelle Basin highlights its petroleum potential. Seismic images show a thick half-graben fill in the western Mentelle Basin that could have provided a deep water source kitchen. There is significant potential for migration up-dip into the eastern Mentelle Basin where a series of tilted fault blocks might provide suitable traps for migrating hydrocarbons. Current Geoscience Australia basin-analysis studies on the Mentelle Basin are expected to provide further evidence for the petroleum potential of the basin, but the lack of wells means that the tectonostratigraphy of the basin is based very strongly on seismic correlations to the better known Vlaming Sub-basin.

5.2. PRELIMINARY DREDGE RESULTS

Dredges in the Perth canyon were planned in close proximity to successful dredges of the BMR 80 survey (Marshall *et al.*, 1989) which recovered a succession of Permo-Triassic to Early Cretaceous rocks, some of which showed high organic content. Almost no samples were recovered from the Jurassic part of the section, which is very thick in other parts of the Vlaming Sub-basin and is of particular interest to petroleum studies. Dredges in the present survey were thus aimed at recovering samples from this part of the section, as well as obtaining additional samples of the older sequences for direct comparison with the Mentelle Basin samples. Despite the presence of good dredging targets (outcrops steeper than 20°) only recent unconsolidated sediments were recovered in the Perth Canyon. The composition of these sediments is discussed in [Chapter 4: Sedimentology](#).

High resolution bathymetry data acquired during the survey from the multi-beam sonar confirmed that the northern Mentelle Basin does not have large canyons suitable for dredging. Analysis of the seismic data collected during survey BMR 80 revealed that lower parts of the larger canyons have gentle slopes and are filled with recent sediments. The thinnest recent sediment cover occurs close to the shelf break where basement or older sediments are more likely to be exposed or have a thin cover. These sites were identified from the high-resolution bathymetry and our sampling program targeted these outcrops, most of which were in the upper parts of the smaller canyons ([Fig. 4.28](#)). Of the nine dredges in this area only two (20DR05 and 22DR06, [Fig. 4.28](#)) recovered rocks representative of the basin fill and one dredge (23DR07) recovered basement rocks.

Dredges recovered from the Vlaming Sub-basin (02DR01, 26DR09-28DR12) and Mentelle Basin (13DR02-15DR04) that did not sample basin fill sediments contained calcilutite and nanno-fossil oozes. These younger sediments are described in [Table 9.17a](#) and [Appendix E](#).

5.2.1. Basin Sediments

Dredge samples 20DR05 and 22DR06 recovered organic-rich, dark brown, terrigenous mudstones. Preliminary palynological analysis of these samples has shown the presence of mixed Aptian to Cenomanian assemblages, including *G. senonicus*, *Spiniferites* sp., frequent *Apteodinium maculatum* (Aptian-Cenomanian), frequent *Odontochitina operculata*, *Cribroperidinium muderongense*, and possibly *Trichodinium castaneum*.

Dredge sample 23DR07 recovered samples of basement with two different lithologies: granitic rock and amphibolite. These rocks are currently being analysed at the University of Tasmania *Centre for Ore Deposit Research* with the view to establish which tectonic terrane they represent. Dredges 06DR08 and 26DR09 recovered carbonate rocks (limestone and chalk) of Middle Eocene age (E. Monteil, Geoscience Australia, *pers. comm.*, 2006) from higher in the sequence.

6. Discussion and Summary

6.1. DISCUSSION

6.1.1. Seabed and Shallow Sub-surface Sedimentology

A principal objective of the survey was to establish the Holocene sedimentology of the blind and shelf-intruding canyons. Generally, the sedimentology of the seabed for the blind canyons and shelf-intruding Perth Canyon is very similar. Indeed, the texture and composition of the seabed for both of the study regions is consistent with that found across the other Australian margins (Potter et al., 2008; Baker et al., 2008; Keene et al., 2008).

Generally, sandier sediments occur at shallower depths, with finer sediments offshore, located on the mid- and lower-slope. Gravel is a minor constituent of all samples, while mud content increases with increasing water depth. The seabed is dominated by carbonate grains, comprised mainly of the skeletons of pelagic foraminifers and nannofossils, with the fossils of benthic organisms a relatively minor constituent, although sponge spicules are common. Carbonate sands and sandy muds are present on the shelf and upper to mid slope regions, respectively.

Sand content is slightly higher in the canyons compared with the adjacent slope environments, and slightly higher in the blind canyons compared with the shelf-intruding Perth Canyon. Despite these minor differences, no other distinct trends in texture or composition were observed between the sediments on the canyon walls and floor for either the blind canyons or the Perth Canyon. Slightly higher sand contents in the canyons could point to hydraulic sorting of the grains from downslope transport and mass movements confined to the canyons. Certainly, downslope transport of sediments is evidenced by the widespread occurrence of slope failures throughout the study area, including in the canyons.

Detailed bathymetry has revealed numerous examples of seabed instability on the mid to lower slope in the Mentelle Basin (see [Appendix J](#)). The seabed morphology is rugose and contains numerous depressions that suggest that the seabed is highly deformed, with multiple failures. Other features indicative of slope failure, including detachment blocks, cracks and fault scarps, are also prevalent. Holocene seismicity in the region is low, and it is likely that these features formed gradually from gravitation processes, associated with sediment dewatering and compaction. Despite these initial conclusions, the causes of the mass movements are presently not well understood and their timing is unknown.

Very little terrigenous material is present in the seabed sediments, concomitant with the overall aridity of the Australian continent and absence of large modern river systems in the southwest. Interestingly, sediments in the Perth Canyon are slightly richer in terrigenous mud. While the sediments are overwhelmingly dominated by carbonate grains, a higher mud content implies that the Perth Canyon may be a conduit for the small amounts of terrigenous material that are sourced from the shelf to the deeper ocean, similar to other large shelf cutting canyons from other continents (e.g., Monterey Canyon, California). Transport of sediment and organic matter from the shelf to the upper slope is implied from oceanographic data with the west and northwest net displacement of water over the study period. The data also reveal that waves are the principal mechanism for resuspending material from the seabed, and were representative of relatively energetic wave conditions, although not extreme conditions, experienced during the survey. Even though this transport

mechanism is likely, the age of the sediments is unknown. It is possible that these sediments were transported to the canyon under present sea level conditions and/or were transported downslope during post-glacial marine transgressions.

The shallow (<5 mbsf) sub-surface sedimentology shows very similar texture and composition to the seabed, being primarily composed of unconsolidated spiculitic, foraminiferal/nannofossil ooze. Dredges contained chalks and dewatered, partially-cemented foraminifer/nannofossil ooze of very similar grain size distributions. This relatively homogenous sediment implies stable and similar depositional processes and environments over time throughout the study region. It also shows that the dominant sediment sources of pelagic material supplemented with smaller amounts of benthic and terrigenous material have also not changed significantly over time.

Despite the relative homogeneity of the texture and composition of the fossil content, the sub-surface sedimentology and physical properties do contain interesting characteristics that may provide evidence of changes to the relative inputs of different sediment sources. Several peaks in magnetic susceptibility occur down cores GC02 and GC05. All of the peaks coincide with intervals of darker (organic-rich?) sediment, and horizontal laminations and inter-beds, which are repeated at regular intervals down the core and associated with the repetition of sediment facies. The three facies are present in similar stratigraphic positions in all of the cores. The stratigraphic sequence of facies is repeated down core at four locations in Busselton and Bunbury Canyons. This regional stratigraphy is interpreted to represent periods of sea level lowstand when organic and terrigenous material from shelf (neritic) sources was being transported to the canyons in greater amounts/rates.

Although the peaks in magnetic susceptibility occur at different depths and we have no age control on the sediments, the pattern in down core magnetic susceptibility and sediment facies suggests an independent but repeated control on the facies development for these cores. Correlation of the facies across the canyons and slope environments points to regional processes influencing the sedimentology of the SW margin. We speculate that these regional trends are associated with high-resolution Quaternary sea-level cycles which influence the amount of organic and terrigenous matter transported to the upper slope, with the peaks representing lowstands and relatively more organic and terrigenous material transported to the upper slope. If these features represent consecutive higher-order (4th – 5th) Quaternary sea-level cycles, then the accumulation rates on the SW margin are in contrast to the relatively slow sediment accumulation rates that have been reported from slope environments offshore of the eastern Australian margin.

6.1.2. Benthic Biota

A secondary aim of the survey was to characterise the benthic biota on the deep SW margin, as the number of benthic biological samples recovered from water depths greater than 2,000 m around Australia are relatively few. In addition, the collection of biota from different seabed environments—specifically from blind and shelf-intruding canyons—provided an opportunity to compare and contrast and document biological transitions.

Fauna sampled and observed in the study area are typical of the benthic and demersal fauna for the mid- to lower-bathyal zone (200-3,000 m) for Australia and for the world's oceans (Zezina, 1998). The shelf-cutting and blind canyons and the adjacent slope environments are depauperate environments. This reflects the generally oligotrophic conditions of Australian waters. Primary production in the surface waters is generally low

and as such little food makes it to the seabed which is a significant limiting factor for organisms in the bathyal zone. Despite this, the sediments themselves have a very high fossil content. Bioturbation marks, including burrows, tracks and mounds are the most common indicators of life and reflect a relatively abundant and active infauna, as shown by the repeated occurrences of traces and specimens of worms and Holothurians in the still images. Motile species such as shrimp, prawns and lobsters are only sparsely distributed.

Given the relatively few samples collected on the survey, it is difficult to draw any firm conclusions about differences in benthic biota between the shelf-cutting and blind submarine canyons and the adjacent slope environment. Comparison with global distributions of bathyal benthic fauna indicates that the benthic biota observed on the present survey comprise the South Australian faunal element (Zezina, 1998). Although not testable in the present study given the paucity of samples and specimens, some infaunal species (e.g., bivalves, brachiopods and gastropods) attain the maximum number of species in the bathyal zone (although a generally smaller total biomass to the shelf zone). Any simplification of faunal patterns with increasing depth on this margin (i.e., reduction in the number of species, and reduction in the number of faunistic elements and provinces) probably mirrors the uniformity of water masses with increasing depth, as shown in the CTD casts. Below, 2,000 m most biogeographical differences would be related to changes in food supply.

6.1.3. Petroleum prospectivity

A third aim of the survey was to assess the petroleum potential of the Vlaming Sub-basin and Mentelle Basin. Rocks collected on the survey have provided the first samples of the basin sediments, despite the thick overburden of pelagic sediments. The interpreted ages for the samples of organic-rich terrigenous mudstones collected from the basins are Albian and Aptian to Cenomanian and Albian-Cenomanian (E. Monteil, Geoscience Australia, *pers. comm.*, 2006). Therefore, rocks dredged at these locations belong to the Coolyena Group (Fig. 1.3) that was deposited during a thermal subsidence basin phase. These rocks lie above the main stratigraphic intervals of interest for petroleum systems.

The preliminary assessment of the basement rocks recovered is that they are from the Pinjarra Orogen, although this needs to be confirmed. These rocks will be compared with basement rocks dredged during survey SS09/2005 (Voyage Summary – SS09/2005) on the Naturaliste Plateau. A better understanding of origin of the basement in the Mentelle Basin will then aid the assessment of heat flow in maturation history of the basin.

On the basis of the material recovered from the canyons and the analyses completed so far, we are unable to conclusively assess the petroleum prospectivity of the Vlaming Sub-basin and Mentelle Basin. More work needs to be completed on the samples collected on the survey, as well as further seismic and sampling needs to be undertaken in the basin regions to fully assess their prospectivity. Samples recovered during the present survey are the first samples ever recovered from the Mentelle Basin and contribute to our understanding of geological evolution of this frontier area. The geological results from this cruise are being incorporated in a regional basin-analysis study which aims to document the tectonostratigraphic history and petroleum potential of the Mentelle Basin.

6.2. SUMMARY

The major scientific outcomes of the survey are as follows:

- Collection of >5,500 km² of multibeam sonar data covering a new area of the seabed in the Mentelle Basin region. These data revealed the true extents of the blind submarine canyons in SW Australia (including two previously unknown canyons), and multiple seabed features that are associated with seabed failure and slope instability, including a 75 km² slump block at the head of Geographe Canyon. Numerous tributary canyons on the mid-slope were also discovered;
- Completion of multibeam sonar mapping of the Perth Canyon. These data filled the remaining gaps to bring the coverage to 100% for the canyon. Along with Bass Canyon, this is only the second large shelf-cutting canyon to be completely mapped with high-resolution multibeam sonar data in Australia;
- Recovery of the first rocks ever to be collected from the Mentelle Basin. These rocks comprised organic-rich terrigenous mudstones that have been dated to be Albian-Cenomanian in age from palynology;
- Recovery of basement rocks close to the surface. These samples now define and confirm the extent of the northern margin of the East Mentelle Basin sequence;
- Collection of the first ever images of the seabed below 2,000 m water depth from the SW Australian margin. The seabed images reveal that the deep-seabed is mostly covered with spiculitic ooze, with rocks cropping out at the surface on the steep flanks of the canyons. Overall, benthic biota are sparse, but the photographic evidence indicates that there is an abundant and active infauna; and
- Collection of the most comprehensive SBP data for the SW Australian margin, which reveal the sediment thickness and sub-surface architecture of the shallow seabed sediments across the mid-slope in the both the Mentelle Basin and Perth Canyon regions.

Even though we experienced bad weather and lost some time due to logistical reasons, the survey achieved its objectives. Data collected on this survey have improved our understanding of the nature and processes of the seabed associated with blind submarine canyons on the SW margin of Australia and surrounding areas, as well as the geology of the East Mentelle Basin. The petroleum potential of the Mentelle Basin is yet to be fully determined but the preliminary results are encouraging with results suggesting sufficient sediment thicknesses and rock types.

7. References

- Backhouse, J., 1978. *Palynological zonation of the Late Jurassic and Early Cretaceous sediments of the Yarragadee Formation, central Perth Basin, Western Australia*. Geological Survey of Western Australia, Report No. 7. Perth. 53pp.
- Berger, W.H., 1970. Planktonic foraminifera: Selective solution and the lysocline. *Marine Geology* **8**, 111-138.
- Beslier, M.-O., Royer, J.-Y., Girardeau, J., Hill, P., Boeuf, E., Buchanan, C., Chatin, F., Jacovetti, G., Moreau, A., Munchy, M., Partouche, C., Robert, U. and Thomas, S., 2004. Une large transition continent - océan en pied de marge sud-ouest australienne : premier résultats de la campagne MARGO/MD110. *Bulletin of the Geological Société de France* **175**, 629-641.
- Best, A.I. and Gunn, D.E., 1999. Calibration of marine sediment core loggers for quantitative acoustic impedance studies. *Marine Geology* **160**, 137-146.
- Borissova, I., 2002. *Geological framework of the Naturaliste Plateau*. Geoscience Australia, Record **2002/20**, Canberra. 44pp.
- Bosley, K.L., Lavelle, J.W., Brodeur, R.D., Wakefield, W.W., Emmett, R.L., Baker, E.T. and Rehmke, K.M., 2004. Biological and physical processes in and around Astoria submarine Canyon, Oregon, USA. *Journal of Marine Systems* **50**, 21-37.
- Bradshaw, B.E., Rollet, N., Totterdell, J.M. and Borissova, I., 2003. *A revised structural framework for frontier basins on the southern and southwestern Australian continental margin*. Geoscience Australia, Record **2003/03**, Canberra. 44pp + 45 plates.
- Carrigy, M.A. and Fairbridge, R.W., 1954. Recent sedimentation, physiography and structure of the continental shelves of Western Australia. *Journal of the Royal Society of Western Australia* **38**, 65-95.
- Carson, B., Baker, E.T., Hickey, B.M., Nittrouer, C.A., DeMaster, D.J., Thorbjarnarson, K.W. and Snyder, G.W., 1986. Modern sediment dispersal and accumulation in Quinault submarine canyon -- A summary. *Marine Geology* **71**, 1-13.
- Cartes, J.E., Company, J.B. and Maynou, F., 1994. Deep-water decapod crustacean communities in the northwestern Mediterranean: influence of submarine canyons and season. *Marine Biology* **120**, 221-229.
- Coleman, P.J., Michael, P.J. and Mutter, J.C., 1982. The origin of the Naturaliste Plateau, SE Indian Ocean; implications from dredged basalts. *Journal of the Geological Society of Australia* **29**, 457-468.
- Collins, L.B., 1988. Sediments and history of the Rottnest Shelf, southwest Australia: a swell-dominated, non-tropical carbonate margin. *Sedimentary Geology* **60**, 15-49.
- Conolly, J.R. and Von Der Borch, C.C., 1967. Sedimentation and physiography of the sea floor south of Australia. *Sedimentary Geology* **1**, 181-220.
- Cresswell, G.R. and Peterson, J.L., 1993. The Leeuwin Current south of Western Australia. *Australian Journal of Marine and Freshwater Research* **44**, 285-303.
- Cresswell, G.R., 1991. The Leeuwin Current - observations and recent models. *Journal of the Royal Society of Western Australia* **74**, 1-14.

- Cresswell, G.R. and Golding T.J., 1980. Observations of a south-flowing current in the southeastern Indian Ocean. *Deep-Sea Research* **27A**, 449-466.
- Crostella, A. and Backhouse, J., 2000. *Geology and petroleum exploration of the central and southern Perth Basin, Western Australia*. Western Australia Geological Survey, Report **57**, Perth. 87pp.
- Damuth, J. E., 1975. Echo character of the western equatorial Atlantic floor and its relationship to the dispersal and distribution of terrigenous sediments. *Marine Geology* **18**, 17-45.
- Damuth, J. E. 1980. Use of high-frequency echograms in the study of near-bottom sedimentation processes in the deep-sea: a review. *Marine Geology* **38**, 51-75.
- Davies, P.J., 1972. *Submarine canyons on the continental margin of southeast Australia*. Bureau of Mineral Resources, Geology and Geophysics, Record **1973/147**, Canberra. 11pp.
- Emery, K.O. and Uchupi, E., 1972. Western North Atlantic Ocean: Topography, rocks, structure, water, life and sediments. *American Association of Petroleum Geology Memoir*, No. 17. 532pp.
- Exon, N.F., Hill, P.J. and Post, A., 2005. Nature and origin of the submarine Albany Canyons off southwest Australia. *Australian Journal of Earth Sciences* **52**, 101-115.
- Folk, R.L., 1954. The distinction between grainsize and mineral composition in sedimentary rock nomenclature. *Journal of Geology* **62**, 334-359.
- Foreman, M.G.G., 1977. *Manual for Tidal Heights Analysis and Prediction*. Pacific Marine Science Report **77-10**. Institute of Ocean Sciences, Patricia Bay, Sidney. 97 pp.
- Freeland, H.J. and Denman, K.L., 1982. A topographically induced upwelling center of southern Vancouver Island. *Journal of Marine Research* **40**, 1069-1093.
- Gardner, W.D., 1989. Baltimore Canyon as a modern conduit of sediment to the deep sea. *Deep Sea Research Part A. Oceanographic Research Papers* **36**, 323-358.
- Gerland, S. and Villinger, H., 1995. Non-destructive density determination on marine sediment cores from gamma-ray attenuation measurements. *Geo-Marine Letters* **15**, 111-118.
- Gingele, F.X., De Deckker, P. and Hillenbrand, C-D., 2004. Late Quaternary terrigenous sediments from the Murray Canyons area, offshore South Australia and their implications for sea level change, palaeoclimate and palaeodrainage of the Murray Darling Basin. *Marine Geology* **212**, 183-197.
- Godfrey, J.S. and Ridgway, K., 1985. The large-scale environment of the poleward flowing Leeuwin Current, Western Australia: Longshore steric height gradients, wind stresses and geostrophic flow. *Journal of Physical Oceanography* **15**, 481-508.
- Granata, T.C., Vidondo, B., Duarte, C.M., Satta, M.P. and Gracia, M., 1999. Hydrodynamics and particles transport associated with a submarine canyon off Blanes (Spain), NW Mediterranean Sea. *Continental Shelf Research* **19**, 1249-1263.
- Haedrich, R.L., Rowe, G.T. and Polloni, P.T., 1980. The megabenthic fauna of the deep sea south of New England, USA. *Marine Biology* **57**, 165-179.

- Haedrich, R.L., Rowe, G.T. and Polloni, P.T., 1975. Zonation and faunal composition of epibenthic populations on the continental slope south of New England. *Journal of Marine Research* **33**, 191-212.
- Harris, P.T., Baker, E.K. and Cole, A.R., 1991. Physical sedimentology of the Australian continental shelf, with emphasis on Late Quaternary deposits in major shipping channels, port approaches and choke points. *Ocean Sciences Institute, University of Sydney, Report No. 51*, Sydney. 505pp.
- Hayes, D.E., Frakes L.A., Barrett, P.J., et al., 1975. *Initial Reports of the Deep Sea Drilling Project 28; Fremantle, Australia to Christchurch, New Zealand; Leg 28*, 19-48.
- Heap, A.D., Dickens, G.R. and Stewart, L.K., 2001. Late Holocene sediment in Nara Inlet, central Great Barrier Reef platform, Australia: sediment accumulation on the middle shelf of a tropical mixed clastic/carbonate systems. *Marine Geology* **176**, 39-54.
- Heap, A.D., Larcombe, P. and Woolfe, K.J., 1999. Storm-dominated sedimentation in a protected basin fringed by coral reefs, Nara Inlet, Whitsunday Islands, Great Barrier Reef. *Australian Journal of Earth Sciences* **46**, 443-451.
- Hill, P.J., De Deckker, P. and Exon, N.F., 2005. Geomorphology and evolution of the gigantic Murray canyons on the Australian southern margin. *Australian Journal of Earth Sciences* **52**, 117-136.
- Hill, P. and De Deckker, P., 2004. *AUSCAN Seafloor mapping and geological sampling survey on the Australian margin by RV Marion Dufrense in 2003: final project report*. Geoscience Australia, Record **2004/04**, Canberra. 136 pp.
- Hooker, S.K., Whitehead, H. and Gowans, S., 1999. Marine Protected Area Design and the Spatial and Temporal Distribution of Cetaceans in a Submarine Canyon. *Conservation Biology* **13**, 592-602.
- Inman, D.L., Nordstrom, C.E. and Flick, R.E., 1976. Currents in submarine canyons; an air-sea-land interaction. *Annual Review of Fluid Mechanics* **8**, 275-310.
- James, N.P., Collins, L.B., Bone, Y. and Hallock, P., 1999. Subtropical carbonates in a temperate realm: Modern sediments on the southwest Australian Shelf. *Journal of Sedimentary Research* **69**, 1297-1321.
- Keene, J., Baker, C., Tran, M. and Potter, A., 2008. *Geomorphology and Sedimentology of the East Marine Region of Australia*. Geoscience Australia, Record **2008/10**. Geoscience Australia, Canberra. 263pp.
- Kennett, J.P. 1982. *Marine Geology*. Prentice-Hall, New Jersey. 813pp.
- Kineke, G.C., Woolfe, K.J., Kuehl, S.A., Milliman, J.D., Dellapenna, T.M. and Purdon, R.D., 2000. Sediment export from the Sepik River, Papua New Guinea: evidence for a divergent sediment plume. *Continental Shelf Research* **20**, 2239-2266.
- Krumbein, W.C. and Sloss, L.L., 1963. *Stratigraphy and Sedimentation*. 2nd edition. WH Freeman and Company, San Francisco. 660pp.
- Lemm, A.J., Hegge, B.J. and Masselink, G., 1999. Offshore wave climate, Perth (Western Australia), 1994-96. *Marine and Freshwater Research* **50**, 95-102.

- Liu, J.T. and Lin H., 2004. Sediment dynamics in a submarine canyon: a case of river-sea interaction. *Marine Geology* **207**, 55-81.
- Marshall, J.F., Ramsay, D.C., Moore, A.M.G., Shafik, S., Graham, T.G. and Needham, J., 1993. *The Vlaming Sub-basin, offshore South Perth Basin*. AGSO, Continental Margins Folio 7, Canberra. 85pp.
- Marshall, J.F., Ramsay, D.C., Lavering, I., Swift, M.G., Shafik, S., Graham, T.G., West, B.G., Boreham, C.J., Summons, R.E., Apthorpe, M. and Evans, P.E., 1989. *Hydrocarbon prospectivity of the offshore Perth Basin*. Bureau of Mineral Resources, Geology and Geophysics, Record **1989/23**, Canberra. 158pp + 53 folded plates.
- Masselink, G. and Hughes, M.G., 2003. *Introduction to Coastal Processes and Geomorphology*. Hodder Arnold, London. 354 pp.
- McCauley, R.D., Jenner, C., Bannister, J.L., Cato, D.H. and Duncan, A., 2000. Blue Whale calling in the Rottnest trench, Western Australia, and low frequency sea noise. *Australian Acoustical Society Conference, Joondalup, Australia, 15-17 November, 2000*. 6pp.
- Miyazaki, S., Cadman, S.J., Vuckovic, V., Davey, S.J. and Conolly, J.R., 1996. *Vlaming Sub-Basin Petroleum Prospectivity Bulletin and Database*. Bureau of Resource Sciences, Canberra. **1996/1**.
- Mullenbach, B.L. and Nittrouer, C.A. *Rapid deposition of fluvial sediment in the Eel Canyon, northern California*. *Continental Shelf Research* **20**, 2191-2212.
- Muller and Gastner, 1971. The "Karbonat-Bombe", a simple device for the determination of the carbonate content in sediments, soils, and other materials. *Neues Jahrbuch fuer Mineralogie* **10**, 466-469.
- Nielsen, P., 1992. Coastal Bottom Boundary Layers and Sediment Transport. *Advanced Series on Ocean Engineering Vol. 4*. World Scientific Publishing, Singapore. 324pp.
- Norvick, M.S., 2003. *Tectonic and stratigraphic history of the Perth Basin*. Geoscience Australia Record **2004/16**, Canberra. 25pp.
- Ogston, A.S., Cacchione, D.A., Sternberg, R.W. and Kineke, G.C., Observations of storm and river flood-driven sediment transport on the northern California continental shelf. *Continental Shelf Research* **20**, 2141-2162.
- Pattiaratchi, C.B. and Buchan, S.J., 1991. Implications of long term climate change for the Leeuwin Current. *Journal of the Royal Society of Western Australia* **74**, 133-140.
- Pawlowicz, R., Beardsley, B. and Lentz, S., 2002. Classical tidal harmonic analysis including error estimates in MATLAB using T_TIDE. *Computers and Geosciences* **28**, 929-937.
- Pearce, A. and Pattiaratchi, C., 1999. The Capes Current: a summer countercurrent flowing past Cape Leeuwin and Cape Naturaliste, Western Australia. *Continental Shelf Research* **19**, 401-420.
- Pickering, K.T., Hiscott, R.N. and Hein, F.J., 1989. *Deep marine environments. Clastic sedimentation and tectonics*. Unwin Hyman, London.
- Playford, P.E., Cockbain, A.E., and Low, G.H., 1976. *Geology of the Perth Basin Western Australia*. Geological Survey of Western Australia, Bulletin **124**, Perth. 311pp.

- Potter, A., Baker, C., Tran, M. and Heap, A.D., 2008. *Geomorphology and Sedimentology of the Northwest Marine Region of Australia*. Geoscience Australia, Record **2008/08**. Geoscience Australia, Canberra. 229pp.
- Potter, A., Southby, C. and Heap, A.D., 2008. *Geomorphology and Sedimentology of the South West Planning Region of Australia*. Geoscience Australia, Record **2008/11**. Geoscience Australia, Canberra. 105pp.
- Pugh, D., 2004. *Changing Sea Levels: Effects of Tides, Weather and Climate*. Cambridge University Press, Cambridge. 265pp.
- Puig, P., Ogston, A.S., Mullenbach, B.L., Nittrouer, C.A. and Sternberg, R.W. 2003. Shelf-to-canyon sediment-transport processes on the Eel continental margin (northern California). *Marine Geology* **193**, 129-149.
- Rennie, S., 2006. Physical processes within the Perth Canyon and their influence on productivity. *EOS Transactions, American Geophysical Union, Ocean Science Meeting Supplement* **87**, Abstract OS45-08.
- Robinson, S.G., 1990. Applications for whole-core magnetic susceptibility measurements of deep-sea sediments: Leg 115 Results. In: Duncan, R.A., Backman, J., Peterson, L.C., *et al.* (Eds.), ODP, *Scientific Results, Ocean Drilling Program Leg 115*, p.737-771. Texas A&M University, College Station.
- Rowe, G.T., Polloni, P.T. and Haedrich, R.L., 1982. The deep-sea macrobenthos on the continental margin of the northwest Atlantic Ocean. *Deep-Sea Research Part A. Oceanographic Research Papers* **29**, 257-278.
- Rowe, G.T., 1971. Observations of bottom currents and epibenthic populations in Hatteras submarine canyon. *Deep-Sea Research* **18**, 569-581.
- Seggie, R., 1990. Geological cross-sections of the Vlaming Sub-basin, South Perth Basin. Bureau of Mineral Resources, Geology and Geophysics, Record **1990/64**, Canberra. 21pp.
- Shepard, F.P., 1973. *Submarine Geology*. 3rd Ed. Harper and Row, New York. 517pp.
- Shepard, F.P., 1972. Submarine Canyons. *Earth Sciences Review* **8**, 1-12.
- Shepard, F.P. and Dill, R.F., 1966. *Submarine Canyons and Other Sea Valleys*. Rand McNally Geology Series, Chicago. 381pp.
- Shepard, F.P., Marshall, N.F., McLoughlin, P.A. and Sullivan, G.G., 1979. *Currents in submarine canyons and other sea valleys*. AAPG Studies in Geology, **8**, American Association of Petroleum Geologists, Tulsa. 173pp.
- Shanmugan, G., Moiola, R.J. and Damuth, J.E., 1985. Eustatic control of submarine fan development. In: Bouma, A., Normark, W. R., and Barnes, N.E., (Eds), 1986. *Submarine fans and related turbidite systems*, Springer Verlag, New York. 351pp.
- Smith, R.L., Huyer, A., Godfrey, J.S. and Church, J.A., 1991. The Leeuwin Current off Western Australia, 1986-1987. *Journal of Physical Oceanography*, **21**, 323-345.
- Snelgrove, P.V.R., Grassle, J.F., Petrecca, R.F., 1994. Macrofaunal response to artificial enrichments and depressions in a deep-sea habitat. *Journal of Marine Research* **52**, 345-369.

- Soulsby, R.L., 1997. *Dynamics of Marine Sands: A manual for practical applications*. Thomas Telford, London. 249pp.
- Soulsby, R.L. and Whitehouse, R.J.S.W., 1997. Threshold of sediment motion in coastal environments. *Proceedings of the Pacific Coasts and Ports 1997 Conference, Christchurch* **1**, p.149-154. University of Canterbury, New Zealand.
- Spring, D.E. and Newell, N.A., 1993. Depositional systems and sequence stratigraphy of the Cretaceous Warnbro Group, Vlaming Sub-basin, Western Australia. *APEA Journal* **33**, 190-204.
- Stagg, H.M.J. and Willcox, J.B., 1991. Structure and hydrocarbon potential of the Bremer Basin, southwest Australia. *Journal of Australian Geology and Geophysics*, **12**, 327-337.
- Stefanescu, C., Morales-Nin, B. and Massuti, E., 1994. Fish assemblages on the slope in the Catalan Sea (western Mediterranean): influence of a submarine canyon. *Journal of Marine Biological Association of the United Kingdom* **74**, 499-512.
- Storey, M., Kent, R.W., Saunders, A.D., Salters, V.J., Hergt, J., Whitechurch, H., Sevigny, J.H., Thirlwall, M.F., Leat, P., Ghose, N.C. and Gifford, M., 1992. Lower Cretaceous volcanic rocks on continental margins and their relationship to the Kerguelen Plateau. In: Wise Jr, S.W., Schlich, R. *et al.*, *Proceedings of Scientific Results, ODP, Leg 120, Central Kerguelen Plateau*, p. 33-53. Texas A&M University, College Station.
- Thompson, R.O.R.Y., 1984. Observations of the Leeuwin Current off Western Australia. *Journal of Physical Oceanography* **14**, 623-628.
- Vetter E.W. and Dayton, P.K. 1999. Organic enrichment by microphyte detritus, and abundance patterns of megafaunal populations in submarine canyons. *Marine Ecology Progress Series* **186**, 137-148.
- Vetter, E.W. 1998. Population dynamics of a dense assemblage of marine detritivores. *Journal of Experimental Marine Biology and Ecology* **226**, 131-161.
- Vetter, E.W. and Dayton, P.K., 1998. Macrofaunal communities within and adjacent to a detritus-rich submarine canyon system. *Deep-Sea Research II* **45**, 25-54.
- Vetter, E.W., 1994. Hotspots of benthic production. *Nature* **372**, 47.
- Vincenty, T., 1975. Direct and inverse solutions of geodesics on the ellipsoid with application of nested solutions. *Survey Review* **23**, 88-93.
- Von der Borch, C.C., 1968. Southern Australian submarine canyons: their distribution and ages. *Marine Geology* **6**, 267-279.
- Von der Borch, C.C., 1967. *Giant submarine canyons*. In: Tyler, M.J., Twidale, C.R. and Ling, J.K. (Eds.), *Natural History of Kangaroo Island*, p47-51. Royal Society of South Australia, Adelaide.
- Voyage Summary–SS09/2005. Nature and origin of the Naturaliste Plateau and Diamantina Zone: a key in understanding the assembly and break-up history of Eastern Gondwana (21 Oct–16 Nov 2005), http://www.marine.csiro.au/nationalfacility/voyagedocs/2005/Summary_SS09-2005pdf.

- Webb, D.J. and Morris, R.J., 1984. DSDP Site 258: evidence for recent nutrient-rich upwelling off Western Australia. Deep Sea Research Part A. *Oceanographic Research Papers* **31**, 1265-1272.
- Weber, M.E., Niessen, F., Kuhn, G. and Wiedicke, M., 1997. Calibration and application of marine sedimentary physical properties using a multi-sensor core logger. *Marine Geology* **136**, 151-172.

8. Acknowledgements

We thank the National Facility Steering Committee for making ship time available on the RV *Southern Surveyor*. Financial support for the survey was provided by Geoscience Australia, Department of the Environment, Water, Heritage and the Arts, and CSIRO. Technical support for the survey was provided by Hiski Kippo and Drew Mills (CSIRO), and Andrew Hislop, Jon Stratton, Ray De Graaf, Tim Johnson, Jack Pittar, and Stan Rucinski (Geoscience Australia). Tony Watson, Billie Poignand, and Haylee Martin of the sedimentology laboratory at Geoscience Australia managed all sample analyses and are thanked for their timely and efficient production of the physical property, texture and composition data. We also thank Capt. Les Morrow, the officers and crew of the RV *Southern Surveyor* for helping us discover something new. The original report benefited from a review by Dr Scott Nichol (Geoscience Australia).

9. Appendices

9.1. Appendix A – Survey Leader's Log

Geoscience Australia Survey 08/2005 – SW Australia
28/09/2005 – 20/10/2005
Survey Leaders Log
RV *Southern Surveyor*
Andrew Heap

Wednesday 28/09/2005: Tested Geoscience Australia's deep-water video camera while alongside. Everything was in working order. Geoscience Australia officers in Fremantle to support mobilisation went ashore and the RV *Southern Surveyor* departed Fremantle Harbour for Survey 08/2005 at 04:25 UTC. Transited to the ADCP mooring site. Successfully deployed the ADCP frame in 27 m of water at 09:21 UTC (location: -32° 02.713', 115° 26.795'). Transited to Area 1 to conduct sampling of the southern flank of the Perth Canyon. Along the way gaps in the existing swath coverage for the canyon were filled. The canyon has now almost 100% swath coverage. Most science crew are finding their sea legs. The ship's computer technician can not network any of Geoscience Australia's computers due to restrictions on the set up. This is a continuing issue that must be resolved.

Thursday 29/09/2005: Transited to Area 1 and completed a CTD at 1651 UTC in 1,450 m water depth at the first dredge station. The underwater video camera was then deployed. However, camera connector broke at 250 m due to heavy swell. The cable was re-potted at 21:00 UTC and will be left to cure for 24 hours. It was decided to continue with CTD's and dredges and complete the cameras together before transiting to Area 2. Commenced dredge on southern flank of Perth Canyon at 23:56 UTC in 2,672 m at -32° 01.367', 114° 41.360'. Upon retrieving the dredge it became apparent that the spooling gear on the port trawl winch was out of sync with the cable. This meant that the spooling gear had to be physically moved across the drum while hauling in the cable. This caused a delay of ~5 hours before the dredge came aboard. When finally aboard, the shear pin had sheared and the dredge chain bag was empty, probably due to the extended period of time it was dragging across the seabed. We obtained approximately 25 kg of spiculitic nannofossil ooze from the pipe dredge and a small piece of vesicular basalt. The problem with the spooling gear has come about because the sockets were replaced the day before we departed and the wire had not been laid out with the new sockets during the sea trials. This means that the crew will need to lay out the cable while at sea to fix the problem. It was decided to abandon sampling of Area 1 and move on to Area 2 to undertake multi-beam sonar survey to give the crew time to fix the spooling problem. Sites in Area 1 will be occupied on the way back to Fremantle. Transited to Area 2 and commenced multi-beam sonar survey. Some science crew are still finding their sea legs.

Friday 30/09/2005: Continued multi-beam sonar survey of the blind submarine canyons in Area 2. Due to heavy weather no repairs could be made to the spooling gear of the

winch drum. We are experiencing swells of up to 5 m and seas of 1.5-2 m with winds of 40 knots ahead of a cold front. The Captain has ordered that no-one is allowed on the outside decks.

Saturday 01/10/2005: Heavy weather continues in the last 24 hours with swells of up to 6 m and winds up to 35 knots, gusting to 60 knots. Multi-beam sonar survey continues. An intriguing picture of the blind canyons is beginning to emerge. The lower regions of the canyons in water depths of 3,500-4,000 m are flat-bottomed and gently sloping indicating that these lower sections are not presently active. The shape and profiles of the canyons are similar to those of the Albany canyons. In terms of seabed habitats and environments, these blind canyons will make an interesting contrast to the Albany canyons and the near-by Perth Canyon. We continue to monitor the weather situation. I am becoming concerned about one science party member who is still not well and does not seem to be getting over her seasickness. We are hoping that the break in the weather over the next 24-48 hours will help.

Sunday 02/10/2005: A rough night last night with swells up to 6 m and winds up to 35 knots, gusting to 55 knots. Multi-beam sonar survey continues with another 200 line-km completed. The submarine canyons in the northeast of the study area have terminated in 1,500-1,700 m water depth. They show well-developed cirques, slump scarps and terraces, indicating that there is some erosion occurring and their morphology is not simply reflecting the morphology of the underlying basement. Some flanks have near vertical sides and have been noted for dredging sites. The weather has moderated and we expect easing conditions for the next 24-36 hours before a freshening of the wind again. The crew have begun repairing the spooling gear on the port trawl winch and 7 stations have been provided the bridge to occupy while it is relatively calm. We are aware that sampling will be in short periods of relatively good (but not ideal) conditions between several days of rough to severe weather. We hope to commence sampling about 0600 UTC.

Monday 03/10/2005: Commenced sampling at station 3 ($-32^{\circ} 49.966'$; $113^{\circ} 54.063'$). A CTD was successfully completed in 2,450 m water depth. We then deployed GA's underwater camera at 1107 UTC ($-32^{\circ} 49.879'$; $113^{\circ} 54.019'$). The camera was lowered to 1,000 m water depth and then lost all communications. Upon retrieval the wire jumped violently at 500 m water depth. When it came to the surface we realised that the camera had parted from the wire and was lost. This is extremely disappointing for all concerned given the amount of effort put into designing and constructing the camera. It appears that the kelems grip had failed due to excess strain put on it because of the swell. The last known position of the camera was $-32^{\circ} 52.164'$; $113^{\circ} 52.375'$ in a water depth of 2,398 m. We will now use the back-up benthos camera for under-water video shots. During the day I had become more concerned about the science party member who was not getting over her sea sickness. In consultation with the Les Morrow (Skipper), Ron Plaschke (CSIRO), Drew Mills (Voyage Manager), Peter Wilkes (P&O) and Peter Harris (GA), I decided to abandon sampling after the camera failure and transit back to Fremantle to drop her off. The transfer was successfully completed at 0330 UTC and she was received by a CSIRO representative (Peter Dunn) and relatives in Perth. Jane Blevin (watch leader) and I both advised her to seek medical attention

immediately after returning to shore. In the shelter of Fremantle Harbour we trialled the benthos camera which worked perfectly. We departed for the study area at 0715 UTC and arrived back at the study site at 1600 UTC. The weather had worsened by this stage and we recommenced multi-beam sonar survey of the study area.

Tuesday 04/10/2005: Continued multi-beam sonar survey of the study area. We collected approximately 150 line-km of swath and sub-bottom profiler data. The good news is that the weather has eased and is becoming more conducive for sampling. A discussion was held on the bridge at 0800 UTC to determine whether conditions were suitable for coring. Conditions were marginal so I decided to postpone an attempt at coring until first light and continue multi-beam sonar survey.

Wednesday 05/10/2005: The weather was suitable today to commence a coring program in Busselton Canyon, a well-developed blind submarine canyon in the northeast of the study area. A 2.3 m gravity core GC01 containing grey-white spiculitic nannofossil ooze was collected from 1,630 m water depth at 00:31 UTC ($-32^{\circ} 36.427'$, $114^{\circ} 20.239'$). At station 5, GC02 was collected from 1,708 m at 04:46 UTC ($-32^{\circ} 35.241'$, $114^{\circ} 21.763'$) and comprised 4.10 m. At station 6, GC03 was collected from 2,386 m at 06:50 UTC ($-32^{\circ} 34.569'$, $114^{\circ} 21.377'$) and comprised 0.42 m. At station 7, GC04 was collected from 2,719 m at 09:21 UTC ($-32^{\circ} 31.701'$, $114^{\circ} 18.444'$) and comprised 0.30 m. The surface of this core was partially cemented and bored by numerous worm tubes. All of the cores collected from Busselton Canyon terminated in stiff grey-white spiculitic nannofossil ooze. We deployed the back-up benthos camera at station 7. The camera reached the bottom at >2,500 m water depth and captured a relatively smooth seafloor comprising nannofossil ooze containing worm trails and what appears to be a sponge. The camera became stuck in the seabed and required some skilful manoeuvring of the ship to come free. Geoscience Australia's winch had trouble retrieving the camera from that water depth and recovery was slow. After the camera was aboard we attempted a CTD at the site. Approximately 200 m below the water surface the CTD wire jumped out of the sheave and caused the winch to jam. Approximately 250 m of wire was lost and the CTD wire will need to be re-terminated. The next 6 hours were lost while the crew retrieved the CTD and tried to fix the winch.

Thursday 06/10/2005: While fine, the conditions have become unsuitable for sampling with winds of 25 knots, gusting to 30 knots associated with an approaching high pressure system from the west. We have re-commenced multi-beam sonar survey of the study area until conditions become favourable for the crew to fix the trawl winch and now also the CTD winch. We have been forced to resume multi-beam sonar survey on an oblique course to our original survey plan due to confused swell and sea conditions. The swath has revealed a series of relatively shallow and straight NW-trending tributary canyons on the upper- to mid-slope that feed the deeper and much broader blind canyons on the mid- to lower slope. The cirques of the canyons are well defined at the ends of the tributary canyons. Some even have morphologies of "plunge-pools" found at the base of waterfalls. The cirques of these canyons could represent underwater knick-points that are migrating up slope. The weather forecast is good for the next 2 days with a high pressure system moving towards us. This will allow the

crew to make the necessary repairs to the winches and we will then recommence sampling in a large un-named blind canyon in the SW of the study area.

Friday 07/10/2005: Completed approximately 250 line-km of multi-beam sonar on a course oblique to our original survey lines. The conditions have become suitable for sampling and I have put together a series of sampling sites targeting the tributary canyons in the east of our study area. At station 8, GC05 was collected from 2,546 m water depth at 20:45 UTC ($-32^{\circ} 33.267'$, $114^{\circ} 19.394'$) and comprised 3.35 m. The core had a distinct and strong smell of ammonia. At station 9, GC06 was collected from 1,308 m at 06:00 UTC ($-32^{\circ} 53.516'$, $114^{\circ} 12.548'$) and comprised 2.12 m. This core terminated in grey-white spiculitic nanno-fossil ooze. GC07 was collected at 07:09 UTC from the same station ($-32^{\circ} 53.546'$, $114^{\circ} 12.514'$) and sampled for geochemistry. CAM03 was collected at station 09 from 09:50 UTC to 11:16 UTC using the benthos underwater stills camera. More than 15 photographs were taken along a 400 m transect. The photographs showed the seabed to be smooth and sedimented. At station 10, GC08 was collected at 14:12 UTC from 1,872 m ($-32^{\circ} 47.796'$, $114^{\circ} 09.929'$) and comprised 3.7 m. This core terminated in grey-white spiculitic ooze. GC09 was collected at 15:35 UTC from the same site ($-32^{\circ} 47.817'$, $114^{\circ} 09.967'$) and sampled for geochemistry. We then abandoned sampling to transit to a way-point to the north of our study area in 4.5 km of water to stream out the port trawl wire in order to fix the spooling problem. The crew began to fix the wire at 22:00 UTC.

Saturday 08/10/2005: Completed repairs to spooling gear on the port trawl winch and transited back to the study area to re-commence sampling in western region of Area 2. I have asked for a written report from Roger Thomas (Chief Engineer) on the cause of the problem and the repairs he has made. At station 11, GC10 was collected from 3,138 m at 1318 UTC ($-32^{\circ} 48.350'$, $113^{\circ} 48.288'$) and comprised 0.40 m. The core terminated in very stiff de-watered brown clay containing large organic fragments. The clay resembles a well-developed soil horizon. Back at station 03, GC12 was collected from 2,475 m at 15:57 UTC ($-32^{\circ} 49.836'$, $113^{\circ} 54.048'$) and comprised 1.95 m. The core terminated in white-tan spiculitic nannofossil ooze. On the floor of the blind "Mentelle Canyon", GC13 was collected from 2,600 m at 18:24 UTC ($-32^{\circ} 49.537'$, $113^{\circ} 51.383'$) and comprised 3.0 m. The core terminated in white-grey spiculitic nannofossil ooze. A CTD was then completed at 20:26 UTC ($-32^{\circ} 49.494'$, $113^{\circ} 51.267'$) followed by a camera run at 23:37 UTC ($-32^{\circ} 49.410'$, $113^{\circ} 51.454'$ to $-32^{\circ} 49.753'$, $113^{\circ} 51.215'$). A total of 12 photographs showed that the seabed of the canyon to be comprised of nannofossil ooze. A sea cucumber and lobster (sp unknown) were captured in the photographs, although burrows and ejecta were common implying a relatively abundant infauna.

Sunday 09/10/2005: The camera at station 12 was completed and recovered from the seabed. By this time the weather had deteriorated and we were experiencing 20-30 knot winds and swells rising to 4 m. The deck crew and engineers did not want to risk deploying the benthic sled in case there was trouble getting the wire back on board. This outcome is very frustrating for all on board given that we lost 20 hours of perfect weather yesterday to fix the trawl wire. Consequently, we recommenced the multi-beam sonar survey of the study area. We have almost completed 100% of the study area and will also spend some time filling in the gaps. We continue to monitor the weather and will

re-commence sampling as soon as conditions allow it. At approximately, 03:30 UTC the swath system crashed with a serious error causing it to lose the entire project to date. Fortunately, all of the data are backed up on the ship's network. Conditions had abated slightly at this time, so we steamed back to station 12 to commence the benthic sled.

Monday 10/10/2005: The swath system was brought back on line during the transit to the benthic sled site. BS02 was deployed in Mentelle Canyon in 2,600 m water depth at 09:46 UTC (-32° 50.294', 113° 50.508' to -32° 50.548', 113° 50.247'). The sled came back with approximately 500 g of white spiculitic mud on the frame. It was apparent that the jaws of the sled did not open during the deployment. We lashed the jaws back to ensure material enters the sled next time. DR02 was then deployed on the cirque wall of Mentelle Canyon in 2,775 m water depth at 15:43 UTC (-32° 52.430', 113° 49.680' to -32° 52.926', 113° 49.277'). The dredge came back 70% full of white-green spiculitic nannofossil ooze. Three types of ooze were recognised, namely: unconsolidated, gluggy and partially-lithified. These three types probably represent increasing age and depth. The gluggy and partially-lithified samples were greenish-grey in colour and may contain abundant glauconite. The wind has abated to <5 knots, but a 3.5-4 m swell remains with us.

Tuesday 11/10/2005: Sampling of the tributary Mentelle Canyon continues. DR03 was deployed in 2,013 m water depth at 00:07 UTC (-32° 57.940', 113° 52.400' to -32° 58.019', 113° 51.895'). The dredge contained spiculitic nannofossil ooze in the pipe dredges. The 5T shear-pin broke on the chain bag, releasing anything inside it. DR04 was deployed in 2,150 m water depth at 06:00 UTC (-32° 57.610', 113° 52.449' to -32° 57.958', 113° 51.058'). The dredge recovered spiculitic nannofossil ooze and a specimen of deep-water coral (*Solenosmilia variabilis*), indicating the presence of rock outcrops. This coral is one of the main reef-building corals on deep-sea seamounts. 16GC11 (collected out of sequence) was deployed in 2,131 m water depth at 12:36 UTC (-32° 56.362', 113° 52.798'). The core recovered 0.10 m and terminated in very stiff, de-watered white to grey-white spiculitic nannofossil ooze contained in the core cutter and core catcher. GC14 was deployed in 2,072 m water depth at 14:57 UTC (-32° 56.143', 113° 53.220'). The core recovered 0.90 m of stiff, de-watered grey-white spiculitic nannofossil ooze. This core was taken in place of a rock dredge at this site due to the inability of the ship to dredge from west to east given current weather conditions.

Wednesday 12/10/2005: Sampling of the tributary Mentelle Canyon continues. GC15 was deployed in 2,085 m water depth at 18:21 UTC (-32° 58.050', 113° 53.877'). The core recovered 1.85 m of white to tan coloured spiculitic nannofossil ooze. GC16 was deployed in 2,170 m water depth at 21:06 UTC (-32° 59.250', 113° 53.644'). The core recovered 0.30 m of semi-consolidated spiculitic nannofossil ooze. A CTD was attempted at 23:08 UTC at this location but had to be aborted due to software problems. A camera tow was completed from 02:41 UTC to 05:05 UTC (-32° 59.226', 113° 53.649' to -33° 00.278', 113° 53.418'), representing a distance of approximately 2 km. Unfortunately, a broken wire on the camera loom shorted out the strobe and no photos were obtained. During the camera deployment the problem with the CTD software was fixed and CTD04 was deployed in 2,199 m water depth at 07:57 UTC (-32° 59.204', 113° 53.641'). A total of 11 water samples were collected based on changing

water properties. BC01 was deployed in 2,200 m water depth at 11:15 UTC and recovered <0.05 m of semi-consolidated spiculitic nannofossil ooze. During the CTD and BC deployments the camera was fixed and CAM06 was deployed in 2,150 m water depth at 14:58 UTC (-32° 59.258', 113° 53.619' to -32° 59.369', 113° 53.611'), representing a distance of approximately 250 m. The camera returned with 5 photographs of the seabed showing numerous burrows and a large feeding trail. Unfortunately the switch on the camera was damaged, but this is repairable.

Thursday 13/10/2005: Sampling moved to another tributary canyon to the NE of the Mentelle Canyon. DR05 was deployed in 2,025 m water depth at 19:43 UTC (-32° 56.562', 113° 58.702' to -32° 56.916', 113° 58.478'). The dredge recovered a dark-brown organic-rich, micaceous terrigenous mudstone (our first rock!) and spiculitic nannofossil ooze. The micaceous mudstone appears heavily weathered and has a similar appearance to the material obtained in the base of GC10 from the base of the Mentelle Canyon. Sampling then moved to the interfluvium between Mentelle and Geographe Canyon. GC17 was deployed at this site in 1,945 m water depth at 01:07 UTC (-32° 56.797', 113° 55.816'). The core recovered 0.61 m of semi-consolidated spiculitic nanno-fossil ooze. Sampling moved to another tributary canyon of Geographe Canyon where DR06 was deployed in 2,097 m water depth at 10:41 UTC (-32° 52.744', 114° 02.866' to -32° 53.978', 114° 02.454'). The dredge recovered micaceous organic-rich dark-brown terrigenous mudstone and white to grey-white spiculitic nannofossil ooze. The mudstone is the same as that recovered from DR05 further to the west.

Friday 14/10/2005: Sampling moved to a large straight tributary of Geographe Canyon to the head-wall of an enormous slump block. DR07 was deployed in 2,320 m water depth up the head-wall at 18:58 UTC (-32° 46.613', 114° 08.582' to -32° 47.478', 114° 09.595'). In the process of dredging this steep wall the dredge stuck fast to the seabed for >2 hours but was finally freed by manoeuvring the ship directly over the dredge. The dredge recovered metamorphosed sediment (gneiss), phyllite and the seemingly ubiquitous spiculitic nannofossil ooze. The rocks in this dredge are the basement rocks that occur close to the surface indicating that the East-Mentelle basin sediments pinch-out on this margin. GC18 was deployed in 1,946 m water depth at 02:12 UTC (-32° 46.942', 114° 08.851') and recovered 0.12 m of solid pteropod hash and silty sand. CTD05 was deployed in 1,950 m water depth at 04:42 UTC (-32° 46.904', 114° 08.836') and 11 water samples were collected throughout the water column for suspended sediment. GC18 was deployed in 2,340 m water depth at 07:16 UTC (-32° 46.436', 114° 08.476') in the depression separating the slump block and head-wall. The core recovered 2.80 m of white unconsolidated spiculitic nannofossil ooze. The core was taken to sample the pelagic sediments that have accumulated in the depression since the slump to possibly determine the minimum age of the slump event. GC19 was deployed at the head of the tributary canyon in 1,562 m at 10:00 UTC (-32° 51.600', 114° 15.017'). The core recovered 3.12 m of spiculitic nannofossil ooze. CAM07 was deployed in 1,515 m water depth at 13:32 UTC (-32° 51.427', 114° 14.949'). A total of 10 photos of the seabed were obtained showing that the seabed was heavily burrowed with many feeding trails evident.

Saturday 15/10/2005: BS02 was deployed in 1,430 m at 15:57 UTC (-32° 51.203', 114° 15.482') and recovered a good haul of spiculitic nannofossil ooze. In addition to the meiofauna,

a variety of worms were collected from the haul as well as whale ear bones. Sampling then moved to the slope environments on the interfluvium of the tributary canyon. The TOPAS sub-bottom profiler showed that the sediments at this site to be very thin (<1 m) and thus the final core site was picked using the sub-bottom profile data where well-bedded sediments were 15 m thick. Despite three attempts at coring the seabed at this site, no recovery was possible, indicating that the sediments are quite hard. Also, the camera appears not to be working. A decision was made to move on to re-occupy our stations in Busselton Canyon in the far NE of the study area. The technicians are working around the clock to get it back on line. We hope that it will be fixed in time for the next station. DR08 was deployed in 1,962 m water depth at 07:51 UTC ($-32^{\circ} 34.887'$, $114^{\circ} 21.270'$ to $-32^{\circ} 35.932'$, $114^{\circ} 20.835'$) and recovered a full dredge containing unconsolidated spiculitic ooze, calcarenite (calcilutite), and abundant marly limestone. Other oddments included manganese crusts and octacoral covered in manganese crusts. GC20 was then deployed on the mid-slope above the canyon in 1,117 m water depth at 13:12 UTC ($-32^{\circ} 37.289'$, $114^{\circ} 25.270'$). The core recovered 5.36 m and terminated in sticky, de-watered spiculitic nannofossil ooze. CAM08 was deployed at this station in 1,092 m water depth at 15:54 UTC ($-32^{\circ} 37.289'$, $114^{\circ} 25.270'$) and collected 11 photos of the seabed. The photos showed the seabed to be heavily burrowed.

Sunday 16/10/2005: Sampling then moved to the cirque of Busselton Canyon where CAM09 was deployed in 1,665 m water depth at 19:28 UTC ($-32^{\circ} 35.297'$, $114^{\circ} 21.731'$) and collected 8 photographs of the seabed. The photographs revealed that the seabed to comprise heavily burrowed spiculitic ooze. A gravity core was attempted in the floor of Busselton Canyon in 3,420 m water depth. While the core hit the seabed it did not return with any sample! We then transited to Perth Canyon filling in gaps in the swath bathymetry to begin a 2-day sampling program. At the first station on the southern margin of the canyon, DR09 was deployed in 2,405 m water depth at 15:47 UTC ($-31^{\circ} 57.877'$, $114^{\circ} 36.473'$ to $-31^{\circ} 58.679'$, $114^{\circ} 35.925'$). The dredge recovered abundant calcilutite and nannofossil ooze. GC21 was then deployed at the end of the dredge tow in 2,037 m water depth at 22:21 UTC ($-32^{\circ} 58.329'$, $114^{\circ} 36.158'$) and recovered 1.31 m. The core terminated in stiff, de-watered spiculitic nannofossil ooze (calcilutite).

Monday 17/10/2005: Sampling then moved to reoccupy stations we had to abandon earlier in the survey due to bad weather. DR10 was deployed in 2,400 m water depth at 01:37 UTC ($-32^{\circ} 02.510'$, $114^{\circ} 39.520'$ to $-32^{\circ} 02.895'$, $114^{\circ} 38.114'$). The dredge recovered a full haul of calcilutite and nannofossil ooze at 2 phases of lithification. DR11 was then deployed in 2,108 m water depth at 07:25 UTC ($-32^{\circ} 03.200'$, $114^{\circ} 38.861'$ to $-32^{\circ} 03.759'$, $114^{\circ} 39.590'$). The dredge recovered a full haul of calcilutite and nannofossil ooze at 3 phases of lithification, as well as a specimen of deep-sea Bamboo Coral. DR12 was then deployed in 2,071 m water depth at 13:30 UTC ($-32^{\circ} 04.322'$, $114^{\circ} 39.893'$ to $-32^{\circ} 04.467'$, $114^{\circ} 40.117'$). The dredge recovered abundant calcilutite and some nannofossil ooze. In all three cases, the dredges hooked up on the seabed indicating significant rock exposure on the southern slopes of the canyon.

Tuesday 18/10/2005: Sampling continued on the southern flank of Perth Canyon with a series of gravity cores at the dredge locations. GC22 was deployed in 2,148 m water depth at

18:38 UTC (-32° 03.904', 114° 40.084') and comprised 1.85 m. The core terminated in indurated calcilutite mixed with nannofossil ooze. GC23 was deployed in 2,115 m water depth at 21:15 UTC (-32° 03.090', 114° 38.912') and comprised 1.19 m. The core terminated in consolidated (but not indurated) calcilutite. GC24 was deployed in 2,360 m water depth at 23:48 UTC (-32° 02.577', 114° 39.500') and comprised 0.5 m. The core terminated in consolidated calcilutite. A series of camera stations was then undertaken in a transect across the southern flank of the Perth Canyon from the interfluvial to the canyon floor. CAM11 was deployed on the interfluvial in 1,251 m at 03:38 UTC (-32° 03.865', 114° 38.200' to -32° 04.054', 114° 38.126'). A total of 7 photos were obtained along a ~400 m long transect. All of the photos showed the seabed to be composed of spiculitic nannofossil ooze. The seabed also contained numerous burrows. CAM12 was deployed on a steep (>20°) slope of the canyon wall in 2,030 m water depth at 08:20 UTC (-32° 03.085', 114° 38.919' to -32° 03.084', 114° 38.916'). The ship stayed on station due to the steep nature of this site. A total of 1 photo was obtained from this station and showed the bottom to comprise spiculitic nannofossil ooze. Interestingly, the photo contained distinctive lineations on the seafloor, probably trawl marks. CAM13 was deployed on the canyon floor in 2,700 m water depth at 13:13 UTC (-32° 01.681', 114° 40.886' to -32° 02.050', 114° 40.803'). A total of 12 photographs were obtained along a ~600 m long transect. The photos showed the canyon floor to be variable with some containing all spiculitic ooze and 1 photograph showing sub-cropping rocks interspersed with spiculitic ooze. Several sponges were seen growing on the sub-cropping rocks.

Wednesday 19/10/2005: The ADCP was recovered successfully at 23:30 UTC and CTD06, CAM14 and GR01, 02 and 03 completed at the site. The grabs contained rocky rubble and calcareous medium sand. We then transited to the head of the Perth Canyon to begin a digital acquisition survey with the side scan sonar and Topas sub-bottom profiler to seek evidence of a lowstand river channel extending across the shelf and feeding into the Perth Canyon. Alas, while we found many interesting features including onlapping reflectors, little incised channels and uncharted wrecks, we could not find any compelling evidence for a lowstand channel in the area that we surveyed. We found evidence of remnant marine deposits comprised of tidal sand ridges and laminated sediments (fan?) at the head of the canyon that would've been in 40-50 m of water at the LGM.

Thursday 20/10/2005: The pilot boarded the RV *Southern Surveyor* at 23:15 UTC and was alongside in Fremantle Harbour at 00:00 UTC. The ship was demobilised and the science and technical party departed for Canberra.

9.2. Appendix B – Shallow Seismic Screen Captures

Figures showing screen captures of select shallow seismic reflection profiles are provided on the data CD-ROM in Windows BMP and JPEG format. The figures are obtained from the TOPAS seismic acquisition program. The filenames are in date and time format: DDMMYYHHMMSS (e.g., 290905112103.bmp).

9.3. Appendix C – CTD Data and Water Samples

Table 9.1 below details the water samples collected on the six successful CTD casts. Water samples were collected to calculate suspended sediment concentrations (SSC) in each of the water masses identified in the water column. The calibrated data for each cast are contained in Excel spreadsheets on the data CD-ROM. The filenames follow the following format: *Survey Number, Station Number, Operation Type, Operation Number* (e.g., SS082005_02CTD01).

Table 9.1. Summary details of suspended sediment samples collected on the survey.

Sample	Latitude	Longitude	Water depth (m)	Filter paper pre weight (g)	Filter paper post weight (g)	SSC (g l ⁻¹)
02CTD01	-32° 03.61'	114° 38.39'	0*	0.1054	0.1136	0.0082
			278	0.1054	0.1123	0.0069
			560	0.1062	0.1125	0.0063
			900	0.1059	0.1133	0.0074
			1356 [#]	0.1064	0.1134	0.0070
02CTD02	-32° 49.97'	113° 54.22'	0*	0.1061	0.1117	0.0056
			100	0.1066	0.1117	0.0051
			200	0.1066	0.1117	0.0051
			500	0.1063	0.1111	0.0048
			850	0.1065	0.1109	0.0044
			1200	0.1067	0.1108	0.0041
			1600	0.1051	0.1096	0.0045
			1900	0.1059	0.1104	0.0045
02CTD03	-32° 49.94'	113° 51.27'	0*	0.1071	0.1163	0.0092
			800	0.1076	0.1141	0.0065
			1500	0.1074	0.1158	0.0084
			2000	0.1075	0.1138	0.0063
19CTD04	-32° 59.20'	114° 53.64'	0*	0.1025	0.1077	0.0052
			10	0.1025	0.1082	0.0057
			25	0.1021	0.107	0.0049
			50	0.102	0.1067	0.0047
			100	0.1073	0.1123	0.0050
			200	0.1075	0.1126	0.0051
			850	0.1065	0.1114	0.0049
			1200	0.1066	0.1117	0.0051
			1600	0.107	0.1117	0.0047
			1900	0.1071	0.1124	0.0053
23CTD05	-32° 46.90'	114° 08.84'	0*	0.1066	0.1132	0.0066
			10	0.1062	0.1125	0.0063
			25	0.1061	0.1125	0.0064
			50	0.1063	0.1127	0.0064
			100	0.1063	0.1127	0.0064
			500	0.1013	0.1076	0.0063
			850	0.1014	0.1069	0.0055
			1200	0.1014	0.107	0.0056
			1600	0.1013	0.1072	0.0059
			1900	0.1016	0.1072	0.0056
01CTD06	-32° 02.65'	114° 26.83'	1950*	0.1014	0.1069	0.0055
			0*	0.1064	0.1136	0.0072
			8	0.1063	0.1134	0.0071
			15	0.1054	0.1129	0.0075
			21	0.1065	0.1144	0.0079

* = Sample collected 2 m below sea surface.

= Sample collected 10 m above seabed.

9.4. Appendix D – Still Photographs

This appendix contains the summary details and brief descriptions of the still photographs taken during the survey. The descriptions are based on the field notes taken on board the ship and a detailed, systematic analysis of the images has not yet been undertaken. The descriptions are thus brief. Digital images of the photographs are contained on the data CD-ROM. Although all photographs were taken on colour film, black and white images are shown as no surface light occurs at the depths the photographs were taken, except for photographs at 01CAM14 which are shown in colour. The black and white images also increased the contrast and improved the clarity of the features on the seabed. Filenames follow the following convention: *Survey number, station number, operation type, operation number, photograph number* (e.g., SS082005_02CAM01_1).

9.4.1. Summary Details of Still Photographs

Table 9.2. Summary details of camera station SS08/2005/02CAM01.

Position	Replicate	Date & time (GMT)	Latitude	Longitude	Water depth (m)	Photo number
1	1	18/10/05 19:28	-32° 04.759'	114° 37.116'	1,280	No Recovery

Table 9.3. Summary details of camera station SS08/2005/07CAM02.

Position	Replicate	Date & time (GMT)	Latitude	Longitude	Water depth (m)	Photo number
1	1	05/10/05 11:27	-32° 31.105'	114° 19.563'	2,369	1

Table 9.4. Summary details of camera station SS08/2005/09CAM03.

Position	Replicate	Date & time (GMT)	Latitude	Longitude	Water depth (m)	Photo number
1	1	06/10/05 09:50	-32° 53.295'	114° 12.590'	1,290	1,2,3
	2	Not Recorded	-32° 53.286'	114° 12.609'	1,290	4,5,6,7,8
2	3	Not Recorded	-32° 53.292'	114° 12.619'	1,290	9,10,11
	4	06/10/05 10:20	-32° 53.337'	114° 12.604'	1,290	12,13
3	5	Not Recorded	-32° 53.335'	114° 12.605'	1,290	14,15
	6	Not Recorded	-32° 53.330'	114° 12.621'	1,290	16,17,18,19,20
4	7	06/10/05 10:42	-32° 53.431'	114° 12.580'	1,290	21,22
	8	Not Recorded	-32° 53.433'	114° 12.581'	1,290	23,24,25
5	9	06/10/05 10:49	-32° 53.433'	114° 12.583'	1,290	26,27
	10	06/10/05 11:01	-32° 53.485'	114° 12.547'	1,290	28,29,30,31,32
6	11	06/10/05 11:05	-32° 53.483'	114° 12.557'	1,290	33,34,35,36
	12	06/10/05 11:09	-32° 53.484'	114° 12.558'	1,290	No Recovery

Table 9.5. Summary details of camera station SS08/2005/12CAM04.

Position	Replicate	Date & time (GMT)	Latitude	Longitude	Water depth (m)	Photo number
1	1	09/10/05 00:06	-32° 49.390'	113° 51.484'	2,594	1,2,3,4
	2	09/10/05 00:10	-32° 49.405'	113° 51.418'	2,590	5,6,7,8,9,10
2	3	09/10/05 00:22	-32° 49.464'	113° 51.411'	2,600	No Recovery
	4	09/10/05 00:26	-32° 49.458'	113° 51.397'	2,595	No Recovery

3	5	09/10/05 00:39	-32° 49.523'	113° 51.374'	2,605	No Recovery
	6	09/10/05 00:41	-32° 49.539'	113° 51.351'	2,605	No Recovery
4	7	09/10/05 00:51	-32° 49.611'	113° 51.290'	2,600	No Recovery
	8	09/10/05 00:54	-32° 49.616'	113° 51.281'	2,605	No Recovery
5	9	09/10/05 01:06	-32° 49.688'	113° 51.250'	2,610	No Recovery
	10	09/10/05 01:08	-32° 49.678'	113° 51.258'	2,620	11
6	11	09/10/05 01:19	-32° 49.753'	113° 51.195'	2,620	12,13,14
	12	09/10/05 01:25	-32° 49.753'	113° 51.215'	2,610	15,16

Table 9.6. Summary details of camera station SS08/2005/19CAM05.

Position	Replicate	Date & time (GMT)	Latitude	Longitude	Water depth (m)	Photo number
1	1	11/10/05 02:42	-32° 59.230'	113° 53.638'	2,160	No Recovery
2	1	11/10/05 02:58	-32° 59.339'	113° 53.581'	2,160	No Recovery
3	1	11/10/05 03:15	-32° 59.472'	113° 53.530'	2,150	No Recovery
4	1	11/10/05 03:35	-32° 59.575'	113° 53.520'	2,145	No Recovery
5	1	11/10/05 03:54	-32° 59.678'	113° 53.473'	2,125	No Recovery
6	1	11/10/05 04:07	-32° 59.814'	113° 53.475'	2,122	No Recovery
7	1	11/10/05 04:24	-32° 59.937'	113° 53.453'	2,100	No Recovery
8	1	11/10/05 04:37	-33° 00.056'	113° 53.465'	2,085	No Recovery
9	1	11/10/05 04:50	-33° 00.161'	113° 53.438'	2,075	No Recovery
10	1	11/10/05 05:05	-33° 00.278'	113° 53.418'	2,060	No Recovery

Table 9.7. Summary details of camera station SS08/2005/19CAM06.

Position	Replicate	Date & time (GMT)	Latitude	Longitude	Water depth (m)	Photo number
1	1	11/10/05 14:58	-32° 59.258'	113° 53.619'	2,150	1,2
	2	11/10/05 15:01	-32° 59.244'	113° 53.616'	2,155	3
2	3	11/10/05 15:14	-32° 59.379'	113° 53.648'	2,160	4
	4	11/10/05 15:19	-32° 59.372'	113° 53.618'	2,150	5

Table 9.8. Summary details of camera station SS08/2005/25CAM07.

Position	Replicate	Date & time (GMT)	Latitude	Longitude	Water depth (m)	Photo number
1	1	13/10/05 13:32	-32° 51.427'	114° 14.949'	1,515	1
	2	13/10/05 13:39	-32° 51.490'	114° 14.904'	1,535	2
2	3	13/10/05 14:58	-32° 51.588'	114° 14.960'	1,535	3
	4	13/10/05 15:01	-32° 51.573'	114° 14.960'	1,525	4,5,6
3	5	13/10/05 15:14	-32° 51.616'	114° 15.069'	1,530	7,8,9
	6	13/10/05 15:19	-32° 51.594'	114° 15.064'	1,520	10,11,12,13

Table 9.9. Summary details of camera station SS08/2005/27CAM08.

Position	Replicate	Date & time (GMT)	Latitude	Longitude	Water depth (m)	Photo number
1	1	14/10/05 15:54	-32° 37.312'	114° 25.270'	1,090	1,2
	2	14/10/05 15:59	-32° 37.344'	114° 25.293'	1,090	3,4,5,6
2	3	14/10/05 16:11	-32° 37.428'	114° 25.272'	1,090	7

3	4	14/10/05 16:18	-32° 37.445'	114° 25.274'	1,092	8
	5	14/10/05 16:31	-32° 37.344'	114° 25.250'	1,092	-
	6	14/10/05 16:39	-32° 37.342'	114° 25.254'	1,092	9,10,11

Table 9.10. Summary details of camera station SS08/2005/05CAM09.

Position	Replicate	Date & time (GMT)	Latitude	Longitude	Water depth (m)	Photo number
1	1	16/10/05 19:28	-32° 35.297'	114° 21.731'	1,665	1,2
	2	16/10/05 19:37	-32° 35.316'	114° 21.684'	1,670	3,4,5,6
2	3	16/10/05 19:55	-32° 35.395'	114° 21.780'	1,665	7
	4	16/10/05 19:58	-32° 35.383'	114° 21.769'	1,665	8
3	5	16/10/05 20:12	-32° 35.494'	114° 21.798'	1,657	-
	6	16/10/05 20:17	-32° 35.515'	114° 21.770'	1,657	9,10,11

Table 9.11. Summary details of camera station SS08/2005/07CAM10.

Position	Replicate	Date & time (GMT)	Latitude	Longitude	Water depth (m)	Photo number
1	1	16/10/05 00:19	-32° 31.723'	114° 18.359'	2,764	-
	2	16/10/05 00:31	-32° 31.733'	114° 18.299'	2,740	-
2	3	16/10/05 00:54	-32° 31.854'	114° 18.321'	2,714	1,2,3
	4	16/10/05 01:00	-32° 31.822'	114° 18.370'	2,800	4
3	5	16/10/05 01:14	-32° 31.927'	114° 18.339'	2,817	5,6
	6	16/10/05 01:19	-32° 31.948'	114° 18.363'	2,817	7,8,9

Table 9.12. Summary details of camera station SS08/2005/30CAM11.

Position	Replicate	Date & time (GMT)	Latitude	Longitude	Water depth (m)	Photo number
1	1	17/10/05 03:38	-32° 03.865'	114° 38.200'	1,280	1
	2	17/10/05 03:46	-32° 03.840'	114° 38.162'	1,280	2,3
2	3	17/10/05 04:08	-32° 03.928'	114° 38.118'	1,250	4
	4	17/10/05 04:19	-32° 03.910'	114° 38.098'	1,265	5
3	5	17/10/05 04:36	-32° 03.041'	114° 38.125'	1,260	6
	6	17/10/05 04:43	-32° 03.054'	114° 38.126'	1,260	7

Table 9.13. Summary details of camera station SS08/2005/02CAM12.

Position	Replicate	Date & time (GMT)	Latitude	Longitude	Water depth (m)	Photo number
1	1	18/10/05 08:20	-32° 03.085'	114° 38.919'	2,035	-
	2	18/10/05 08:28	-32° 03.088'	114° 38.907'	2,030	-
2	3	18/10/05 08:34	-32° 03.081'	114° 38.915'	2,025	-
	4	18/10/05 08:41	-32° 03.082'	114° 38.910'	2,035	1
3	5	18/10/05 08:47	-32° 03.084'	114° 38.914'	2,030	-
	6	18/10/05 08:53	-32° 03.084'	114° 38.916'	2,030	-

Table 9.14. Summary details of camera station SS08/2005/29CAM13.

Position	Replicate	Date & time (GMT)	Latitude	Longitude	Water depth (m)	Photo number
1	1	18/10/05 13:13	-32° 01.681'	114° 40.886'	2,680	1,2

	2	18/10/05 13:18	-32° 01.685'	114° 40.889'	2,665	3,4
2	3	18/10/05 13:37	-32° 01.803''	114° 40.918'	2,660	5
	4	18/10/05 13:44	-32° 01.818'	114° 40.935'	2,645	6,7
3	5	18/10/05 14:02	-32° 01.941'	114° 18.893'	2,650	8
	6	18/10/05 14:10	-32° 01.943'	114° 18.877'	2,630	9
4	7	18/10/05 14:31	-32° 02.060'	114° 18.811'	2,615	10
	8	18/10/05 14:35	-32° 02.060'	114° 18.803'	2,605	11

Table 9.15. Summary details of camera station SS08/2005/01CAM14.

Position	Replicate	Date & time (GMT)	Latitude	Longitude	Water depth (m)	Photo number
1	1	19/10/05 01:44	-32° 02.638'	115° 26.609'	32	1

9.4.2. Photograph Descriptions

Table 9.16. Descriptions of still photographs collected on the survey.

SampleID	Replicate	Photo no.	Description
07CAM02	1	1	Mottled sediment. Small ball shaped sponge. Cylindrical shaped faeces and faint trails visible.
09CAM03	1	1	Bad photo.
		2	Mottled, bioturbated surface.
		3	Same image as photo 2.
	2	4	Mottled and bioturbated sediment. Small mounds and several small holes visible.
		5	Mottled and bioturbated sediment. Small mounds, small holes and several larger holes visible.
		6	Same image as photo 5.
		7	Same image as photo 5.
		8	Bad photo.
	3	9	Bad photo.
		10	Bad photo.
		11	Bad photo.
	4	12	Bad photo.
		13	Mottled and bioturbated sediment. Several holes (asymmetric) and small rounded mounds of sand.
	5	14	Mottled and bioturbated sediment. Stalked glass sponge (hexactinellid).
		15	Mottled and bioturbated sediment. Large depression.
	6	16	Mottled and bioturbated sediment. Small mounds.
		17	Mottled and bioturbated sediment. 5-6 large holes at bottom (crustacean or worm) Mounds from worms.
	7	18	Same image as photo 17.
		19	Bad photo.
		20	Bad photo.
	8	21	Mottled and bioturbated sediment. Large holes (crustacean?). Excavated sediment next to holes.
		22	Mottled and bioturbated sediment.
		23	Same image as photo 22.
	9	24	Same image as photo 22.
		25	Bad photo.
	10	26	Mottled and bioturbated sediment. Mounds visible.
		27	Same image as photo 26.
	11	28	Bad photo.
		29	Mottled and bioturbated sediment. Shrimp. Mounds and holes.
		30	Same image as photo 29.
		31	Same image as photo 29.
		32	Bad photo.
	11	33	Bad photo.
		34	Mottled and bioturbated sediment. Two large holes.

		35	Same image as photo 34.
		36	Same image as photo 34.
	12	-	No photo.
12CAM04	1	1	Bad photo.
		2	Bad photo.
		3	Sediment. Clump of hard rock?
		4	Same image as photo 3.
	2	5	Bad photo.
		6	Bad photo.
		7	Bad photo.
		8	Bad photo.
		9	Bad photo.
		10	Mottled and bioturbated sediment.
	3	-	No photo.
	4	-	No photo.
	5	-	No photo.
	6	-	No photo.
	7	-	No photo.
	8	-	No photo.
	9	-	No photo.
	10	11	Mottle and bioturbated sediment. Holothurian.
	11	12	Mottled and bioturbated sediment. Two ball shaped sponges. Faint trail marks and small cylindrical faeces.
		13	Mottled sediment. Small ball shaped sponge.
		14	Same image as photo 13.
	12	15	Mottled sediment. Two rounded sponges at bottom.
		16	Squat lobster (galatheid). Probably hard ground under thin silt layer.
19CAM06	1	1	Mottled and bioturbated sediment. Mollusc trails.
		2	Bad photo.
	2	3	Raised spiral trail (holothurian faeces).
	3	4	Small sponge- ball shape. Fan marks are feeding trails, most likely of crustacean, possibly worm.
	4	5	Trails most likely molluscs. Holes- probably worms, possibly crustaceans.
25CAM07	1	1	Mottled and bioturbated sediment. Small ball shaped sponges. Larger holes most likely crustaceans.
		2	Mottled and bioturbated sediment. Several holes. Several small ball shaped clumps, possibly sponges.
		3	Mottled and bioturbated sediment. Small sponges. Trails most likely molluscs. Several holes.
		4	Mottled and bioturbated sediment. Faeces trail. Small ball shaped sponge. Two large holes.
	5	5	Mottled sediment. Lots of small ball shaped sponges with holes and cylindrical shaped faeces. Octocoral.
		6	Bad photo.
		7	Mottled and bioturbated sediment. Trails- probably molluscs. Small ball shaped sponges.
		8	Mottled and bioturbated sediment. Holes and trails with several small round clumps, probably sponges.
		9	Very mottled sediment. Sponges and hole.
	6	10	Mottled sediment. Trails. Several small ball shaped sponges. Some small cylindrical shaped faeces.
		11	Mottled sediment. Several small ball shaped sponges with holes. Cylindrical shaped faeces.
		12	Same image as photo 11.
		13	Same image as photo 11.
27CAM08	1	1	Mottled sediment. Crustacean hole next to weight. Octocorals. Fish-eel.
		2	Mottled sediment. Three holes at top. Two stalks near holes.
	2	3	Mottled sediment. Octocoral.
		4	Same image as photo 2.
		5	Mottled sediment. Circular array of small holes (~7). Octocorals. Small mounds.
		6	Same image as photo 5.

	3	7	Mottled sediment. Swimming shrimp. Several small holes, mounds and trails.
	4	8	Mottled sediment. Small mounds. Unknown small black object in centre photo.
	5	-	No photos.
	6	9	Mottled sediment. Swimming shrimps. Trails most likely worms.
		10	Mottled sediment. Small mounds and hole. Trails.
		11	Same image as photo 10.
05CAM09	1	1	Mottled sediment. Several trails and small mounds.
	2	2	Mottled and bioturbated sediment. Old trails- most likely mollusc. Small mounds- old worm traces.
		3	Same image as photo 2.
		4	Same image as photo 2.
	3	5	Mottled sediment. Several trails and small mounds.
	4	6	Mottled sediment. Several holes and mounds.
		7	Mottled sediment. Large mound with hole. Trails and faeces.
	5	-	No photos.
	6	8	Mottled and bioturbated sediment. Holes- most likely crustaceans, possibly worms.
07CAM10	1	-	No photos.
	2	-	No photos.
	3	1	Mottled and bioturbated sediment. Sponge (ball). Trail-possibly mollusc. Fan trail. Crustacean in burrow. Some cylindrical faeces.
		2	Same image as photo 1.
		3	Bad photo.
	4	4	Mottled sediment. Several trails. Cylindrical shaped faeces.
	5	5	Mottled sediment. Small rounded sponge. Small mounds and some trails visible.
		6	Bad photo.
	6	7	Mottled sediment. Clump of faeces. Domed mound surrounded by numerous small holes.
		8	Same image as photo 7.
		9	Bad photo.
30CAM11	1	1	Mottled sediment. Faint mollusc trails
	2	2	Mottled sediment. Several holes (~7). Near camera trigger- one large asymmetric hole.
		3	Same image as photo 2.
	3	4	Mottled sediment. Asymmetric holes- mostly crustaceans. Hole in centre- worm. Whiptail.
	4	5	Mottled sediment. Rig of holes and small built up hole near centre. Mostly worms.
	5	6	Mottled sediments. Large built-up hole. Several other small holes.
	6	7	Mottled sediment. Several holes and mounds. Lots of small whitish mounds (ripple marks?).
02CAM12	1	-	No photos.
	2	-	No photos.
	3	-	No photos.
	4	1	Parallel marks probably man-made, possibly trawl marks, but look very irregular spacing so more likely something else. Trails cut over parallel marks.
	5	-	No photos.
	6	-	No photos.
29CAM13	1	1	Mottled sediment. 8 rounded sponges. Spiral holothurian faeces. Octocorals.
		2	Mottled sediment. Trails- most likely molluscs. Faeces.
	2	3	Mottled sediment. Holes - most likely crustaceans. Faeces.
		4	Mottled sediment and subcrop. Long straggling colonies. Octocorals, commensal brittlestar, anemone, possibly cerianthid.
	3	5	Mottled sediment. Small ball shaped sponges. Small mounds and cylindrical faeces. Fan mark- feeding trails, most likely crustacean, possibly worm.
	4	6	Mottled sediment. Spiral trail- holothurian faeces. Lots of other faeces.
		7	Mottled sediment. Small cylindrical holothurian faeces.
	5	8	Mottled sediment. Ball shaped sponge. Cylindrical faeces and mounds present.
	6	9	Mottled sediment. Ball shaped sponge. Cylindrical faeces, trails and mounds present.

	7	10	Mottled sediment. A few cylindrical shaped faeces.
	8	11	Mottled sediment. Few small holes and cylindrical shaped faeces.
01CAM14	1	1	Calcareous sand covered with Ecklonia kelp and other brown algae (<i>Neafypus obliquus</i>).
	2	2	Same image as photo 1

9.5. Appendix E – Dredge Descriptions

Table 9.17a. Dredge sub-sample descriptions: rock-type, mineralogy, description, colour and lithification/induration.

SampleID	Rock type	Mineralogy	Description	Colour	Lithification/ Induration
02DR01/A	Calcareous nannofossil ooze with diatoms and sponge spicules.	N/A	Biogenic + siliciclastic	2.5Y 8/2	Unconsolidated to semi-consolidated (firm).
02DR01/B	Basalt, vesicular, glassy, fragment.	Glassy texture, not detectable from hand specimen.			Very hard, glassy.
13DR02/A	Calcareous nannofossil ooze with glauconite (no spicules).	Carbonate and siliceous.	Biogenic + siliciclastic	Pale yellow (5Y 8/2) to white (5Y 8/1)	Partially consolidated, stiff.
13DR02/B	Calcareous nannofossil ooze with minor spicules.	Carbonate and siliceous.	Biogenic	White (5Y 8/1)	Semi consolidated with clots of sticky. clay
13DR02/C	Calcareous nannofossil ooze.	Carbonate and siliceous.	Biogenic	White (5Y 8/1)	Liquefied, unconsolidated.
14DR03/A	Calcareous nannofossil ooze with spicules.	Carbonate and siliceous.	Biogenic	Pale yellow (5Y 8/2) to white (5Y 8/1)	Partial consolidated with clots of clay.
15DR04/A1	Calcareous, spiculitic nannofossil ooze (stiff and dewatered).		Biogenic		Unlithified, loose.
15DR04/A2	Calcareous, spiculitic nannofossil ooze (unconsolidated).		Biogenic		Unlithified, loose.
15DR04/C	Deep-water coral (<i>Solenosmilia vanabilis</i>).		Reef building corals on seamounts.		
20DR05/A	Mudstone	Clay and mica.	Terrigenous clastic, micaceous, carbonaceous + organic fragments.	Dark brown (5Y 2/1)	Well indurated, weathered to soft, stiff clay.
20DR05/B	Calcareous nannofossil ooze.		Biogenic	White (5Y 8/1)	Stiff, dewatered, indurated.
20DR05/C	Calcareous nannofossil ooze.		Biogenic		Unconsolidated, liquefied.
22DR06/A	Siliceous mudstone.	Clay, mica, silt.	Terrigenous, clastic, mica, organic fragments.	Dark brown (5Y 2/1)	Well indurated, weathered, soft. Some stiff clays.
22DR06/B	Calcareous nannofossil ooze with silica spicules.	Silt and clay.	Biogenic	White to grey-white	Stiff, dewatered, very gluggy.
23DR07/A	Megacrystic garnet bearing granite or gneiss.	K-feldspar, quartz, biotite, plagioclase, almandine	Plutonic igneous or high grade metamorphic.	Generally pink to grey	Lithified but weathered.

		garnet.			
23DR07/B	Granulite, metamorphosed dolerite, amphibolite.	Pyroxene, amphibole, garnet.	High grade metamorphic-maybe some retrogression.	Black (5Y 2.5/1)	Lithified and well indurated.
23DR07/C	Nannofossil ooze with spicules (stiff).	Silt and clay-sized grains and matrix.	Biogenic	White (5Y 8/1)	Stiff, slightly dewatered with sticky clay clots.
23DR07/D	Calcareous nannofossil ooze.	Silt and clay-sized grains and matrix.	Biogenic	White (5Y 8/1)	Liquefied
06DR08/A1	Calcareous nannofossil ooze.	Calcite and silica.	Biogenic	White to grey-white	Unlithified, soft, unconsolidated.
06DR08/A2	Calcareenite	Calcite and silica.	Biogenic	White to grey-white	Partial lithified, indurated.
06DR08/A3	Calclutite (mudstone).		Biogenic, pelagic.	White	Partially lithified to lithified
06DR08/B	Marl (limestone).	Glauconite and olivine.	Bioclastic, biogenic.	Grey-green	Lithified, well indurated.
06DR08/D	Manganese crust.	Manganese	Clastic	Black	Lithified, friable.
06DR08/E	Octacoral with manganese crust.	Manganese and calcite.	Bioclastic	Black	N/A
26DR09/A1	Calclutite (mudstone).	Calcareous, minor quartz	Biogenic, possible quartz, silt and clay. minerals.	Light-yellowish brown (2.5Y 6/3)	Friable
26DR09/A2	Calclutite (mudstone).	Calcareous, minor quartz	Biogenic, possible quartz silt and clay minerals. HCl reaction.	Pale yellow (2.5Y 7/3)	Friable
26DR09/B	Calclutite (mudstone).	Calcareous, minor quartz	Biogenic, possible quartz silt and clay minerals.	Light-grey (2.5Y 7/2)	Indurated
26DR09/C	Calclutite (mudstone), soft chalk.	Nannofossil ooze, calcareous	Biogenic, strong HCl reaction.	White (5Y 8/1)	Consolidated, sticky.
26DR09/E	Calcareous nannofossil ooze.	Calcareous	Biogenic	Light grey (5Y 7/1)	Liquefied
02DR10/A1	Calcareous bioclastic.	Calcite, silica	Biogenic (quartz, silt and clay).	White to light grey (2.5Y 7/2)	Unlithified, unconsolidated.
02DR10/A2	Calcareous bioclastic.	Calcite, silica	Biogenic (quartz, silt and clay).	White to light grey (2.5Y 7/3)	Partially lithified, friable.
02DR10/C	Calcareous bioclastic.	Calcite (HCl reaction), black grains?	Biogenic	Yellow-brown (2.5YR 6/3)	Lithified, indurated.
02DR11/A1	Calcareous with sponge spicules.	Calcite, silica	Biogenic, pelagic.	Light grey (5Y 7/1)	Unconsolidated
02DR11/A2	Calcareous with sponge spicules.	Calcite, silica, quartz	Biogenic, pelagic.	Light grey (5Y 7/1); White (5Y 8/1)	Partially lithified, loose.
02DR11/A3	Calclutite. Calcareous with some silica and weathered surface.	Calcite, silica, quartz	Biogenic, pelagic.	Light grey (2.5Y 7/2)	Semi-lithified, friable.

02DR11/A4	Calcilutite. Calcareous, (silica?).		Biogenic, pelagic.	Light yellowish brown (2.5Y 6/3)	Lithified, indurated.
02DR11/C	Bamboo coral (Deep sea coral).				
28DR12/A	Calcilutite (carbonate mudstone).	Calcareous	Biogenic, silty quartz. HCl reaction.	Light grey (2.5Y 7/2)	Indurated
28DR12/B1	Calcareous nannofossil ooze with spicules.	Carbonate, silica spicules	Biogenic		Liquefied
28DR12/B2	Calcareous nannofossil ooze with spicules.	Carbonate, silica spicules	Biogenic		Unconsolidated, sticky.

Table 9.17b. Dredge sub-sample descriptions continued: sedimentary structures, fabric, particle size, fossil content, interpretation.

SampleID	Sedimentary structures	Fabric	Particle size	Fossil content	Interpretation
02DR01/A	None	Sedimentary with thin manganese crust.	Clay (ooze)	Forams, diatoms, sponge spicules under hand lens.	Nannofossil ooze, pelagic, abundant sponge spicules.
02DR01/B	N/A	N/A	N/A	N/A	Sub-aerial volcanic, to submarine extrusion.
13DR02/A	None	Very well sorted.	Silt and clay	Nannofossils	Minor manganese or organic crust on part of sample.
13DR02/B		Very well sorted.	Silt and clay	Nannofossils	
13DR02/C	None	Very well sorted.	Silt and clay	Nannofossils	
14DR03/A	None	Very well sorted.	Silt and clay	Nannofossils	
15DR04/A1	None	Moderately sorted.	Silt and clay	Nannofossils/ forams/ ?ostracods.	Pelagic drape- deep sea. Age unknown.
15DR04/A2	None	Moderately sorted.	Silt and clay	Nannofossils/forams/ ostracods.	Pelagic drape- deep sea. Age unknown.
15DR04/C	N/A	N/A	N/A		
20DR05/A	Filled burrows.	Bedding not apparent. Very well sorted.	Silt and clay	?Fossil fragments or contamination.	Similar to Bremer Sub-basin mudstones; possible Berriasian to Aptian age. Lacustrine/flood plain.
20DR05/B	None	Very well sorted.	Silt and clay	Nannofossils	
20DR05/C	None	Very well sorted.	Silt and clay	Nannofossils	
22DR06/A	Burrows filled with nanno-ooze.	Homogenous, well sorted, no bedding.	Silt and clay	None apparent.	Terrigenous mudstone.
22DR06/B	None	Well sorted.	Silt and clay	Nannofossils and foraminifers.	Deep sea ooze.
23DR07/A	N/A	Course grained K-spar phenocrysts bands in a medium to fine grained ground mass of subhedral quartz, biotite, plagioclase and garnet.	Course phenocrysts + medium – fine grained (Phenocrysts up to 3 cm)	N/A	Possibly a product of pegmatitic melt. Per aluminous in composition. Basement, Albany Fraser?
23DR07/B	N/A	Granulitic	Medium to fine grained (equi-granular)	N/A	Granulite facies/ amphibolite facies. Basement: Albany Fraser?
23DR07/C	None apparent.	Very well sorted.	Silt and clay	Nannofossils	
23DR07/D	None apparent.	Very well sorted.	Silt and clay	Nannofossils	

06DR08/A1	None	Well sorted, grain supported.	Silt and clay	None apparent.	Calcareous nannofossil ooze (modern).
06DR08/A2	Horizontal bedding.	Well sorted, grain supported.	Silt and clay	None apparent.	Calcareenite
06DR08/A3	None apparent.	Well sorted.	Silt and clay	None apparent.	Consolidated ooze in weathering ??.
06DR08/B	Horizontal bedding.	Well sorted, grain supported.	Silt	Fossil plant.	Calcareenite.
06DR08/D	N/A	Matrix	N/A	N/A	Marl (limestone). Contains fossil plant on fresh surface.
06DR08/E	N/A	N/A	N/A	Octacoral	Manganese crust.
					Deep-sea octacoral, very old due to manganese crust.
26DR09/A1	Possible bioturbation.	Very well sorted.	Silt and clay	?Nannofossils	
6DR09/A2	Possible bioturbation.	Very well sorted.	Silt and clay	?Nannofossils	
26DR09/B	Boring and possible bioturbation.	Very well sorted.	Silt and clay	?Nannofossils	
26DR09/C		Very well sorted.	Silt and clay	Nannofossils and spicules	
26DR09/E		Very well sorted.	Silt and clay	Nannofossils and spicules.	Deep sea marine (Holocene).
02DR10/A1	None apparent.	Well sorted, grain supported.	Silt and clay	Nannofossils	Deep sea calcareous ooze.
02DR10/A2	None apparent.	Well sorted, grain supported.	Silt and clay	Borings/burrows and nannofossils.	Calclutite. Weathering surface apparent.
02DR10/C	None apparent.	Well sorted, grain supported.	Silt and clay	Nannofossils?	Marl (muddy limestone).
02DR11/A1	None apparent.	Well sorted, grain supported.	Silt and clay	Nannofossils	Pelagic ooze.
02DR11/A2	None apparent.	Well sorted, grain supported.	Silt and clay	Nannofossils	Deep sea marine (Pelagic) chalk.
02DR11/A3	Burrows/ weathered surface.	Well sorted, grain supported.	Silt and clay	Nannofossils	Deep sea marine calcareous (mudstone).
02DR11/A4	None apparent.	Well sorted, grain supported.	Silt and clay	Nannofossils	Deep sea marine calclutite (mudstone).
28DR12/A	?Relict fabric of bioturbation.	Some colour variation (re-oxidised carbonate mud), very well sorted.	Silt and clay	?Nannofossils	
28DR12/B1	None	Very well sorted.	Silt and clay	Nannofossils, spicules.	
28DR12/B2	None	Very well sorted.	Silt and clay	Nannofossils, spicules.	

9.6. Appendix F – Textural Characteristics of Seabed Sediments

Table 9.18. Textural characteristics of seabed sediment samples collected during SS08/2005 Survey.

SampleID	Latitude	Longitude	Gravel (%)	Sand (%)	Mud (%)	CaCO ₃ (Bulk%)	CaCO ₃ (Sand%)	CaCO ₃ (Mud%)
04GC01	-32° 36.43'	114° 20.24'	0.17	35.59	64.24	87.9	94.0	87.4
05GC02	-32° 35.24'	114° 21.76'	0.00	11.19	88.81	83.0	I/S	80.9

06GC03	-32° 34.57'	114° 21.38'	0.00	11.23	88.77	80.9	I/S	78.6
07GC04	-32° 31.70'	114° 18.44'	0.00	9.13	90.87	69.7	I/S	80.0
08GC05	-32° 33.27'	114° 19.39'	0.00	15.82	84.18	78.0	I/S	71.3
09GC06	-32° 53.52'	114° 12.35'	0.00	20.53	79.47	85.0	I/S	86.1
10GC08	-32° 47.80'	114° 09.93'	0.00	27.89	72.11	81.4	I/S	81.3
11GC10	-32° 48.35'	113° 48.29'	0.00	31.67	68.33	79.8	92.9	78.8
13GC12	-32° 49.84'	113° 54.05'	0.00	19.60	80.40	81.9	91.6	82.2
12GC13	-32° 49.57'	113° 51.38'	0.00	22.65	77.35	82.4	I/S	82.9
17GC14	-32° 56.14'	113° 53.22'	0.00	22.76	77.24	83.2	92.5	84.2
18GC15	-32° 58.05'	113° 53.88'	0.34	19.56	80.10	83.2	90.6	83.3
19GC16	-32° 59.25'	113° 53.64'	0.15	14.31	85.54	82.6	89.0	82.7
21GC17	-32° 56.80'	113° 55.82'	0.00	9.13	90.87	83.8	91.0	83.7
23GC18A	-32° 46.94'	114° 08.85'	0.67	20.17	79.16	82.6	91.1	83.2
24GC18	-32° 46.44'	114° 08.48'	0.00	24.98	75.02	80.4	I/S	83.6
25GC19	-32° 51.60'	114° 15.02'	0.00	11.11	88.89	82.3	86.4	84.6
27GC20	-32° 37.32'	114° 25.27'	0.09	16.51	83.40	84.5	90.7	85.6
26GC21	-31° 58.33'	114° 36.16'	0.00	12.54	87.46	80.9	I/S	81.5
28GC22	-32° 03.90'	114° 40.08'	0.00	13.16	86.84	77.7	I/S	80.9
02GC23	-32° 03.09'	114° 38.91'	0.00	8.09	91.91	79.7	I/S	82.7
02GC24	-32° 02.58'	114° 39.50'	0.00	6.38	93.62	79.3	I/S	82.3
02DR01/A	-32° 02.85'	114° 39.29'	0.05	10.87	89.07	80.2	78.0	83.2
13DR02/A	-32° 52.29'	113° 50.78'	0.00	2.35	97.65	72.0	I/S	73.2
14DR03/A	-32° 57.82'	113° 53.55'	0.02	13.07	86.91	80.6	69.5	81.5
15DR04/A1	-32° 57.73'	113° 52.09'	0.00	19.29	80.71	78.2	84.0	83.9
20DR05/C	-32° 55.95'	113° 58.88'	0.00	22.98	77.02	81.5	87.0	83.2
22DR06/B	-32° 52.89'	114° 02.89'	0.04	23.24	76.72	82.8	89.9	83.6
23DR07/D	-32° 46.54'	114° 08.50'	0.00	18.16	81.84	81.0	88.2	83.2
06DR08/A1	-32° 34.31'	114° 21.44'	0.00	15.59	84.41	81.2	86.0	83.5
26DR09/E	-31° 57.37'	114° 36.42'	0.00	13.57	86.43	76.7	79.1	80.4
02DR10/A1	-32° 01.96'	114° 39.65'	0.06	10.72	89.22	77.3	I/S	81.1
02DR11/A1	-32° 02.88'	114° 38.91'	0.00	10.18	89.82	78.1	I/S	82.0
28DR12/B1	-32° 04.01'	114° 40.03'	0.09	12.41	87.50	78.2	77.1	81.7
12BS01	-32° 50.92'	113° 50.51'	0.00	9.65	90.35	90.2	92.4	90.0
25BS02/A	-32° 15.41'	113° 15.02'	0.17	18.43	81.40	83.2	86.2	85.0

I/S = insufficient sample for analysis.

Table 9.19. Textural characteristics of seabed sediment samples collected on previous surveys.

Survey	Sample ID	Latitude	Longitude	Gravel (%)	Sand (%)	Mud (%)	CaCO ₃ (Bulk%)	CaCO ₃ (Sand%)	CaCO ₃ (Mud%)
296	GR32	-31° 36.72'	115° 10.69'	7.81	92.13	0.06	92.1	96.4	I/S
296	GR33	-31° 39.26'	115° 01.43'	8.65	90.66	0.69	93.6	95.2	I/S
296	GR34	-31° 39.31'	114° 58.68'	0.13	39.09	60.78	83.7	85.3	86.1
296	GR35	-31° 41.83'	114° 52.68'	0.06	31.41	68.54	84.2	86.4	85.9
296	GR36	-31° 43.62'	114° 45.45'	0.38	44.83	54.80	86.2	91.8	85.7
296	GR37	-33° 00.02'	114° 34.73'	0.49	55.31	44.20	85.6	88.6	87.6

296	GR50	-34° 02.20'	114° 27.11'	5.66	93.96	0.38	92.4	91.4	I/S
296	GR51	-33° 02.25'	114° 48.48'	1.00	70.09	28.91	86.7	89.8	I/S
80	GC02	-31° 51.20'	115° 01.29'	0.08	19.43	80.49	80.9	91.2	82.6
80	GC03	-30° 07.00'	114° 01.00'	0.00	14.39	85.61	87.6	I/S	91.7
80	GC04	-30° 07.00'	114° 17.00'	0.54	23.90	75.56	83.6	I/S	87.2
80	GC08	-31° 14.00'	114° 44.00'	0.01	30.86	69.12	78.2	92.3	85.8
80	DR02	-31° 52.00'	114° 55.40'	0.00	7.47	92.53	68.9	78.8	73.1
80	DR03	-30° 06.98'	113° 44.64'	0.00	12.29	87.71	81.0	89.9	82.9
80	DR04	-31° 13.64'	114° 35.96'	0.08	38.55	61.37	87.8	93.4	87.7
80	DR05	-32° 00.20'	114° 57.50'	0.00	22.43	77.57	51.8	47.4	58.2
80	DR06	-32° 00.70'	114° 58.00'	0.01	12.65	87.34	81.8	89.8	85.0
80	DR08	-32° 01.67'	114° 59.61'	0.01	12.07	87.92	82.5	89.5	86.0
80	DR09	-32° 02.50'	115° 01.13'	0.11	12.72	87.17	81.5	87.9	83.3
80	DR10	-32° 01.70'	114° 58.60'	0.02	12.55	87.43	82.4	89.3	83.7
80	DR12	-31° 59.35'	115° 01.50'	0.00	15.97	84.03	82.8	88.6	83.9
80	DR13	-31° 57.70'	115° 04.50'	2.11	22.55	75.33	76.3	32.6	71.2
80	DR14	-32° 03.60'	114° 45.00'	4.21	23.49	72.31	78.5	42.0	72.9
80	DR15	-32° 03.10'	114° 45.50'	0.06	8.72	91.22	77.3	82.5	81.4
80	DR16	-32° 06.00'	114° 43.00'	0.12	9.21	90.67	78.2	81.2	81.5
80	DR17	-32° 06.05'	114° 43.00'	0.06	16.59	83.34	77.4	90.5	79.9
80	DR18	-31° 57.40'	114° 44.20'	0.00	8.32	91.68	76.4	89.2	81.5
80	DR19	-31° 59.80'	114° 39.50'	0.06	9.62	90.32	79.4	86.9	82.4
80	DR20	-32° 00.00'	114° 38.00'	0.00	15.39	84.61	75.7	81.4	79.3
80	DR21	-31° 50.05'	114° 37.60'	1.05	15.14	83.81	74.3	68.9	77.1
80	DR23	-31° 48.00'	114° 39.00'	0.00	15.65	84.35	80.2	84.1	80.9
81	GC01	-31° 53.40'	114° 34.50'	0.05	13.68	86.26	77.3	89.7	70.1
SS09/2005	DRGA-1A	-32° 14.40'	114° 23.20'	0.00	38.45	61.55	37.8	46.0	36.9
SS09/2005	DRGA-2B	-32° 49.63'	114° 13.00'	0.00	12.07	87.93	82.4	91.5	84.4
SS09/2005	DR01	-32° 46.25'	114° 09.31'	0.00	25.93	74.07	81.5	87.7	84.6
SS09/2005	DR02	-32° 16.22'	114° 29.69'	2.89	30.76	66.35	79.8	85.0	83.9

I/S = insufficient sample for analysis.

Table 9.20. Mean grainsize and Folk classification of seabed sediment samples collected during SS08/2005 Survey.

SampleID	Mean grainsize (mm)	Descriptive mean grainsize	Folk classification
04GC01	0.09321	very fine sand	sandy mud
05GC02	0.05202	coarse silt	sandy mud
06GC03	0.04087	coarse silt	sandy mud
07GC04	0.03484	coarse silt	mud
08GC05	0.04923	coarse silt	sandy mud
09GC06	0.05971	coarse silt	sandy mud
10GC08	0.03943	coarse silt	sandy mud
11GC10	0.08031	very fine sand	sandy mud
03GC12	0.05264	coarse silt	sandy mud
12GC13	0.05651	coarse silt	sandy mud
17GC14	0.06133	coarse silt	sandy mud

18GC15	0.04698	coarse silt	sandy mud
19GC16	0.07158	very fine sand	sandy mud
21GC17	0.07077	very fine sand	mud
23GC18A	0.04962	coarse silt	sandy mud
24GC18	0.04140	coarse silt	sandy mud
25GC19	0.04548	coarse silt	sandy mud
27GC20	0.06375	very fine sand	sandy mud
26GC21	0.05451	coarse silt	sandy mud
28GC22	0.05065	coarse silt	sandy mud
02GC23	0.03359	coarse silt	sandy mud
02GC24	0.03523	coarse silt	sandy mud
02DR01/A	0.03608	coarse silt	sandy mud
13DR02/A	0.02556	medium silt	mud
14DR03/A	0.04047	coarse silt	sandy mud
15DR04/A	0.04691	coarse silt	sandy mud
20DR05/C	0.05190	coarse silt	sandy mud
22DR06/B	0.05681	coarse silt	sandy mud
23DR07/D	0.04708	coarse silt	sandy mud
06DR08/A	0.04873	coarse silt	sandy mud
26DR09/E	0.03874	coarse silt	sandy mud
02DR10/A1	0.03192	coarse silt	sandy mud
02DR11/A1	0.03398	coarse silt	mud
28DR12/A	0.03286	coarse silt	sandy mud
12BS01	0.02846	coarse silt	sandy mud
25BS02/A	0.05191	medium silt	sandy mud

Table. 9.21. Mean grainsize and Folk classification of seabed sediment samples collected on previous surveys.

Survey	SampleID	Mean grainsize (mm)	Descriptive mean grainsize	Folk classification
296	GR32	0.6154	coarse sand	gravelly sand
296	GR33	0.5516	coarse sand	gravelly sand
296	GR34	0.0668	very fine sand	sandy mud
296	GR35	0.0674	very fine sand	sandy mud
296	GR36	0.1308	fine sand	sandy mud
296	GR37	0.0954	very fine sand	Muddy sand
296	GR50	0.4116	medium sand	gravelly sand
296	GR51	0.1713	fine sand	slightly gravelly muddy sand
80	GC02	0.0687	very fine sand	sandy mud
80	GC03	0.0543	coarse silt	sandy mud
80	GC04	0.0947	very fine sand	sandy mud
80	GC08	0.0866	very fine sand	sandy mud
80	DR02	0.0177	medium silt	sandy mud
80	DR03	0.0424	coarse silt	sandy mud
80	DR04	0.0870	very fine sand	sandy mud
80	DR05	0.0387	coarse silt	sandy mud
80	DR06	0.0506	coarse silt	sandy mud

80	DR08	0.0420	coarse silt	sandy mud
80	DR09	0.0417	coarse silt	sandy mud
80	DR10	0.0378	coarse silt	sandy mud
80	DR12	0.0454	coarse silt	sandy mud
80	DR13	0.0425	coarse silt	slightly gravelly sandy mud
80	DR14	0.0589	coarse silt	slightly gravelly sandy mud
80	DR15	0.0358	coarse silt	sandy mud
80	DR16	0.0357	coarse silt	sandy mud
80	DR17	0.0540	coarse silt	sandy mud
80	DR18	0.0390	coarse silt	sandy mud
80	DR19	0.0392	coarse silt	sandy mud
80	DR20	0.0493	coarse silt	sandy mud
80	DR21	0.0462	coarse silt	slightly gravelly sandy mud
80	DR23	0.0448	coarse silt	sandy mud
81	GC01	0.0552	coarse silt	sandy mud
SS09/2005	DRGA-1A	0.0523	coarse silt	sandy mud
SS09/2005	DRGA-2B	0.0306	coarse silt	sandy mud
SS09/2005	DR01	0.0585	coarse silt	sandy mud
SS09/2005	DR02	0.0627	very fine sand	slightly gravelly sandy mud

Table 9.22. Composition point counting results for SS08/2005 seabed samples.

SampleID	Planktic foraminifera	Benthic foraminifera	Sponge spicules	Ostracods	Radiolarians	Pteropods	Mineral grains	Fragments	Other/ Unknown	Count
04GC01	229	10	0	2	0	10	0	83	3	337
05GC02	212	5	2	0	7	0	1	93	1	321
06GC03	220	5	15	2	7	0	0	60	0	309
08GC05	234	3	3	0	9	0	0	55	1	305
09GC06	102	3	14	0	6	0	0	180	2	307
10GC08	206	6	43	1	8	0	0	59	1	324
11GC10	284	5	0	1	0	0	0	41	2	333
03GC12	270	4	0	0	0	0	0	51	0	325
12GC13	320	7	1	0	0	0	0	54	1	383
17GC14	295	4	0	2	0	2	1	57	1	362
18GC15	238	3	0	2	3	0	0	66	0	312
19GC16	236	8	6	1	2	0	1	77	2	333
21GC17	239	8	4	2	0	0	1	83	1	338
23GC18A	355	7	4	1	1	1	1	88	0	458
24GC18	262	7	0	0	0	0	0	45	1	315
25GC19	213	4	13	0	11	1	0	67	2	311
27GC20	116	4	99	13	29	12	0	676	2	951
26GC21	116	6	177	2	19	0	0	197	0	517
28GC22	272	13	0	0	7	0	0	33	0	325
02GC23	277	3	23	1	0	0	0	44	5	353

02GC24	252	7	32	1	4	0	0	39	0	335
12BS01	329	2	0	0	0	0	0	8	0	339
25BS02/A	237	6	0	1	1	3	4	113	0	365
02DR01/A	289	7	0	0	7	0	1	45	25	374
13DR02/A	314	22	0	1	0	0	0	26	0	363
14DR03/A	346	5	0	1	3	0	0	46	0	401
15DR04/A	297	6	0	0	0	0	0	35	0	338
20DR05/C	235	8	12	0	4	0	0	78	1	338
22DR06/B	239	6	0	0	3	1	0	72	2	323
23DR07/D	322	6	0	1	2	0	1	73	0	405
06DR08/A	256	2	0	0	3	1	1	61	0	324
26DR09/E	313	6	0	0	1	0	0	16	1	337
02DR10/A1	288	6	7	1	1	0	0	40	4	347
02DR11/A1	250	5	34	1	9	0	0	70	5	374
28DR12/A	316	8	0	1	2	0	3	38	2	370

Table 9.23. Composition point counting results for SS08/2005 seabed samples, expressed as percentages.

SampleID	Planktic foraminifera	Benthic foraminifera	Sponge spicules	Ostracods	Radiolarians	Pteropods	Mineral grains	Fragments	Other/Unknown	Total
04GC01	68.0	3.0	0.0	0.6	0.0	3.0	0.0	24.6	0.9	100
05GC02	66.0	1.6	0.6	0.0	2.2	0.0	0.3	29.0	0.3	100
06GC03	71.2	1.6	4.9	0.6	2.3	0.0	0.0	19.4	0.0	100
08GC05	76.7	1.0	1.0	0.0	3.0	0.0	0.0	18.0	0.3	100
09GC06	33.2	1.0	4.6	0.0	2.0	0.0	0.0	58.6	0.7	100
10GC08	63.6	1.9	13.3	0.3	2.5	0.0	0.0	18.2	0.3	100
11GC10	85.3	1.5	0.0	0.3	0.0	0.0	0.0	12.3	0.6	100
03GC12	83.1	1.2	0.0	0.0	0.0	0.0	0.0	15.7	0.0	100
12GC13	83.6	1.8	0.3	0.0	0.0	0.0	0.0	14.1	0.3	100
17GC14	81.5	1.1	0.0	0.6	0.0	0.6	0.3	15.7	0.3	100
18GC15	76.3	1.0	0.0	0.6	1.0	0.0	0.0	21.2	0.0	100
19GC16	70.9	2.4	1.8	0.3	0.6	0.0	0.3	23.1	0.6	100
21GC17	70.7	2.4	1.2	0.6	0.0	0.0	0.3	24.6	0.3	100
23GC18A	77.5	1.5	0.9	0.2	0.2	0.2	0.2	19.2	0.0	100
24GC18	83.2	2.2	0.0	0.0	0.0	0.0	0.0	14.3	0.3	100
25GC19	68.5	1.3	4.2	0.0	3.5	0.3	0.0	21.5	0.6	100
27GC20	12.2	0.4	10.4	1.4	3.0	1.3	0.0	71.1	0.2	100
26GC21	22.4	1.2	34.2	0.4	3.7	0.0	0.0	38.1	0.0	100
28GC22	83.7	4.0	0.0	0.0	2.2	0.0	0.0	10.2	0.0	100
02GC23	78.5	0.8	6.5	0.3	0.0	0.0	0.0	12.5	1.4	100
02GC24	75.2	2.1	9.6	0.3	1.2	0.0	0.0	11.6	0.0	100
12BS01	97.1	0.6	0.0	0.0	0.0	0.0	0.0	2.4	0.0	100
25BS02/A	64.9	1.6	0.0	0.3	0.3	0.8	1.1	31.0	0.0	100
02DR01/A	77.3	1.9	0.0	0.0	1.9	0.0	0.3	12.0	6.7	100

13DR02/A	86.5	6.1	0.0	0.3	0.0	0.0	0.0	7.2	0.0	100
14DR03/A	86.3	1.2	0.0	0.2	0.7	0.0	0.0	11.5	0.0	100
15DR04/A	87.9	1.8	0.0	0.0	0.0	0.0	0.0	10.4	0.0	100
20DR05/C	69.5	2.4	3.6	0.0	1.2	0.0	0.0	23.1	0.3	100
22DR06/B	74.0	1.9	0.0	0.0	0.9	0.3	0.0	22.3	0.6	100
23DR07/D	79.5	1.5	0.0	0.2	0.5	0.0	0.2	18.0	0.0	100
06DR08/A	79.0	0.6	0.0	0.0	0.9	0.3	0.3	18.8	0.0	100
26DR09/E	92.9	1.8	0.0	0.0	0.3	0.0	0.0	4.7	0.3	100
02DR10/A1	83.0	1.7	2.0	0.3	0.3	0.0	0.0	11.5	1.2	100
02DR11/A1	66.8	1.3	9.1	0.3	2.4	0.0	0.0	18.7	1.3	100
28DR12/A	85.4	2.2	0.0	0.3	0.5	0.0	0.8	10.3	0.5	100

Table 9.24. Total foraminifera and total fragments excluding other categories (%).

Sample ID	Total foraminifera	Total fragments
04GC01	74.2	25.8
05GC02	70.0	30.0
06GC03	78.9	21.1
08GC05	81.2	18.8
09GC06	36.8	63.2
10GC08	78.2	21.8
11GC10	87.6	12.4
03GC12	84.3	15.7
12GC13	85.8	14.2
17GC14	84.0	16.0
18GC15	78.5	21.5
19GC16	76.0	24.0
21GC17	74.8	25.2
23GC18A	80.4	19.6
24GC18	85.7	14.3
25GC19	76.4	23.6
27GC20	15.1	84.9
26GC21	38.2	61.8
28GC22	89.6	10.4
02GC23	86.4	13.6
02GC24	86.9	13.1
12BS01	97.6	2.4
25BS02/A	68.3	31.7
02DR01/A	86.8	13.2
13DR02/A	92.8	7.2
14DR03/A	88.4	11.6
15DR04/A	89.6	10.4
20DR05/C	75.7	24.3
22DR06/B	77.3	22.7
23DR07/D	81.8	18.2
06DR08/A	80.9	19.1
26DR09/E	95.2	4.8

02DR10/A1	88.0	12.0
02DR11/A1	78.5	21.5
28DR12/A	89.5	10.5

Table 9.25. Composition point counting results for seabed sediment samples collected on previous surveys.

SampleID	Planktic foraminifera	Benthic foraminifera	Sponge spicules	Ostracods	Radiolarians	Pteropods	Mineral grains	Fragments	Other/Unknown	Count
SS09/2005/DRGA1A	169	4	21	0	9	0	37	67	0	307
SS09/2005/DR01	316	5	5	2	2	0	0	40	1	371
SS09/2005/DR02	288	6	0	0	0	0	0	19	0	313
SS07/2005/GR36	131	26	1	0	0	15	0	142	0	315
SS07/2005/GR51	84	30	1	0	0	5	3	188	0	311
BMR80/DR04	46	6	5	1	10	18	0	246	0	332
BMR80/DR05	148	13	0	4	5	6	0	144	1	321

Table 9.26. Composition point counting results for seabed sediment samples collected on previous surveys, expressed as percentage.

SampleID	Planktic foraminifera	Benthic foraminifera	Sponge spicules	Ostracods	Radiolarians	Pteropods	Mineral grains	Fragments	Other/Unknown	Count
SS09/2005/DRGA1A	55.0	1.3	6.8	0.0	2.9	0.0	12.1	21.8	0.0	100
SS09/2005/DR01	85.2	1.3	1.3	0.5	0.5	0.0	0.0	10.8	0.3	100
SS09/2005/DR02	92.0	1.9	0.0	0.0	0.0	0.0	0.0	6.1	0.0	100
SS07/2005/GR36	41.6	8.3	0.3	0.0	0.0	4.8	0.0	45.1	0.0	100
SS07/2005/GR51	27.0	9.6	0.3	0.0	0.0	1.6	1.0	60.5	0.0	100
BMR80/DR04	13.9	1.8	1.5	0.3	3.0	5.4	0.0	74.1	0.0	100
BMR80/DR05	46.1	4.0	0.0	1.2	1.6	1.9	0.0	44.9	0.3	100

Table 9.27. Total foraminifera and total fragments excluding other categories (%).

SampleID	Total foraminifera	Total fragments
SS09/2005/DRGA1A	72.1	27.9
SS09/2005/DR01	88.9	11.1
SS09/2005/DR02	93.9	6.1
SS07/2005/GR36	52.5	47.5
SS07/2005/GR51	37.7	62.3
BMR80/DR04	17.4	82.6
BMR80/DR05	52.8	47.2

Grainsize distribution graphs and associated data from the Malvern are also contained on the data CD-ROM in pdf format.

9.7. Appendix G – Core Logs

The core logs contain the physical property data (wet bulk density, p-wave velocity, magnetic susceptibility, fractional porosity, and colour), texture and composition information, visual log (including digital images) and comments on specific features. The core logs are contained on the data CD-ROM in jpg format. The filenames follow the convention: *GA Survey Number, Station Number, Operation Type, Operation Number* (e.g., SS082005_04GC01). High-resolution digital photographs of selected intervals are also contained in the Appendix. The filenames follow the convention: *GA Survey Number, Station Number, Operation Type, Operation Number, Interval Depth* (e.g., SS082005_04GC01_18_45cm).

9.8. Appendix H – Textural Characteristics for Sub-surface Sediments

Data contained in this Appendix are based on sieve analysis and carbonate bomb analysis, and are thus expressed as weight percents. Grainsize distributions for all of the sub-surface samples are expressed as volume percentages measured from the Malvern™ Mastersizer-2000 laser particle analyser and can be found on the accompanying data CD-ROM. Grainsize distribution graphs and associated data from the Malvern are contained on the data CD-ROM in pdf format. The filenames follow the convention: *7-digit Lab Number, GA Survey Number, Station Number, Operation Type, Operation Number, and Sub-sample Depth Interval* (e.g., 1828827 SS082005/04GC01/10-12cm).

9.9. Appendix I – Multi-sensor Core Logger Data

The multi-sensor core logger data is the processed physical property data for the cores (i.e., wet bulk density, p-wave velocity, magnetic susceptibility, fractional porosity, and colour). Compromised and unreliable data have been removed. The data are contained in Excel spreadsheets and the filenames follow the convention: *GA Survey Number, Station Number, Operation Type, Operation Number* (e.g., SS082005_04GC01). The unprocessed data and the processing files can be downloaded from Geoscience Australia's marine samples database (MARS) (<http://www.ga.gov.au/oracle/mars>).

9.10. Appendix J – Slope Stability Report

The report contained in this appendix is an initial assessment of the seabed stability of the mid to lower slope of the Mentelle Basin. The assessment is based on a detailed interpretation of the geomorphology and shallow seismic data, where features associated with mass movements are identified. The report is provided as a separate document on the data CD-ROM in pdf format.